ENVIRONMENTAL CHAMBER STUDIES FOR DEVELOPMENT OF AN UPDATED PHOTOCHEMICAL MECHANISM FOR VOC REACTIVITY ASSESSMENT

Final Report to

California Air Resources Board, Contract 92-345
Coordinating Research Council, Inc., Project M-9
National Renewable Energy Laboratory, Contract ZF-2-12252-07

by

William P. L. Carter,
Dongmin Luo, and Irina L. Malkina

November 26, 1997

College of Engineering,
Center for Environmental Research and Technology
University of California, Riverside, CA 92521

96:AP:070F

ABSTRACT

A series of indoor environmental chamber experiments were conducted to fill gaps in the data base needed for evaluation of gas-phase photochemical mechanisms for assessing the effects of emissions of volatile organic compounds (VOCs) on ambient air quality. Two large dual-mode indoor Teflon bag chambers, one irradiated by blacklights and the other by xenon arc light, were employed. Alternative methods for measuring light intensity in these chambers were evaluated. It was found that quartz tube NO_2 actinometry provides satisfactory data for the blacklight chamber, but that Cl_2 - n-butane irradiations provide a better method for the xenon arc chamber. The effects of varying humidity on results and reproducibility of chamber experiments were examined. It was found that differences between dry runs and runs at ~50% RH were minor and should not significantly affect mechanism evaluation results, but that runs with humidities approaching 100% RH may have problems. Incremental reactivity experiments, where a test compound is added to NOx-air irradiations of reactive organic gas (ROG) surrogates representing ambient pollution, were conducted for representative compounds using the xenon arc chamber. These were needed to supplement the much larger data base of incremental reactivity experiments in blacklight chambers. The results were consistent with model predictions and the large data base of incremental reactivity experiments in blacklight chambers, if the aromatics mechanisms was modified to account for differences in light source. An extensive series of single aromatic - NO_x experiments were carried out using both light sources to provide data needed to develop, adjust, and evaluate mechanisms for benzene, toluene, ethylbenzene, o-, m-, and p-xylenes, and all three trimethylbenzene isomers. The current version of the detailed SAPRC mechanism (SAPRC-93) did not correctly account for isomeric differences and tended to underpredict reactivities in the xenon arc chamber. Much better fits could be obtained if yields of two lumped fragmentation products, representing different photodecomposition action spectra, are optimized separately for each isomer. However, such adjustments still did not provide satisfactory fits for benzene, and could not simulate the data for the other aromatics in all respects. The data base obtained in this study will be an important resource for evaluating updated mechanisms which are under development.

ACKNOWLEDGEMENTS

The authors wish to acknowledge and thank Mr. Bart Croes of the CARB, Mr. Tim Belian of the CRC, and Mr. Brent Bailey of NREL for their support of this project and their patience with the delays in completing this report. Dr. Joseph Norbeck, Director of the University of California, Riverside's College of Engineering Center for Environmental Research and Technology (CE-CERT) provided funding needed to move the environmental chamber facility to CE-CERT, and additional support needed to carry out this project. Valuable assistance in constructing the chamber facility and conducting the experiments for this program was provided by Mr. Dennis Fitz and Mr. Kurt Bumiller. Mr. Fitz also assisted in administration of this program. Assistance in conducting the experiments was provided by Ms. Kathalena M. Smihula, Mr. David Cocker and Ms. Amy Lishan Ng. Mr. Patrick Sekerka and Mr. Jeff Friend provided assistance in constructing the chamber facility at CE-CERT.

The opinions and conclusions in this document are entirely those of the authors. Mention of trade names and commercial products does not constitute endorsement or recommendation for use.

EXECUTIVE SUMMARY

Introduction and Background

The formation of ground-level ozone is caused by the gas-phase interactions of emitted volatile organic compounds (VOCs) and oxides of nitrogen (NO_x) in the presence of sunlight. Although traditional VOC control strategies to reduce ozone have focused on reducing the total mass of VOC emissions, strategies which take into account these differences in "reactivities" of VOCs might provide a means for additional ozone reduction which could supplement mass-based controls. Examples include conversion of motor vehicles to alternative fuels and solvent substitutions. Implementing reactivity-based strategies requires a reliable means to quantify the effects of emissions of different types of VOCs on ozone formation. Such estimates require use of computer airshed models, since the effects of the VOCs on ozone formation depend both on the nature of the environment where the VOC is emitted and on the VOC's atmospheric reactions. Since the predictions of such models can be no more reliable than the chemical mechanisms upon which they are based, it is critical that the chemical mechanisms used for the VOCs be able to accurately predict the effects of VOCs on ozone formation under various conditions.

The chemical mechanisms used in airshed models are based on our knowledge and theories concerning the elementary gas-phase reactions which are believed to be involved in ground-level ozone formation. However, the processes by which VOCs and NO_x interact to form ozone are complex, and our knowledge of them is incomplete. Therefore, no model calculation of reactivity can be considered to be reliable unless it has been shown that it can accurately predict ozone impacts under a variety of conditions. The only practical way to do this is to carry out environmental chamber experiments and then determine if the mechanism can accurately predict the ozone impacts that were observed. Although ozone impacts in chambers will not be quantitatively the same as they are in the atmosphere, in appropriately designed experiments they will be affected by the aspects of the chemical mechanisms that affect reactivities in the atmospheres.

While the chamber database used in evaluating atmospheric chemical mechanisms has been quite extensive, there has been a number of major gaps and data needs, particularly with regard to evaluating mechanisms for VOC reactivity assessment for a wide variety of individual VOCs. To address this need, the Statewide Air Pollution Research Center (SAPRC) at the University of California at Riverside (UCR), subsequently in conjunction with the College of Engineering, Center for Environmental Research and Technology (CE-CERT), has conducted a multi-year environmental chamber program to provide data needed to improve the reliability of chemical mechanisms for use in predicting effects of VOC emission

changes on ozone formation. Two phases of this program have been completed and reported previously. In the first phase, we measured the effects of the addition of 36 representative VOCs to irradiations of a simplified mixture representing pollutants in the atmosphere under conditions where ozone is most sensitive to VOCs, using an indoor chamber with a blacklight light source. It was found that effects of the VOCs on ozone formation in these systems differed significantly, even after differences in their atmospheric reaction rates were taken into account. All these experiments were carried out using the same highly simplified reactive organic gas (ROG) surrogate to represent reactive VOC pollutants from other sources and using relatively low ROG/NO_x levels representing maximum incremental reactivity (MIR) conditions. In the second phase of this program, the effects of varying ROG surrogate and NO_x levels were examined, and it was found that both had significant effects on reactivity. In addition, a limited number of experiments was carried out in a chamber using a new xenon arc light source, which provided a spectrum more representative of sunlight than blacklights. The results of these first two phases were used to evaluate the SAPRC-90 chemical mechanism which was used to calculate the MIR reactivity scale which was used in the California Air Resources Board's Clean Fuel/Low Emissions Vehicle regulations, and to evaluate an updated version of that mechanism, designated SAPRC-93, which was developed in part using data from the Phase I study. The updated mechanism simulated reasonably well most of the data obtained, and could account for the observed effects of variations of ROG surrogate and NO_x on VOC reactivity. However, it did not satisfactorily account for reactivity differences among some aromatic isomers, and there were indications that it could not adequately simulate the effects of varying the light source on reactivities of aromatic compounds.

Although these two phases of the program have been successful in providing data needed for mechanism evaluation, important gaps have remained. The large data base of reactivity experiments from the previous phases of the programs were obtained using a blacklight light source, and verification was needed that consistent results would be obtained using a more realistic xenon arc light source. There was a need for single aromatic - NO_x experiments to develop, adjust, and evaluate aromatic mechanisms which can account for isomeric differences and correctly predict effects of changing light source. There were also data gaps related to our ability to characterize chamber conditions for mechanisms evaluation purposes, as well as the need for additional mechanism evaluation data. There was a concern about uncertainties in light intensity measurements in our indoor chambers, since they relied on a single method which might not be satisfactory for the xenon arc chamber. There was also a concern about the effects of humidity on results of chamber experiments carried out for mechanism evaluations, and whether the model was appropriately accounting for these effects. The third phase of this program, which is discussed in this report, was designed to address these needs.

Objectives

The overall objective of this phase of the program was to conduct environmental chamber experiments needed to fill critical data gaps in the data base needed for evaluating mechanisms for VOC reactivity assessment. The program had four major elements, whose specific objectives were as follows:

- Obtain data needed to validate the light intensity measurement methods used in indoor chamber runs for mechanism evaluations, and determine the most appropriate method for the indoor chambers used in our laboratories for mechanism evaluation.

- Obtain data concerning effects of humidity on results of environmental chamber experiments used for mechanism evaluation, assess how humidity affects experimental reproducibility, and determine if current mechanisms and chamber effects models appropriately represent effects of changing humidity.

- Conduct incremental reactivity experiments using the xenon arc light source for representatives of the major class of VOCs, which can be compared with the large data base of incremental reactivity results obtained in blacklight chambers, and which can be used to assess whether current models adequately represent the effects of changing light source on reactivity.

- Conduct aromatic - NO_x experiments, with varying light sources and aromatic and NO_x levels, which are needed to develop, adjust, and evaluate mechanisms for a variety of aromatic isomers.

The results and conclusions of each of these elements of this program are summarized below.

Experiments Carried Out

The environmental chamber experiments which were carried out for this program are summarized on Table ES-1. Experiments were conducted in both the CE-CERT Dividable Teflon Chamber (DTC) with the blacklight light source, and the CE-CERT xenon arc Teflon Chamber (CTC) with the xenon arc light source. Both the DTC and (after a few initial experiments) the CTC consist of dual FEP Teflon reaction bags, with volumes of ~5000 liters and ~3500 liters, respectively. This design allows for irradiation of two mixtures at the same time, making them well suited for incremental reactivity experiments or systematically varying reactant concentrations. As indicated on Table ES-1, irradiations of various aromatic isomers (at differing aromatic and NO_x levels), actinometry experiments, and various other control and characterization runs were carried out in both chambers. In addition, a number of replicate propene - NO_x and toluene - NO_x were carried out at various humidities in the DTC as part of the humidity effects study, and incremental reactivity experiments for representative compounds, using two types of ROG surrogates, were carried out in the CTC. The results of characterization runs were used to derive or evaluate the chamber characterization model used in simulating the mechanism evaluation runs. The mechanism evaluation runs were simulated using both the SAPRC-93 mechanism

Table ES-1. Summary of environmental chamber experiments carried out for this program.

	Number of Runs	
	Blacklight	Xenon Arc
Actinometry Runs [a]		
NO2 Actinometry - Quartz Tube	22	13
NO2 Actinometry - Steady State	7	5
Cl2 - n-Butane Actinometry	3	3
Humidity Effects Study [b]		
Propene - NOx		
Dry [c]	20	
~50% RH	14	
~100% RH	3	
Toluene - NOx		
Dry	7	
~50% RH	4	
~100% RH	1	
Incremental Reactivity [a]		
Carbon Monoxide		2
n-Octane		2
Propene		2
Toluene		2
m-Xylene		2
Formaldehyde		2
Acetaldehyde		2
Aromatic Isomer - NOx [b]		
Benzene		4
Toluene	10	8
Ethylbenzene	4	4
o-xylene	6	6
m-xylene	11	7
p-xylene	6	6
1,2,3-trimethylbenzene	6	3
1,2,4-trimethylbenzene	5	4
1,3,5-trimethylbenzene	7	5
Other Single Compound - NOx [b]		
Formaldehyde	2	6
Acetaldehyde	1	4
Ethene		1
Propene		12
Other Characterization and control [a]	14	25

[a] Dual sided experiments counted as one run.
[b] Each single sided experiment counted as a separate experiment.
[c] Also includes control and mechansim evaluation runs.

and a mechanism with modified representations for aromatics developed based on these experiments. The conclusions and recommendations which result from these new data are summarized below.

Summary Of Conclusions

Evaluation of Light Intensity Measurements for Indoor Chambers. Two alternative methods for measuring light intensity, one based on the photostationary relationship between NO, NO_2, and O_3, and the other based on measuring the rate of photolysis of Cl_2, were evaluated and compared with the quartz tube NO_2 actinometry method which has been the primary indoor chamber light intensity monitoring method in our previous studies. The steady-state method was found to be prone to irreproducibility and was judged not to be satisfactory as a routine method for monitoring light intensity. However, if obviously anomalously low data are rejected, then results from these experiments are quite consistent with the quartz tube method in the blacklight chamber, and with the Cl_2 actinometry method in both chambers. The Cl_2 actinometry method, where the rate of Cl_2 photolysis is determined by measuring the rate of consumption of n-butane resulting from its reaction with Cl atoms, appears to be the more reliable approach, giving reproducible results which were also consistent with the other methods. The agreement between the Cl_2 actinometry results and the NO_2 actinometry using the quartz tube method in the blacklight chamber tends to validate both approaches, since they are based on quite different principles.

The quartz tube NO_2 actinometry method is concluded not to be satisfactory for obtaining absolute light intensities in the xenon arc chamber because of the inhomogeneous nature of the light source, but it provides probably the best indication of the absolute and relative trends in light intensity in the blacklight chamber. The Cl_2 actinometry method appears to be the best approach for determining the absolute light intensity in the xenon arc chamber, with absolute spectral intensity data taken from each experiment providing the most precise measurement of changes in relative intensity with time.

Humidity Effects. The existing chamber data base for mechanism evaluation has been obtained using differing humidities, but until this program systematic studies of effects of humidity on results of environmental chamber experiments, mechanism evaluation, and experimental reproducibility have been limited, and restricted primarily to examining the effects of humidity on wall reactions. In this study, good reproducibility was obtained for all runs carried out with similar initial reactant concentrations and humidities, indicating that humidity is not a significant factor affecting reproducibility of chamber experiments for mechanism evaluation. However, increasing the humidity to near 100% causes reductions in peak O_3 concentrations in both the propene - NO_x and toluene - NO_x systems which could not be accounted for by N_2O_5 hydrolysis or other known homogeneous or heterogeneous processes in the model. This is believed to be due to a heterogeneous effect which becomes important as the system approaches

saturation. In addition, there was an inconsistency between the magnitude of the chamber radical source that was necessary to model the results of the ~100% RH n-butane - NO_x and that which was consistent with the results of the propene or toluene - NO_x experiments at that humidity. Because of this, it is concluded that experiments with humidities near 100% should not be used for mechanism evaluation until we have a much better understanding of the surface processes which may be operating as the system approaches saturation. It was also observed that the formaldehyde yields in both the toluene and the propene systems declined as the humidity was increased, though the possibility of this being due to sample line losses has not been ruled out.

Other than the formaldehyde yields, the differences between results of experiments with dry air and those at ~50% RH are minor, and almost within the normal run-to-run variability of chamber experiments. The small difference should not significantly affect results of most mechanism evaluations. Therefore, we conclude that there are no significant humidity effects which complicate use of chamber data obtained from dry to ~50% RH conditions. This indicates that humidity should not be a significant complication in modeling chamber experiments with actual auto exhaust (where humidity is also a component) provided that the humidity in such experiments are not allowed to approach saturation.

Fortunately, most of the existing chamber data base for mechanism evaluation consist of experiments carried out under dry to ~50% RH conditions. Earlier SAPRC chamber experiments were carried out at ~50% RH air, while most of the more recent runs were carried out using dry air to minimize surface effects. Although the University of North Carolina (UNC) uses ambient air, steps are taken now to dry the air to minimize condensation on the walls in the morning, and the humidity would tend to decrease during the run due to heating. However, earlier UNC runs should be examined for possible high humidity conditions when being used for mechanism evaluation. It is uncertain at which humidity level between ~50% and ~100% RH the problems indicated by our data may become significant. It may be that these problems may be near-saturation effects which become important primarily as the humidity approaches ~100%, though there are insufficient data to evaluate this.

Xenon Arc Reactivity Experiments. Much of the work in the first two phases consisted of incremental reactivity experiments carried out using blacklight light sources, and this phase of the program provided the first data concerning incremental reactivities using the more realistic xenon arc light source. The results of these experiments for this program indicated that there are no unexplained light source effects on incremental reactivities of these compounds. The model which gave good simulations of the incremental reactivities of the non-aromatic compounds in the blacklight chamber experiments gave equally good (and in some cases slightly better) simulations of the incremental reactivities observed in

these xenon arc chamber experiments. In the case of the aromatics, good simulations of the results of the xenon arc reactivity experiments were obtained once the mechanisms were reoptimized to be consistent with the single aromatic - NO_x experiments carried out in this chamber. Thus, the same mechanism, with appropriate photolysis rates for the light source, gives similar and generally satisfactory predictions of incremental reactivities for experiments using both light sources. Therefore, the differences between blacklights and solar lighting can be accounted for in model simulations of incremental reactivity, supporting the applicability of the large blacklight chamber reactivity data base for mechanism evaluation for ambient air reactivity predictions.

Aromatic Isomer Mechanism Evaluation Data. Despite progress in recent years in our understanding of aromatic chemistry, it is still necessary to use parameterized mechanisms, optimized to fit chamber data, to represent their atmospheric reactions. This study provided the data needed to significantly improve the parameterization and performance of aromatics mechanisms. These data confirmed that the existing SAPRC mechanism (SAPRC-93) does not correctly predict reactivity differences among aromatic isomers, and tends to underpredict aromatic reactivities when irradiated with the xenon arc light source. Therefore, a reparameterization of the aromatic mechanism is clearly necessary.

The performance of the aromatic mechanism in simulating these data was improved dramatically by a relatively simple reparameterization, involving no changes in the existing mechanism other than product yield parameters. The change involved allowing the yield of the methyl glyoxal ("MGLY") model species to be optimized, along with that for the uncharacterized product species "AFG2". This resulted in the model being able to adequately represent the reactivity with the xenon arc light source, while still satisfactorily simulating the blacklight chamber experiments. Since previously the α-dicarbonyl model species used in the mechanism (of which MGLY is the most reactive) were based on measured glyoxal or methylglyoxal yields, this indicates that there are apparently other uncharacterized photoreactive aromatic fragmentation products with action spectra more closely representing that for methylglyoxal than that of acrolein (which is used for AFG2).

It was also found that, as expected, separate optimizations of MGLY and AFG2 yields for each aromatic isomer resulted in significantly improved model performance for these compounds. Previously ethylbenzene was assumed to react like toluene, all dialkylbenzens to react like m-xylene, and all trialkyl-benzenes to react like the 1,3,5 isomer. Ethylbenzene appears to have much lower yields of photoreactive ring fragmentation products than does toluene, and likewise p-xylene and 1,2,4-trimethylbenzene also have lower yields of these products than do their other isomers. On the other hand, the overall reactive

fragmentation product yields for o- and m-xylene are quite similar, as are 1,2,3- and 1,3,5-trimethylbenzene. This suggests that there may be a "para" substituent effect which somehow causes reduced total yields of photoreactive fragmentation products, since this is the one feature that distinguishes p-xylene and 1,2,4-trimethylbenzene from their other isomers. Although this may be merely a coincidence, until we have a better understanding of the details of the aromatic ring fragmentation process and the reactivity characteristics of the products formed, this provides the best basis for estimating mechanistic parameters for the higher aromatic isomer for which evaluation data are not available for mechanism optimization.

The effects of these changes to the aromatic mechanisms on atmospheric reactivity assessments have not been definitively assessed, since we are still in the process of updating the overall mechanism. However, preliminary calculations indicate that the relative MIRs for some aromatics increase by ~50%, others increase by about the same amount, and others are not significantly changed. Relative MIRs for most of the non-aromatic VOCs decrease by ~6-10%, presumably because of the net increase for the aromatics present in urban atmospheres. Relative reactivities for most alternatively fueled vehicle exhaust mixtures being evaluated by the CARB do not appear to be significantly affected.

While the new parameterized mechanism performs significantly better in simulating the new, more comprehensive aromatic mechanism evaluation data base, it is not satisfactory in every respect, and is clearly an oversimplification to what is actually happening. For example, no mechanism could satisfactorily simulate both the blacklight and xenon arc chamber data for benzene. Although benzene is not a particularly important compound to predicting ozone formation, poor model performance for the simplest aromatic suggests fundamental problems with the aromatic mechanism. The reoptimized mechanism also systematically overpredicts the initial rate of O_3 formation at the beginning of the blacklight experiments for toluene while underpredicting the ozone formation rate in the middle periods of both chambers, has similar discrepancies for many of the other isomers, and tends to underpredict the maximum ozone yields for most xylenes and trialkylbenzenes. Various other adjustments and optimizations, such as assuming that some aromatic products react with O_3, have been tried without significantly improving overall model performance.

Presumably, a better understanding of the details of the aromatic photooxidation process, and the reactivities characteristics of the major reactive products formed, will result in improved aromatic mechanisms. This will require an identification *and quantification* of the major aromatic ring opening products which account for their reactivity, and, equally important, information on their rates and mechanisms. Such studies are being carried out at a number of laboratories, though it will probably be a number of years before sufficient information is available to have a significant impact on predictive

reactivity modeling. Until such information is available, we will have no choice but to use parameterized mechanisms. We are in the process of a complete update of the SAPRC mechanisms, which will include a re-assessment of how aromatics mechanisms are parameterized. The data obtained in this work will play a crucial role in the development, evaluation, and optimization of any new aromatics mechanisms which may result from this ongoing mechanism development effort.

TABLE OF CONTENTS

LIST OF TABLES

LIST OF FIGURES

INTRODUCTION

Background

The formation of ground-level ozone is caused by the gas-phase interactions of emitted volatile organic compounds (VOCs) and oxides of nitrogen (NO_x) in the presence of sunlight. Although traditional VOC control strategies to reduce ozone have focused on reducing the total mass of VOC emissions, not all VOCs are equal in the amount of ozone formation they cause. Control strategies which take into account these differences in "reactivities" of VOCs might provide a means for additional ozone reduction which could supplement mass-based controls. Examples include conversion of motor vehicles to alternative fuels and solvent substitutions. However, implementing reactivity-based strategies requires a reliable means to quantify the effects of emissions of different types of VOCs on ozone formation, which depends on the nature of the environment where the VOC is emitted, as well as on the VOCs' atmospheric reactions. Such estimates require use of computer airshed models, which in turn require a model for airshed conditions and a mechanism for the VOCs' atmospheric chemical reactions, and a mechanism for the relevant reactions of the other atmospheric species which are present. Therefore, the predictions of such models can be no more reliable than the chemical mechanisms upon which they are based.

Atmospheric chemical mechanisms for use in airshed models are developed based on our knowledge and theories concerning the elementary gas-phase reactions which are believed to be involved in ground-level ozone formation. This in turn is based on basic laboratory kinetic and mechanistic studies, as well as our fundamental knowledge of chemistry in general. However, the processes by which VOCs and NO_x interact to form ozone are highly complex (e.g., NRC, 1991; Atkinson, 1990) and a number of aspects of the mechanisms have to be estimated, parameterized, or simplified for the purpose of developing usable mechanisms for airshed model calculations (e.g., Gery et al. 1988; Carter, 1990; Stockwell et al. 1990). Because of this, no model calculation of reactivity can be considered to be reliable unless it has been shown that it can accurately predict ozone impacts under a variety of conditions. The only practical way to do this is to carry out environmental chamber experiments, and then model the experiments to determine if the mechanism can accurately predict the ozone impacts that were observed. Although ozone impacts in chambers will not be quantitatively the same as they are in the atmosphere (Carter and Atkinson, 1989; Carter et al. 1995a), in appropriately designed experiments they will be affected by the aspects of the chemical mechanisms that affect reactivities in the atmospheres. If the mechanism cannot correctly predict the ozone impacts observed in the chamber, it is because it is representing one (or more) of these effects incorrectly, and thus would not be expected to correctly predict ozone formation in the atmosphere. If the mechanism correctly predicts the ozone impacts in a variety of experiments designed

to encompass conditions sensitive to all these effects, then one would have greater confidence in its ability to predict ozone reactivity in the atmosphere.

There are basically four types of chamber experiments which are used to evaluate chemical mechanisms for airshed models. Single VOC - NO_x - air experiments provide the most straightforward test of a VOC's mechanism because interpretation of the results are not complicated by mechanisms of other VOCs. For that reason, previous mechanism development and evaluation (e.g., Gery et al. 1988; Carter, 1990; Stockwell et al. 1990; Carter and Lurmann, 1990, 1991) have focused primarily on modeling such experiments, and they have served as the basis of the development of the parameterized aromatics mechanisms currently in use. However, such experiments do not provide a realistic representation of atmospheric conditions, where many different types of VOCs are reacting together. In addition, such experiments are of limited utility for VOCs, such as alkanes, which do not have significant radical sources in their mechanisms, because the results are highly sensitive to uncertain chamber effects (Carter and Lurmann, 1990, 1991; Carter et al. 1982).

Mixture - NO_x - air experiments have the advantages that, with appropriately chosen mixtures, they can provide a more realistic simulation of the chemical environment present in polluted atmospheres, and are also much less sensitive to chamber effects than single compound runs which do not have radical initiators. They are essential for evaluating the performance of mechanisms as a whole, and this has been their role in previous mechanism evaluations (Carter and Lurmann, 1990, 1991; Gery et al. 1988). However, they are obviously not particularly useful for evaluating mechanisms of single VOCs because it is difficult to identify the source of cases of poor model performance, and because compensation of errors can sometimes make erroneous mechanisms appear to give good model performance. Because the relative importance of the compensating factors may be different in the atmosphere than in the chamber experiment, such a mechanism would likely give erroneous predictions in simulations of the atmosphere.

Incremental reactivity experiments, which consist of determining the effects of adding a test compound to a standard (base case) reactive organic gas (ROG) - NO_x - air mixture, combines the advantages of both single VOC and mixture - NO_x experiments. Like mixture - NO_x experiments, with an appropriate choice of the base case ROG "surrogate" mixture (Carter et al. 1995a), they can present a realistic representation of the chemical environment in the atmosphere. In addition, they are relatively insensitive to chamber effects, and to the extent that chamber effects influence the results, they would affect both the added VOC and base case experiments to a similar extent, and thus, to a first order approximation, tend to be cancelled out when looking at the difference. Like single compound experiments, they isolate the effect of the single compound, and provide direct data on its impact on ozone

[and other measures, such as overall radical levels (Carter et al. 1993a, 1995a)] in a chemically realistic environment. They provide the best available means for evaluating the mechanisms for low-reactivity compounds such as alkanes (and many of the VOC exemption candidates) without the complications of chamber effects which plague use of low reactivity VOC - NO_x experiments for mechanism evaluation. Varying the NO_x levels or the composition of the base case ROG surrogate in the experiments provide a means for evaluating the mechanism under varying chemical conditions, which is necessary to assure satisfactory performance in varying atmospheric simulations.

Regardless of what type of experiment is employed, the results will be influenced by chamber effects such as the nature of the light source, heterogeneous reactions on the chamber walls, reactant offgasing, possibly background reactants in the matrix air or impurities introduced with other reactants, and other such artifacts. Appropriate representation of these effects must be included in the model calculations when evaluating the mechanisms, or compensating errors will be introduced (Jeffries et al. 1992). Because of this, various characterization experiments are used to derive or evaluate chamber effects models for such evaluations. The most important characterization experiments involve actinometry runs to measure the light intensity, and runs to measure the magnitude of the chamber radical source, but other types of characterization experiments can also be important in some circumstances (Carter et al. 1982; Carter and Lurmann, 1990, 1991; Carter et al. 1995b,c).

The primary gas-phase atmospheric chemical mechanisms currently being used in the United States in models for control strategy assessment applications are the Carbon Bond IV (CB4) (Gery et al. 1988), the RADM-2 (Stockwell et al. 1990), and the SAPRC-90 (Carter, 1990) mechanisms. Of these, only the SAPRC-90 mechanism is applicable for reactivity assessment of individual VOCs, currently being capable of separately representing reactions of approximately 250 classes of compounds (Carter, 1990; unpublished results from this laboratory). The others represent most types of VOCs using a limited number of lumped or surrogate model species, for efficient representation of ambient mixtures. However, despite their differences in level of detail and in some cases treatment of uncertain processes, they were developed and evaluated using primarily the same environmental chamber data (Carter and Lurmann, 1990, 1991; Gery et al. 1988). These consisted primarily of indoor, with a limited number of outdoor, chamber experiments carried out at the Statewide Air Pollution Research Center (SAPRC) at the University of California at Riverside (UCR) (Carter et al. 1995b), and of a large number of outdoor chamber runs from the University of North Carolina (UNC) (Jeffries et al. 1982, 1985a-c, 1990). The SAPRC and RADM-2 mechanisms were developed and evaluated primarily using the indoor chamber runs, with the outdoor runs being used primarily for confirmation (Carter, 1990; Carter and Lurmann, 1991; Stockwell et al. 1990), while the CB4 was developed and evaluated using primarily the UNC chamber data, with a relatively limited number of

SAPRC runs being modeled for confirmation (Gery et al. 1988). Nevertheless, the three mechanisms perform quite similarly in simulating this chamber data base, at least for runs with the individual VOCs they are all designed to represent, and for runs with mixtures designed to simulate ambient conditions (Carter and Lurmann, 1990, 1991, unpublished results from this laboratory).

Although the chamber data base used in evaluating these three mechanisms was quite extensive, including single VOC - NO_x runs with a number of individual compounds representing important classes of emitted VOCs and a variety of mixture - NO_x runs, there has been a number of major gaps and data needs, particularly with regard to evaluating mechanisms for VOC reactivity assessment for a wide variety of individual VOCs. In particular, there were many types of important VOCs for which well-characterized chamber data were either unavailable, limited to only one type of chamber, or (in the case or alkane - NO_x runs) unsuitable for mechanism evaluation. There were no incremental reactivity experiments designed to evaluate mechanisms under conditions applicable to the development of the Maximum Incremental Reactivity (MIR) scale (Carter, 1994), which the California Air Resources Board (CARB) has adopted for use in setting reactivity-based vehicle emissions standards (CARB, 1993). In addition, the available data were insufficient to assess the effects of chamber, light source, and humidity on mechanism evaluation results.

Summary and Progress for this Program

Therefore, SAPRC, subsequently in conjunction with the College of Engineering, Center for Environmental Research and Technology (CE-CERT), has conducted a multi-year environmental chamber program to provide data needed to improve the reliability of chemical mechanisms for use in predicting effects of VOC emissions changes on ozone formation. This program has been carried out in three phases, under joint funding from the California Air Resources Board (CARB), the Coordinating Research Council (CRC), the South Coast Air Quality Management District (SCAQMD) (Phases 1 and 2) and the National Renewable Energy Laboratory (NREL) (Phases 2 and 3). The results of the two phases have been reported previously (Carter et al. 1993a, 1995a,c), and the results of the third and final phase are documented in this report. To place these results in perspective, the results of the first two will be briefly summarized.

Progress in Previous Phases of this Study

In the first phase of this program, we measured the incremental reactivities of 36 representative VOCs under maximum incremental reactivity conditions using a simplified "mini-surrogate" mixture to represent reactive organic gases (ROGs) in the atmosphere (the base ROG surrogate), and using an indoor chamber with a blacklight light source. The results were described in a report entitled "Environmental

Chamber Studies of Maximum Incremental Reactivities of Volatile Organic Compounds" (Carter et al. 1993a), and in two journal articles (Carter et al. 1995d; Carter, 1995a). It was found that incremental reactivities of VOCs varied widely, even after differences in their atmospheric reaction rates were taken into account. An updated version of the SAPRC-90 mechanism, referred to as the "SAPRC-93" mechanism in the subsequent discussion, was developed during this time period, in part to take into account the results of this study (Carter et al. 1993b; Carter, 1995a). That mechanism was found to be able to simulate the experimental reactivity data to within the experimental uncertainty for approximately half the VOCs studied, and qualitatively predicted the observed reactivity trends. However, the results indicated the need for refinements to the mechanisms for a number of compounds, including branched alkanes, alkenes, aromatics, acetone, and possibly even formaldehyde. The possibility that some of the discrepancies were due to uncertainties in the model for the base case experiment could not be ruled out. In addition, the data for some of the compounds provided an imprecise test of the mechanism because of run-to-run variability of conditions.

The second phase of the program consisted of two major components. In the first, documented by a report titled "Environmental Chamber Studies of Atmospheric Reactivities of Volatile Organic Compounds: Effects of ROG Surrogate and NO_x" (Carter et al. 1995a), a series of chamber experiments were carried out to assess the effects of variations of NO_x and the base ROG surrogate on the incremental reactivities of representative VOCs. As with the previous phase, an indoor chamber using blacklights was employed, though a dual chamber designed for more efficient and precise incremental reactivity experiments was employed. The base ROG surrogate consisted either of a 8-component mixture whose use as the ROG surrogate was predicted in model simulations to give the same incremental reactivities as an ambient mixture, or by an "ethylene surrogate" consisting of ethylene alone. The data obtained, combined with the Phase 1 results, show that VOCs have a greater range of incremental reactivities in experiments using the Phase 1 mini-surrogate or the ethylene surrogate than when the more realistic 8-component surrogate is used. Reducing NO_x had a large effect on VOC reactivities, with ozone reactivities of propene, *trans*-2-butene, acetaldehyde, and the aromatics becoming negative in the low NO_x experiments, and those for the other VOCs decreasing significantly. These observed dependencies of reactivity on ROG surrogate and NO_x were consistent with the predictions of the SAPRC-93 mechanism. The mechanism was found to perform well in simulating reactivities in the experiments with the more complex surrogate, but had some problems in the simulations of the reactivities of the simpler surrogates. Thus, while there are still problems with the current mechanisms, they may not necessarily have a large effect in simulations of ambient reactivity. It was concluded that while use of simpler surrogates will not give reactivities which correlate well with those in the atmosphere, because they are more sensitive to VOC differences they provide better tests for the models which must be used for atmospheric predictions.

A second component of the Phase 2 study was an investigation whether current mechanisms give consistent predictions in simulations of experiments using different chambers and light sources. The results of this component is described in a report entitled "Environmental Chamber Studies of Volatile Organic Compounds, Effects of Varying Chamber and Light Source" (Carter et al. 1995c). The blacklights used in the Phase 1 and 2 reactivity studies have different spectral characteristics than natural sunlight, and data were needed to test whether the model can take these differences into account. A new indoor Xenon Teflon Chamber (XTC) using a xenon arc light source, which gives a better representation of the solar spectrum than blacklights, was constructed and was then used to conduct representative single compound and surrogate - NO_x runs, and comparable runs were carried out in the blacklight chambers used for the reactivity studies and in the SAPRC outdoor chamber. The results these experiments, and of comparable earlier SAPRC experiments which were used in the development and evaluation of the SAPRC-90, RADM-2, and CB4 mechanisms, were then simulated using the SAPRC-93 mechanism. Some variability and chamber differences were observed, but there did not appear to be a consistent light source effect in the simulations of the aldehyde, ethene, and propene experiments. The simulations of the XTC and SAPRC outdoor runs were generally consistent with each other, suggesting that the model can appropriately account for differences between the XTC light source and sunlight. However, a potentially significant discrepancy was seen in the simulations of aromatic and surrogate runs, where the model, which gave reasonably good ozone predictions in the blacklight chamber runs, underpredicted ozone formation in the xenon arc and outdoor runs. The model did not give consistent predictions in simulations of earlier SAPRC Evacuable Chamber (EC) runs, which also used a xenon arc light source but had a different surface type than the chambers used in this study. The SAPRC EC was found to have much larger surface effects than the Teflon chambers now in use (Carter et al. 1982), which may be affecting evaluation results. It was concluded that additional xenon arc chamber experiments with aromatics are needed to evaluate whether current SAPRC aromatic mechanisms, which are optimized to fit blacklight chamber or EC experiments, can appropriately simulate aromatic reactivity under ambient conditions.

Elements of this Phase of the Program

The third phase of this program consisted of several elements, all aimed at providing data needed to fill several important gaps in the environmental chamber data base relevant to VOC reactivity assessment. These consisted of (1) obtaining data concerning effects of humidity on mechanism evaluation results and experimental reproducibility; (2) verifying the light intensity measurement methods used in indoor chamber runs for mechanism evaluations; (3) conducting incremental reactivity experiments using the xenon arc light source; and (4) conducting aromatic isomer - NO_x runs needed for mechanism evaluation. The background and needs for each of these elements are summarized briefly below.

Humidity Effects. The existing chamber data base for mechanism evaluation has been carried out in chambers using different light sources, surfaces, and levels of humidification of the matrix air. The Phase 2 study provided needed data concerning effects of changing the light source, and indicated apparent differences, at least for aromatics, in evaluation results using the SAPRC EC and XTC, which both use a xenon arc light source. In addition to the different surface employed, the EC and XTC runs differ in that the former used air humidified to ~50% RH, while the latter used dried air. Humidification is also a difference between the UNC outdoor chamber runs, which uses ambient air (with partial drying in some cases), and the SAPRC outdoor chamber, using very dry purified air. Dry air is preferred in most or our current experiments because it tends to minimize surface effects (Carter et al. 1982; Pitts et al. 1983). Since humidity may influence surface effects, it may also affect run-to-run reproducibility, but this also has not been studied. To determine whether humidity may be a significant factor in affecting mechanism evaluation results and run-to-run reproducibility, and to provide a bridge between data from different chambers, a number of replicate propene - NO_x and toluene - NO_x runs were carried out at various levels of humidity, ranging from dry to nearly 100% RH.

Light Intensity Measurements. Accurate light source measurement is obviously critical to mechanism evaluation, since light provides the energy which drives the transformations being studied. Most of the light intensity characterization for the indoor runs for Phases 1 and 2 were based on applications of the quartz tube NO_2 actinometry method of Zafonte et al. (1977), modified to take into account updated rate constants (Carter et al. 1993a; 1995b). A limited number of determinations using the steady state NO_x - ozone method were carried out in the XTC as part of Phase 2, but the results were inconclusive because of insufficient data (Carter et al. 1995b,c). To obtain additional information to verify the light source measurements, additional actinometry experiments using the steady-state method were carried out in both the DTC and xenon arc chamber, and the applicability of a new method, based on Cl_2 photolysis in the presence of n-butane, was investigated.

Xenon Arc Reactivity Experiments. Much of the work in the first two phases consisted of incremental reactivity experiments carried out using blacklight light sources. However, the second phase results indicated that there are differences in mechanism evaluation results using the new XTC chamber, particularly for aromatics or mixtures containing aromatics. To evaluate the applicability of the Phase 1 and Phase 2 incremental reactivity results to lighting conditions more representative of sunlight, reactivity experiments were carried out for representative compounds using both the simple ROG surrogate used in Phase 1, and the more realistic ROG surrogate used in Phase 2.

Aromatic Isomer Mechanism Evaluation Data. Despite progress in recent years in our understanding of aromatic chemistry (e.g., Atkinson, 1994, and references therein), it is still necessary to use parameterized mechanisms, optimized to fit chamber data, to represent the atmospheric reactivities of these compounds. The SAPRC-90 and the SAPRC-93 mechanisms assumed that all xylene isomers and other dialkyl benzenes could be represented by mechanisms which were optimized to fit m-xylene chamber data, that all trialkyl benzenes could be represented by a mechanism optimized for 1,3,5-trimethylbenzene, and that all monoalkylbenzenes could be represented by one optimized for toluene. The RADM and CB4 mechanisms had similar approximations, except that they also lumped all the higher aromatics with xylenes. Both Phase 1 and Phase 2 results indicated problems with these parameterized aromatic mechanisms, and the need for an improved data base of chamber data for evaluating them. The Phase 1 results showed that there were significant reactivity differences among aromatic isomers which were not well represented by the SAPRC-93 and earlier mechanisms. In addition, the XTC runs indicated that the SAPRC-90 and SAPRC-93 mechanisms could not correctly account for effects of changing light source. This indicated a clear need to develop optimized aromatic mechanisms for each of the aromatic isomers, which can simulate aromatic runs using both types of light sources. To obtain the data needed for this purpose, single aromatic - NO_x experiments were carried out for the various alkylbenzene isomers in both blacklight and xenon arc chambers, at various NO_x levels and aromatic/NO_x ratios.

METHODS

Environmental Chambers

The two chamber systems employed in this study were the CE-CERT "Dividable Teflon Chamber" (DTC) with the blacklight light source and the CE-CERT Dividable Xenon-arc Teflon Chamber (CTC). The DTC and (after run CTC093) the CTC were designed to allow simultaneous irradiations of the base case and the test experiments under the same reaction conditions. Each chamber is actually two adjacent FEP Teflon reaction bags which can be simultaneously irradiated using the same light source and the same temperature control system. These are referred to as the two "sides" of the chamber (Side A and Side B) in the subsequent discussion. The sides are interconnected with two ports, each with a box fan, which rapidly exchanges their contents to insure that reactants which are desired to have equal concentrations in each side are equalized. In addition, a fan is located in each of the reaction bags to rapidly mix the reactants within each chamber. The ports connecting the two reactors can then be closed to allow separate injections on each side, and separate monitoring of each. This design is optimized for carrying out incremental reactivity experiments such as those for this program.

Blacklight Chamber

The CE-CERT DTC was modeled after the SAPRC DTC which was employed in the Phase 2 work, and which is described in detail elsewhere (Carter et al. 1995a,b). It consists of two ~5000-liter 2-mil heat-sealed FEP Teflon reaction bags located adjacent to each other and fitted inside an 8'x8'x8' framework, and which uses two diametrically opposed banks of 32 Sylvania 40-W BL blacklights as the light source. Because this has the largest volume of all the indoor chambers currently used at CE-CERT, it is well suited for studies of relatively low volatile compounds such as the C_{12+} n-alkanes. The lighting system in the DTC was found to provide so much intensity that only half the lights were used for the blacklights. The unused blacklights were covered with aluminum foil, and were used to bring the chamber up to the temperature it will encounter during the irradiation before the uncovered lights are turned on. The air conditioner for the chamber room was turned on before and during the experiments. Four air blowers which are located in the bottom of the chamber were used to help cool the chamber and to mix the contents of the chamber.

During the course of this program, the reaction bags used were those which were used previously in the SAPRC DTC for the Phase 2 work. In addition, the run numbering was consecutive, so the first run for this program, DTC-124, was the first run after this chamber was set up at CE-CERT.

Xenon Arc Chamber

The CE-CERT CTC is modeled after the SAPRC XTC used in the Phase 2 work, and the same NREL-funded xenon arc lighting system was used. The SAPRC XTC and the light source it employed are described in detail elsewhere (Carter et al. 1995c). When first constructed, the CTC consisted of a single ~6,000-liter reaction bag located in one end of a ~9'x14' room, with four 6.3 kW xenon arc lights mounted on the wall opposite the reactors. All surfaces are covered with reflectively polished aluminum paneling to maximize the light intensity and homogeneity. Each of the four lamps had borosilicate inner and outer filters which were the same as those in the XTC for the Phase 2 work, and which were not replaced during the course of the program. The radiative power per lamp using these filters was stated as 114,350 microwatts per square centimeter at 48 cm from the light. The lamps were operated at a constant power setting of 4.0 kW for all experiments discussed here, which is ~60% of maximum. The air conditioner for the chamber room was turned on before and during the experiment. The four lamps were turned on to warm up the lamps and to preheat the chamber at least 30 minutes prior to irradiation. A shutter was used to shield the chamber from the lights when they were warming up. It was raised to begin the irradiation. Four blowers located on the ceiling were turned on to force cooling air down into the chamber room to cool the chamber during the irradiation.

After run CTC083, the single bag was removed and was replaced by two adjacent ~3,500-liter reaction bags, with ports and blowers designed to mix the contents of the reactors, similar to the dual chamber design of the DTC. The system of blowers which mixed the contents of the chambers was redesigned somewhat to minimize leakage, which was more evident in the smaller volume of this chamber than in the larger DTC. The dual CTC was operated at slightly positive pressure so leaks were manifested by a slow reduction of the reactors' volume rather than dilution. The chamber was used in this mode for the incremental reactivity experiments carried out for this program.

Experimental Procedures

Mechanism Evaluation, Reactivity and Other Organic - NO_x Experiments

Similar experimental procedures were employed for experimental runs carried out in both chamber systems, and were generally modeled after the procedure employed for SAPRC indoor chamber experiments which are described in detail elsewhere (Carter et al. 1995b). The reaction bags (or bag) were flushed with dry purified air for 14 hours (6pm-8am) on the nights before experiments. An AADCO air purification system was employed. The continuous monitors were connected prior to reactant injection and the data system began logging data from the continuous monitoring systems. The reactants were injected as described below (see also Carter et al. 1993a,, 1995d). For incremental reactivity experiments, the common reactants were injected in both sides simultaneously using a three-way (one inlet and two

outlets connected to side A and B respectively) bulb of 2 liters in the injection line and were well mixed before the chamber was divided. For the DTC and later CTC runs the contents of each side were blown into the other using two box fans located between them. Mixing fans were used to mix the reactants in the chamber during the injection period, but these were turned off prior to the irradiation. The sides were then separated by closing the ports which connected them, after turning all the fans off to allow their pressures to equalize. After that, reactants for specific sides in divided chamber runs (the test compound in the case of reactivity experiments) were injected and mixed. The irradiation began by turning on the lights and proceeded for 6 hours. In the case of the CTC, the sliding panel was lowered between the lights and the reaction bags, and the lights were turned on and allowed to stabilize for 30 minutes prior to the irradiation being started by raising the panel. After the run, the chamber was emptied by allowing the bag to collapse, and then flushed with purified air. The contents of the reactors were vented into a fume hood.

For humidified runs, a 5-liter bulb containing distilled water was placed in a temperature-controlled heater to humidify the dry air output from the AADCO air purification system. In general, the heater temperature was set to 40° C and the flow through the water bulb was set to 150 SCFH. The system was designed so that the air out of the bulb would be at ~100% RH. The humidified air was then mixed with dry air at the appropriate proportion to achieve the desired humidity of the air entering the chamber. For the most humidified runs, the appropriately humidified air was used to flush the chamber overnight prior to the experiment. For a few earlier runs, the chamber was flushed with dry air overnight, and then partially deflated and filled with humidified air immediately prior to the experiment.

The procedures for injecting the various types of reactants were as follows. The NO and NO_2 were prepared for injection using a high vacuum rack. Known pressure of NO, measured with MKS Baratron capacitance manometers, were expanded into Pyrex bulbs with known volumes, which were then filled with nitrogen (for NO) or oxygen (for NO_2). The contents of the bulbs were then flushed into the chamber with ADDCO air. The other gas reactants were prepared for injection either using a high vacuum rack or using gas-tight syringes. The gas reactants in a gas-tight syringe were usually diluted to 100-ml with nitrogen in the syringe. The volatile liquid reactants were injected, using a micro syringe, into a 1-liter Pyrex bulb equipped with stopcocks on each end and a port for the injection of the liquid. The port was then closed and one end of the bulb was attached to the injection port of the chamber and the other to a dry air source. The stopcocks were then opened, and the contents of the bulb were flushed into the chamber with a dry air for approximately 5 minutes, while being heated with a heat gun. Formaldehyde was prepared in a vacuum rack system by heating paraformaldehyde in an evacuated bulb until the pressure corresponded to the desired amount of formaldehyde. The bulb was then closed and detached

from the vacuum system and its contents were flushed into the chamber with dry air through the injection port.

Quartz Tube Actinometry Experiments

The light intensity in the DTC and CTC chambers was normally monitored by periodic NO_2 actinometry experiments utilizing the quartz tube method of Zafonte et al. (1977), with the data analysis method modified as discussed by Carter et al. (1995c). In DTC actinometry experiments, the tube was oriented horizontally and usually located in the middle of chamber (~4 ft high) and between two bags. (The height of the tube was varied in a few early runs to determine if this had an effect on the results.) The NO_2 flow was set to 1 liter/min. The lights were turned on after stable NO and NO_2 initial concentrations were obtained. The irradiation time was about 20 minute, which allowed us to get stable NO and NO_2 data after the lights were turned on. The concentrations of NO and NO_2 were recorded prior to, during, and after the irradiation.

The procedure employed with the CTC was similar to that for the DTC, except that the tube was located immediately in front of the reaction bag(s), on the side of the lights. The same location was employed for the dual reactor configuration as for the initial single bag mode. The lights were turned on to stabilize for 30 minutes before opening the shutter and exposing the chamber and actinometry tube to the light.

NO_x - O_3 Steady State Actinometry Experiments

A limited number of steady state actinometry experiments, where the NO_2 photolysis rate was determined by simultaneously measuring NO, NO_2, and O_3 when irradiated in air, were carried out for comparison with our standard actinometry method, discussed below. In these experiments, a Monitor Labs model 8410 ozone analyzer, which works on the principle of chemiluminescence from the reaction between ozone and ethylene, was used to monitor ozone instead of a Dasibi model 1003AH ozone analyzer, which was used in the chamber experiments. This ozone analyzer was employed because it provides faster response and better sensitivity for lower ozone concentrations which must be monitored in these experiments. The analyzer was usually located close to the chamber to minimize any reaction occurring in the sampling line. Oxides of nitrogen were monitored using Thermo Electron Co. Model 14B analyzer, as employed in the chamber experiments. After background of the chamber was checked using ozone and NO_x analyzers, a few torr of NO_2 in 1-liter bulb, which was prepared using vacuum rack system, was introduced into the chamber. Box fans and mixing fans were turned on to mix the contents of the chamber and ozone and NO_x were monitored before and during the irradiation. The data were recorded until stable concentrations of O_3, NO, and NO_2 were observed.

Cl_2 - n-Butane Actinometry Experiments

A limited number of Cl_2 actinometry experiments were also carried out to provide an alternative measurement of light intensity. Since we could not monitor Cl_2 directly, its photolysis rate was determined indirectly from the consumption of n-butane due to its rapid reaction with Cl atoms formed when Cl_2 photolyses. The procedures for these experiments were similar to that for the organic - NO_x runs discussed above, except that shorter irradiation times were employed. Approximately 100-150 ppb of Cl_2 and ~1 ppm of n-butane were injected into the chamber prior to the irradiation. The Cl_2 was prepared using vacuum methods and the amount injected determined by measuring its pressure with a precision capacitance monometer in a known volume. *n*-Butane was monitored prior to and at ~20-30 minute intervals during the irradiation, which proceeded until there was no further change in n-butane concentrations (usually ~2 hours).

Analytical Methods

Ozone and nitrogen oxides (NO_x) were continuously monitored using commercially available continuous analyzers with Teflon sampling lines inserted directly into the chambers. The sampling lines from each side of the chamber were connected to solenoids which switched from side to side every 10 minutes, so the instruments alternately collected data from each side. Ozone was monitored using a Dasibi 1003AH UV photometric ozone analyzer and NO and total oxides of nitrogen (including HNO_3 and organic nitrates) were monitored using a Teco Model 14B chemiluminescent NO/NO_x monitor. The output of these instruments, along with that from the temperature and formaldehyde instruments, were attached to a computer data acquisition system, which recorded the data at 10 minute intervals for ozone, NO and temperature (and at 15 minutes for formaldehyde), using 30 second averaging times. This yielded a sampling interval of 20 minutes to take data from each side.

The Teco instrument and Dasibi CO analyzer were calibrated with a certified NO and CO source and CSI gas-phase dilution system. It was done prior to the chamber experiment for each run. The NO_2 converter efficiency check was carried out on regular intervals. The Dasibi ozone analyzer was calibrated against a transfer standard ozone analyzer approximately every three months. In addition, for each experiment the Dasibi was checked with a CSI ozone generator (set to 400 ppb) to insure that the instrument worked properly. The details were discussed elsewhere (Carter et al. 1995d).

Organic reactants other than formaldehyde were measured by gas chromatography with FID or ECD detectors as described elsewhere (Carter et al. 1993a). GC samples were taken for analysis at intervals from 20 minutes to 30 minutes either using 100 ml gas-tight glass syringes or by collecting the 100 ml sample from the chamber onto a Tenax-GC solid adsorbent cartridge. These samples were taken

from ports directly connected to the chamber after injection and before irradiation and at regular intervals after irradiation. Two sampling methods were employed for injecting the sample onto the GC column, depending on the volatility or "stickiness" of the compound. For analysis of the more volatile species (which includes all the components of the base case surrogates employed in this study), the contents of the syringe were flushed through a 2 ml or 3 ml stainless steel or 1/8" Teflon tube loop and subsequently injected onto the column by turning a gas sample valve. The calibrations for the GC analyses for most compounds were carried out by sampling from chambers or vessels of known volume into which known amounts of the reactants were injected, as described previously (Carter et al. 1995d).

Formaldehyde was monitored using a diffusion scrubber system based on the design of Dasgupta and co-workers, as described elsewhere (Carter et al., 1993a, 1995b). This system alternately collected data in sample, zero, and calibrate mode, for a 20 minute cycle time. The readings at the end of the time period for each mode, averaged for 30 seconds, were recorded on the computer data acquisition system, which subsequently processed the data to apply the calibration and zero corrections. This yielded formaldehyde data every 40 minutes for each side for divided chamber runs. A separate sampling line from the chamber was used for the formaldehyde analysis.

The analytical methods and calibration procedures employed in this work are similar to those employed previously in SAPRC chamber experiments, which are described in detail elsewhere (Carter et al. 1995b.)

Characterization Methods

Three temperature thermocouples for each chamber were used to monitor the chamber temperature, two of which were located in the sampling line of continuous analyzers to monitor the temperature in each side. The third thermocouple was located in the chamber enclosure for the DTC, or above the ceiling in the forced air inlet system in the case of the CTC. Only one temperature thermocouple was used in the sampling line for the CTC when it was in its initial single reactor mode. The temperature in these experiments were typically 21-25°C for DTC and 25-30°C for CTC. The temperature thermocouples in the sampling lines were shielded using insulating material covered with aluminum foil.

The light intensity in the DTC and CTC chambers was monitored primarily by periodically conducting actinometry experiments as discussed above. This was done primarily using the quartz tube method, but occasionally the other types of methods were also employed. For the CTC, information concerning both the spectrum and relative changes in the light intensity was also obtained from spectra

taken using a LiCor LI1600 spectraradiometer located on a post in front of the reaction bag(s). The spectral data for the CTC are discussed later in this report.

The dilution of in these chambers due to sampling is expected to be small because the flexible reaction bags can collapse as sample is withdrawn for analysis. However, some dilution occurs with the age of reaction bags because of small leaks. This was particularly true for the DTC, which employed older reaction bags during the course of this program, and whose mixing system was subsequently found to be a source of leaks. Information concerning dilution in an experiment was obtained from relative rates of decay of added VOCs which react with OH radicals with differing rate constants (Carter et al. 1993b; 1995d). Most experiments had more reactive compounds, such as m-xylene or n-octane, present either as a reactant or added in trace amounts to monitor OH radical levels, and small amounts (~0.1 ppm) of n-butane were added to experiments if needed to provide a less reactive compound for the purpose of monitoring dilution. In addition, specific dilution check experiments such as CO-NO were carried out. Based on the results of these tests, the average dilution in sides A and B in the DTC reactors were found to be 1.1±0.5 and 3.4±0.9 %-hour^{-1}, respectively. The leakage was somewhat less in the CTC in the single reactor mode (runs CTC011-CTC082), with an average dilution rate of 0.4±0.6 %-hour^{-1}. The dilution was even less for the CTC in the dual chamber mode (runs CTC083 and those following) because of the improved design of the mixing system, and the positive pressure operation of the chamber when it was in the divided mode. In this case, there was no significant difference in the dilution rate between the two CTC reactors, and the average dilution rate was 0.1±0.3 %-hr^{-1}. These were used as defaults when modeling runs where dilution information could not be derived.

During the humidified runs, the relative humidity was measured by a certified NIST traceable Digital Hygrometer/Thermometers whose relative humidity (RH) range is 10-95%. The response time is 30 seconds to 3 minutes. The measurement was accomplished by inserting the sensor into the chamber (side A of DTC or side B of CTC) through the hole which is used to empty the contents of the chamber after the experiment. It was taken out after stable reading was obtained. The RH was measured several times before and during the experiment, and generally the readings did not change with time.

Data Analysis Methods

Quartz Tube Actinometry Experiments

The quartz tube actinometry experiments involved measuring changes in NO and NO_2 concentrations after flowing through an irradiated quartz tube of known volume and known rate. As discussed by Zafonte et al. (1977), the NO_2 photolysis rates, k_1, can then be calculated by

$$k_1 = \frac{[NO]^{light} - [NO]^{dark}}{[NO_2]^{light} + ½ ([NO]^{light} - [NO]^{dark})} \times \frac{F}{V} \times \frac{1}{\Phi} \quad \text{(I)}$$

where $[NO]^{dark}$ and $[NO_2]^{dark}$ are the NO and NO_2 concentrations prior to entering the tube or when the lights are off, $[NO]^{light}$ and $[NO_2]^{light}$ are their concentrations as measured after exiting from the irradiated tube, F is the flow rate, V is the volume of the tube exposed to the light, and Φ is an effective quantum yield factor. Based on model simulations of typical quartz tube actinometry experiments in a blacklight chamber, Carter et al. (1995b) derived $\Phi = 1.66 \pm 0.02$, which was used in processing all the quartz tube actinometry data for this program.

Steady State Actinometry Experiments

As indicated above, the "photostationary state" actinometry method involved photolysis of low concentrations of NO and NO_2 in otherwise pure air in the chamber, and simultaneously measuring NO, NO_2, and O_3. Because of the photostationary state established by the rapid reactions

$$NO_2 + h\nu \rightarrow NO + O(^3P) \quad (1)$$

$$O(^3P) + O_2 + M \rightarrow O_3 + M$$

$$NO + O_3 \rightarrow NO_2 + O_2 \quad (2)$$

the NO_2 photolysis rate, k_1, is given by

$$k_1 = \frac{k_2 [O_3] [NO]}{[NO_2]} \quad \text{(II)}$$

where k_2, the rate constant for the reaction between NO and O_3, is 27.5 ppm^{-1} min^{-1} at 300° K, the approximate temperature of our experiments. The NO, NO_2, and O_3 were measured approximately each 20 minutes on alternate sides of the chamber, and the k_1 was calculated using Equation (II) for each time period where the measurements were made. The tabulated results of these experiments give the average k_1 values for each side of the chamber.

Cl_2 Actinometry Experiments

The Cl_2 actinometry experiments involved measuring rates of decay of n-butane when photolyzed in the presence of Cl_2. Cl_2 undergoes relative rapid photolysis under the conditions of our experiments, with a half life of ~10 minutes in the DTC and ~17 minutes in the CTC. The photolysis of Cl_2 gives rise to two Cl atoms, each of which reacts rapidly with n-butane.

$$Cl_2 + h\nu \rightarrow 2\ Cl \qquad (3)$$
$$Cl + \text{n-butane} \rightarrow \text{products}$$

Under the conditions of this experiment, model calculations indicate that the above are the only reactions significantly affecting concentrations of Cl_2 or n-butane. (In particular, consumption of n-butane by reaction with OH radicals is calculated to be negligible. Although the reactions of Cl with n-butane will form peroxy radicals which would generate OH in the presence of NO_x, in the absence of NO_x they either undergo termination, or react to form HO_2, which is consumed primarily by self-reaction forming H_2O_2.) Therefore, from integrating the kinetic differential equations involved, the concentration of n-butane at time=t, $[n\text{-}C_4]_t$, is given by

$$[n\text{-}C_4]_t = [n\text{-}C_4]_0 - 2\ [Cl_2]_0\ (1 - e^{-k_3\ t}) \qquad (III)$$

where $[n\text{-}C4]_0$, and $[Cl_2]_0$ are the initial n-butane and Cl_2 concentrations and k_3 is the Cl_2 photolysis rate. Equation (II) cannot be solved analytically since $[Cl_2]_0$ is not known precisely, but $[n\text{-}C4]_0$, $[Cl_2]_0$, and k_3 can be derived from Equation (II) and the measured $[n\text{-}C_4]_t$ data by nonlinear least-squares optimization. Because there was no apparent differences in the n-butane decay rates measured on the two sides of the DTC or dual chamber CTC runs, the data from both sides of the chamber were used together in the optimizations, to improved the precision of the results.

NO_2 photolysis rates, k_1, can be derived from the measured Cl_2 photolysis rates given the relevant absorption cross sections, quantum yields, and spectral distributions. If it is assumed that Cl_2 photodecomposes with unit quantum yield (Atkinson et al. 1996), then

$$k_1 = k_3 \frac{\int SD_\lambda\ \sigma(Cl_2)_\lambda\ d\lambda}{\int SD_\lambda\ \sigma(NO_2)_\lambda\ \Phi(NO_2)_\lambda\ d\lambda} \qquad (IV)$$

where $SD\lambda$ is the measured relative spectral distribution of the light source, $\sigma(NO_2)_\lambda$ and $\Phi(NO_2)_\lambda$ are the absorption cross sections and quantum yields for NO_2 at wavelength λ. Based on the NO_2 absorption cross sections and quantum used in the current SAPRC mechanism (Carter, 1990; Carter et al. 1993b), the $\sigma(Cl_2)_\lambda$ are the absorption cross sections for Cl_2 taken from the latest IUPAC evaluation (Atkinson et al. 1996), the spectral distribution recommended by Carter et al. (1995b) for modeling blacklight chamber runs, and the average of the measured spectral distributions for the CTC runs, we obtain,

$$k_1 = 2.89\ k_3 \text{ (for the DTC)} \qquad (V)$$

and

$$k_1 = 5.15\ k_3 \text{ (for the CTC)} \qquad \text{(VI)}$$

These were used to convert the Cl_2 actinometry results to NO_2 photolysis rates in the DTC or CTC, to allow direct comparison with the NO_2 actinometry results.

Reactivity Data

As indicated above, a number of experiments for this program were incremental reactivity experiments. These consist of simultaneous irradiation of a "base case" reactive organic gas (ROG) surrogate - NO_x mixture in one of the dual reaction chambers, together with an irradiation, in the other reactor, of the same mixture with a test compound added. The results were analyzed to yield two measures of VOC reactivity: the effect of the added VOC on the amount of NO reacted plus the amount of ozone formed, and integrated OH radical levels. These are discussed in more detail below.

The first measure of reactivity is the effect of the VOC on the change in the quantity $[O_3]$-[NO], or $([O_3]_t$-$[NO]_t)$-$([O_3]_0$-$[NO]_0)$, which is abbreviated as $d(O_3$-NO) in the subsequent discussion. As discussed elsewhere (e.g., Johnson, 1983; Carter and Atkinson, 1987; Carter and Lurmann, 1990, 1991, Carter et al. 1993b, 1995a), this gives a direct measure of the amount of conversion of NO to NO_2 by peroxy radicals formed in the photooxidation reactions, which is the process that is directly responsible for ozone formation in the atmosphere. (Johnson calls it "smog produced" or "SP".) The incremental reactivity of the VOC relative to this quantity, which is calculated for each hour of the experiment, is given by

$$IR[d(O_3\text{-NO})]_t^{VOC} = \frac{d(O_3\text{-NO})_t^{test} - d(O_3\text{-NO})_t^{base}}{[VOC]_0} \qquad \text{(VII)}$$

where $d(O_3\text{-NO})_t^{test}$ is the $d(O_3$-NO) measured at time t from the experiment where the test VOC was added, $d(O_3\text{-NO})_t^{base}$ is the corresponding value from the corresponding base case run, and $[VOC]_0$ is the amount of test VOC added. An estimated uncertainty for IR[$d(O_3$-NO)] is derived based on assuming a ~3% uncertainty or imprecision in the measured $d(O_3$-NO) values. This is consistent with the results of the side equivalency test, where equivalent base case mixtures are irradiated on each side of the chamber.

Note that reactivity relative to $d(O_3$-NO) is essentially the same as reactivity relative to O_3 in experiments where O_3 levels are high, because under such conditions $[NO]_t^{base} \approx [NO]_t^{test} \approx 0$, so a change $d(O_3$-NO) caused by the test compound is due to the change in O_3 alone. However, $d(O_3$-NO) reactivity has the advantage that it provides a useful measure of the effect of the VOC on processes responsible for O_3 formation even in experiments where O_3 formation is suppressed by relatively high NO levels.

The second measure of reactivity is the effect of the VOC on integrated hydroxyl (OH) radical concentrations in the experiment, which is abbreviated as "IntOH" in the subsequent discussion. This is an important factor affecting reactivity because radical levels affect how rapidly all VOCs present, including the base ROG components, react to form ozone. If a compound is present in the experiment which reacts primarily with OH radicals, then the IntOH at time t can be estimated from

$$IntOH_t = \int_0^t [OH]_\tau \, d\tau = \frac{\ln\left(\frac{[tracer]_0}{[tracer]_t}\right) - D\,t}{kOH^{tracer}}, \qquad \text{(VIII)}$$

where $[tracer]_0$ and $[tracer]_t$ are the initial and time=t concentrations of the tracer compound, kOH^{tracer} is its OH rate constant, and D is the dilution rate in the experiments. The latter was found to be small and was assumed to be negligible in our analysis. The concentration of tracer at each hourly interval was determined by linear interpolation of the experimentally measured values. M-xylene was used as the OH tracer in these experiments because it is a surrogate component present in all experiments, its OH rate constant is known (the value used was 2.36×10^{-11} cm^3 $molec^{-1}$ s^{-1} [Atkinson, 1989]), and it reacts relatively rapidly.

The effect of the VOC on OH radicals can thus be measured by its IntOH incremental reactivity, which is defined as

$$IR[IntOH]_t = \frac{IntOH_t^{test} - IntOH_t^{base}}{[VOC]_0} \qquad \text{(IX)}$$

where $IntOH_t^{test}$ and $IntOH_t^{base}$ are the IntOH values measured at time t in the added VOC and the base case experiment, respectively. The results are reported in units of 10^6 min. The uncertainties in IntOH and IR[IntOH] are estimated based on assuming a ~2% imprecision in the measurements of the m-xylene concentrations. This is consistent with the observed precision of results of replicate analyses of this compound.

Modeling Methods

Atmospheric Photooxidation Mechanism

The chemical mechanism used in the model simulations in this report is given in Appendix A. It is based on that documented by Carter (1990), and can explicitly represent a large number of different types of organic compounds, but uses a condensed representation for many of the reactive organic products. The reactions of inorganics, CO, formaldehyde, acetaldehyde, peroxyacetyl nitrate, propanaldehyde, peroxypropionyl nitrate, glyoxal and its PAN analog, methylglyoxal, and several other product compounds are represented explicitly. The reactions of unknown photoreactive products formed

from aromatic hydrocarbons are represented by model species "AFG1" and "AFG2", whose yields and photolysis parameters are adjusted based on fits of model simulations to environmental chamber experiments. Most of the higher molecular weight oxygenated product species are represented using the "surrogate species" approach, where simpler molecules such as propanaldehyde or 2-butanone are used to represent the reactions of higher molecular weight analogues that are assumed to react similarly. A chemical operator approach is used to represent peroxy radical reactions, as discussed in detail by Carter (1990). Generalized reactions with variable rate constants and product yields are used to represent the primary emitted alkane, alkene, aromatic, and other VOCs (with rate constants and product yields appropriate for the individual compounds being represented in each simulation); the tables in the Appendix list only those VOCs (or groups of VOCs) used in the simulations in this work.

Prior to this work the Carter (1990) mechanism was updated as described in previous reports for this program (Carter et al. 1993a,b; 1995a,c), and by Carter (1995a). This is referred to as the "SAPRC-93" mechanism in the subsequent discussion. In addition, based on the results of the aromatic isomer experiments carried out for this program, several modifications were made to the way the unknown aromatic fragmentation products were represented. This is referred to as the "revised mechanism" in the subsequent discussion, and is discussed in the results section in conjunction with the discussion of the modeling of those experiments.

We are in the process of developing an updated version of the SAPRC mechanism under funding from a separate CARB program, which incorporates recent kinetic and mechanistic data which became available after the base mechanism used in this report was developed. Although preliminary calculations have been carried out using this mechanism, including simulations of some of the experiments discussed in this report, its development and evaluation will be the subject of a subsequent report.

Environmental Chamber Simulations

The use of environmental chamber experiments for mechanism evaluation requires including in the model appropriate representations of chamber-dependent effects such as wall reactions and characteristics of the light source. The methods used in this study are based on those discussed in detail by Carter and Lurmann (1990, 1991), updated as discussed by Carter et al. (1995b,c). Table 1 gives a summary of the methods used, and the values of the parameters used when modeling the specific experiments for this study. The photolysis rates were derived from results of actinometry experiments and direct measurements of the spectra of the light sources, as discussed in greater detail later in this report. The thermal rate constants were calculated using the temperatures measured during the experiments, with the small variations of temperature with time during the experiment being taken into account. The

computer programs and modeling methods employed are discussed in more detail elsewhere (Carter et al. 1995b). The derivation of chamber effects parameters specific to this study are discussed where appropriate in the "Characterization Results" section, below.

Table 1. Values of chamber-dependent parameters used in the model simulations of the environmental chamber experiments for this study.

Parm.	Value(s)	Discussion
k(O3W)	1.1×10^{-4} min^{-1} (Dry DTC) 1.5×10^{-4} min^{-1} (~50% RH DTC) 1.5×10^{-4} min^{-1} (~100% RH DTC) 8.5×10^{-4} min^{-1} (CTC)	k(O3W) is rate constant for unimolecular wall loss of O_3. Value used for dry DTC runs is based on results of DTC221 (see Table 8). Value used for humidified DTC runs is the default O_3 dark decay rate for Teflon bag chambers based on results of a number of such experiments by Carter et al. (1995b). The value used for the CTC runs is based on the results of runs CTC053 and CTC106, which are reasonably consistent with each other.
k(N25I) k(N25S)	2.8×10^{-3} min^{-1}, 1.5×10^{-6} - k_g ppm^{-1} min^{-1}	k(N25I) is unimolecular decay of N_2O_5 to the walls. K(N25S) is the rate constant for bimolecular reaction with H_2O, forming two HNO_3. The value used for the DTC is based on the N_2O_5 decay rate measurements in a similar chamber reported by Tuazon et al. (1983). Although we previously estimated their rate constants were lower in the larger Teflon bag chambers (Carter and Lurmann, 1990, 1991), we now consider it more reasonable to use the same rate constants for all such chambers (Carter et al., 1995b).
k(NO2W) yHONO	1.6×10^{-4} min^{-1} 0.2	k(NO2W) is the rate constant for a unimolecular decay of NO_2 to the walls, forming HONO with a yield of yHONO. The values used for both chambers are based on dark NO_2 decay and HONO formation measured in a similar chamber by Pitts et al. (1984). This is assumed to be the same in all Teflon bag chambers (Carter et al. 1995b).
k(XSHC)	≤250 min^{-1}	k(XSHC) is the rate constant for a unimolecular conversion of HO to HO_2, which is equivalent to the reaction of OH with CO. It is used to represent the effect of background VOC reactants, and is estimated by modeling pure air irradiations carried out in this reactor. Not an important parameter affecting model predictions except for pure air or NO_x-air runs.
RS/K1	0.17 ppb (dry DTC) 0.2 ppb (≥~50% RH DTC) 0.07 ppb (CTC)	The continuous chamber radical source as a light-dependent flux of OH radicals, whose rate (in units of concentration per time) is given by the NO_2 photolysis rate (k_1) multiplied by the parameter RS/K1. The parameter RS/K1 is derived from model simulations of n-butane - NO_x and CO - NO_x experiments as discussed in the text and by Carter et al. (1995c). The RS/K1 values used for the dry and ~50% RH DTC runs and for the CTC are based on averages which fit the n-butane - NO_x experiments summarized on Table 6. For the ~100% RH DTC runs, model simulations of the propene - NO_x and toluene - NO_x experiments were much better fit using the value using the ~50% RH n-butane runs rather than the high value (0.08 ppb) obtained from the single ~100% n-butane - NO_x run DTC177. See text.

Table 1 (continued)

Parm.	Value(s)	Discussion
E-NO2/K1	Same as RS/K1 (DTC) 0.04 ppb (CTC)	The rate of NO_2 offgasing from the chamber walls (in concentration per unit time) is obtained by multiplying the parameter E-NO2/K1 by the NO_2 photolysis rate. Model simulations of acetaldehyde - air runs, summarized on Table 7, are used to derive this parameter. For the DTC chamber, the results of these runs are consistent with assuming E-NO2/K1 ≈ RS/K1. For the CTC, the value used is based on the results of CTC019.
HONO-F	0.0	HONO-F is the fraction of initially present NO_2 which is assumed to be converted to HONO prior to the start of the run. When the light-induced radical source is represented by a continuous OH flux, best fits to most n-butane - NO_x experiments are obtained if this is assumed to be negligible. (Note that this is not the case if the continuous radical source is represented by NO_x offgasing. This alternative representation will be investigated when the updated version of the mechanism is evaluated, and is beyond the scope of the present report.)

RESULTS AND DISCUSSION

Chronological listings of all the environmental chamber experiments carried out during this phase of the program are given in Table 2 for the experiments in the blacklight chamber (DTC), and in Table 3 for the CTC runs using the xenon arc light source. As shown on the tables, a number of different types of experiments were carried out to address the various objectives of this program. Actinometry experiments were conducted to measure the light intensity by various methods. Other characterization and control runs were carried out to determine chamber-dependent parameters, or to verify that the standard assumptions used to model chamber effects (Carter et al. 1995b) are appropriate for these runs. A set of replicate propene - NO_x and toluene - NO_x experiments were carried out in the DTC at various humidities to determine if there are humidity effects which are not appropriately accounted for in the chamber model. Several formaldehyde - NO_x, acetaldehyde - NO_x, and ethene - NO_x experiments were carried out in both chambers for comparison with previous runs in the existing chamber data base and to serve as controls. A series of NO_x-air irradiations of various aromatic compounds, namely benzene, toluene, ethylbenzene, o-, m-, and p-xylene, and 1,2,3-, 1,2,4- and 1,3,5-trimethylbenzene, were carried out in both chambers to provide data needed to develop updated mechanisms for these compounds. Finally, a series of incremental reactivity experiments were carried out in the xenon arc chamber to evaluate whether incremental reactivity results obtained using this light source are consistent with the large data base of incremental reactivity results using blacklight chambers. The results of experiments, and the implication of these results to the development and evaluation of the atmospheric photooxidation mechanisms, are discussed in the following section.

Results of Characterization and Control Experiments

Tables 2 and 3 also show the various types of control and characterization runs which were carried out in conjunction with the experiments for this program. These consist of actinometry experiments whose results are discussed in more detail in a separate section, ozone dark decay experiments to measure the loss rate of O_3 to the walls, n-butane - NO_x and CO - NO_x experiments to measure the chamber radical source, pure air and acetaldehyde - air irradiations to measure the NO_x wall offgasing rates, and replicate propene - NO_x and surrogate - NO_x control experiments. In addition, several aldehyde - NO_x and ethene - NO_x experiments were carried out for comparison with similar experiments in other chambers. The relevant results of these experiments are given in the "comments" column of the tables, or are given in separate tables as discussed below. Except as noted below, the results were as expected based on results of other experiments in similar chambers (Carter et al. 1995b).

Table 2. Chronological listing of the blacklight chamber experiments carried out during this phase of the program.

Run	Date	Run Title	Description	Comments
		New chamber enclosure installed at CE-CERT Atmospheric Processes Laboratory. Old SAPRC DTC bag installed		
DTC124	2/24/94	NO_2 Actinometry (also DTC125)	Measure NO_2 photolysis rate using the quartz tube method. Measurements made with 100% and 50% lights using different banks of lights, and in different positions.	NO_2 photolysis rate not significantly affected by position or which bank used. Average NO_2 photolysis rate with all lights was 0.59 min^{-1}, and with 50% lights was 0.30 min^{-1}. See Table 4.
DTC126	3/9/94	O_3 Decay	Measure ozone dark decay rate. Ozone injected into the chamber and monitored in the dark.	Apparent O_3 decay rate increases with time. Initial rate slower than predicted by standard chamber model, final rate faster. Possible bag leakage. See Table 8.
DTC127	3/9/94	Pure Air Irradiation.	Characterization run to evaluate offgasing effects.	40 ppb O_3 formed in six hour. This is not inconsistent with predictions of default chamber model for this reaction bag, though the run could not be modeled because of lack of CO data.
DTC128	3/10/94	Propene - NOx	Control run to establish reproducible conditions, and dry propene run for humidity effects study.	Results in normal range and in good agreement with model predictions.
DTC129	3/11/94	Propene - NOx	Replicate of previous run.	Results in normal range and in good agreement with model predictions.
		Runs were carried out for another program. This included a number of runs at ~50% RH		
DTC145	5/3/94	n-Butane - NOx	Characterization run to determine magnitude of chamber radical source. (This is measured by the parameter RS/K1, which is the OH radical input rate used in model simulations to fit the data, divided by the NO_2 photolysis rate.)	NO oxidation rate indicated an RS/K1 value of 0.25 ppb, which is approximately 4 times higher than typical for Teflon reactors at this temperature, and ~25% higher than default for this chamber with these reaction bags. See Table 6.
DTC146	5/4/94	Propene - NOx	Control run to establish reproducible conditions, and dry propene run for humidity effects study.	Results in normal range. See Table 10.
DTC147	5/6/94	NO2 Actinometry (also DTC148)	Measure NO_2 photolysis rate using the quartz tube method. Measurements made with 100% and 50% lights using different banks of lights, and in different positions.	NO_2 photolysis rate not significantly affected by position or which bank used. Average NO_2 photolysis rate with all lights was 0.51 min^{-1}, and with 50% lights was 0.26 min^{-1}. See Table 4.
DTC149	5/10/94	Formaldehyde - NOx	Control run for comparison with previous formaldehyde runs and for evaluating light characterization model.	See Table 9. Model underpredicted O_3 formation rate but consistent with formaldehyde decay rate.
DTC150	5/11/94	Acetaldehyde - NOx	Control run for comparison with previous formaldehyde runs and for evaluating light characterization model.	See Table 9. O_3 formation rate consistent with predictions of model.

Table 2 (continued)

Run	Date	Run Title	Description	Comments
DTC151	5/12/94	Toluene - NOx	Run for toluene mechanism evaluation and control run for humidity effects study. Benzaldehyde and cresol data collected.	See Table 11.
DTC153		Propene - NOx (A), Toluene-NOx (B)	Replicate control runs for humidity effect study	See Tables 10 and 11.
DTC154	5/18/94	Tracer - NOx	Characterization run to determine magnitude of chamber radical source.	NO oxidation rate indicated an RS/K1 value of 0.2 ppb, which is the default for this chamber with these reaction bags.
DTC155	5/19/94	Propene - NOx (B), Toluene-NOx (A)	Low NOx propene and NOx run	See Tables 10 and 11.
DTC156	5/20/94	Pure Air Irradiation	Probable contamination with uncertain amount of NO	Run not modelable
DTC157		NO_2 Actinometry	Measure NO_2 photolysis rate using the quartz tube method. Measurements made with 100% and 50% lights using different banks of lights, and in different positions.	NO_2 photolysis rate not significantly affected by position or which bank used. NO2 photolysis rate with all lights was 0.45 min^{-1}, and average with 50% lights was 0.24 min^{-1}. See Table 4.
DTC158	5/24/94	Propene - NOx (A), Toluene-NOx (B)	Replicate dry run for humidity effects study.	See Tables 10 and 11. Data for propene run not used for model evaluation because measured initial propene disagreed with amount injected.
DTC159	5/25/94	Propene - NOx (A), Ethene - NOx (B)	Replicate propene run and ethene run for comparison with previous ethene experiments.	See Tables 10 and 11. Data for propene run not used for model evaluation because initial propene disagreed with amount injected.
DTC160	5/26/94	Propene - NOx (RH=50%)	Replicate 50% RH run for humidity effects study.	See Table 10. Data not used for model evaluation because measured initial propene disagreed with amount injected.
DTC161	5/27/94	Propene - NOx (RH=50%)	Replicate 50% RH run for humidity effects study.	See Text. Data not used for model evaluation because measured initial propene disagreed with amount injected.
DTC162	6/1/94	Propene - NOx (RH=50%)	Replicate 50% RH run for humidity effects study.	See Table 10.
DTC163	6/2/94	Propene - NOx (A), Toluene-NOx (B) (RH=50%)	Replicate 50% RH run for humidity effects study.	See Table 10. No toluene data, so Side B run is not modelable.
DTC164	6/3/94	Propene - NOx (B), Toluene-NOx (A) (RH=50%)	Replicate 50% RH run for humidity effects study.	See Tables 10 and 11.
DTC166	6/7/94	Propene - NOx (A), Toluene-NOx (B) (RH=50%)	Replicate 50% RH run for humidity effects study.	See Tables 10 and 11.

Table 2 (continued)

Run	Date	Run Title	Description	Comments
DTC167	6/8/94	Propene - NOx (B), Toluene-NOx (A) (RH=50%)	Replicate 50% RH run for humidity effects study.	See Tables 10 and 11.
DTC168	6/9/94	Propene - NOx (A), Toluene-NOx (B)	Replicate dry run for humidity effects study. Determine if results of dry run followed by a series of humidified runs are any different than standard dry run.	See Tables 10 and 11.
DTC169	6/10/94	Propene - NOx (A), Toluene-NOx (B)	Replicate dry run for humidity effects study.	See Tables 10 and 11.
DTC170	6/14/94	Propene - NOx (B), Toluene-NOx (A)	Replicate dry run for humidity effects study.	See Tables 10 and 11.
DTC171	6/15/94	n-Butane - NOx	Characterization run to determine magnitude of chamber radical source.	NO oxidation rate indicated an RS/K1 value of 0.2 ppb, which is the default for this chamber with these reaction bags. See Table 6.
DTC172	6/16/94	Propene - NOx (A), Toluene-NOx (B) (RH=50%)	50% RH run for humidity effects study. Chamber flushed with dry air overnight, then with humidified air.	See Tables 10 and 11.
DTC173	6/17/94	Propene - NOx (B), Toluene-NOx (A) (RH=50%)	50% RH run for humidity effects study. Chamber flushed with dry air overnight, then with humidified air.	See Table 10. No toluene data. Side B not modelable.
DTC174	6/18/94	NO_2 Actinometry	NO_2 actinometry by quartz tube method. Replicate measurements in same position.	Average NO_2 photolysis rate was 0.23 min^{-1}. See Table 4.
DTC174	6/18/94	NO2 Actinometry (Photostationary state)	NO2 actinometry by photostationary state method.	See Table 4. NO2 photolysis rate was 0.245 min-1.
DTC175	6/21/94	Propene - NOx (RH=100%)	Replicate ~100% RH run for humidity effects study.	Good side equivalency. See Table 10.
DTC176	6/22/94	Propene - NOx (A), Toluene-NOx (B) (RH=~100%)	Replicate ~100% RH run for humidity effects study.	See Tables 10 and 11.
DTC177	6/23/94	n-Butane - NOx (RH=100%)	Characterization run to determine magnitude of chamber radical source at ~100% RH.	NO oxidation rate indicated a RS/K1 value of 0.8 ppb., which is 4 times higher than the value obtained from the 50% RH and dry runs, and which is also inconsistent with the results of modeling the propene runs. See Table 6.
DTC178	6/24/94	Propene - NOx (Dry following Wet flush)	Run for humidity effects study. Chamber flushed with ~100% air overnight, then filled with dry air.	See Table 10.
DTC179	6/28/94	Propene - NOx (B), Toluene-NOx (A)	Replicate dry run for humidity effects study.	See Tables 10 and 11.

Table 2 (continued)

Run	Date	Run Title	Description	Comments
DTC182	7/19/94	Propene - NOx (RH=50%)	Replicate 50% RH run for humidity effects study.	Measured initial reactants somewhat outside the range of the other replicate runs. See Table 10.
DTC183	7/20/94	n-Butane - NOx (RH=50%)	Characterization run to determine magnitude of chamber radical source at 50% RH.	NO oxidation rate indicated an RS/K1 value of 0.25 ppb, which is within the range observed for the dry runs with this reaction bag. See Table 6.
DTC185	7/22/94	Acetaldehyde - air (RH=50%)	Characterization run to determine the magnitude of NOx offgasing at 50% RH.	Ozone formation rate is consistent with a NOx offgasing rate which is equal to default radical input rate for dry and 50% RH runs in this chamber and set of reaction bags. See Table 7.
DTC186	7/26/94	n-Butane - NOx (RH=20%)	Characterization run to determine magnitude of chamber radical source at ~50% RH.	NO oxidation rate indicated an RS/K1 value of 0.2 ppb, which is within the range observed for the dry runs with this reaction bag. See Table 6.
DTC187	7/27/94	Propene +NOx	Replicate dry run for humidity effects study.	Measured initial reactants somewhat outside the range of the other replicate runs. See Table 10.
DTC188	7/28/94	m-Xylene - NOx	Aromatic mechanism evaluation run.	See Table 13.
DTC189	7/29/94	m-Xylene - NOx	Aromatic mechanism evaluation run.	See Table 13.
DTC190	8/2/94	Propene (A) & Toluene (B) - NOx	Replicate dry run for humidity effects study.	Measured initial reactants somewhat outside the range of the other replicate runs. See Tables 10 and 11.
DTC191	8/3/94	m-Xylene - NOx	Aromatic mechanism evaluation run.	See Table 13.
DTC192	8/4/94	m-Xylene - NOx	Aromatic mechanism evaluation run.	See Table 13.
DTC193	8/5/94	m-Xylene - NOx	Aromatic mechanism evaluation run.	See Table 13.
DTC194	8/10/94	135-TMB - NOx	Aromatic mechanism evaluation run.	See Table 13.
DTC195	8/11/94	135-TMB - NOx	Aromatic mechanism evaluation run.	See Table 13.
DTC196	8/12/94	135-TMB - NOx	Aromatic mechanism evaluation run.	See Table 13.
DTC197	8/15/94	NO_2 Actinometry (Photostationary state)	NO_2 actinometry by photostationary state method.	NO_2 photolysis rate was 0.186 min^{-1}, which is low compared to other determinations around this time. See Table 4.
DTC198	8/16/94	p-Xylene - NOx	Aromatic mechanism evaluation run.	See Table 13.
DTC199	8/17/94	p-Xylene - NOx	Aromatic mechanism evaluation run.	See Table 13.
DTC200	8/18/94	p-Xylene - NOx	Aromatic mechanism evaluation run.	See Table 13.
DTC201	8/19/94	124-TMB - NOx	Aromatic mechanism evaluation run.	See text. (Possible leak in Side B. Side B data not used for modeling.)

Table 2 (continued)

Run	Date	Run Title	Description	Comments
DTC202	8/23/94	NO_2 Actinometry	NO_2 actinometry by quartz tube method.	Average NO_2 photolysis rate was 0.23 min^{-1}. See Table 4.
DTC202	8/23/94	NO_2 Actinometry (Photostationary state)	NO_2 actinometry by photostationary state method.	Average NO_2 photolysis rate was 0.24 min^{-1}. See Table 4.
DTC203	8/23/94	124-TMB - NOx	Aromatic mechanism evaluation run.	See Table 13.
DTC204	8/24/94	124-TMB - NOx	Aromatic mechanism evaluation run.	See Table 13.
DTC205	8/26/94	Propene - NOx	Replicate propene run to determine standard run conditions.	Results in normal range and consistent with model predictions.
DTC206	8/30/94	135-TMB - NOx (A), m-Xylene - NOx (B)	Aromatic mechanism evaluation run.	See Table 13.
DTC207	8/31/94	o-Xylene - NOx	Aromatic mechanism evaluation run.	See Table 13.
DTC208	9/1/94	o-Xylene - NOx	Aromatic mechanism evaluation run.	See Table 13.
DTC209	9/2/94	o-Xylene - NOx	Aromatic mechanism evaluation run.	See Table 13.
DTC210	9/6/94	NO2 Actinometry	NO2 actinometry by quartz tube method.	Average NO2 photolysis rate was 0.21 min-1. See Table 4.
DTC210	9/6/94	NO_2 Actinometry (Photostationary state)	NO_2 actinometry by photostationary state method.	Average NO_2 photolysis rate was 0.22 min^{-1}. See Table 4.
DTC211	9/7/94	123-TMB - NOx	Aromatic mechanism evaluation run.	See Table 13.
DTC212	9/8/94	123-TMB - NOx	Aromatic mechanism evaluation run.	See Table 13.
DTC213	9/9/94	123-TMB - NOx	Aromatic mechanism evaluation run.	See Table 13.
DTC214	9/13/94	Biacetyl Actinometry	Light intensity measurement by biacetyl decay rate.	Not used for light characterization because of uncertainty in quantum yields. Included in chamber data base for future use.
DTC215	9/14/94	n-Butane - NOx	Characterization run to determine magnitude of chamber radical source.	NO oxidation rate indicated an RS/K1 value of 0.1 ppb, which is about half the default rate used for this chamber with these reaction bags. See Table 6.
DTC216	9/15/94	Acetaldehyde - air	Characterization run to determine the magnitude of NOx offgasing.	Ozone formation rate is consistent with a NOx offgasing rate which is equal to default radical input rate fin this chamber and set of reaction bags. See Table 7.
DTC218	9/20/94	Formaldehyde - NOx	Control run for comparison with previous formaldehyde runs and for evaluating light characterization model.	See Table 9. Model slightly underpredicted O_3 formation rate but consistent with formaldehyde decay rate. Consistent with results of other formaldehyde - NOx runs in this chamber.

Table 2 (continued)

Run	Date	Run Title	Description	Comments
DTC219	9/21/94	Tracer - NOx	Characterization run to determine magnitude of chamber radical source.	NO oxidation rate is consistent with the default RS/K1 value for these reaction bags, which is 0.2 ppb.
DTC220	9/22/94	Pure Air Irradiation	Characterization run to evaluate offgasing effects.	40 ppb O3 formed in six hour. This is not inconsistent with predictions of default chamber model for this reaction bag, though the run could not be modeled because of lack of CO data.
DTC221	9/23/94	Dark O_3 Decay	Ozone injected in the chamber and decay monitored in the dark. CO also present to monitor dilution.	See Table 8. Dilution rates as measured by CO decay in Sides A and B were 1.5 and 3%/hour, respectively, which are near the averages observed for these reactors. O_3 decay, after correcting for dilution, was 0.6%/hour.
DTC222	9/29/94	NO_2 Actinometry	NO_2 actinometry by quartz tube method.	Average NO_2 photolysis rate was 0.24 min^{-1}. See Table 4.
DTC223	9/29/94	Ethylbenzene - NOx	Aromatic mechanism evaluation run.	See Table 13.
DTC224	9/30/94	Ethylbenzene - NOx	Aromatic mechanism evaluation run.	See Table 13.

Light Characterization Results

Blacklight Chamber Actinometry Results

Table 4 gives the results of all the actinometry measurements carried out in the CE-CERT DTC chamber up to the time it was constructed until well after the time period for most of the experiments covered in this report, and Figure 1 shows a plot of these data against DTC run number. The time period is extended beyond that applicable to most experiments for this program to provide better long-term trend information, and also to show the results of the Cl_2 actinometry experiments, which were carried out after the other experiments for this program were completed.

The banks of blacklights around the DTC chamber are switched such that alternative lights can be turned on or off independently, allowing the chamber to be operated at either 50% or 100% light intensity. All of the experimental runs for this program were at 50% light intensity using the same set of lights, and thus this was the case for most of the actinometry experiments as well. However, as indicated on Table 4, several of the earlier quartz tube experiments were conducted with all the lights on, or with the light banks which were normally off turned on, and visa-versa. In addition, as also noted on the table, a few experiments were also carried out with the quartz tube in a different position than that

Table 3. Chronological listing of the xenon arc chamber experiments carried out during this phase of the program.

Run	Date	Run Title	Description	Comments
			New single reaction bag installed	
CTC011	10/4/94	Pure Air Irradiation	No added reactants. Run to evaluate background effects in newly installed reaction bag.	Approximately 11 pob O_3 formed at end of 6 hours, which is approximately half that fit by standard chamber model. Best fit with NOx offgasing rate reduced by factor of 2, and no background VOC reactivity.
CTC012	10/5/94	Propene - NOx	Standard control run to test for consistency with previous experiments. Also, conditioning of new reaction bag.	See Table 9. Results reasonably consistent with model predictions.
CTC013	10/13/94	n-Butane - NOx	Characterization run to evaluate chamber model for chamber radical source.	See Table 6. Radical source approximately half the average for this reactor.
CTC014	10/7/94	Acetaldehyde - NOx	Control run for comparison with similar runs in other chambers.	See Table 9. Ozone formation and NO oxidation somewhat slower than model predicted.
CTC015	10/13/94	Acetaldehyde - NOx	Control run for comparison with similar runs in other chambers.	See Table 9. Ozone formation and NO oxidation somewhat slower than model predicted.
CTC016	10/14/94	Formaldehyde - NOx	Control run for comparison with similar runs in other chambers.	See Table 9. Results consistent with model predictions.
CTC017	10/17/94	NO_2 Actinometry	Measure light intensity using steady state method.	See Table 5.
CTC018	10/18/94	Propene - NOx	Standard control run to evaluate consistency and reproducibility of chamber conditions.	See Table 9. Results consistent with model predictions.
CTC019	10/19/94	Acetaldehyde + Air	Control run to test chamber model for NOx offgasing.	20 ppb O_3 and 2 ppb PAN formed at end of run. Reasonably consistent with prediction of chamber model based on assuming NO_x offgasing rate is the same as the radical source rate which fit CTC-020. See Table 7.
CTC020	10/20/94	n-Butane - NOx	Characterization run to evaluate chamber model for chamber radical source.	See Table 6. Radical source slightly more than half the average for this reactor.
CTC021	10/21/94	CO - NOx	Intended to be control run to test chamber model for radical source, but turned out not to be suitable for modeling because the CO was not purified	Run not suitable for modeling because CO was not purified. (Previous experience has shown that an impurity in CO causes anomalously high reactivity.
CTC022	10/24/94	NO2 Actinometry	Measure light intensity using steady state method.	See Table 5.

Table 3 (continued)

Run	Date	Run Title	Description	Comments
CTC023	10/25/94	Propene - NOx	Standard control run to evaluate consistency and reproducibility of chamber conditions.	See Table 9. Results were in reasonably good agreement with model predictions.
CTC024	10/26/94	Formaldehyde - NOx	Run for comparison with results of formaldehyde runs in other chambers.	See Table 9. O_3 yield slightly higher than model predicted.
CTC025	10/27/94	Ethene - NOx	Run for comparison with results of formaldehyde runs in other chambers.	See Table 9. O_3 yield was lower than model prediction.
CTC026	10/28/94	Toluene - NOx	Run for comparison with results of similar runs in other chambers, and for toluene mechanism evaluation.	See Table 13.
CTC027	11/2/94	NO2 Actinometry	Measure light intensity using steady state method.	See Table 5.
CTC028	11/3/94	n-Butane - NOx	Temperature control problems.	No LiCor data for this run through CTC048. Radical source near average for this reactor. See Table 6.
CTC029	11/8/94	m-Xylene - NOx	Run for comparison with results of similar runs in other chambers, and for m-xylene mechanism evaluation.	See Table 13.
CTC030	11/9/94	135-TMB - NOx	Aromatic mechanism evaluation run.	See Table 13.
CTC031	11/10/94	CO - NOx	Control run to test chamber model for radical source.	See Table 6. Radical source near average for this reactor.
CTC032	11/11/94	Acetaldehyde - NOx	Run for comparison with results of similar runs in other chambers, and evaluation of light source model.	Results reasonably consistent with model predictions.
CTC033	11/15/94	Toluene - NOx	Aromatic mechanism evaluation run.	One light out for part of run. Data not suitable for mechanism evaluation.
CTC034	11/16/94	Toluene - NOx	Aromatic mechanism evaluation run.	See Table 13.
CTC035	11/17/94	m-Xylene - NOx	Aromatic mechanism evaluation run.	See Table 13.
CTC036	11/18/94	m-Xylene - NOx	Aromatic mechanism evaluation run.	See Table 13.
CTC037	11/21/94	NO2 Actinometry	Measure light intensity using both quartz tube and steady state method.	See Table 5.
CTC038	11/22/94	o-Xylene - NOx	Aromatic mechanism evaluation run.	See Table 13.
CTC039	11/23/94	o-Xylene - NOx	Aromatic mechanism evaluation run.	See Table 13.
CTC040	11/31/94	NO2 Actinometry	Measure light intensity using both quartz tube and steady state method.	See Table 5.
CTC041	12/1/94	p-Xylene - NOx	Aromatic mechanism evaluation run.	See Table 13.

Table 3 (continued)

Run	Date	Run Title	Description	Comments
CTC042	12/2/94	n-Butane - NOx	Control run to test chamber model for radical source.	See Table 6. Radical source slightly higher than average for this reactor.
CTC043	12/5/94	p-Xylene - NOx	Aromatic mechanism evaluation run.	See Table 13.
CTC044	12/6/94	p-Xylene - NOx	Aromatic mechanism evaluation run.	See Table 13.
CTC045	12/7/94	n-Butane - NOx	Control run to test chamber model for radical source.	See Table 6. Radical source near average for this reactor.
CTC046	12/8/94	o-Xylene - NOx	Aromatic mechanism evaluation run.	See Table 13.
CTC047	12/12/94	p-Xylene - NOx	Aromatic mechanism evaluation run.	See Table 13.
CTC048	12/13/94	Toluene - NOx	Aromatic mechanism evaluation run.	See Table 13. LiCor returned from calibration.
CTC049	12/14/94	Propene - NOx	Standard control run to evaluate consistency and reproducibility of chamber conditions.	Results consistent with model predictions.
CTC050	12/15/94	135-TMB - NOx	Aromatic mechanism evaluation run.	See Table 13.
CTC051	12/18/94	NO_2 Actinometry	Measure light intensity using both quartz tube and steady state method.	See Table 5.
CTC052	12/19/94	Pure Air Irradiation	Control run to evaluate chamber model for background effects.	70 ppb O_3 formed at end of run, much greater than model predictions. May have been NO contamination problems. NO data appear to be anomalous. Concluded that run not suitable for model evaluation.
CTC053	12/20/94	Ozone Dark Decay	Characterization run to evaluate the ozone wall loss rate.	O_3 dark decay rate was 8.5×10^{-4} min^{-1}, which is approximately 60% the value used in the standard chamber model for Teflon bag reactors. See Table 8.
CTC054	12/21/94	123-TMB - NOx	Aromatic mechanism evaluation run.	See Table 13.
CTC056	1/5/95	124-TMB - NOx	Aromatic mechanism evaluation run.	See Table 13.
CTC057	1/6/95	Ethylbenzene - NOx	Aromatic mechanism evaluation run.	See Table 13.
CTC058	1/10/95	n-Butane - NOx	Control run to test chamber model for radical source.	See Table 6. Radical source slightly higher than average for this reactor.
CTC059	1/11/95	Propene - NOx	Standard control run to evaluate consistency and reproducibility of chamber conditions.	See Table 9. Results consistent with model predictions.
CTC061	1/13/95	CO - NOx	Control run to test chamber model for radical source.	See Table 6. Radical source near average for this reactor.
CTC062	1/17/95	NO_2 Actinometry	Measure light intensity using both quartz tube and steady state method.	See Table 5.

Table 3 (continued)

Run	Date	Run Title	Description	Comments
CTC063	1/18/95	Toluene - NOx	Aromatic mechanism evaluation run.	NO_x data appear to be anomalous. Run not modelable.
CTC065	1/25/95	Toluene - NOx	Aromatic mechanism evaluation run.	See Table 13.
CTC066	1/25/95	m-Xylene - NOx	Aromatic mechanism evaluation run.	See Table 13. One light out for part of run.
		Lamp A replaced. Filters not changed. No significant change in spectrum observed.		
CTC068	1/27/95	o-Xylene - NOx	Aromatic mechanism evaluation run.	See Table 13.
CTC069	1/31/95	p-Xylene - NOx	Aromatic mechanism evaluation run.	See Table 13.
CTC070	2/1/95	p-Xylene - NOx	Aromatic mechanism evaluation run.	See Table 13.
CTC071	2/2/95	135-TMB - NOx	Aromatic mechanism evaluation run.	See Table 13.
CTC072	2/3/95	Acetaldehyde - NOx	Control run for comparison with similar runs in other chambers.	See Table 9. Ozone formation and NO oxidation rates slightly lower than model predicted.
CTC073	2/7/95	135-TMB - NOx	Aromatic mechanism evaluation run.	See Table 13.
CTC074	2/8/95	n-Butane - NOx	Control run to test chamber model for radical source.	See Table 6. Radical source near average for this reactor.
CTC075	2/9/95	123-TMB - NOx	Aromatic mechanism evaluation run.	See Table 13.
CTC076	2/10/95	123-TMB - NOx	Aromatic mechanism evaluation run.	See Table 13.
CTC077	2/14/95	Formaldehyde - NOx	Control run for comparison with similar runs in other chambers.	See Table 9. Ozone formation and NO oxidation rates slightly higher than model predicted.
CTC078	2/16/95	Propene - NOx	Standard control run to evaluate consistency and reproducibility of chamber conditions.	Results consistent with model predictions. Maximum O_3 slightly higher than predicted by model.
CTC079	2/17/95	Toluene - NOx	Aromatic mechanism evaluation run.	See Table 13.
CTC080	2/21/95	m-Xylene - NOx	Aromatic mechanism evaluation run.	See Table 13.
CTC081	2/22/95	o-Xylene - NOx	Aromatic mechanism evaluation run.	See Table 13.
CTC082	2/23/95	NO_2 Actinometry	Measure light intensity using both quartz tube and steady state method	See Table 5.
			Dual Reaction Bags Installed	
CTC083	3/2/95	Propene - NOx	Standard control run to evaluate consistency and reproducibility of chamber conditions. Also condition chamber and serve as a side equivalency test.	Results are consistent with model predictions and results of previous propene runs in this chamber. Good side equivalency.

Table 3 (continued)

Run	Date	Run Title	Description	Comments
CTC084	3/3/95	n-Butane - NOx	Control run to test chamber model for radical source.	Radical source consistent with other determinations in these reactors. See Table 6.
CTC085	3/5/95	Dilution and Leak Tests	Monitored dark decay of CO and other species.	Some evidence of leakage. Valves tightened
CTC086	3/7/95	Propene - NOx	Standard control run to evaluate consistency and reproducibility of chamber conditions.	Maximum O_3 somewhat higher than predicted by model.
CTC087	3/9/95	Aborted formaldehyde run	Control run for comparison with similar runs in other chambers.	HCHO analysis problems
CTC088	3/10/95	NO_2 Actinometry	Measure light intensity using steady state method.	See Table 5.
CTC089	3/14/95	Toluene - NOx	Aromatic mechanism evaluation run.	See Table 13.
CTC090	3/16/95	CO - NOx	Control run to test chamber model for radical source.	Radical source consistent with other determinations in these reactors. See Table 6.
CTC091	3/16/95	o-Xylene - NOx (A), 124-TMB - NOx (B)	Aromatic mechanism evaluation run.	See Table 13.
CTC092	3/17/95	Ethylbenzene - NOx	Aromatic mechanism evaluation run.	See Table 13.
CTC093	3/21/95	124-TMB - NOx	Aromatic mechanism evaluation run.	See Table 13.
CTC094	3/22/95	m-Xylene - NOx	Aromatic mechanism evaluation run.	See Table 13.
CTC095	3/23/95	Formaldehyde - NOx	Run for comparison with results of formaldehyde runs in other chambers.	Good agreement with model predictions.
CTC096	3/24/95	Pure Air Irradiation	Characterization run to test chamber model for background effects.	30 ppb O_3 formed at end of run, in good agreement with predictions of chamber model using NO_x offgasing rate consistent with lower range of radical source.
CTC097	3/27/95	NO2 Actinometry	Measure light intensity using quartz tube method.	See Table 5.
CTC098	3/28/95	135-TMB - NOx (A), Ethylbenzene - NOx (B)	Aromatic mechanism evaluation run.	See Table 13.
CTC099	3/29/95	n-Butane - NOx	Control run to test chamber model for radical source.	Radical source consistent with other determinations in these reactors. See Table 6.
CTC100	3/30/95	Mini-Surrogate - NOx	Run to determine appropriate conditions for mini-surrogate base case run for reactivity experiments. Side Equivalency test.	Almost no ozone formed.

Table 3 (continued)

Run	Date	Run Title	Description	Comments
CTC101	3/31/95	Mini-Surrogate - NOx	Repeat of mini-surrogate run with lower NOx and higher ROG surrogate to get O_3 levels similar to mini-surrogate experiments in Phase 1 of the program.	Approximately 0.2 ppm O_3 formed at the end of 6 hours, which is still lower than in most Phase 1 mini-surrogate base case runs. Good side equivalency.
CTC102	4/5/95	Propene +NOx	Standard control run to evaluate consistency and reproducibility of chamber conditions.	See Table 9. Results are consistent with model predictions.
CTC103	4/6/95	Mini-Surrogate - NOx	Repeat of mini-surrogate run with lower NO_x to get higher O_3 levels, while still being in maximum reactivity conditions.	Approximately 0.3 ppm O_3 formed at the end of 6 hours, which is within the range of most Phase 1 mini-surrogate base case runs. Good side equivalency.
CTC105	4/12/95	Mini-Surrogate + CO (B)	Measure the incremental reactivity of representative compounds.	See Table 12.
CTC106	4/14/95	Ozone Dark Decay	Characterization run to determine ozone wall loss rate. CO also present to measure dilution.	Results consistent with other ozone dark decay experiments in Teflon bag chambers. See Table 8.
CTC107	4/18/95	Mini-Surrogate + Acetaldehyde (A)	Measure the incremental reactivity of representative compounds.	See Table 12.
CTC108	4/19/95	Mini-Surrogate + Toluene (B)	Measure the incremental reactivity of representative compounds.	See Table 12.
CTC109	4/21/95	Mini-Surrogate + m-Xylene (A)	Measure the incremental reactivity of representative compounds.	See Table 12.
CTC110	4/25/95	Mini-Surrogate + n-Octane (B)	Measure the incremental reactivity of representative compounds.	See Table 12.
CTC113	4/28/95	Mini-Surrogate - NOx	Measure the incremental reactivity of representative compounds.	See Table 12.
CTC114	5/3/95	n-Butane +NOx	Control run to test chamber model for radical source.	Radical source consistent with other determinations in these reactors. See Table 6.
CTC115	5/4/95	Propene - NOx	Standard control run to evaluate consistency and reproducibility of chamber conditions.	Results are consistent with model predictions.
CTC117	5/10/95	Full Surrogate - NOx	Measure the incremental reactivity of representative compounds.	See Table 12.
CTC118	5/11/95	Full Surrogate - NOx	Measure the incremental reactivity of representative compounds.	See Table 12.
CTC120	5/16/95	n-Butane - NOx	Control run to test chamber model for radical source.	Radical source consistent with other determinations in these reactors. See Table 6.
CTC123	5/23/95	Full Surrogate + CO (A)	Measure the incremental reactivity of representative compounds.	See Table 12.

Table 3 (continued)

Run	Date	Run Title	Description	Comments
CTC127	6/1/95	Full Surrogate +Toluene (B)	Measure the incremental reactivity of representative compounds.	See Table 12. Lamp problems in later period of run.
CTC128	6/2/95	Full Surrogate + m-Xylene (A)	Measure the incremental reactivity of representative compounds.	See Table 12.
CTC129	6/5/95	NO_2 Actinometry	Measure light intensity using quartz tube and steady state methods.	See Table 5.
CTC130	6/6/95	Full Surrogate + Propene (B)	Measure the incremental reactivity of representative compounds.	See Table 12. Lamp problems in later period of run.
CTC131	6/7/95	Full Surrogate + n-Octane (A)	Measure the incremental reactivity of representative compounds.	See Table 12. Lamp problems in later period of run.
CTC132	6/8/95	Propene - NOx	Standard control run to evaluate consistency and reproducibility of chamber conditions.	Results are consistent with model predictions.
CTC133	6/9/95	Formaldehyde - NOx	Control run for comparison with similar runs in other chambers.	See Table 9. Ozone formation and NO oxidation slightly faster than model predictions.
CTC135	6/14/95	n-Butane - NOx	Control run to test chamber model for radical source.	Radical source consistent with other determinations in these reactors. See Table 6.
CTC136	6/18/95	Chlorine actinometry.	Measure light intensity using Chlorine + n-butane method.	See Table 5.
CTC137	6/19/95	NO_2 Actinometry	Measure light intensity using quartz tube and steady state methods.	See Table 5.
CTC138	6/20/95	Full Surrogate + Formaldehyde (B)	Measure the incremental reactivity of representative compounds.	See Table 12. Lamp problems in later period of run.
CTC139	6/21/95	Chlorine actinometry.	Measure light intensity using Chlorine + n-butane method.	See Table 5.
CTC140	6/22/95	Full Surrogate + Formaldehyde (A)	Measure the incremental reactivity of representative compounds.	See Table 12. Lamp problems in later period of run.
CTC142	6/27/95	Mini-Surrogate + Propene (B)	Measure the incremental reactivity of representative compounds.	See Table 12. Lamp problems in later period of run.
CTC143	6/28/95	Pure-Air Irradiation	Characterization run to test chamber model for background effects.	30 ppb O_3 formed at end of run, in good agreement with predictions of chamber model using NO_x offgasing rate consistent with lower range of radical source.
CTC144	6/29/95	NO_2 Actinometry	Measure light intensity using quartz tube method.	See Table 5.

Table 3 (continued)

Run	Date	Run Title	Description	Comments
			Chamber inactive for a period.	
			Runs for other programs carried out in conjunction with the following.	
CTC145	11/30/95	NO_2 Actinometry	Measure light intensity using quartz tube method.	See Table 5.
CTC166	3/8/96	NO_2 Actinometry	Measure light intensity using quartz tube method.	See Table 5.
CTC177	3/8/96	NO_2 and Chlorine Actinometry	Measure light intensity using quartz tube method.	See Table 5.

normally employed. As expected, the NO_2 photolysis rates in the experiments with 100% lights were, to within experimental variability, twice those with the normal 50% light intensity, and there was no significant effect as to which set of lights were used. The data also indicate that the measured NO_2 photolysis rates were not highly sensitive to variations in the height of the actinometry tube when located between the two reactors.

Figure 1 shows that the light intensity as measured by the quartz tube method declined relatively rapidly during the first ~40 or so experiments after the chamber was constructed and the new lights were installed, and then declined slowly after that. The rapid decline following installation of new lights is similar to that observed for other blacklight chambers (Carter et al. 1995b), although the gradual, apparently linear, decline in intensity after the initial "burn in" period was not observed previously. The quartz tube actinometry data were fit by the empirical function

$$k_1\ (min^{-1}) = 0.242\ [1 + 0.298\ e^{-0.0497\ (RunNo-120)}]\ [1 - 0.00074\ (RunNo-120)] \qquad (X)$$

where RunNO is the DTC run number. Equation (X) was used to compute the "fit to tube data" line on Figure 1, and to derive the NO_2 photolysis rates for modeling the DTC experiments for this work.

Table 4 and Figure 1 show that the results of approximately half of the steady-state actinometry experiments were in good agreement with the quartz tube results. However, other steady-state experiments gave k_1 values which were ~25-30% lower than indicated by the quartz tube data. We suspect that the data from runs 229 and 234 probably should be rejected because inappropriately long sample lines may have been used, but unfortunately the log books are unclear on the procedure for those particular runs. The low results for run 197 are more difficult to explain. This variability suggests that

Table 4. Summary of results of actinometry experiments in the DTC Blacklight chamber.

Run	Date	Lights Used	Light Banks	Tube Loc. [b]	NO_2 Phot. Rate (min^{-1}) Tube	Steady State A	Steady State B
DTC-124	2/24/94	100%	1-4	[c]	0.59		
		100%	1-4	[c]	0.59		
		100%	1-4		0.56		
		50%	1&3	[c]	0.30		
		50%	2&4	[c]	0.30		
		50%	1&3	[c]	0.30		
		50%	1&3		0.29		
		50%	2&4		0.29		
DTC-125	2/25/94	100%	1-4	[d]	0.61		
		100%	1-4	[d]	0.60		
		50%	1&3	[d]	0.31		
		50%	2&4	[d]	0.31		
		50%	2&4	[d]	0.31		
		50%	1&3	[d]	0.31		
DTC-147	5/5/94	100%	1-4		0.51		
		50%	1&3		0.26		
		50%	2&4		0.27		
DTC-148	5/9/94	100%	1-4		0.51		
		50%	1&3		0.26		
		50%	2&4		0.27		
DTC-157	5/23/94	100%	1-4		0.45		
		50%	1&3		0.25		
		50%	2&4		0.23		
DTC-174	6/18/94	50%	[a]		0.24		0.24
		50%	[a]		0.23		
		50%	[a]		0.23		

Run	Date	Lights Used	Light Banks	NO_2 Phot. Rate (min^{-1}) Tube [b]	Steady State A	Steady State B	Cl_2
DTC-197	8/15/94	50%	[a]		0.19		
DTC-202	8/23/94	50%	1&3	0.24	0.24	0.23	
		50%	1&3	0.24			
		50%	1&3	0.22			
DTC-210	9/6/94	50%	1&3	0.21	0.22	0.22	
		50%	1&3	0.21			
		50%	1&3	0.21			
DTC-222	9/26/94	50%	1&3	0.24	0.22	0.22	
		50%	1&3	0.23			
DTC-229	7/17/95	50%	1&3	0.23	0.16	0.16	
DTC-234	7/24/95	50%	1&3	0.23	0.15	0.14	
DTC-245	8/14/95	50%	1&3	0.23			
DTC-254	8/28/95	50%	1&3	0.23			
DTC-287	10/30/95	50%	1&3	0.22			
DTC-297	11/27/95	50%	1&3	0.21			
DTC-300	1/24/96	50%	1&3	0.22			
DTC-326	3/11/96	50%	1&3	0.21			
DTC-343	4/29/96	50%	1&3	0.21			
DTC-341	4/25/96	50%	[a]				0.23
DTC-356	5/20/96	50%	[a]				0.21
DTC-367	6/10/96	50%	1&3	0.19			
DTC-392	8/5/96	50%	1&3	0.19			
DTC-407	9/4/96	50%	1&3	0.18			0.20
DTC-429	10/14/96	50%	1&3	0.18			

[a] Information not available.
[b] Unless otherwise noted, tube was located between the reaction bags 5' from the floor.
[c] Tube located between reaction bags 3'5" from the floor.
[d] Tube was located inside reaction bag B.

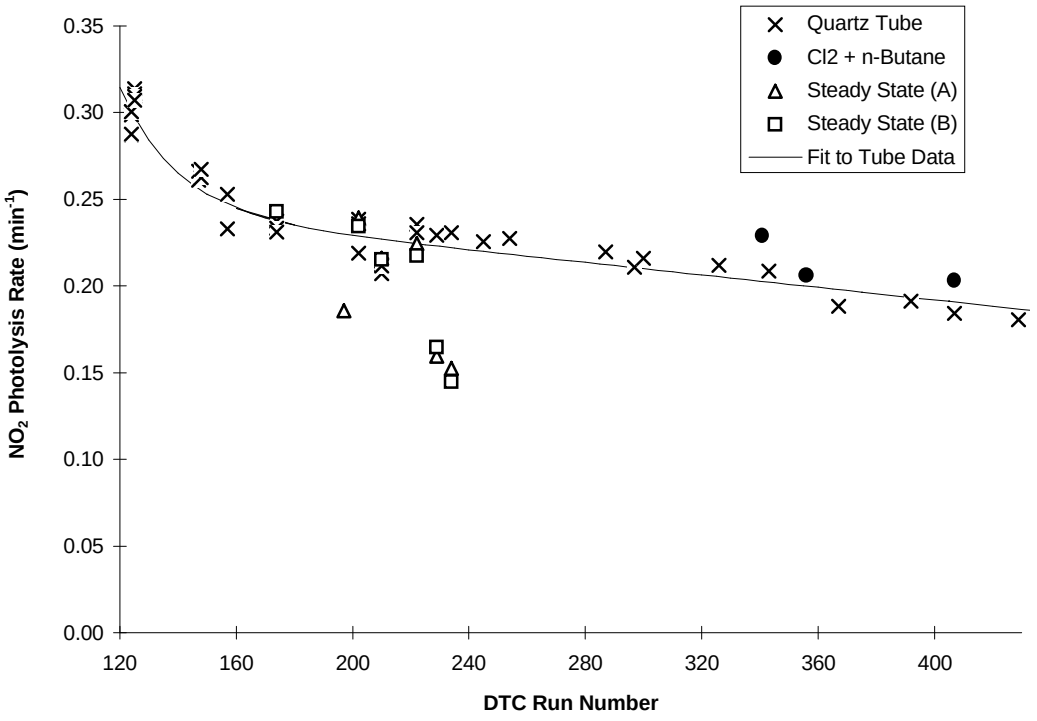

Figure 1. Plots of results of actinometry experiments in the DTC chamber against run number.

Figure 1. Plots of results of actinometry experiments in the blacklight chamber against run number.

this actinometry method may have inherent variability problems, or that inappropriate procedures may have been employed. Because of this, these steady-state actinometry results should probably be considered to be lower limits to the true light intensity. Therefore, the most that can be concluded from these experiments is that they are not inconsistent with the results of the quartz tube method, but they do not provide conclusive validation for the accuracy of the quartz tube method for this chamber.

On the other hand, Table 4 and Figure 1 show that the results of the Cl_2 actinometry experiments are much less variable, and are in reasonably good agreement with the results of the quartz tube method. They tend to be slightly higher (by ~7% on the average) than predicted using Equation (X), though clearly they are consistent to within the experimental variability. If the difference is real, it could be due to quantum yields for Cl_2 photolysis being slightly less than unity, resulting in an overestimation of the NO_2 photolysis rate when derived from the Cl_2 photolysis rate using Equation (IV). However, the consistency of these two very different actinometry methods tend to support the validity of both the quartz tube and the Cl_2 actinometry methods.

Xenon Arc Chamber Spectral Data

The spectral distributions in the CTC chamber were measured approximately four times during each chamber run using a LiCor 1600 portable spectral radiometer which was located on a post immediately in front of the reaction bag(s). The LiCor was located in the same position relative to the

lights for all experiments, so its data could also be used to monitor changes in relative intensity as well as changes in spectral distribution (see Carter et al. 1995c). This is shown on Figure 2, which gives plots of intensities (in units proportional to photons per unit area) against CTC run number for selected wavelengths. The discontinuities around runs 28-48 and after run 144 are due to results of factory recalibrations of the instruments which were carried out around those times. Except for these discontinuities, it can be seen that there is a very slight decline in intensity with time, with the relative rate of decline decreasing with increasing wavelength. Relatively slow changes in spectral characteristics are expected because the lights and filters were well conditioned prior to this program, and the lights and filters were not changed except as noted below.

The discontinuities in the spectral trends resulting from recalibrations of the spectraradiometer indicated that it was somewhat out of calibration in the runs prior to the calibration, and that corrections to the data were appropriate. Corrected spectral intensity trends were derived for each wavelength based on assuming that the spectra for the runs immediately following the calibrations were correct, that the decline with intensity with time is linear at any given wavelength, and that the rate of decline in intensity (i.e., the slope divided by the intercept) also varies linearly with wavelength. The latter assumption was supported by the wavelength dependence of the trend slope/intercept ratios derived separately for each wavelength, but was made to smooth out the variability in the data at the lower wavelengths. The resulting trend lines, derived by nonlinear least-squares optimization, are also shown on Figure 2.

These corrected trend lines were used to derive the spectral distributions which were used when modeling the CTC experiments for this program. However, rather than calculating a separate spectrum for each experiment which is only slightly different from the previous and subsequent one, the experiments were grouped into sets of ~30 consecutive runs, and an averaged spectrum was used for modeling each experiment in a group.

The corrected trends in spectral intensities can also be used, in conjunction with the NO_2 absorption cross sections and quantum yields used in the model (see Appendix A), to calculate the relative trends in the NO_2 photolysis rates (k_1 values) for these experiments. The resulting calculated k_1 trend, scaled by a factor to make them consistent with the results of the actinometry experiments as discussed in the following section, are shown on Figure 3. Based on this trend, the NO_2 photolysis rate is calculated to decline by only ~8% during the period of the CTC runs listed on Table 2.

The occasional low points on the plots are due to runs where individual lamps malfunctioned; data from such runs are not used for mechanism evaluation. The first of those is run CTC-066, where a lamp

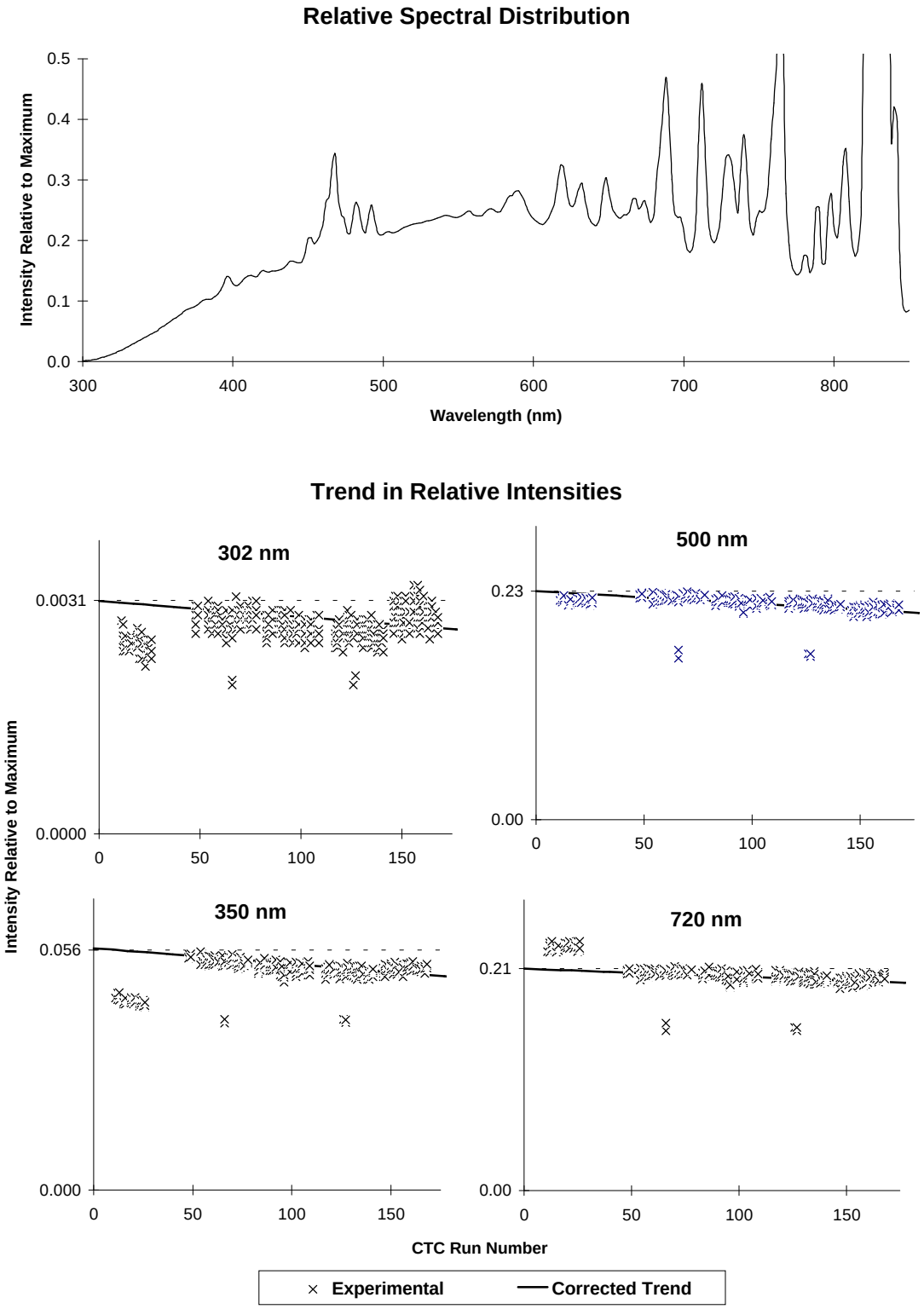

Figure 2. Representative spectrum of the xenon arc light source for the CTC chamber and trends in relative intensities with time at selected wavelengths.

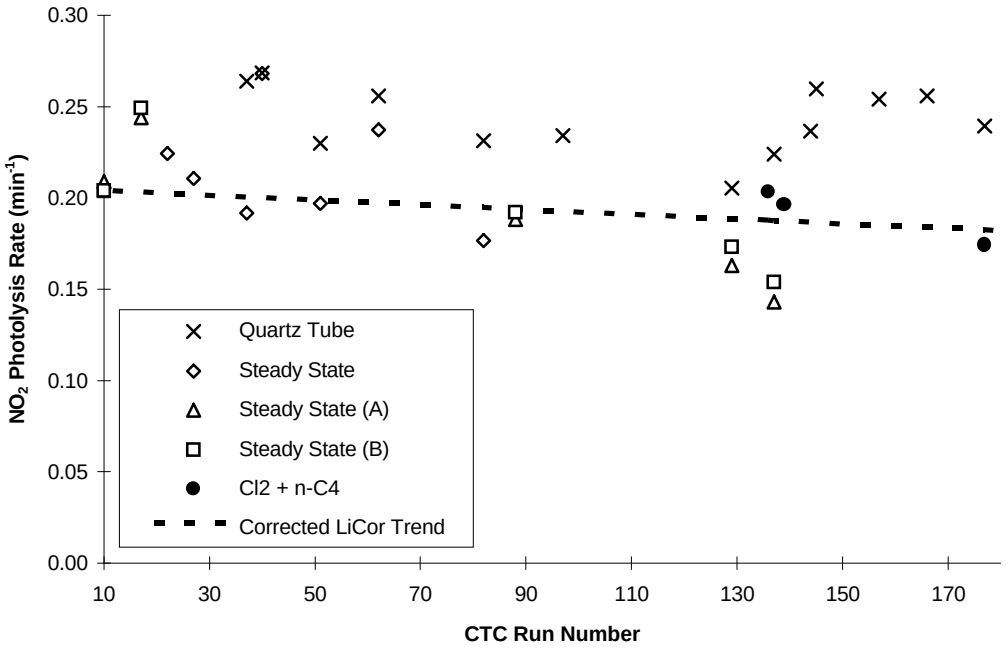

Figure 3. Plots of results of actinometry experiments in the xenon arc chamber against run number, and calculated k1 trend based on corrected trends in spectral intensities measured using the LiCor spectraradiometer.

Figure 3. Plots of results of actinometry experiments in the xenon arc chamber against run number, and calculated k_1 trend based on corrected trends in spectral intensities measured using the LiCor spectraradiometer.

failed completely and had to be replaced. However, the inner and outer filters with the failed lamp were preserved and were used with the new lamp. The spectrum taken of the new lamp (with the old filters) had no significant difference between the spectra of the old lights, nor, as indicated on Figure 2, was there any discontinuity in the spectral intensity caused by this lamp replacement. This indicates that it is primarily the aging of the filters, not the lamps, which is the primary factor causing the gradual change in spectral intensity with time. The old filters were deliberately kept to avoid the more rapid changes in spectral intensity which were observed when the lamps were new (Carter et al. 1995b).

Xenon Arc Chamber Actinometry Results

Table 5 gives the results of all the actinometry measurements carried out in the CTC, and Figure 3 shows a plot of these data against CTC run number. As with the DTC, the time period is extended beyond that applicable to this program to provide better long-term trend information, and to show the results of the Cl_2 actinometry experiments.

The actinometry results indicate that any change in light intensity with time during the period of these experiments is less than the precision of these data, but is not inconsistent with the gradual decline calculated using the trend in spectral intensities derived as discussed above. The quartz tube actinometry results are higher, by ~30% on the average, than the results using the steady-state or Cl_2 photolysis method. This is as expected because the quartz tube is located in front of reaction bags and slightly

Table 5. Summary of results of actinometry experiments in the CTC Xenon arc chamber.

Run	Date	NO_2 Photolysis Rate (min^{-1})				
		Tube	Steady State			Cl_2
			A	B	Single	
CTC-010	9/19/94		0.209	0.204		
CTC-017	10/17/94		0.244	0.249		
CTC-022	10/24/94				0.224	
CTC-027	10/31/94				0.211	
CTC-037	11/21/94	0.264			0.192	
CTC-040	11/28/94	0.268			0.268	
CTC-051	12/16/94	0.230			0.197	
CTC-062	1/17/95	0.256			0.237	
CTC-082	2/23/95	0.231			0.177	
CTC-088	3/10/95		0.188	0.192		
CTC-097	3/27/95	0.234				
CTC-129	6/5/95	0.205	0.163	0.173		
CTC-136	6/15/95					0.203
CTC-137	6/19/95	0.224	0.143	0.154		
CTC-139	6/21/95					0.196
CTC-144	6/29/95	0.237				
CTC-145	11/30/95	0.260				
CTC-157	1/10/96	0.254				
CTC-166	3/8/96	0.256				
CTC-177	11/27/96	0.240				0.174

Table 5. Summary of results of the actinometry experiments carried out in the CE-CERT xenon arc chamber.

closer to the lights. Because of this, the results of the photostationary state or Cl_2 actinometry methods are considered to be more appropriate for deriving absolute photolysis rates for modeling.

As with the DTC, the data using the steady-state actinometry method show more scatter than those using the Cl_2 actinometry method, but in this case the results of the two methods agree to within the variability of the data. Because the Cl_2 actinometry results have greater precision, are consistent with the quartz tube results for the DTC, and are not inconsistent with the steady-state results for this chamber, they are considered to be the most reliable indicator of the actual absolute light intensity in this chamber. On the other hand, they are not suitable for determining the trend in light intensity with time, since Cl_2 actinometry data are available only for the ending period of this program. The LiCor trend data, corrected to take into accounts results of instrument calibrations as discussed above, provide the most precise indication of how overall light intensity varies with time throughout the entire period. Therefore, for modeling purposes, the corrected LiCor k_1 trend data, multiplied by a calibration factor to minimize the least squares difference between them and the NO_2 photolysis rates derived from the results of the three

Cl_2 actinometry experiments, are used to derive the NO_2 photolysis rates for modeling the CTC runs. This corrected and calibrated k_1 trend is shown as the dotted line on Figure 3. Note that the results of the steady-state actinometry experiments are not inconsistent with this trend line.

Results of Chamber Radical Source Determination

Other than light intensity, the most important chamber-dependent parameter for modeling chamber runs is the chamber radical source (Carter et al. 1982; Carter and Lurmann, 1990, 1991; Carter et al. 1995c). As discussed by Carter et al. (1995c), we now believe that the most reliable method for determining this is modeling n-butane - NO_x or CO - NO_x irradiations. Table 6 summarizes all the n-butane - NO_x and CO - NO_x runs carried out in the chambers employed for this study, along with the radical input rates which gave best agreements between experimental and model simulated NO oxidation rates. (The radical input rates are given as RS/k_1, which is the ratio of the OH input to the NO_2 photolysis rate, as indicated on Table 1, above.) For comparison purposes, Table 6 also shows radical input rates derived in model simulations of the n-butane - NO_x and CO - NO_x runs carried out in other Teflon bag indoor chambers, including those employed in the previous phases of this study. These chambers were of similar construction and the experiments carried out under similar conditions, so the radical input rates in them should be comparable. As indicated on Table 1, the average values (shown on the right-hand column of Table 6) were used as the basis for deriving the radical source rates to use when conducting model simulations for the various experimental runs for this report.

Table 6 shows that the radical input rates for the dry runs in the CE-CERT DTC chamber during this reporting period were approximately a factor of three higher than observed in the SAPRC DTC during phase 2, and also in the CE-CERT DTC after the reactors were changed. We have no obvious explanation for this higher radical source, since the reaction bags employed were the same as those employed in the SAPRC DTC; in effect, the chamber was moved from SAPRC to CE-CERT and installed in a new enclosure of similar design. One possibility is that between the time the reactors were installed at CE-CERT and the time of the experiments for this program were carried out, a number of experiments employing siloxanes were carried out at variable humidity to determine their aerosol forming potential (Carter et al. 1994). Experiments employing α-pinene were also carried out. (Aerosol formation occurred in the α-pinene but not the siloxane runs.) It is unlikely that contamination by these compounds could be the problem, since siloxanes and pinenes have been studied in our chambers previously with no noticeable effects on the chamber radical source. [In addition, siloxanes are radical inhibitors (Carter et al. 1992), so, if anything, contamination by them should suppress radicals.] Another possibility is that conducting runs under humidified conditions may have affected the characteristics of the walls in subsequent runs. However, the radical source rates in the SAPRC ITC runs, which were

Table 6. Summary of results of n-butane - NOx and CO - NOx experiments for chamber radical source determinations.

Run	Initial			RH	k1	T	RS/k1 (ppb)		
	NO_x	n-C_4	CO		(min^{-1})	(deg K)	A	B	Avg.
				SAPRC ITC (Runs for past programs)					
ITC507	0.09	3.7		~50%	0.37	301	0.074		0.080 +_ 0.005
ITC533	0.10	3.0		~50%	0.36	303	0.079		
ITC939	0.53	4.9		~50%	0.35	301	0.081		
ITC948	0.26	4.7		~50%	0.35	301	0.086		
				SAPRC ETC (Phase 1 runs)					
ETC214	0.49	3.9		dry	0.35	299	0.017		0.024 +_ 0.009
ETC318	0.52	4.2		dry	0.35	298	0.030		
				SAPRC DTC (Phase 2 runs)					
DTC058	0.24	3.5		dry	0.39	301	0.063	0.051	0.057 +_ 0.008
				CE-CERT DTC (Phase 3 runs)					
DTC145	0.65	4.3		dry	0.26	298	0.22	0.14	0.17 +_ 0.05
DTC171	0.59	4.1		dry	0.24	298	0.20	0.20	
DTC215	0.54	4.4		dry	0.23	299	0.11	0.13	
				CE-CERT DTC (Varied humidity)					
DTC183	0.57	4.2		~50%	0.23	298	0.25	0.32	0.25 +_ 0.05
DTC186	0.57	4.3		~20%	0.23	298	0.20	0.25	
DTC177	0.52	4.4		~100%	0.24	299	0.79	0.91	0.85 +_ 0.09
				CE-CERT DTC (New reactors - Runs for other programs)					
DTC228	0.28	1.5		dry	0.22	297	0.051	0.046	0.060 +_ 0.015
DTC236	0.26	3.5		dry	0.22	296	0.079	0.064	
				SAPRC XTC (Phase 2 runs)					
XTC085	0.55	3.8		dry	0.26	302	0.080		0.079 +_ 0.001
XTC098	0.57	4.0		dry	0.25	303	0.078		
				CE-CERT XTC (CTC) (Phase 3 runs) - Single reactor					
CTC013	0.45	3.0		dry	0.20	303	0.035		0.071 +_ 0.029
CTC020	0.26	3.6		dry	0.20	304	0.040		
CTC028	0.27	3.7		dry	0.20	304	0.051		
CTC031	0.26		85	dry	0.20	300	0.090		
CTC042	0.26	3.7		dry	0.20	301	0.113		
CTC045	0.46	3.6		dry	0.20	301	0.092		
CTC058	0.26	3.5		dry	0.20	299	0.103		
CTC061	0.23		85	dry	0.20	300	0.049		
CTC074	0.25	3.6		dry	0.20	297	0.062		
				CE-CERT XTC (CTC) (Phase 3 runs) - Dual reactors					
CTC084	0.25	3.9		dry	0.20	299	0.052	0.049	0.067 +_ 0.018
CTC090	0.26		89	dry	0.19	294	0.070	0.086	
CTC099	0.27	3.4		dry	0.19	295	0.070	0.108	
CTC114	0.24	3.6		dry	0.19	296	0.065	0.068	
CTC120	0.26	3.5		dry	0.19	294	0.040	0.054	
CTC135	0.26	3.4		dry	0.19	294	0.068	0.074	

all carried out under humidified conditions, are lower than radical source rates the CE-CERT DTC with this reactor, and are not significantly higher than those carried out under dry conditions in the other reactors.

The DTC runs carried out at ~50% RH had slightly higher radical source rates than the dry runs, though the difference is not significantly outside the run-to-run variability. On the other hand, the radical source in the ~100% RH run was factor of ~5 higher than measured in the dry runs. However, the results of model simulations of the ~100% RH propene runs, discussed below, were not consistent with this high radical source, suggesting that the ~100% RH n-butane run may be anomalous.

The radical source rates in the CTC chamber were very close to the ranges of values observed in the other chambers, except for the CE-CERT DTC runs with the reactor used in this program. There was no significant difference between the radical source in the single larger reactor or the dual smaller reactor systems. For that reason a single average RS/K1 value was used when modeling all the CTC runs for this report.

Other Characterization Results

Other characterization runs which were periodically carried out consisted of acetaldehyde - air irradiations to measure NO_x offgasing rates and O_3 dark decay runs to measure the wall loss rates. The acetaldehyde - air experiments are summarized on Table 7, which also shows the NO_x offgasing rate (normalized to the NO_2 photolysis rate — see Table 1) which fit the ozone formation rates in these experiments. The NO_x offgasing rates in the DTC appear to be the same in dry and 50% RH runs, and average 0.18±0.02 ppb x k_1. The CTC acetaldehyde - air run indicates a lower NO_x offgasing rate of 0.04 ppb x k_1. These NO_x offgasing rates are very close to the radical input rates in these chambers, suggesting that these both may be the manifestation of the same process. Jeffries (private communication) suggested that this may be due to HONO offgasing, which, because of the rapid photolysis of HONO, amounts to a radical source as well as a NO_x source. Preliminary calculations indicate that using this to represent these effects is also consistent with the characterization runs, though non-negligible amounts of initial HONO also have to be assumed to successfully simulate the n-butane - NO_x experiments. This alternative method for representing these effects will be evaluated further in conjunction with the evaluations of the fully updated SAPRC mechanism, which is beyond the scope of this report.

The results of the ozone decay experiments carried out for this program are summarized on Table 8. To allow for correction for dilution due to leakage (which was significant in the DTC but minor in the CTC), ~50 ppm CO was also added in most of these experiments, and its decay rate was also

Table 7. Summary of acetaldehyde - air characterization runs to measure NO_x offgasing rates.

Run	RH	k_1 (min^{-1})	T (K)	Acetald. (ppm)	Final O_3 (min)	Final O_3 (ppb)	E-NO_2/k_1 (ppb)
DTC185A	50% RH	0.233	299	0.48	390	54	0.17
DTC185B				0.49	380	57	0.20
DTC216A	dry	0.226	299	0.65	370	44	0.15
DTC216B				0.68	380	50	0.19
CTC019	dry	0.203	304	0.51	360	21	0.042

Table 8. Summary of ozone dark decay runs.

Run	RH	T (K)	O_3 (ppm)	Avg. Decay rate (% hr^{-1}) O_3	CO	O_3 (corr)	Notes
DTC126A	dry	295	0.35	0.5%	-	-	[a]
DTC126B			0.35	0.7%	-	-	
DTC221A	dry	295	0.87	1.7%	1.1%	0.7%	[b]
DTC221B	dry	295	0.90	3.7%	3.1%	0.6%	
CTC053	dry	292	0.82	0.5%	0.1%	0.4%	[c]
CTC106A	dry	288	0.63	0.7%	0.1%	0.6%	
CTC106B			0.62	0.6%	0.1%	0.5%	

[a] Decay rate increases with time, due to apparent leakage. Ozone decay rate computed for first 130 minutes only. No dilution data available, so this is an
[b] upper limit to true O3 decay rate.
[c] Data for t=1.5-6 hours, after decay rates stabilized.
Data for t=2-6 hours, after CO concentrations stabilized.

Table 7. Summary of acetaldehyde - air characterization runs to measure NO_x offgasing rates.

Table 8. Summary of ozone dark decay runs

monitored. The results indicated O_3 decay rates of ~6% $hour^{-1}$ in both chambers, which is well within the range observed previously for large Teflon bag reactors. Note that although the DTC during this period had higher than usual radical and NO_x input rates, the O_3 decay rates for these reactors was within the normal range. The effects of humidity on O_3 decay rates were not determined, but it should be noted that these decay rates are comparable to the average O_3 decay of ~0.9% $hour^{-1}$ determined at 50% RH in the SAPRC ITC (Carter and Lurmann, 1990; Carter et al. 1995b).

Pure air irradiations were also carried out periodically as controls for evaluating background effects. However, these runs are less useful for precise characterization of chamber-dependent parameters because they are sensitive both to background VOC and CO levels as well as to NO_x offgasing, meaning that no single parameter can be unambiguously determined by modeling them. The chronological run

listings on Tables 2 and 3 summarize their results. Generally, model simulations assuming NO_x input rates determined from the acetaldehyde - air runs were reasonably consistent with the results of these runs, and indicated no significant levels of background reactivity other than that attributable to the CO which was known to be present.

Results of Control Experiments

As indicated on Tables 2 and 3, a number of replicate propene - NO_x experiments were carried out to verify consistency of chamber conditions, and several aldehyde - NO_x and ethene - NO_x experiments were carried out in both the DTC and CTC for comparison with mechanism evaluation data in other chambers. An unusually large number of replicate propene runs were carried out in the DTC as part of the humidity effects and reproducibility study, and these are discussed in the following section. Table 9 summarizes the conditions and selected results of these experiments, excluding those which were carried out at variable humidity (which are discussed in the following section), or were judged to be unsuitable for modeling because of data or characterization problems, as noted in Tables 2 or 3. A number of these runs consisted of simultaneous irradiations of the same mixture in both sides of the chamber, and in all cases good side equivalency of the results were obtained. In those cases, only the run in Side A is included in the listing on Table 9.

Model simulations of these experiments using the SAPRC-93 mechanism indicated that the results were consistent with previous evaluation results using this mechanism (e.g., Carter et al. 1995c), and these results will not be discussed further here. These runs have been added to the data base for mechanism evaluation, and will be used in the upcoming evaluation of the updated version of the SAPRC mechanism, which will be described in a subsequent report.

Results of Humidity Effects and Reproducibility Study

A number of replicate propene - NO_x and toluene - NO_x experiments were carried out in the DTC to determine how varying the humidity affected the experimental results and reproducibility, and how it affected results of mechanism evaluations. One of the incentives for this study was to investigate the source of variability in the ability of the model to simulate replicate propene - NO_x experiments which are routinely carried out as controls in conjunction with our environmental chamber studies. While many experiments are well fit by the model, occasionally runs are carried out where the model performs poorly for no apparent reason. Therefore, this study involved an evaluation of reproducibility as well as humidity effects. Replicate toluene - NO_x as well as propene - NO_x runs were carried out to determine if different results are obtained for different chemical systems. As indicated on Table 2, typically these

Table 9. Summary of conditions and selected results of the single compound - NO_x control and mechanism evaluation experiments.

Run	T (K)	k_1 (min^{-1})	NO_x (ppm)	VOC (ppm)	Max O_3 (ppm)	Δ ([O_3]-[NO]) (ppm) 1 hr	2 hr	3 hr	5 hr
				Formaldehyde - NO_x [a]					
DTC149A	298	0.25	0.32	0.42	0.10	0.14	0.22	0.28	0.34
DTC218A	299	0.23	0.28	0.40	0.09	0.10	0.17	0.22	0.28
CTC016	303	0.20	0.24	0.82	0.34	0.15	0.26	0.34	0.46
CTC024	302	0.20	0.17	0.35	0.13	0.07	0.13	0.17	0.24
CTC077	299	0.20	0.16	0.29	0.11	0.07	0.12	0.16	0.22
CTC095A	294	0.19	0.26	0.42	0.05	0.06	0.12	0.16	0.22
CTC116A	296	0.19	0.24	0.36	0.04	0.06	0.12	0.16	0.21
CTC133A	296	0.19	0.26	0.38	0.06	0.07	0.13	0.17	0.23
				Acetaldehyde - NO_x					
DTC150A	298	0.25	0.14	1.67	0.25	0.09	0.15	0.20	0.29
CTC014	303	0.20	0.23	0.92	0.11	0.07	0.13	0.18	0.26
CTC015	303	0.20	0.24	0.90	0.09	0.06	0.12	0.17	0.24
CTC032	301	0.20	0.28	1.10	0.12	0.10	0.16	0.21	0.29
CTC072	298	0.20	0.26	1.03	0.09	0.09	0.15	0.20	0.27
				Ethene - NO_x					
CTC025	302	0.20	0.51	2.27	0.59	0.06	0.15	0.28	0.65
				Propene - NO_x					
DTC129A	299	0.29	0.47	0.96	0.74	0.21	0.51	0.87	1.08
DTC146A	298	0.26	0.51	1.05	0.67	0.13	0.36	0.67	1.07
DTC153A	297	0.25	0.51	1.07	0.71	0.15	0.41	0.79	1.11
DTC155B	298	0.25	0.10	0.38	0.30	0.06	0.18	0.32	0.39
DTC168A	299	0.24	0.52	1.15	0.71	0.18	0.49	0.91	1.12
DTC170B	299	0.24	0.51	1.08	0.67	0.20	0.53	0.94	1.10
DTC179B	299	0.24	0.50	1.18	0.66	0.19	0.50	0.91	1.07
DTC187A	299	0.23	0.57	1.09	0.73	0.13	0.35	0.67	1.15
DTC190A	299	0.23	0.57	1.16	0.74	0.17	0.47	0.90	1.18
DTC205A	299	0.23	0.57	1.06	0.71	0.16	0.41	0.77	1.15
CTC012	302	0.20	0.42	0.77	0.57	0.06	0.18	0.34	0.78
CTC018	303	0.20	0.47	0.97	0.72	0.09	0.25	0.54	1.00
CTC023	301	0.20	0.50	1.10	0.74	0.11	0.32	0.72	1.08
CTC049	301	0.20	0.50	1.15	0.64	0.14	0.38	0.82	1.00
CTC059	300	0.20	0.49	1.07	0.67	0.08	0.26	0.54	1.00
CTC078	298	0.20	0.47	1.13	0.71	0.11	0.30	0.61	1.04
CTC083A	298	0.20	0.51	1.22	0.69	0.10	0.26	0.50	1.01
CTC086A	295	0.20	0.44	1.18	0.70	0.09	0.28	0.59	1.02
CTC086B	295	0.20	0.44	1.20	0.69	0.11	0.30	0.63	1.03
CTC102A	295	0.19	0.49	1.10	0.60	0.10	0.25	0.48	0.93
CTC115A	295	0.19	0.47	1.12	0.62	0.09	0.23	0.44	0.93
CTC132A	293	0.19	0.49	1.13	0.65	0.10	0.26	0.50	0.96

[a] Only Side A run is listed if the run had the same mixture irriadiated on both sides and showed good side equivalency.

involved carrying out simultaneous toluene - NO_x and propene - NO_x experiments in the two DTC reactors.

The conditions and results of the replicate propene - NO_x and toluene - NO_x experiments are summarized on Tables 10 and 11, respectively. These tables give the conditions, measured initial reactant concentrations, maximum O_3, and hourly change in ($[O_3]$-[NO]) for each experiment. Averages are also shown for all runs of the same type, and Figure 4 shows plots of the average d(O_3-NO) data for the various types of experiments.

Tables 10 and 11 indicate that the amounts of ozone formation and NO oxidation in given type or run were reproducible to within 5 ppb or better, or ~5% by the end of the run. There appeared to be no significant effect of variations on how long the chamber was flushed with humidified or dry air prior the run, nor were there significant differences in dry runs following a series of humidified runs. Some irreproducibility was observed in the ability of the model to simulate some of the individual propene runs, and this was the main reason a large number of replicates were carried out for this study. However, this apparent irreproducibility was concluded to be an artifact due to measurement error, and not a real chamber effect. In particular, the runs where the model performed poorly were DTC158-161, where the initial measured propene was ~30-40% less than the other replicate runs, despite the fact that there was no known differences in the amounts of propene gas injected, and that the ozone formation and NO oxidation rates were also essentially the same. Once these runs are rejected from model evaluation set, no significant inconsistencies between model simulations and experimental results are observed.

The data on Tables 10 and 11 and Figure 4 indicate that humidity has very little effect on NO oxidation and O_3 formation rates in the 0 - 50% RH range. However, as the humidity is increased to near 100%, there is a significant reduction in the maximum O_3 yields in both the propene - NO_x and the toluene - NO_x systems. On the other hand, the initial NO oxidation and O_3 formation rates are not significantly affected. The latter observation suggests that the chamber radical source is not playing a large role in these humidity effects, at least for this particular set of reaction bags.

Results of model simulations of the averaged conditions of the propene and toluene experiments are also shown on Figure 4. These simulations use the same initial reactant concentrations, but the appropriate $[H_2O]$ levels and chamber effects parameters for the different humidities. The main chamber effect parameter which was varied was the radical input rates (RS/K1), which were derived based on modeling the n-butane runs as discussed above (see Table 6). (The updated aromatics mechanism, described later in this report, was used in the toluene - NO_x simulations.) The model simulations are

Table 10. Conditions and selected results of the replicate propene - NO_x experiments carried out in the humidity effects and reproducibility study.

Run	Note	T	k_1	Propene	NO_x	D ($[O_3]$ - [NO]) (ppm)					Maximum (ppm)		
		(K)	(min^{-1})	(ppm)	(ppm)	t=1	t=2	t=3	t=5	t=6	O_3	Formald.	Acetald.
						Dry Runs							
DTC128A		299	0.29	0.89	0.48	0.19	0.45	0.79	1.08	1.10	0.73	0.46	0.35
DTC128B		299	0.29	0.87	0.49	0.20	0.47	0.80	1.08	1.10	0.73	0.48	0.34
DTC129A		299	0.29	0.96	0.47	0.21	0.51	0.87	1.08		0.74	0.46	0.49
DTC129B		299	0.29	0.94	0.47	0.21	0.51	0.86	1.07		0.73	0.48	0.45
DTC146A		298	0.26	1.05	0.51	0.13	0.36	0.67	1.07	1.10	0.67	0.47	0.47
DTC146B		298	0.26	1.04	0.52	0.14	0.38	0.69	1.05	1.08	0.64	0.47	0.43
DTC153A		297	0.25	1.07	0.51	0.15	0.41	0.79	1.11	1.10	0.71	0.47	0.57
DTC158B		298	0.25	(0.73) [a]	0.51	0.16	0.48	0.90	1.11	1.09	0.72	0.53	0.44
DTC159A		298	0.25	(0.69) [a]	0.51	0.19	0.50	0.92	1.12	1.09	0.72	0.54	0.45
DTC169A		299	0.24	1.15	0.55	0.16	0.44	0.87	1.15	1.14	0.73	0.50	0.60
DTC170B		299	0.24	1.08	0.51	0.20	0.53	0.94	1.10	1.07	0.67	0.48	0.58
DTC178B		299	0.24	1.01	0.53	0.14	0.40	0.75			0.63	0.48	0.48
DTC179B		299	0.24	1.18	0.50	0.19	0.50	0.91	1.07	1.06	0.66	0.48	0.50
DTC187B		299	0.23	1.04	0.59	0.14	0.38	0.71	1.15	1.17	0.70	0.50	0.36
DTC190A		299	0.23	1.16	0.57	0.17	0.47	0.90	1.18	1.15	0.74	0.58	0.45
DTC205A		299	0.23	1.06	0.57	0.16	0.41	0.77	1.15		0.71	0.53	0.52
DTC205B		299	0.23	1.11	0.60	0.18	0.45	0.81	1.15	1.16	0.68	0.52	0.54
DTC168A	[b]	299	0.24	1.15	0.52	0.18	0.49	0.91	1.12	1.10	0.71	0.49	0.56
DTC178A	[c]	299	0.24	1.03	0.52	0.15	0.40	0.75			0.67	0.49	0.54
DTC187A	[b]	299	0.23	1.09	0.57	0.13	0.35	0.67	1.15	1.19	0.73	0.53	0.40
Average		298.6	0.25	1.04	0.52	0.17	0.45	0.81	1.11	1.11	0.70	0.49	0.47
St.Dev		0.5	0.02	0.09	0.04	0.03	0.05	0.08	0.04	0.04	0.03	0.03	0.08
Rel.St.Dev			9%	9%	8%	15%	12%	10%	4%	3%	5%	7%	17%
						~50% RH Runs							
DTC160A		298	0.25	(0.64) [a]	0.49	0.21	0.48	0.81	1.02	1.01	0.63	0.35	0.40
DTC160B		298	0.25	(0.64) [a]	0.50	0.19	0.44	0.80	1.05	1.03	0.65	0.35	0.39
DTC161A		298	0.24	(0.63) [a]	0.50	0.17	0.40	0.72	1.02	1.02	0.62	0.35	0.36
DTC161B		298	0.24	(0.63) [a]	0.50	0.18	0.43	0.77	1.03	1.04	0.63	0.34	0.35
DTC162A		299	0.24	1.05	0.51	0.14	0.35	0.65	1.07	1.11	0.69	0.40	0.54
DTC162B		299	0.24	1.04	0.52	0.14	0.36	0.67	1.05	1.10	0.67	0.36	0.51
DTC163A		299	0.24	1.09	0.48	0.17	0.43	0.80	1.03	1.01	0.65	0.39	0.49
DTC164B		299	0.24	1.10	0.52	0.19	0.49	0.90	1.10	1.09	0.70	0.43	0.50
DTC166A		299	0.24	1.15	0.50	0.17	0.44	0.82	1.04	1.02	0.64	0.39	0.50
DTC167B		299	0.24	1.13	0.50	0.23	0.57	0.91	1.02	0.98	0.63	0.38	0.48
DTC182A		298	0.23	1.15	0.61	0.18	0.45	0.78	1.14	1.16	0.69	0.43	0.44
DTC182B		298	0.23	1.12	0.62	0.20	0.48	0.79	1.10	1.12	0.63	0.40	0.37
DTC172A	[d]	298	0.24	1.13	0.48	0.24	0.56	0.90	1.01	0.98	0.61	0.38	0.55
DTC173B	[d]	298	0.24	1.20	0.51	0.28	0.63	0.93	0.99		0.59	0.37	0.52
Average		298.5	0.24	1.10	0.53	0.18	0.44	0.78	1.06	1.06	0.65	0.40	0.48
St.Dev		0.6	0.00	0.04	0.05	0.03	0.06	0.08	0.04	0.05	0.03	0.02	0.05
Rel.St.Dev			2%	4%	10%	14%	13%	10%	4%	5%	4%	6%	11%
						~100% RH Runs							
DTC175A		299	0.24	1.07	0.50	0.22	0.46	0.72	0.91	0.88	0.50	0.33	0.50
DTC175B		299	0.24	1.05	0.51	0.24	0.50	0.76	0.94	0.92	0.52	0.31	0.46
DTC176A		299	0.24	1.14	0.46	0.25	0.54	0.80	0.80	0.76	0.47	0.33	0.52
Average		298.8	0.24	1.08	0.49	0.23	0.50	0.76	0.88	0.85	0.50	0.32	0.50
St.Dev		0.3	0.00	0.05	0.02	0.02	0.04	0.04	0.07	0.09	0.02	0.01	0.03
Rel.St.Dev			0%	5%	5%	7%	7%	5%	8%	10%	4%	3%	6%

[a] Measured initial reactant was inconsistent with the amount injected. Run not modelable. Data not used to compute average.

[b] Follows series of humidified runs.

[c] Flushed with ~100% RH air overnight, then filled with dry air.

[d] Dry flush overnight, then chamber flushed with humidified air immediately prior to run.

Table 11. Conditions and selected results of the replicate toluene - NOx experiments carried out in the humidity effects and reproducibility study.

Run	Note	T	k_1	Toluene	NO_x	D ($[O_3]$ - [NO]) (ppm)					Maximum (ppm)	
		(K)	(min^{-1})	(ppm)	(ppm)	t=1	t=2	t=3	t=5	t=6	O_3	Formald.
						Dry Runs						
DTC153B		297	0.250	2.64	0.51	0.11	0.47	0.79	0.83	0.79	0.47	0.058
DTC158A		298	0.246	2.49	0.50	0.07	0.41	0.71	0.83	0.79	0.48	0.064
DTC169B		299	0.240	2.82	0.56	0.17	0.54	0.83	0.78		0.42	0.059
DTC170A		299	0.239	2.52	0.49	0.09	0.42	0.74	0.86	0.81	0.47	0.064
DTC179A		299	0.235	2.26	0.51	0.07	0.38	0.70	0.87	0.82	0.48	0.068
DTC190B		299	0.232	2.36	0.58	0.11	0.44	0.76	0.89	0.85	0.48	0.066
DTC168B	[a]	299	0.240	2.42	0.53	0.13	0.48	0.79	0.80	0.76	0.43	0.063
Average		298.6	0.24	2.50	0.53	0.11	0.45	0.76	0.84	0.80	0.46	0.063
St.Dev		0.6	0.01	0.19	0.03	0.03	0.05	0.05	0.04	0.03	0.02	0.003
Rel.St.Dev			3%	7%	6%	32%	12%	6%	5%	4%	5%	0.054
						~50% RH Runs						
DTC164A		299	0.242	2.57	0.50	0.10	0.41	0.71	0.79	0.75	0.44	0.055
DTC166B		299	0.241	2.61	0.52	0.13	0.45	0.72	0.77	0.74	0.41	0.046
DTC167A		299	0.241	2.45	0.50	0.12	0.44	0.72	0.78	0.74	0.43	0.043
DTC172B	[b]	298	0.238	2.48	0.49	0.22	0.53	0.74	0.74	0.71	0.37	0.050
Average		298.8	0.24	2.53	0.50	0.15	0.46	0.72	0.77	0.73	0.41	0.048
St.Dev		0.5	0.00	0.08	0.01	0.05	0.05	0.01	0.02	0.02	0.03	0.005
Rel.St.Dev			1%	3%	2%	36%	11%	2%	3%	3%	7%	0.110
						~100% RH Run						
DTC176B		299	0.237	2.25	0.48	0.19	0.44	0.61	0.69	0.65	0.32	0.038

[a] Follows series of humidified runs.

[b] Dry flush overnight, then chamber flushed with humidified air immediately prior to run.

Table 11. Conditions and selected results of the replicate toluene - NO_x experiments carried out in the humidity effects and reproducibility study.

consistent with the results of the dry and 50% RH runs that they predicted very little effect of humidity in this range, and gave good simulations to the results of the propene runs. The simulations of the dry and ~50% RH toluene runs were not quite as good as the simulations of the propene runs, but the discrepancies in the middle part of the runs are more likely due to deficiencies in the toluene mechanism than to poorly characterized chamber or humidity effects.

The model does not perform nearly as well in simulating the ~100% RH experiments as it does for the dry or moderate RH runs. The simulations using the high radical source rate indicated by the one ~100% RH n-butane run (DTC177) significantly overpredict the initial NO oxidation and O_3 formation rates in the experiments with both propene and toluene. This suggests that the high radical source indicated in DTC177 may be an anomaly which is not applicable to the ~100% RH propene and toluene runs. Much better predictions of initial NO oxidation and O_3 formation rates in the ~100% RH propene and toluene runs are obtained if the same radical source is used as when modeling the ~50% RH runs,

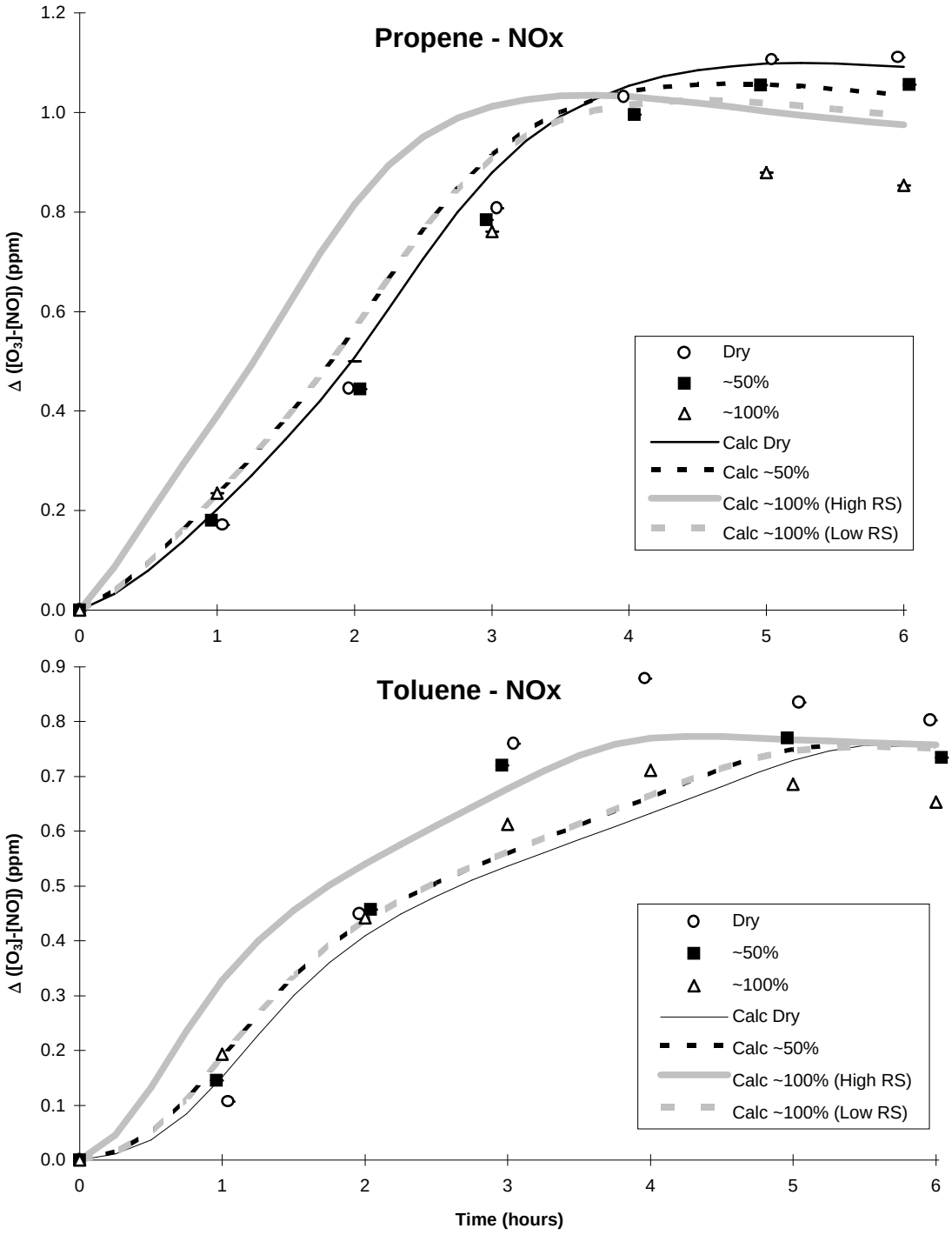

Figure 4. Experimental and calculated concentration - time plots of average $\Delta([O_3]-[NO])$ data in the replicate propene - NO_x and toluene - NO_x experiments carried out in the humidity effects and reproducibility study.

as indicated by the curves on Figure 4 indicated "Low RS". However, those simulations do not correctly predict the reduction in peak O_3 yields observed at ~100% RH in both the propene and toluene runs, relative to the corresponding runs at lower humidities. Therefore, whatever is causing this peak O_3 suppression at high RH is not being correctly represented in the chamber model.

The most obvious humidity-dependent process which can cause suppressed peak O_3 yields at higher humidities is the reaction

$$N_2O_5 + H_2O \rightarrow\rightarrow 2\ HNO_3 \qquad (4)$$

This reaction has the effect of reducing peak O_3 yields in the experiments where the peak O_3 is NO_x-limited (such as both the propene and toluene runs used in this study) because it acts as an effective NO_x sink. In the mechanism used in this work, Reaction (4) is assumed to have both a gas-phase and a heterogeneous component, with the gas-phase $k_4 = 1.0 \times 10^{-21}$ cm^3 $molec^{-1}$ s^{-1} (Tuazon et al. 1983; Carter, 1990), and the humidity-dependent component of the heterogeneous process is assumed to be negligible in Teflon bag reactors (see Table 1, above). If this reaction were enhanced by humidity to a greater extent than assumed in this model, it might account for the observed suppression of peak O_3 at the highest humidities.

However, model calculations where k_4 is varied indicate that this reaction cannot account for the observed O_3 suppression. If k_4 is adjusted to fit the peak O_3 in the ~100% RH runs (i.e., increased to ~8.0×10^{-21}), the model tends to underpredict the peak O_3 (i.e., overpredict the humidity suppression of O_3) in the ~50% RH runs. Thus if this were the cause of the effect, the reaction must have a higher than first order dependence in H_2O. Perhaps more significantly, it was found that, in contrast to the propene - NO_x runs, the peak O_3 in the toluene - NO_x experiments are quite insensitive to reasonable variations in k_4. In particular, using the increased k_4 which fits the O_3 yields in the ~100% RH propene runs has almost no effect on predicted O_3 formation in the ~100% RH toluene - NO_x experiments. Therefore, the suppression in the peak O_3 yield in the ~100% RH toluene runs cannot be caused by this process.

Table 10 also shows the maximum formaldehyde and acetaldehyde concentrations observed in the propene experiments, and the maximum formaldehyde in the toluene runs is shown on Table 11. It can be seen that while humidity has no apparent effect on the acetaldehyde yields in the propene runs, increasing the humidity measurably increases the formaldehyde in both the propene and toluene systems. This is also shown on Figure 5, which shows all the experimental formaldehyde plots in the propene and toluene runs, together with the formaldehyde profiles calculated with the averaged conditions dry and

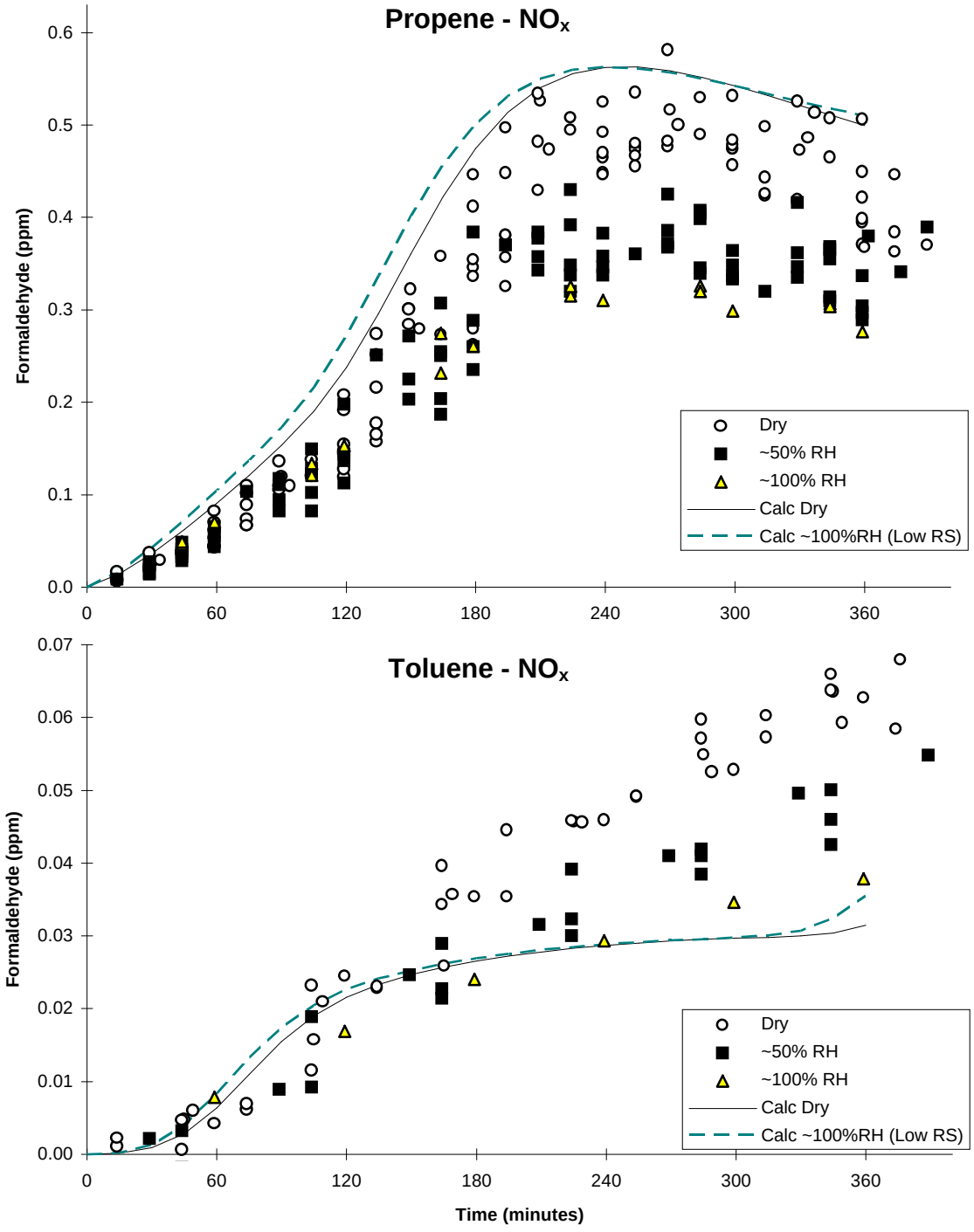

Figure 5. Experimental and calculated concentration - time plots of the formaldehyde data in the replicate propene - NO_x and toluene - NO_x experiments carried out in the humidity effects and reproducibility study.

100% RH model. (The 100% RH model used the lower radical source which gave the better fits to the O_3 formation and NO oxidation data.) Figure 4 shows that the apparent reduction in formaldehyde yields due to humidity is not predicted by the model for either system.

Additional information is required before it can be determined if the apparent reduction in formaldehyde formation with increasing humidity reflects a gas-phase process or some chamber or analytical process. If it is a gas-phase process, it would probably have to be due to some water-induced loss process for formaldehyde rather than humidity affecting its formation rate from the precursor molecules, since a similar suppression is observed in both the formaldehyde and toluene systems. One possibility in this regard would be water involvement in the reactions of formaldehyde with HO_2, which is believed to primarily involve the following equilibrium process,

$$HCHO + HO_2 \rightarrow [HOOCH_2O\cdot] \rightarrow HOCH_2OO\cdot$$
$$HOCH_2OO\cdot \rightarrow HO_2 + HCHO$$

resulting in no net reaction under atmospheric conditions (see Atkinson et al. 1996, and references therein). However, it is possible that $HOCH_2OO\cdot$ may react with water via

$$HOCH_2OO\cdot + H_2O \rightarrow \begin{array}{l} O..O..H \\ | \quad : \\ HOC..H..OH \end{array} \rightarrow HC(O)OH + HO. + H_2O \qquad (5)$$

which would result in a net loss of formaldehyde around the latter periods of the runs. A value of $k_4 \approx 10^{-16}$ cm^3 $molec^{-1}$ s^{-1} would account for the observed effects of humidity on the formaldehyde yields in these experiments.

A more likely explanation for the apparent effect of humidity on formaldehyde yields is loss of formaldehyde on the sampling lines. Modeling ~50% RH formaldehyde - NO_x runs carried out in the SAPRC EC or ITC provides no indication that formaldehyde wall losses are significant (Carter and Lurmann, 1990, 1991; Carter et al. 1995c). However, the formaldehyde sampling procedures used in the earlier studies did not involve sampling lines as long as those employed for formaldehyde monitoring in these DTC experiments. A negative humidity interference in the formaldehyde analysis is considered to be unlikely because the sampling method involves dissolving formaldehyde into a water solution through a semi-permeable membrane (Carter et al. 1995a,b). We will be investigating the possibility of these artifacts further in conjunction with our ongoing environmental chamber studies of reactivities of methanol and other alternative fueled vehicle exhausts (Carter, 1995b).

Xenon Arc Chamber Incremental Reactivity Experiments

To assess the effects of light source on incremental reactivity data and mechanism evaluation results, one component of this program consisted of carrying out incremental reactivity experiments for selected representative compounds in the xenon arc chamber. The compounds studied included carbon monoxide, n-octane, propene, toluene, m-xylene, and formaldehyde. The CO, n-octane, propene, toluene, and m-xylene experiments were conducted using both the mini-surrogate employed in the Phase 1 study (Carter et al. 1993a, 1995d) and the full surrogate employed in Phase 2 (Carter et al. 1995a), while the formaldehyde experiments employed only the full surrogate, and the one acetaldehyde experiment employed the mini-surrogate. All experiments used relatively low ROG/NO_x "maximum reactivity" conditions, since previous studies showed that results of reactivity experiments under those conditions are the most sensitive to mechanism differences.

The conditions and selected results of these experiments are summarized on Table 12, concentration-time plots for the d(O_3-NO) and m-xylene data in the base case experiments are shown on Figures 6 and 7, respectively, and plots of reactivity results for the various compounds studied are shown on Figures 8-14. Results of model simulations of these data are also shown on these figures.

Table 12 and Figures 6 and 7 show that good reproducibility was obtained for the base case experiments, except for the base case for the mini-surrogate propene run CTC142, where lower than the usual amounts of m-xylene and n-hexane were used due to a reactant injection error. Figure 8 shows that the addition of CO had a positive effect on d(O_3-NO) and a very small negative effect on integrated OH radical levels, as measured by the consumption rates of m-xylene. The positive effect on d(O_3-NO) is due to the single NO to NO_2 conversion in its reactions, and the small effect on radicals is expected because it has no significant radical sources or sinks in its mechanism. Figure 9 shows that the effect of n-octane depended significantly on which ROG surrogate was used, being small and mostly positive for the full surrogate, but had a large negative effect on OH radical levels regardless of which surrogate was used. This is consistent with previous results, and is explained by the fact that n-octane has very negative indirect reactivities due to its strong radical inhibiting processes caused by organic nitrate formation, which are balanced by strong positive direct reactivity effects due to the multiple NO to NO_2 conversions which occur in its oxidation, with the relative importances of these two effects being affected by the nature of the ROG surrogate employed (Carter et al. 1995a). Figures 10-13 show that propene, toluene, m-xylene, and formaldehyde have a positive effect on d(O_3-NO) and OH radicals with both surrogates, which is attributed to the fact that all of these compounds have radical sources in their mechanisms. The effect on radicals was quite small in the propene mini-surrogate run, because the O_3 + propene run is a major radical source in that system, and very little O_3 formation occurred in that run

Table 12. Summary of conditions and selected results of the incremental reactivity experiments carried out in the xenon arc chamber.

Run	Surg Type	Initial Reactants (ppm) NOx	Surg	Test VOC	t=2 Δ ([O_3]-[NO]) (ppm) Base	Test	IR	t=5 Δ ([O_3]-[NO]) (ppm) Base	Test	IR	t=5 IntOH (10^{-6} min) Base	Test	IR
							Carbon Monoxide						
CTC105A	Mini [a]	0.30	5.31	89	0.11	0.18	0.0009 ± 0.0001	0.41	0.58	0.0019 ± 0.0002	15.5	13.2	-0.026 ± 0.017
CTC123B	Full [b]	0.40	5.72	89	0.35	0.53	0.0020 ± 0.0002	0.58	0.84	0.0029 ± 0.0003	21.6	19.9	-0.020 ± 0.017
							n-Octane						
CTC110A	Mini	0.30	5.23	0.34	0.11	0.08	-0.108 ± 0.012	0.45	0.35	-0.30 ± 0.05	16.7	11.2	-16 ± 5
CTC131B	Full	0.39	5.67	1.07	0.33	0.32	-0.018 ± 0.013	0.58	0.63	0.05 ± 0.02	21.7	12.8	-8.4 ± 1.5
							Propene						
CTC142A	Mini	0.37	3.47	0.14	0.06	0.09	0.22 ± 0.02	0.25	0.35	0.69 ± 0.09	8.6	10.3	12 ± 11
CTC130A	Full	0.39	5.53	0.41	0.32	0.52	0.48 ± 0.05	0.57	0.83	0.65 ± 0.08	21.9	26.6	11 ± 4
							Toluene						
CTC108A	Mini	0.31	4.99	0.48	0.10	0.19	0.192 ± 0.014	0.40	0.65	0.51 ± 0.05	14.7	23.7	19 ± 3
CTC127A	Full	0.39	5.30	0.73	0.33	0.46	0.17 ± 0.02	0.54	0.71	0.23 ± 0.04	19.3	26.1	9 ± 2
							m-Xylene						
CTC109B	Mini	0.31	4.92	0.081	0.11			0.43	0.63	2.4 ± 0.3	16.6	22.3	71 ± 20
CTC128B	Full	0.41	5.86	0.076	0.35	0.43	1.1 ± 0.2	0.60	0.75	2.0 ± 0.4	21.2	25.3	54 ± 21
							Formaldehyde						
CTC138A	Full	0.40	5.61	0.27	0.34	0.42	0.30 ± 0.06	0.58	0.69	0.40 ± 0.10	21.7	24.4	10 ± 6
CTC140B	Full	0.36	5.64	0.31	0.30	0.39	0.27 ± 0.05	0.55	0.66	0.34 ± 0.08	21.5	25.5	13 ± 5
							Acetaldehyde						
CTC107B	Mini	0.31	5.22	0.56	0.10	0.18	0.136 ± 0.011	0.43	0.37	-0.10 ± 0.03	15.3	7.8	-13 ± 3

[a] The mini-surrogate consisted of n-hexane (0.4 ppm), ethene (0.7 ppm) and m-xylene (0.14 ppm). N-hexane and m-xylene in run CTC142 were somewhat lower, being 0.25 ppm and 0.08 ppm, respectively.

[b] The full surrogate consisted of n-butane (~0.5 ppm), n-octane (~0.13 ppm), ethene (~0.09 ppm), propene (~0.07 ppm), trans-2-butene (~0.07 ppm), toluene (~0.12 ppm), m-xylene (~0.12 ppm), and formaldehyde (0.10 ppm).

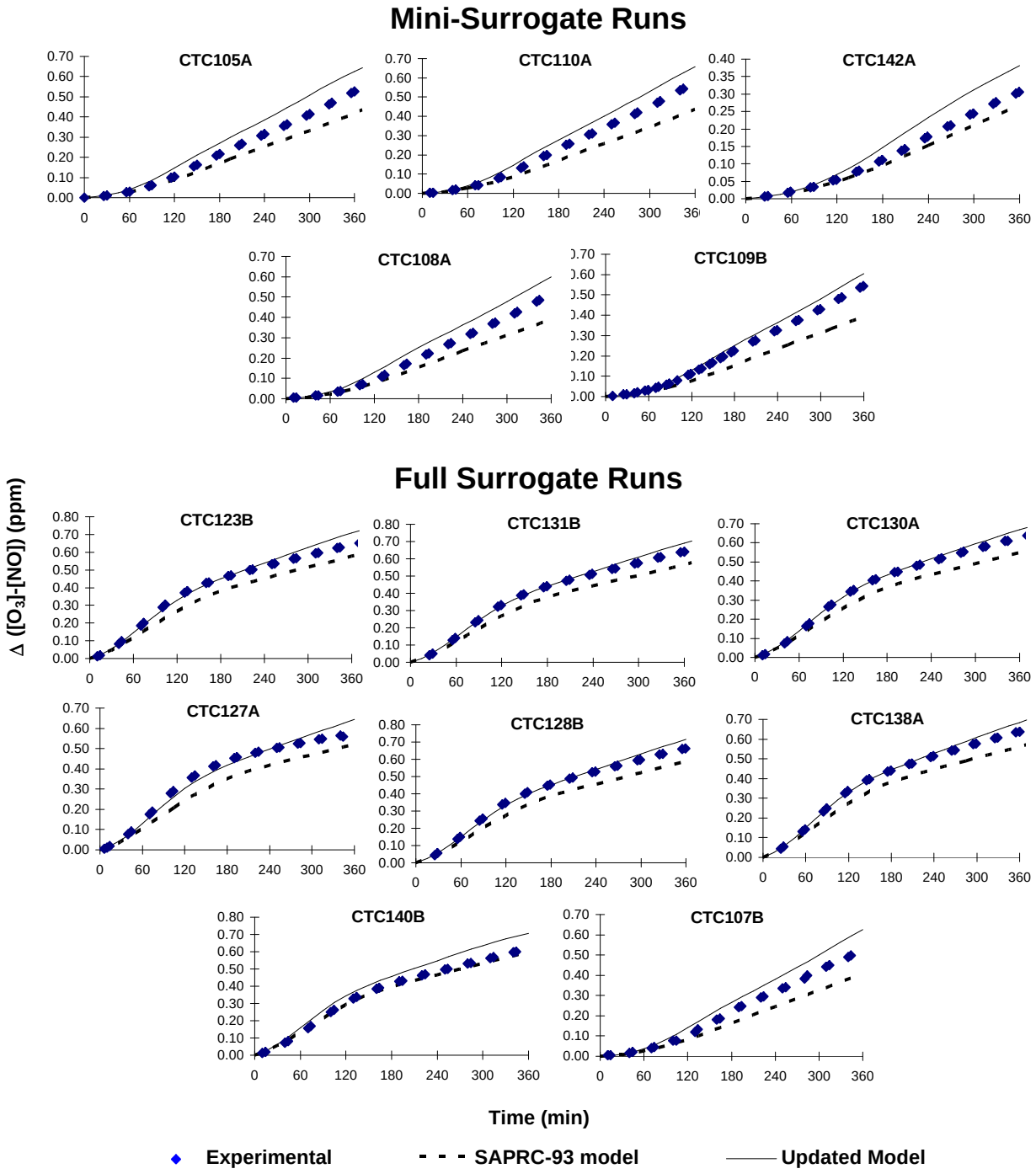

Figure 6. Plots of experimental and calculated $\Delta([O_3]-[NO])$ data in the base case surrogate - NO_x runs carried out in the xenon arc chamber.

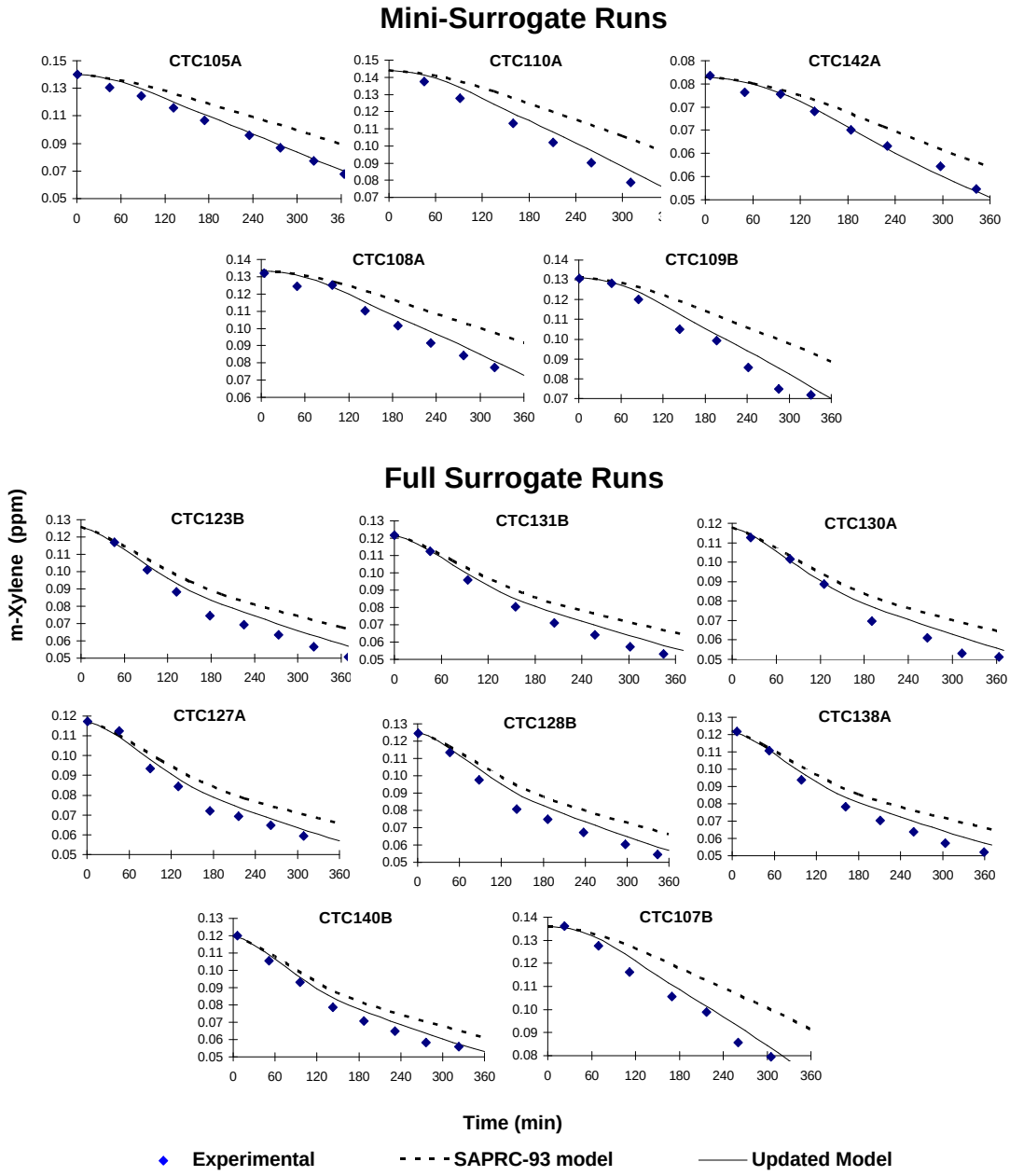

Figure 7. Plots of experimental and calculated m-xylene data in the base case surrogate - NO_x runs carried out in the xenon arc chamber.

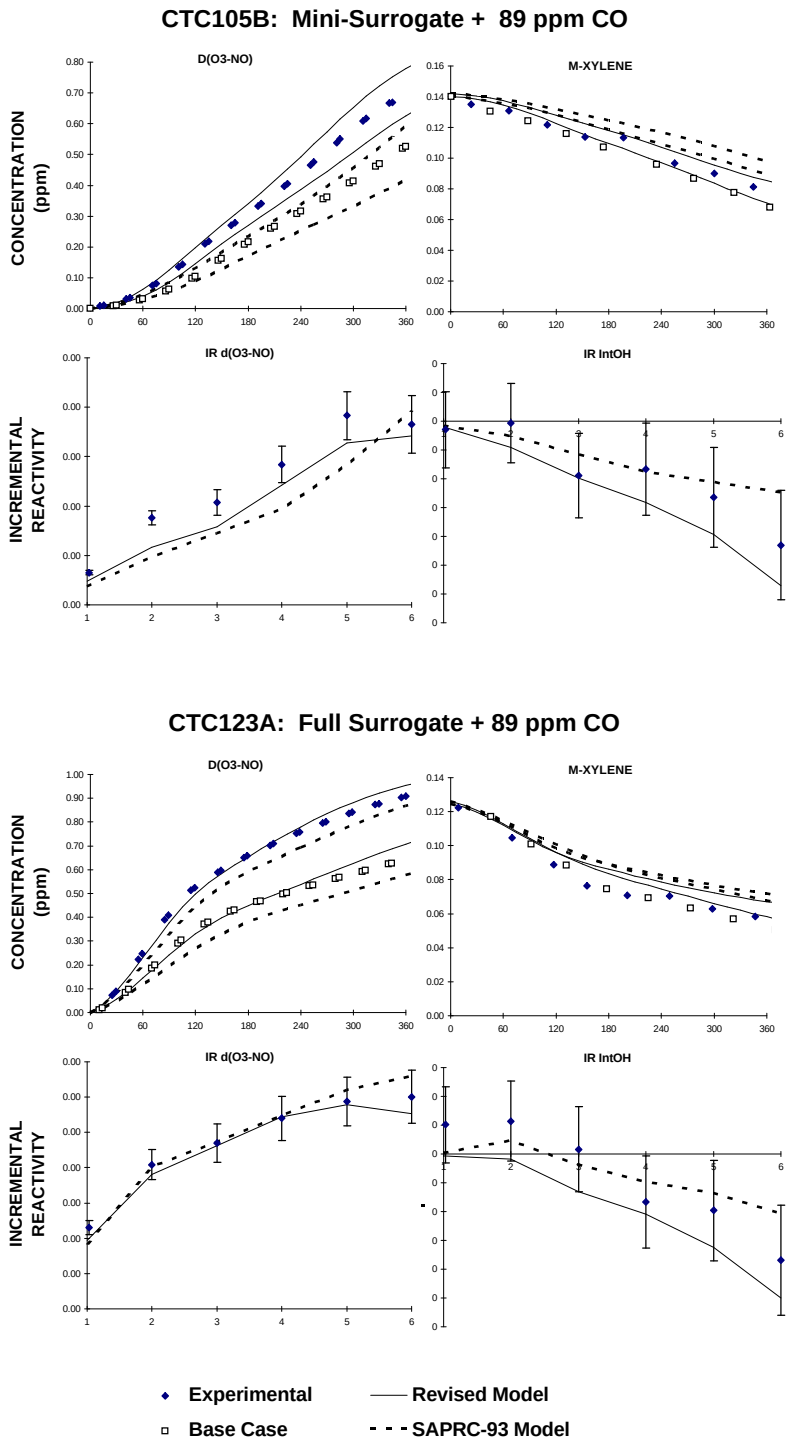

Figure 8. Plots of experimental and calculated incremental reactivity for carbon monoxide from xenon arc experiments carried out for this program.

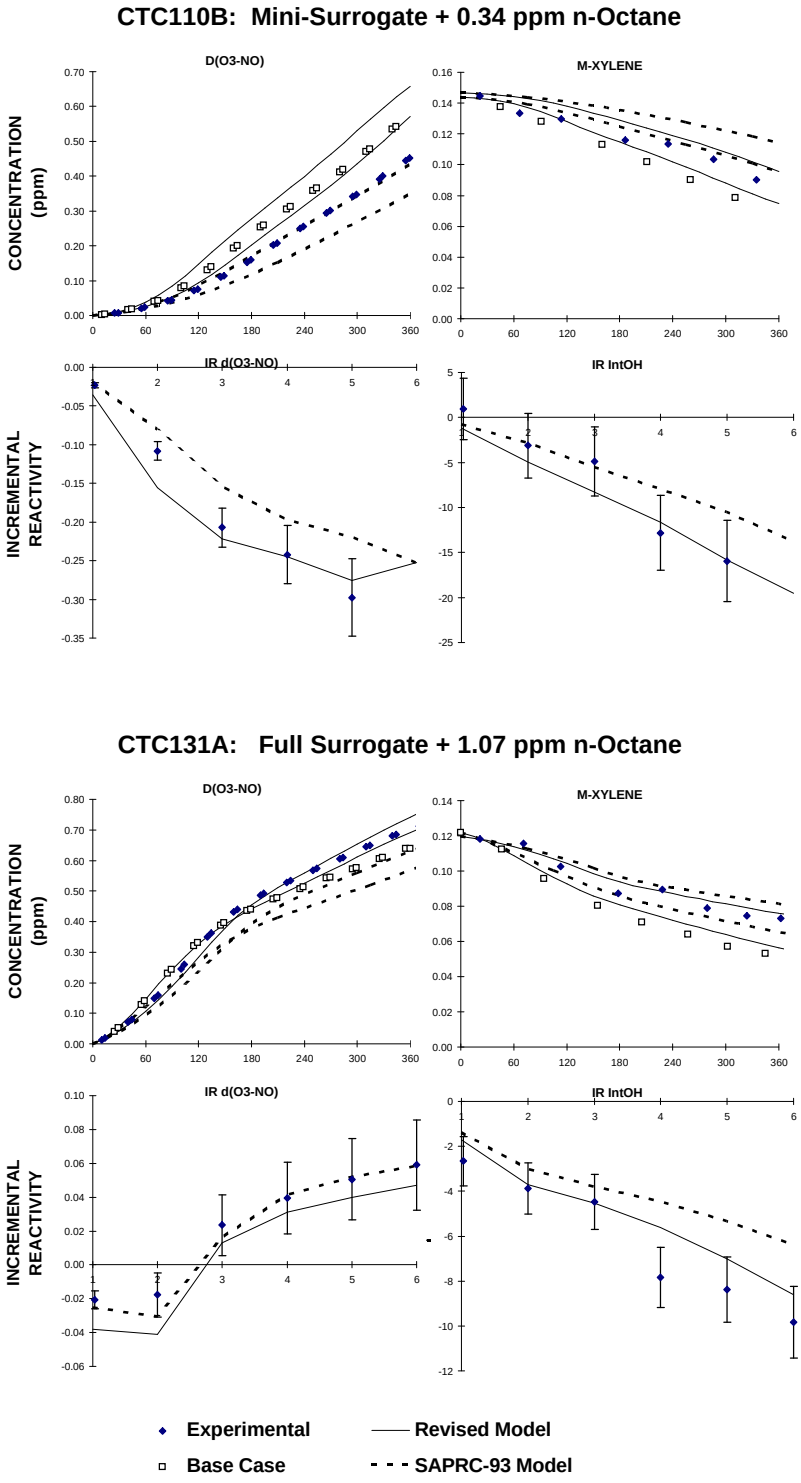

Figure 9. Plots of experimental and calculated incremental reactivity for n-octane from xenon arc experiments carried out for this program.

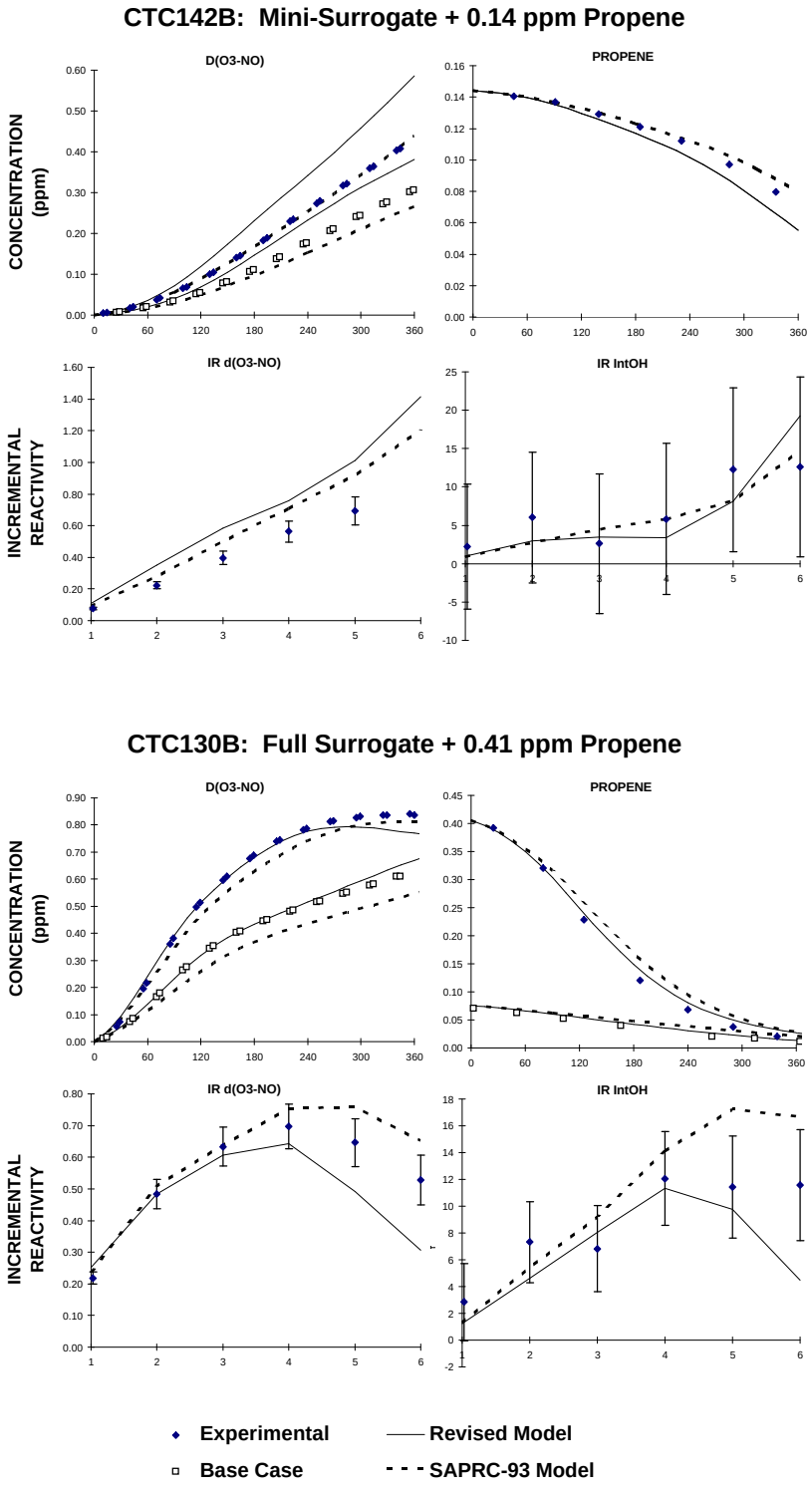

Figure 10. Plots of experimental and calculated incremental reactivity for propene from xenon arc experiments carried out for this program.

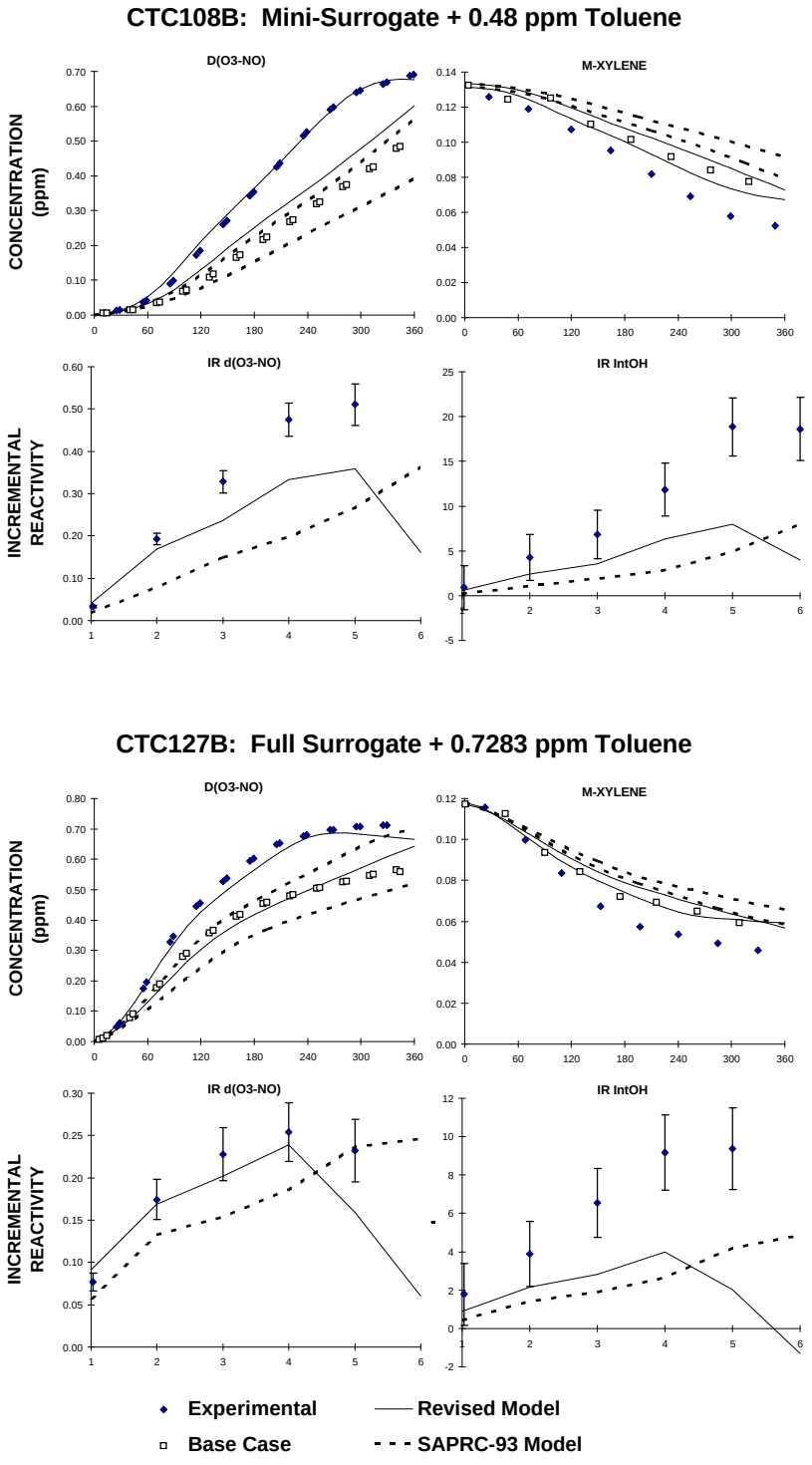

Figure 11. Plots of experimental and calculated incremental reactivity for toluene from xenon arc experiments carried out for this program.

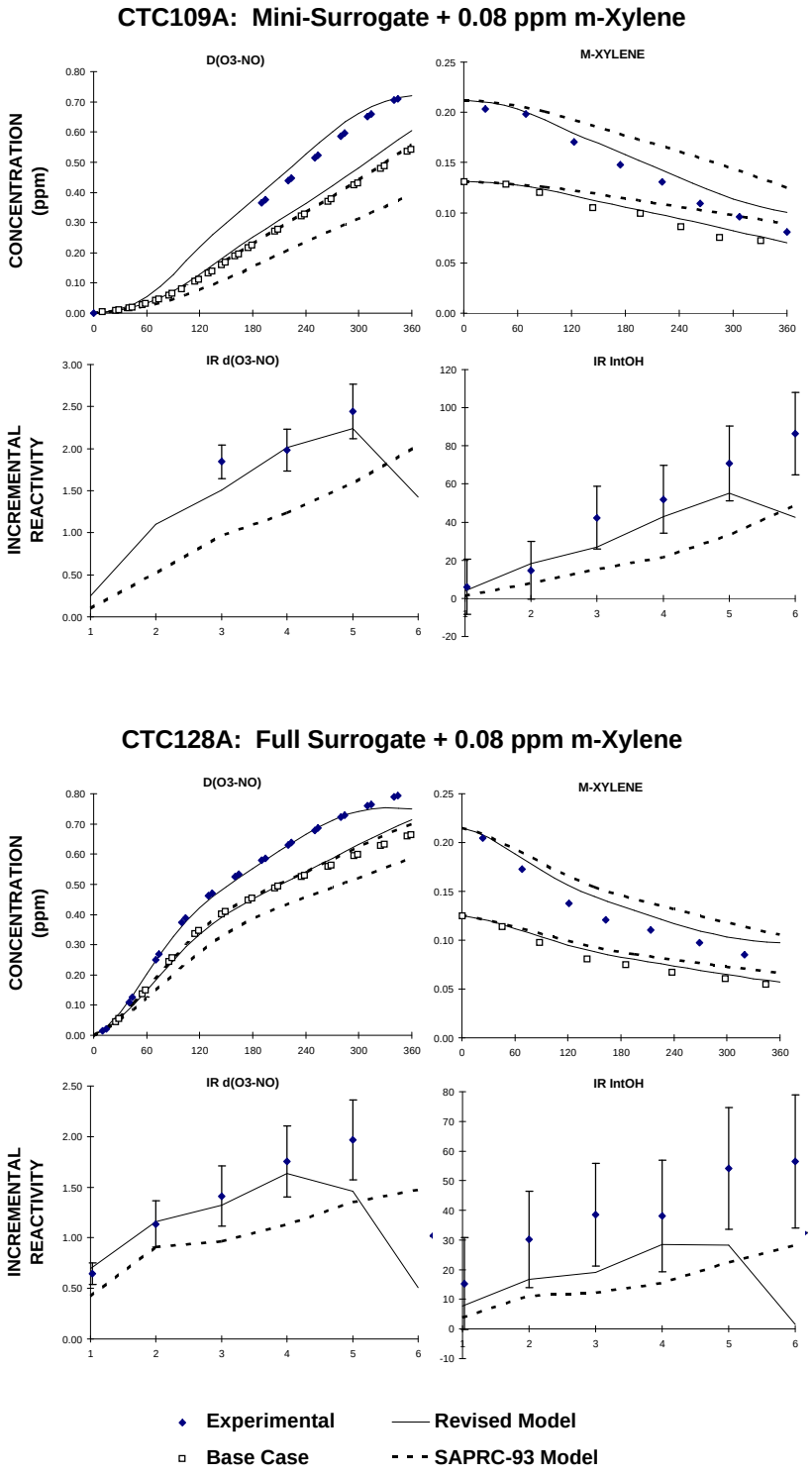

Figure 12. Plots of experimental and calculated incremental reactivity for m-xylene from xenon arc experiments carried out for this program.

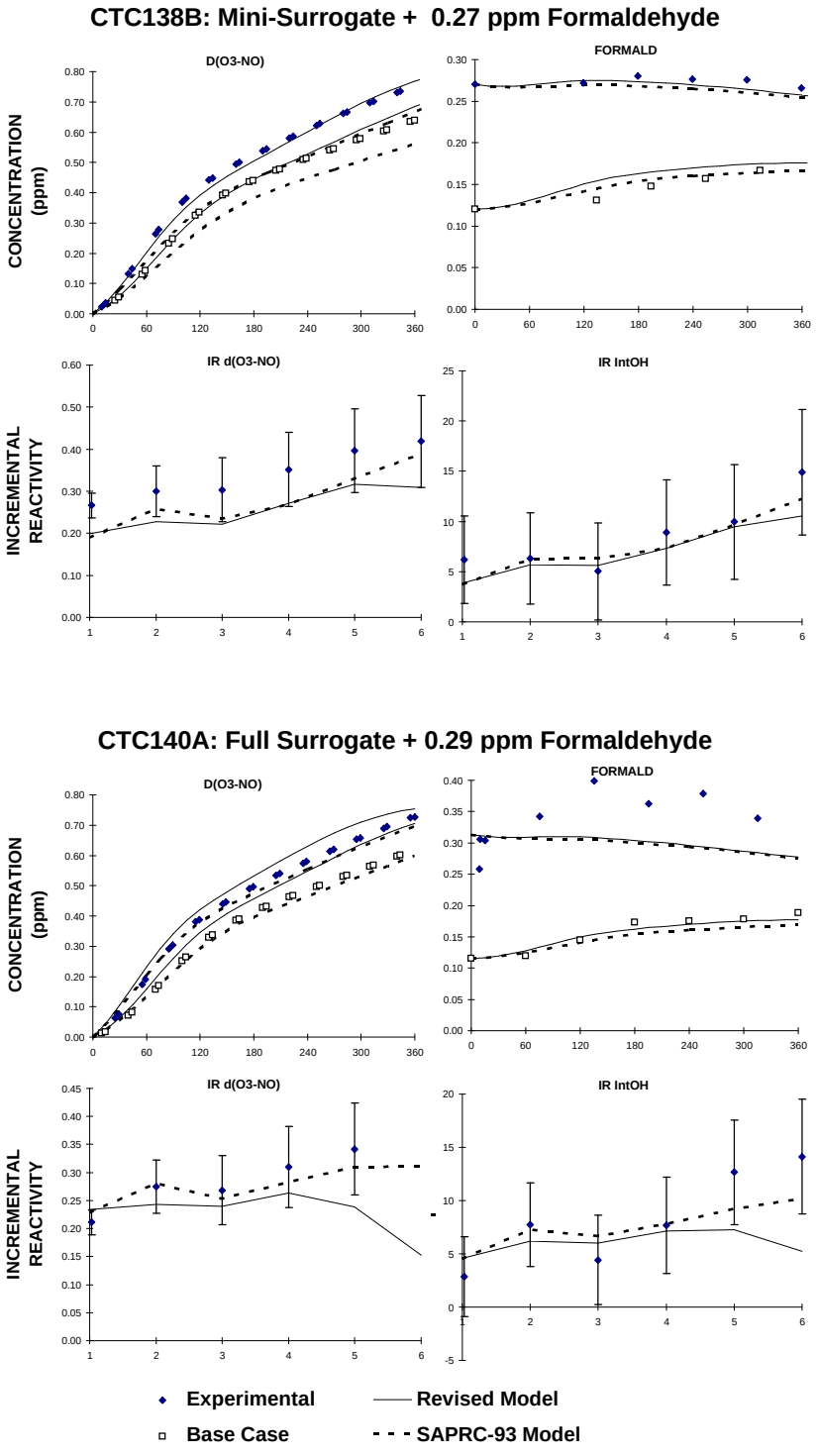

Figure 13. Plots of experimental and calculated incremental reactivity for formaldehyde from xenon arc experiments carried out for this program.

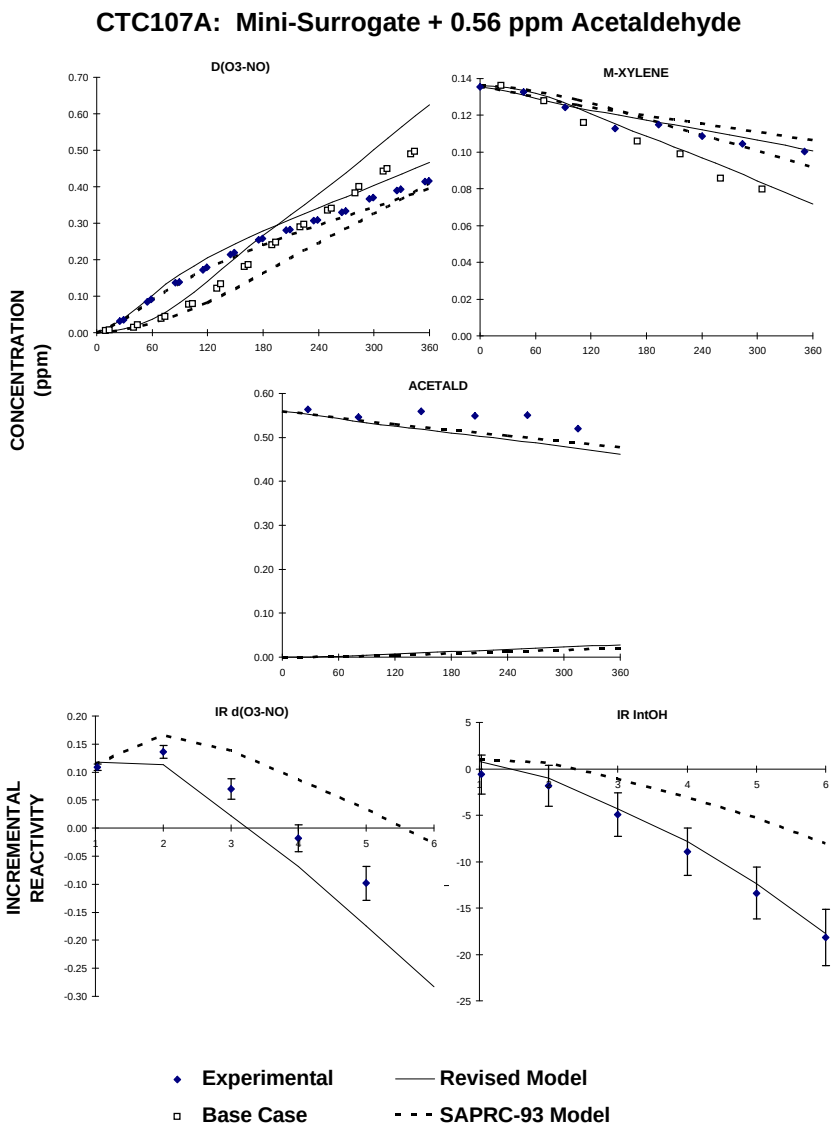

Figure 14. Plots of experimental and calculated incremental reactivity for acetaldehyde from xenon arc experiments carried out for this program.

because of the low base ROG surrogate injections. Figure 14 shows that acetaldehyde has a positive effect on d(O_3-NO) during the initial stages of the mini-surrogate experiment, but its effect becomes negative later, and it has an inhibiting effect on radicals which also becomes relatively more important at later stages of the run. This is attributed to radical inhibition due to the formation of PAN, which becomes important only after most of the initially present NO has been consumed. All these results are qualitatively similar to the results of similar experiments carried out previously in the blacklight chambers, and can be explained in the same way (Carter et al. 1993a; 1995a).

The major reason these experiments were carried out is for mechanism evaluation. Figures 6-14 show results of model simulations carried out using the same SAPRC-93 mechanism which was evaluated in our previous reports for this program (Carter et al. 1993a,b; 1995a,c,d; Carter, 1995a), and also results of calculations with the SAPRC-93 mechanism with reoptimized aromatics mechanisms derived as discussed in the following section. Figures 6 and 7 show that the SAPRC-93 mechanism has a slight tendency to underpredict NO oxidation and O_3 formation in the base case experiments, and also consistently underpredicts m-xylene consumption rates, indicating that it is underpredicting OH radical levels in simulations of experiments in this chamber. This is consistent with results of model simulations of the limited number of xenon arc chamber runs carried out in Phase 2 of this program (Carter et al. 1995c), which indicated that the SAPRC-93 mechanism consistently underpredicted transformation rates in aromatic and mixture runs using this light source. The revised aromatic mechanism, which was adjusted to improve model performance in this regard (see below) performs much better in simulating the m-xylene consumption rates, though it still tends to underpredict them in the later stages of the runs. It also gives better simulations of d(O_3-NO) in the full surrogate runs, though it has a slight tendency to overpredict d(O_3-NO) in the mini-surrogate runs — to about the same extent that SAPRC-93 underpredicts it. This is consistent with the other results of the evaluation of the revised mechanism, which are discussed in more detail later in this report.

Figures 8-14 show the results of the model simulations of the incremental reactivities of the various compounds studied. Figures 8-10 and 13 show that the SAPRC-93 and modified aromatic mechanisms perform reasonably well in simulating the reactivity results for CO, n-octane, propene and formaldehyde. The small differences between the reactivity predictions of the SAPRC-93 and the revised aromatic mechanisms for these compounds can be attributed to the differences in their ability to simulate the base case runs, with the mechanism performing better in simulating the base case generally also performing better in simulating the incremental reactivity. In the case of acetaldehyde (Figure 14), the SAPRC-93 tends to overpredict the reactivity (or underpredict inhibition), while the revised aromatic mechanism has the opposite bias. This also can be attributed to differences in the mechanisms in

simulating the base case experiment, since an overprediction of O_3 formation rate in the base case will cause an overprediction of inhibition (underprediction of reactivity) due to the formation of PAN. If adjusted for the differences in the simulation of the base case, both mechanisms can be considered to be reasonably consistent with the acetaldehyde reactivity data. Thus, for these non-aromatic compounds, the results of these xenon arc chamber experiments are entirely consistent with the predictions of the current versions of the SAPRC mechanisms, and indicate no significant light source effect which is not being appropriately represented in the model.

The situation with the aromatics is somewhat different. Consistent with the Phase 2 results and the results of the single compound aromatic - NO_x experiments discussed in the following section, the incremental reactivities of both toluene and m-xylene in the xenon arc chamber were found to be consistently higher than predicted by the SAPRC-93 mechanism. This was the case for both d(O_3-NO) and IntOH reactivities, and for both ROG surrogates. The discrepancies were greater for the mini-surrogate runs compared with the full surrogate, which is consistent with the greater sensitivity of the full surrogate runs to mechanism differences which was observed in the Phase 2 study (Carter et al. 1995a). The discrepancy was also somewhat greater for toluene than for m-xylene. As expected, the modified aromatic mechanism, which was reoptimized to improve its performance in simulating single aromatic - NO_x experiments in this chamber as discussed in the following section, performs somewhat better in simulating these experiments. However, it still tends to underpredict the reactivities of toluene (though to a lesser extent than SAPRC-93), and somewhat underpredicts the reactivities of m-xylene in the final stages of the experiments. Note that the data from these incremental reactivity experiments were not used in the optimization of the modified aromatic mechanisms shown in these calculations.

Aromatic Experiments and Mechanism Adjustments

Summary of Experiments and Initial Model Simulations

The largest single component of this phase of the program consisted of NO_x - air irradiations of various aromatic compounds carried out in both the blacklight and xenon arc chamber to provide data needed for developing and evaluating their mechanisms. This included various aromatic isomers for which data suitable for systematic mechanism evaluation were highly limited, and a more complete data base using the xenon arc light source. The compounds studied included toluene, ethylbenzene, o-, m-, and p-xylene, and 1,2,3-, 1,2,4- and 1,3,5-trimethylbenzene. For all these compounds experiments were carried out at least two different NO_x levels, and two different aromatic / NO_x ratios, in both the blacklight and xenon arc chambers. In addition, a limited number of benzene - NO_x irradiations were carried out in the xenon arc chamber, for comparison with previous runs carried out using a blacklight light source.

The conditions and selected results of the aromatic - NO_x experiments carried out for mechanism evaluation for this program are summarized on Table 13, Appendix B gives concentration-time plots for the d(O_3-NO) (Figures B-1 - B-9), the reactant aromatic (Figures B-10 - B-17), and the formaldehyde (Figures B-18 - B-25) data for all these experiments, and plots of the d(O_3-NO), reactant aromatic, and formaldehyde data for selected runs are shown on Figures 15-17, respectively. In addition, benzaldehyde and o-cresol was monitored in three of the toluene - NO_x experiments, and concentration - time data for these species are given in Figure 18. For comparison purposes, Appendix B also contains plots of d(O_3-NO) data from aromatic - NO_x experiments carried out in previous programs, including runs used for the development of previous versions of the SAPRC mechanism.

Figures 15-18 and the plots in Appendix B also show results of model simulations of these experiments using the version of the SAPRC mechanism (SAPRC-93) which was employed in the model simulations for the reports for the previous phases of this program (Carter et al. 1993a, 1995c; Carter, 1995a). Consistent with the results of those previous studies, while the SAPRC-93 mechanism performs reasonably well in simulating experiments using compounds and in chambers for which it was evaluated, its performance is not as satisfactory in simulating experiments carried out in the xenon arc chamber, nor in simulating results of experiments for aromatic isomers other than those for which the mechanism was developed. In particular, the mechanism consistently underpredicts NO oxidation and O_3 formation rates in the CTC chamber for all compounds except for ethylbenzene, p-xylene and 1,2,4-trimethylbenzene. On the other hand, the SAPRC-93 mechanism overpredicts O_3 formation and NO oxidation rates for ethylbenzene in the blacklight chamber, and for p-xylene, and 1,2,4-trimethylbenzene in both chambers.

As indicated previously, uncertain portions of the aromatic mechanisms, particularly those representing the reactive aromatic ring fragmentation products, must be represented in a parameterized manner, and derived based on adjustments to the mechanisms to fit results of aromatic - NO_x chamber experiments. The SAPRC-93 aromatic mechanisms were derived by adjusting them to fit results of toluene, m-xylene, or 1,3,5-trimethylbenzene - NO_x experiments carried out in blacklight chambers or in the SAPRC EC. Although the SAPRC EC employs a xenon arc light source with a spectrum similar to the CTC, it has a more reactive surface with a higher radical source than the Teflon bag reactors used for the CTC. This higher radical source would tend to reduce the sensitivity of the results to uncertainties in the aromatic mechanisms. Thus, while the SAPRC-93 mechanism tends to underpredict the rates of O_3 formation and NO oxidation in Teflon bag chambers using xenon arc or sunlight light sources (i.e., the SAPRC XTC and OTC and the CE-CERT CTC), Figures B-10 through B-12 show that the discrepancies were much less for the SAPRC EC, and were not judged to indicate a significant bias at the time the SAPRC-90 and SAPRC-93 mechanisms were developed. However, the bias towards

Table 13. Summary of conditions and selected results of the aromatic - NOx experiments carried out for mechanism evaluation.

Run	T (K)	k_1 (min^{-1})	NO_x (ppm)	VOC (ppm)	Max O_3 (ppm)	Δ ([O_3]-[NO]) (ppm) 1 hr	3 hr	5 hr
				Benzene - NO_x				
CTC159A	303	0.185	0.28	33.6	0.37	0.05	0.55	0.53
CTC159B	303	0.185	0.27	16.2	0.33	0.03	0.33	0.51
CTC160A	302	0.190	0.52	18.0	0.04	0.01	0.09	0.24
CTC160B	302	0.190	0.52	33.6	0.44	0.02	0.20	0.61
				Toluene - NO_x				
DTC155A	298	0.248	0.10	0.64	0.20	0.08	0.29	0.28
DTC151A	298	0.252	0.32	1.84	0.39	0.06	0.63	0.62
DTC151B	298	0.252	0.33	1.82	0.38	0.06	0.66	0.62
DTC170A	299	0.239	0.49	2.52	0.47	0.09	0.74	0.86
DTC179A	299	0.235	0.51	2.26	0.48	0.07	0.70	0.87
DTC158A	298	0.246	0.50	2.49	0.48	0.07	0.71	0.83
DTC153B	297	0.250	0.51	2.64	0.47	0.11	0.79	0.83
DTC168B	299	0.240	0.53	2.42	0.43	0.13	0.79	0.80
DTC169B	299	0.240	0.56	2.82	0.42	0.17	0.83	0.78
DTC190B	299	0.232	0.58	2.36	0.48	0.11	0.76	0.89
CTC089B	295	0.194	0.27	0.49	0.08	0.00	0.06	0.21
CTC079	298	0.195	0.26	0.50	0.12	0.01	0.10	0.27
CTC089A	295	0.194	0.26	0.51	0.09	0.01	0.06	0.19
CTC048	301	0.199	0.25	0.95	0.31	0.01	0.36	0.50
CTC033	300	0.201	0.29	1.03	0.32	0.02	0.34	0.54
CTC026	302	0.202	0.27	2.01	0.35	0.09	0.55	0.54
CTC034	305	0.201	0.52	2.21	0.47	0.05	0.71	0.81
CTC065	300	0.197	0.66	0.97	0.05	0.03	0.13	0.36
				Ethylbenzene - NO_x				
DTC223B	299	0.224	0.27	0.76	0.21	0.02	0.18	0.34
DTC223A	299	0.224	0.26	1.52	0.33	0.05	0.34	0.55
DTC224B	298	0.224	0.55	0.70	0.02	0.03	0.13	0.27
DTC224A	298	0.224	0.53	1.62	0.19	0.05	0.28	0.51
CTC092A	295	0.194	0.27	1.03	0.14	0.02	0.15	0.30
CTC092B	295	0.194	0.27	1.96	0.30	0.04	0.30	0.51
CTC057	300	0.198	0.27	2.03	0.31	0.03	0.33	0.51
CTC098B	295	0.193	0.49	1.88	0.05	0.02	0.11	0.29
				o-Xylene - NO_x				
DTC209B	299	0.227	0.13	0.14	0.26	0.04	0.23	
DTC209A	299	0.227	0.12	0.26	0.28	0.10	0.36	
DTC207A	299	0.228	0.28	0.30	0.38	0.05	0.35	0.56
DTC207B	299	0.228	0.30	0.66	0.41	0.16	0.64	0.62
DTC208B	300	0.227	0.56	0.28	0.10	0.03	0.27	0.47

Table 13 (continued)

Run	T (K)	k_1 (min^{-1})	NO_x (ppm)	VOC (ppm)	Max O_3 (ppm)	Δ ([O_3]-[NO]) (ppm) 1 hr	3 hr	5 hr
			o-Xylene - NO_x (continued)					
DTC208A	300	0.227	0.52	0.57	0.56	0.07	0.58	0.90
CTC038	301	0.201	0.25	0.30	0.38	0.02	0.34	0.56
CTC091A	295	0.194	0.28	0.46	0.35	0.04	0.41	0.58
CTC081	298	0.195	0.26	0.54	0.36	0.09	0.53	0.56
CTC068	302	0.197	0.26	0.64	0.38	0.08	0.58	0.57
CTC039	301	0.201	0.48	0.16	0.00	0.01	0.06	0.16
CTC046	303	0.200	0.50	0.30	0.04	0.01	0.08	0.30
			m-Xylene - NO_x					
DTC193B	299	0.231	0.13	0.15	0.28	0.11	0.35	0.39
DTC193A	299	0.231	0.13	0.29	0.26	0.20	0.37	0.36
DTC192B	298	0.231	0.15	0.53	0.27	0.33	0.38	0.36
DTC189B	299	0.232	0.26	0.11	0.20	0.04	0.25	0.36
DTC206B	299	0.228	0.28	0.25	0.38	0.11	0.48	0.61
DTC189A	299	0.232	0.25	0.25	0.39	0.11	0.48	0.59
DTC192A	298	0.231	0.30	0.53	0.42	0.30	0.65	
DTC188A	299	0.232	0.55	0.13	0.02	0.02	0.14	0.29
DTC188B	299	0.232	0.57	0.23	0.25	0.06	0.42	0.61
DTC191A	298	0.232	0.57	0.53	0.59	0.16	0.81	1.01
DTC191B	298	0.232	0.59	1.10	0.61	0.47	1.03	0.91
CTC035	301	0.201	0.28	0.16	0.36	0.04	0.33	0.51
CTC029	300	0.202	0.27	0.32	0.42	0.08	0.57	0.63
CTC036	302	0.201	0.51	0.16	0.09	0.01	0.18	0.38
CTC080	298	0.195	0.51	0.53	0.54	0.10	0.79	0.94
CTC094A	294	0.194	0.49	0.56	0.46	0.09	0.62	0.82
CTC094B	294	0.194	0.49	0.57	0.46	0.10	0.64	0.82
CTC066	300	0.197	0.56	0.32	0.32	0.04	0.43	0.69
			p-Xylene - NO_x					
DTC200B	299	0.229	0.13	0.20	0.19	0.02	0.14	0.25
DTC200A	299	0.229	0.13	0.38	0.27	0.04	0.21	0.37
DTC198A	299	0.230	0.26	0.42	0.17	0.03	0.15	0.32
DTC198B	299	0.230	0.27	0.84	0.38	0.04	0.29	0.57
DTC199B	299	0.230	0.55	0.43	0.02	0.03	0.15	0.32
DTC199A	299	0.230	0.55	0.83	0.15	0.03	0.21	0.48
CTC043	301	0.200	0.25	0.19	0.01	0.00	0.04	0.10
CTC041	300	0.200	0.26	0.38	0.11	0.01	0.09	0.25
CTC047	301	0.200	0.28	0.97	0.36	0.03	0.23	0.53
CTC069	302	0.197	0.24	2.00	0.39	0.01	0.38	0.59
CTC044	301	0.200	0.51	0.39	0.01	0.00	0.03	0.09
CTC070	301	0.197	0.50	2.02	0.54	0.02	0.29	0.72

Table 13 (continued)

Run	T (K)	k_1 (min^{-1})	NO_x (ppm)	VOC (ppm)	Max O_3 (ppm)	Δ ([O_3]-[NO]) (ppm) 1 hr	3 hr	5 hr
			1,2,3-Trimethylbenzene - NO_x					
DTC213B	299	0.226	0.11	0.09	0.25	0.07	0.25	0.33
DTC213A	299	0.226	0.11	0.14	0.28	0.14	0.37	0.38
DTC211A	299	0.227	0.25	0.13	0.36	0.08	0.39	0.53
DTC211B	299	0.227	0.26	0.30	0.42	0.23	0.63	0.61
DTC212B	299	0.227	0.54	0.16	0.16	0.06	0.40	0.54
DTC212A	299	0.227	0.51	0.31	0.55	0.14	0.67	0.89
CTC076	297	0.196	0.26	0.18	0.34	0.06	0.41	0.55
CTC054	302	0.199	0.23	0.21	0.35	0.09	0.49	0.53
CTC075	298	0.196	0.52	0.23	0.28	0.03	0.43	0.61
			1,2,4-Trimethylbenzene - NO_x					
DTC204B	298	0.228	0.12	0.09	0.18	0.03	0.15	0.25
DTC204A	298	0.228	0.12	0.17	0.29	0.05	0.23	0.37
DTC201A	299	0.229	0.25	0.17	0.23	0.04	0.23	0.38
DTC203B	298	0.229	0.54	0.17	0.04	0.04	0.19	0.38
DTC203A	298	0.229	0.51	0.34	0.21	0.04	0.30	0.55
CTC056	300	0.198	0.25	0.23	0.30	0.01	0.21	0.41
CTC091B	295	0.194	0.28	0.46	0.37	0.04	0.34	0.58
CTC093A	294	0.194	0.48	0.48	0.26	0.03	0.30	0.53
CTC093B	294	0.194	0.49	1.13	0.51		0.57	0.85
			1,3,5-Trimethylbenzene - NO_x					
DTC196B	300	0.230	0.14	0.08	0.27	0.14	0.33	0.38
DTC196A	300	0.230	0.13	0.17	0.28	0.21	0.38	0.39
DTC206A	299	0.228	0.27	0.14	0.42	0.17	0.50	0.63
DTC194A	299	0.231	0.26	0.17	0.43	0.18	0.50	0.61
DTC194B	299	0.231	0.28	0.34	0.41	0.33	0.59	0.56
DTC195B	300	0.231	0.56	0.17	0.33	0.11	0.45	0.58
DTC195A	300	0.231	0.55	0.34	0.63	0.26	0.80	0.94
CTC073	297	0.196	0.26	0.17	0.36	0.09	0.45	0.55
CTC050	303	0.199	0.27	0.19	0.36	0.15	0.54	0.57
CTC098A	295	0.193	0.48	0.20	0.33	0.06	0.49	0.66
CTC030	300	0.202	0.52	0.32	0.61			
CTC071	300	0.197	0.52	0.33	0.59	0.23	0.85	0.99

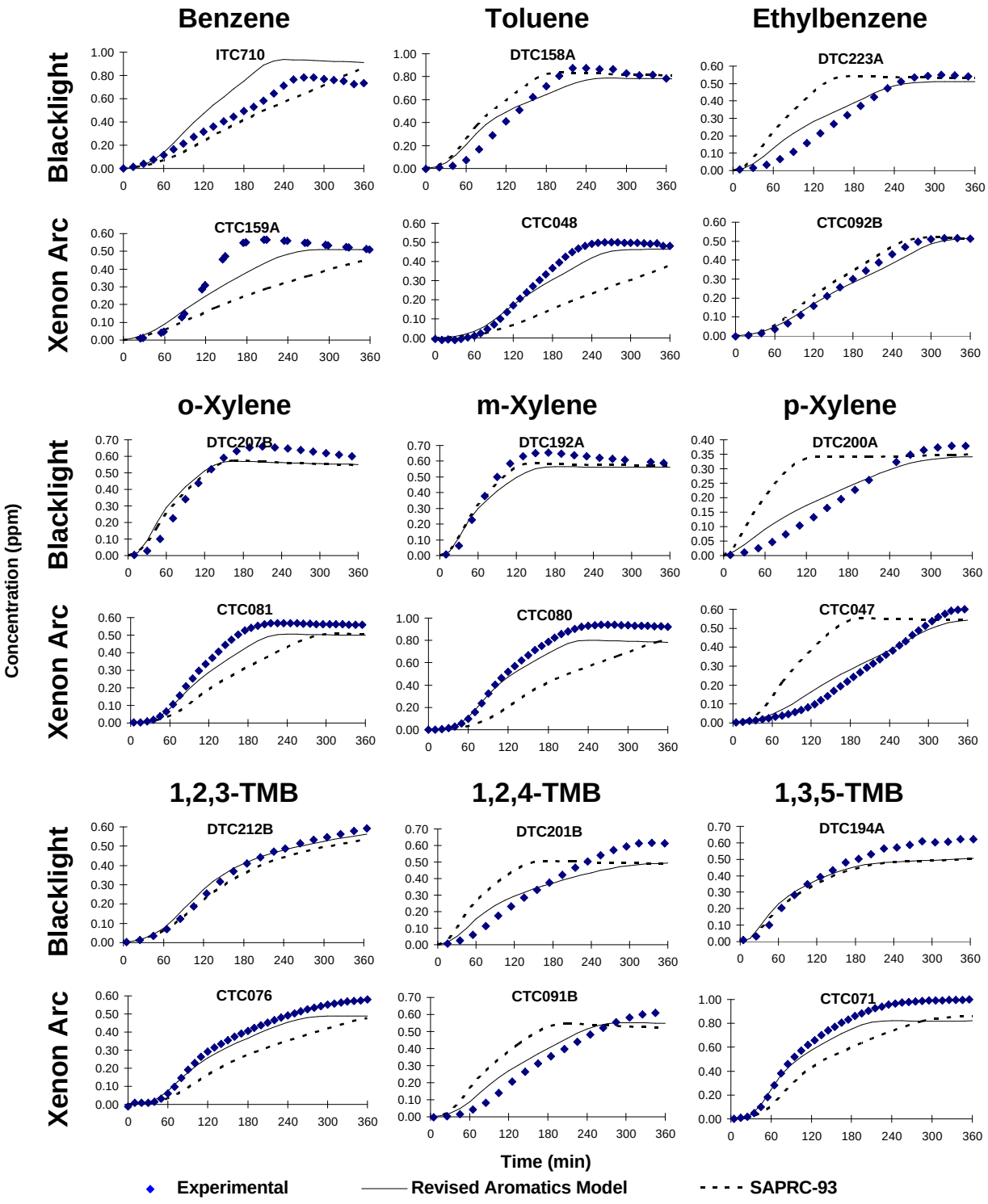

Figure 15. Experimental and calculated concentration - time plots for $\Delta([O_3]-[NO])$ for representative aromatic - NO_x experiments carried out for mechanism evaluation.

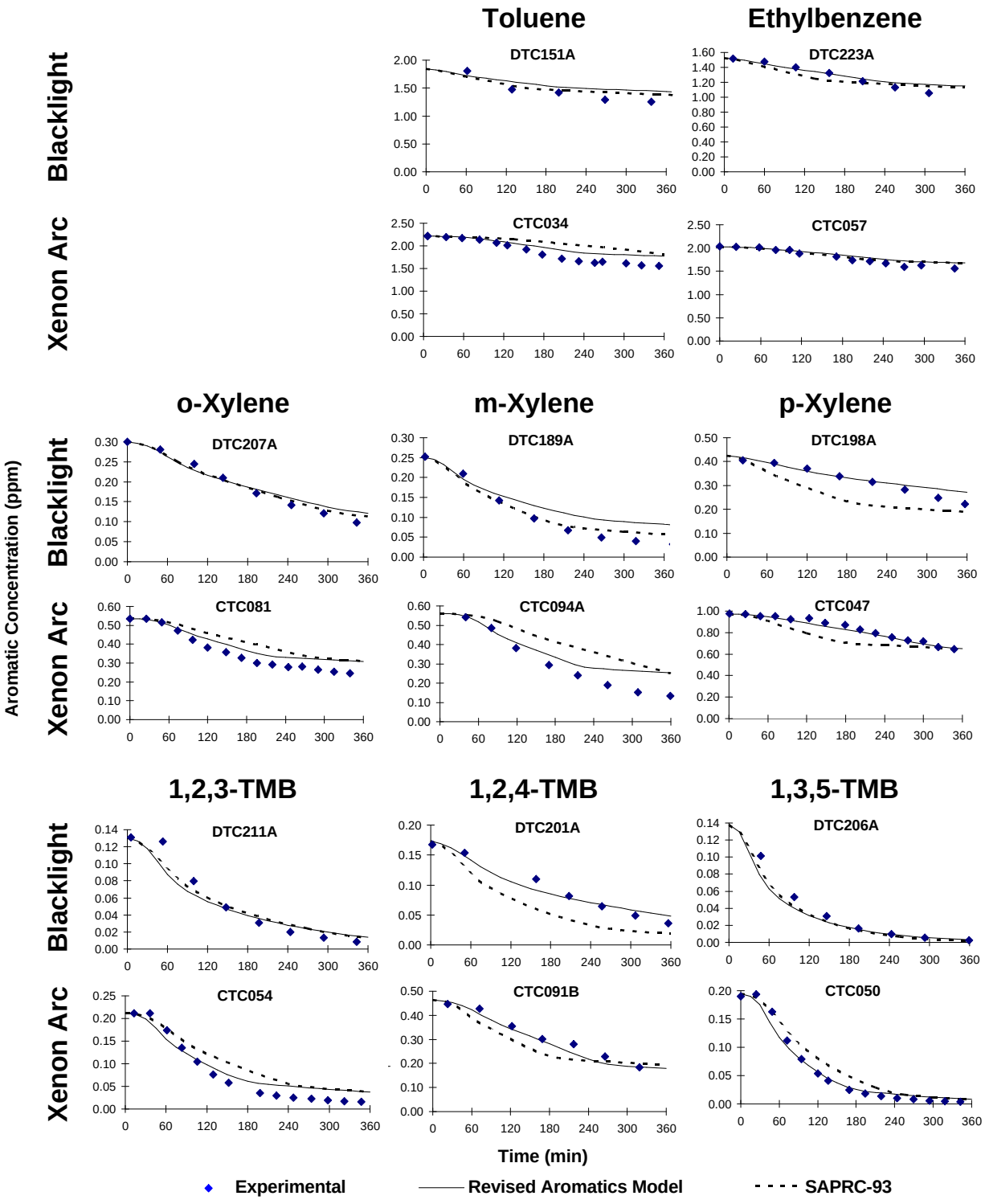

Figure 16. Experimental and calculated concentration - time plots the reactant aromatic in representative aromatic - NO_x experiments carried out for mechanism evaluation.

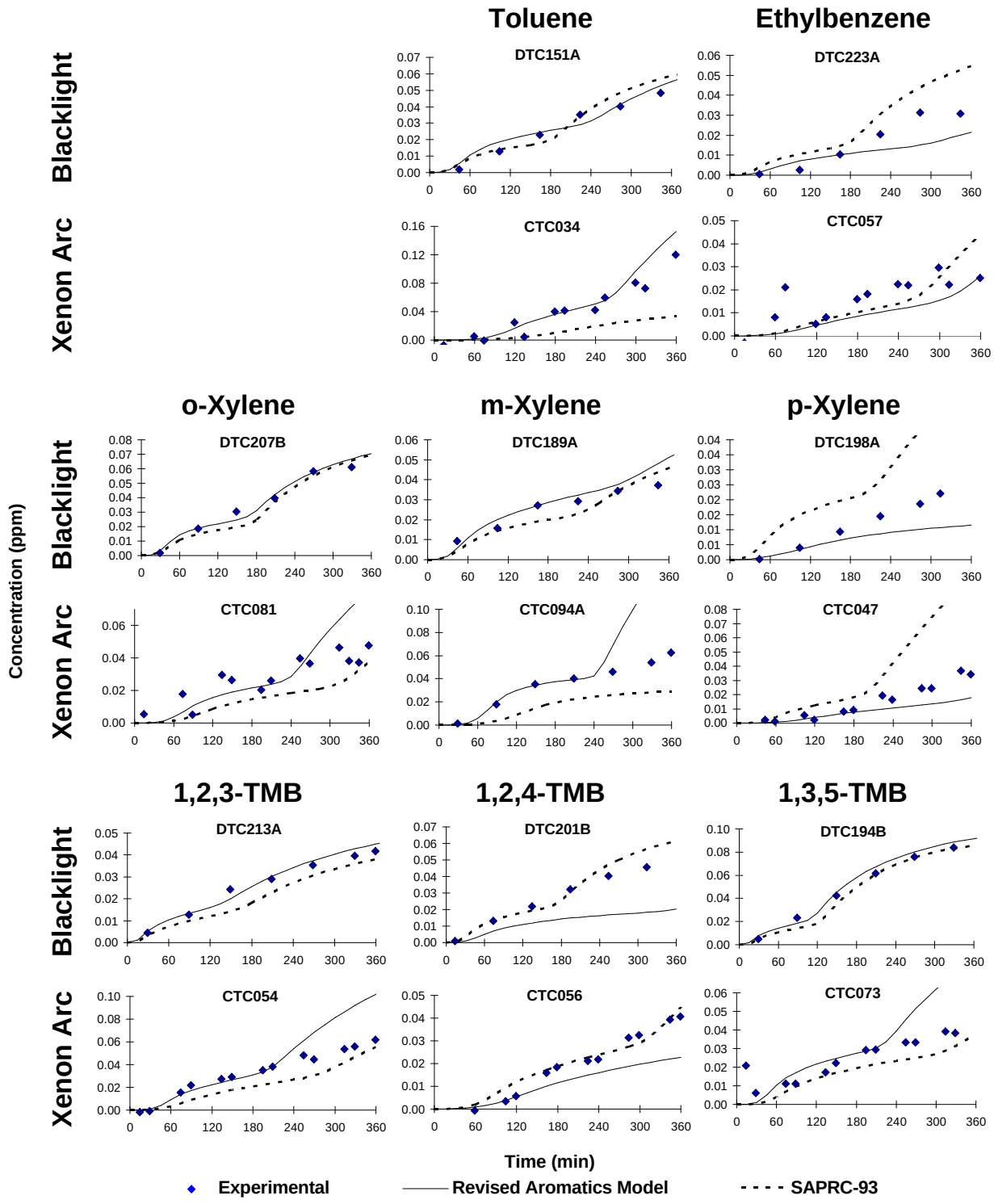

Figure 17. Experimental and calculated concentration - time plots for formaldehyde in representative aromatic - NO_x experiments carried out for mechanism evaluation.

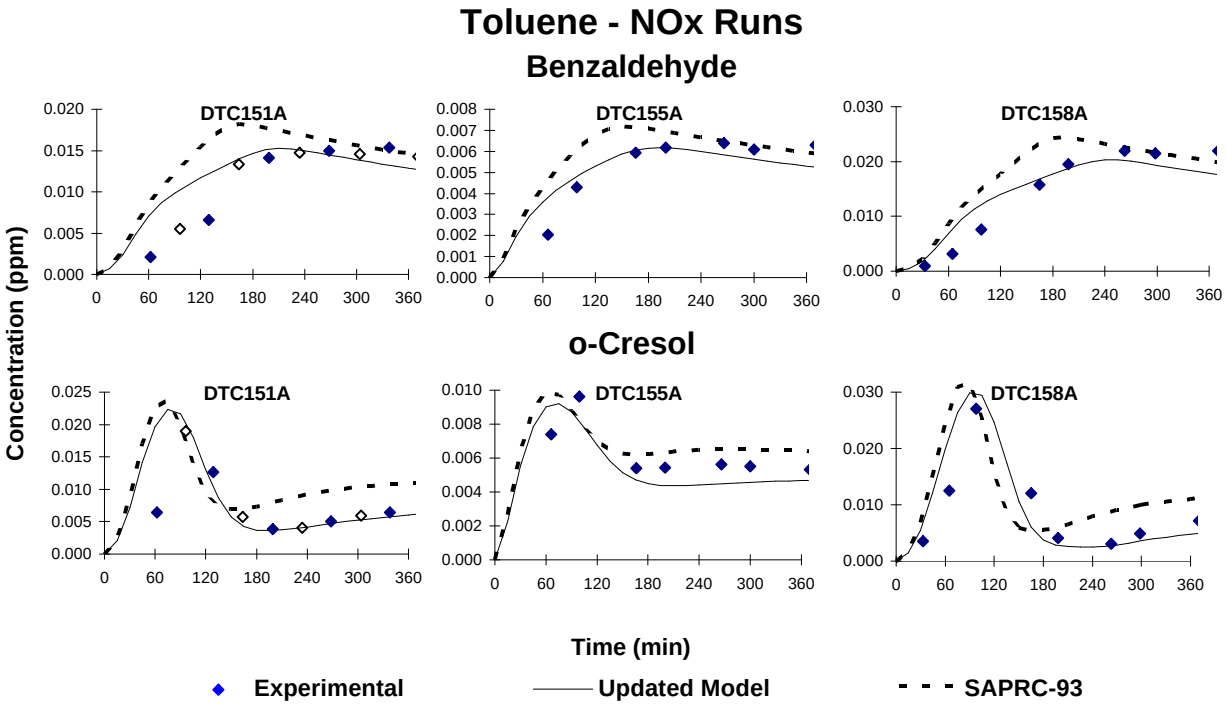

Figure 18. Experimental and calculated concentration-time plots for benzaldehyde and o-cresol in toluene - NO_x experiments DTC151A, DTC155A, and DTC158A.

Figure 18. Experimental and calculated concentration - time plots for benzaldehyde and o-cresol in toluene - NO_x experiments DTC151, DTC155A, and DTC158A.

underprediction is clear in the case of the chambers with the lower radical sources, indicating unacceptable performance of the mechanism.

Reparameterization and Optimization of the Aromatic Mechanisms

In the SAPRC-90 and SAPRC-93 mechanisms, the aromatic ring fragmentation products are represented in their measured yields for toluene, m-xylene, or 1,3,5-trimethylbenzene, and by a lumped uncharacterized aromatic fragmentation product designated "AFG2", which reacted with a similar mechanism as methyl glyoxal, but whose yield and photolysis rates were adjusted based on model simulations of experiments for those three compounds (Carter, 1990). The treatment was similar in the case of benzene, except that the uncharacterized products were represented by a separate species "AFG1", whose mechanism, other than photolysis rate, was assumed to be similar to glyoxal. Best fits to the evaluation data were obtained if the action spectrum of the uncharacterized products are assumed to be similar to that for acrolein (Carter et al. 1993a; Carter, 1995a). Table 14 summarizes the yields of the products which were used, as well as the adjusted photolysis rates used for AFG2 or AFG1. As indicated on the table, because of lack of data available at the time, the ring fragmentation product parameters for ethylbenzene (and all other monoalkylbenzenes) were assumed to be the same as for toluene, those for the other xylene isomers (and other disubstituted benzenes) were assumed to be the same as for m-

Table 14. Summary of optimized parameters in the aromatic photooxidation

Aromatic	Adjusted Products [a] MGLY	AFG1	AFG2	Runs used in Optimizations [b]
SAPRC-93 Mechanism [c]				
Benzene	0	1.75	0	ITC560, ITC561, ITC562
Toluene	0.131	0	0.49	EC266, EC270, EC271, EC273, ITC699, DTC042A, D
Ethylbenzene				Same as Toluene
m-Xylene	0.37	0	0.75	EC344, EC345, ITC702, DTC076, ETC222
o-Xylene				Same as m-Xylene
p-Xylene				Same as m-Xylene
1,3,5-Trimethylbenzer	0.62	0	0.75	EC901, EC903, ITC703, ITC706, ITC709
1,2,3-Trimethylbenzene				Same as 1,3,5-Trimethylbenzene
1,2,4-Trimethylbenzene				Same as 1,3,5-Trimethylbenzene
Reoptimized Mechanism [d]				
Benzene	0	1.44	0	ITC560, ITC561, ITC562, ITC710, CTC159A, CTC159B, CTC160A, CTC160B
Toluene	0.96	0	0.26	CTC079, CTC048, CTC026, CTC034, CTC065, DTC042B, DTC155A, DTC151A, DTC170A,
Ethylbenzene	0.20	0	0.18	CTC057, CTC092A, CTC092B, CTC098B, DTC223A, DTC223B, DTC224A, DTC224B
m-Xylene	1.67	0	0.45	CTC035, CTC029, CTC036, CTC080, CTC094A, CTC094B, DTC193B, DTC193A, DTC192B, DTC189B, DTC206B, DTC189A, DTC192A, DTC188A, DTC188B, DTC191A, DTC191B, DTC073A, DTC294A, DTC294B, DTC295A,
o-Xylene	0.81	0	0.58	CTC038, CTC039, CTC046, CTC068, CTC081, CTC091A, DTC207A, DTC207B, DTC208A, DTC208B, DTC209A, DTC209B
p-Xylene	0.17	0	0.15	CTC041, CTC043, CTC044, CTC047, CTC070, DTC198A, DTC198B, DTC199A, DTC199B,
1,3,5-Trimethylbenzer	1.18	0	0.61	CTC030, CTC050, CTC071, CTC073, DTC194A, DTC194B, DTC195A, DTC195B, DTC196A,
1,2,3-Trimethylbenzer	1.13	0	0.65	CTC054, CTC075, CTC076, DTC211A, DTC211B, DTC212A, DTC212B, DTC213A, DTC213B
1,2,4-Trimethylbenzer	0.41	0	0.25	CTC056, CTC091B, CTC093A, CTC093B, DTC201A, DTC201B, DTC203A, DTC203B, DTC204A,

[a] MGLY is methyl glyoxal, AFG is AFG1 for benzene, AFG2 for the alkylbenzenes.

[b] ITC is the SAPRC Indoor Teflon chamber; EC is the SAPRC Evacuable chamber, and ETC is the SAPRC Indoor Teflon Chamber #2. Run ETC076 was carried out in the SAPRC DTC. The SAPRC chambers are described by Carter et al. (1995b). The other DTC and the CTC runs were carried out for this program.

[c] MGLY yields were not optimized; values used are based on experimental yields from toluene, m-xylene, or 1,3,5-trimethylbenzene. Photolysis rate for AFG1 and AFG2 are calculated using absorption cross sections of acrolein, with overall quantum yields of 0.029 and 0.615, respectively.

[d] MGLY represents other uncharacterized aromatic products as well as methylglyoxal. Photolysis rate for AFG1 and AFG2 are calculated using absorption cross sections of acrolein, with overall quantum yields of 0.077 and 1.0, respectively.

xylene,and those for the other tri- and poly-substituted benzenes were assumed to be the same as for 1,3,5-trimethylbenzene.

The data obtained in this work indicated that the assumption that similar parameters can be used for different isomers is often inappropriate, and also that the parameterization is not appropriate even for the compounds for which they were adjusted. Re-optimization of the existing parameters based on the new data did not yield satisfactory results, since parameter values which fit the blacklight chamber results tended to underpredict O_3 formation and NO oxidation rates in the xenon arc chamber, while those which fit the xenon arc data tended to overpredict them for the blacklight experiments. This means that representing all the unknown ring fragmentation products by a single model species with the action spectrum of acrolein is not sufficient to adequately represent how the atmospheric reactivities of the aromatic compounds respond to changes in lighting conditions.

After examining a number of alternative approaches, it was found that the best results for the alkylbenzenes were obtained if a second lumped aromatic fragmentation product was added to the mechanism, with an independently adjusted yield for each compound. This second product was essentially the same as AFG2, but it was assumed to photolyze with the same action spectrum as methyl glyoxal. Since the AFG2 mechanism is essentially the same as that of methyl glyoxal except for its action spectrum, this second product has essentially the same mechanism as methyl glyoxal, and thus the two can be lumped together. In other words, instead of using the methyl glyoxal yield based on the actual observed yields for each compound, its yield is optimized, along with that for AFG2, to achieve the best results in the model simulations in the chamber experiments. Using this approach allowed NO oxidation and O_3 formation rates in aromatic - NO_x experiments in both the blacklight chamber and the XTC and CTC xenon arc chambers experiments to be reasonably well simulated with the same mechanism. Separate optimizations were done for each isomer to account for their differences in reactivity.

Table 14 lists the reoptimized parameters for the revised mechanisms for the aromatic compounds, and also indicated the runs and the data which were used in the optimizations. It can be seen that there are substantial differences between the parameters which best fit the ethylbenzene data and those for toluene, that those for m-xylene are not very representative of those for o- and (especially) p-xylenes, nor are those for 1,3,5-trimethylbenzene very representative of those for the 1,2,4- isomer. On the other hand, the 1,2,3-trimethylbenzene parameters are very close to those for the 1,3,5- isomer.

Results of model simulations of the aromatic runs carried out using this reoptimized mechanisms are included with the concentration-time plots for the aromatic runs in Figures B-1 through B-9 and B-13

through B-28 in Appendix B, where they can be compared with the data and the simulations using the SAPRC-93 mechanism. In addition, as indicated above, Figures B-10 through B-12 in Appendix B include experimental and calculated concentration-time plots for $d(O_3\text{-NO})$ in the earlier aromatic - NO_x experiments, including the EC and ITC runs used in the derivation of the SAPRC-93 mechanism. Note that the curves with the dotted lines refer to the results of the SAPRC-93 calculations, while those using the solid lines are calculated using the reoptimized model.

The plots in Figure 15 and in Appendix B show that the revised mechanism performs at least as well or better in simulating the $d(O_3\text{-NO})$ data than does the SAPRC-93 mechanism. Figures B-10 through B-12 show that the revised mechanism preforms about the same as the SAPRC-93 mechanism in simulating the earlier ITC and EC runs used to derive the latter mechanism, with the EC data being relatively insensitive to the parameter reoptimizations. In addition, Figures B-10 and B-11 show that the reoptimization eliminated the bias in the earlier mechanism towards underprediction of O_3 formation and NO oxidation rates in the SAPRC outdoor chamber (OTC) runs, though the reoptimized mechanism may have a bias towards overprediction for those experiments. (The OTC data were not used in the optimization because of the greater uncertainty in characterizing lighting and other conditions for outdoor runs.)

However, there are a number of runs where the $d(O_3\text{-NO})$ data are still not particularly well fit by the reoptimized mechanism. The most significant discrepancies appear to be for p-xylene (Figure B-5) and benzene (Figure B-9), where it is clear that the parameterization is not adequately representing all processes which significantly affect O_3 formation and NO oxidation. In the case of p-xylene, it tends to underpredict O_3 formation around the later periods of low aromatic/NO_x runs, while it overpredicts the initial rates of NO oxidation and O_3 formation in the high aromatic/NO_x runs. The model seems to have the opposite problem in the case of the benzene runs, having a tendency to underpredict the ozone formation rates in some (but not all) of the high aromatic/NO_x runs, and to overpredict NO oxidation and O_3 formation in some (but again not all) of the lower aromatic/NO_x runs. In addition, the model has a small, but generally consistent, tendency to underpredict peak O_3 levels in xylene and trimethylbenzene - NO_x runs where the maximum ozone formation potentials have been achieved. Examining alternative mechanistic possibilities or parameterizations, including adding O_3 + aromatic product reactions, has not significantly improved mechanism performance in this regard.

Figures 16 and B-13 through B-20 show that the updates to the mechanism generally improve the predictions of the aromatic consumption rates in those runs where it improves the $d(O_3\text{-NO})$ predictions, as one might expect. Since the aromatic consumption is due to reaction with OH radicals, this means that

the mechanism correctly predicts OH radical levels during most of these experiments. However, even the reoptimized model often underpredicts the aromatic consumption rates around the end of high aromatic/NO_x experiments with toluene, and o- and m-xylenes, suggesting that the model may not be appropriately representing radical sources and/or sinks in aromatic systems once NO_x is consumed.

Figures 17 and B-21 through B-28 show the experimental and calculated formaldehyde concentrations for the alkylbenzene - NO_x experiments for this program. The model fits the data reasonably well for the toluene, o-xylene and ethylbenzene runs, though there may be a slight bias towards underprediction for ethylbenzene. The model also fits most of the data for the m-xylene and 1,3,5-trimethylbenzene runs, except for the end of high aromatic/NO_x experiments in the CTC, where the model predicts an increase in formaldehyde levels which is not observed experimentally. The model has a bias towards underpredicting formaldehyde in the p-xylene and 1,2,4-trimethylbenzene runs. Given the highly approximate representation of the aromatic products, and the fact that formaldehyde is believed to be formed only from the reactions of these products (i.e., it is not a primary product), the fact that the model preforms as well as it does probably should be considered to be fortuitous. Note that the formaldehyde data were not used in the optimizations of the mechanisms.

Figure 18 shows the experimental and calculated concentration-time profiles for benzaldehyde and o-cresol in the three toluene - NO_x experiments where such data were obtained. Note that the yields of these products assumed in the mechanism are based on laboratory data and were not adjusted to fit chamber data (Carter, 1990, and references therein). It can be seen that the model fits remarkably well, with the slight overpredictions in the initial formation rates for both products in DTC151 being consistent with a similar overprediction in the initial NO oxidation and O_3 formation rate for the same experiment (see Figure B-1).

Effect of Reparameterization on Simulations of Previous Incremental Reactivity Experiments

The single aromatic - NO_x experiments shown in Appendix B are not the only chamber data useful for evaluating these aromatic mechanisms. The results of incremental reactivity experiments employing aromatics in the xenon arc chamber have been discussed above, and results of model simulations of these experiments are shown on Figures 11 and 12, above. In addition, a number of aromatic incremental reactivity experiments have been carried out in the SAPRC ETC or DTC during the previous two phases of these programs, and a few of incremental reactivity experiments for toluene carried out in the SAPRC ITC were reported previously by Carter and Atkinson (1987). The conditions and selected experimental and calculated results of these previous experiments are summarized on Table 15. Note that all these previous runs were carried out using blacklight light sources.

Table 15. Summary of conditions and experimental and calculated results for previous aromatic incremental reactivity experiments.

Run	Surg	Initial Reactants (ppm)			IR {Δ ([O_3]-[NO])} (ppm/ppm VOC), t=2			IR {Δ ([O_3]-[NO])} (ppm/ppm VOC), t=5			IR (IntOH) (10^6 min/ppm VOC), t=5		
	Type [a]	NOx	Surg	Test VOC	Experimental	SAPRC-93 [b]	Revised	Experimental	SAPRC-93	Revised	Experimental	SAPRC-93	Revised
							Benzene						
ETC265	Mini	0.49	4.4	5.78	0.015 ± 0.004	0.024 +0.008	0.040 +0.025	0.066 ± 0.008	0.063 -0.003	0.084 +0.018	2.0 ± 0.3	0.5 -1.5	1.4 -0.7
ETC263	Mini	0.48	4.3	6.77	0.012 ± 0.003	0.025 +0.013	0.042 +0.030	0.050 ± 0.007	0.057 +0.007	0.064 +0.014	1.3 ± 0.3	0.4 -0.9	0.9 -0.4
DTC039B	Full	0.18	4.0	7.39	0.001 ± 0.003	0.007 +0.005	0.011 +0.009	-0.011 ± 0.003	-0.006 +0.005	-0.005 +0.006	-1.5 ± 0.2	-2.4 -0.8	-1.9 -0.4
							Toluene						
ETC064	Mini	0.55	3.9	0.06	0.3 ± 0.5	0.4 +0.1	0.3 +0.1	1.0 ± 0.7	0.9 -0.1	0.7 -0.3	18 ± 41	23 +5	14 -3
ETC069	Mini	0.50	3.7	0.10	0.5 ± 0.3	0.4 -0.0	0.3 -0.1	1.4 ± 0.5	1.0 -0.4	0.7 -0.7	82 ± 24	26 -56	16 -66
ETC061	Mini	0.51	3.8	0.17	0.6 ± 0.2	0.43 -0.16	0.35 -0.24	1.7 ± 0.3	1.06 -0.62	0.76 -0.92	50 ± 13	29 -21	17 -33
ETC101	Mini	0.50	3.4	0.17	0.19 ± 0.09	0.28 +0.09	0.23 +0.04	0.89 ± 0.12	0.75 -0.15	0.59 -0.30	26 ± 7	19 -7	12 -13
ETC103	Mini	0.52	3.5	0.18	0.25 ± 0.08	0.26 +0.01	0.22 -0.04	0.98 ± 0.11	0.76 -0.23	0.60 -0.38	30 ± 6	19 -11	12 -17
DTC023A	Full	0.47	3.9	0.49	0.41 ± 0.05	0.38 -0.03	0.31 -0.10	0.76 ± 0.08	0.67 -0.09	0.62 -0.14	29 ± 3	22 -7	13 -16
DTC030B	Full	0.17	3.9	1.05	0.01 ± 0.02	0.02 +0.02	0.03 +0.02	-0.09 ± 0.02	-0.05 +0.04	-0.06 +0.03	-10 ± 1	-12 -2	-12 -1
ITC455	4-HC	0.08	3.3	0.09	0.1 ± 0.3	-0.1 -0.2	-0.1 -0.2	-0.3 ± 0.3	-0.4 -0.1	-0.4 -0.0	-20 ± 16	-34 -15	-33 -13
ITC451	4-HC	0.09	3.4	0.17	0.12 ± 0.14	-0.12 -0.24	-0.11 -0.23	-0.15 ± 0.14	-0.33 -0.17	-0.32 -0.16	-3 ± 8	-29 -27	-28 -26
							Ethylbenzene						
ETC455	Mini	0.53	4.1	0.10	0.1 ± 0.2	0.3 +0.1	0.2 +0.0	0.5 ± 0.5	0.8 +0.3	0.4 -0.1	-13 ± 19	17 +30	6 +19
ETC451	Mini	0.52	4.3	0.11	0.0 ± 0.2	0.3 +0.3	0.2 +0.1	0.3 ± 0.4	0.8 +0.4	0.4 +0.0	5 ± 19	17 +12	6 +1
ETC313	Mini	0.53	4.1	0.25	0.1 ± 0.1	0.3 +0.2	0.2 +0.1	0.6 ± 0.2	0.8 +0.2	0.4 -0.2	2 ± 8	19 +17	6 +4
							o-Xylene						
ETC311	Mini	0.49	4.4	0.06	1.2 ± 0.4	1.1 -0.2	1.1 -0.1	3.4 ± 0.7	2.8 -0.6	2.5 -0.9	70 ± 31	73 +3	61 -9
ETC315	Mini	0.48	4.4	0.06	1.0 ± 0.4	1.1 +0.1	1.2 +0.1	3.2 ± 0.7	3.0 -0.2	2.7 -0.6	62 ± 30	80 +18	67 +4
							m-Xylene						
ETC259	Mini	0.46	4.3	0.05	1.0 ± 0.4	1.8 +0.9	1.7 +0.7	4.2 ± 0.9	4.4 +0.2	3.5 -0.7	94 ± 36	121 +27	84 -10
ETC261	Mini	0.51	3.9	0.06	1.4 ± 0.4	1.9 +0.5	1.7 +0.4	4.6 ± 0.9	4.1 -0.5	3.3 -1.3	127 ± 36	109 -18	76 -51
ETC301	Mini	0.48	4.3	0.06	0.9 ± 0.4	1.9 +1.0	1.8 +0.9	3.5 ± 0.8	4.5 +0.9	3.5 +0.0	102 ± 34	120 +18	82 -20
ETC207	Mini	0.52	4.3	0.08	2.8 ± 0.3	2.0 -0.7	1.9 -0.9	6.7 ± 0.7	4.6 -2.1	3.8 -2.9	61 ± 25	122 +61	85 +24
DTC025A	Full	0.47	4.1	0.08	1.9 ± 0.3	1.8 -0.1	1.6 -0.3	3.6 ± 0.5	3.5 -0.1	3.1 -0.6	129 ± 19	121 -8	72 -57
DTC068B	Full	0.48	3.7	0.06	2.0 ± 0.3	1.8 -0.2	1.7 -0.3	3.7 ± 0.5	3.5 -0.2	3.1 -0.7	126 ± 25	114 -12	72 -53
DTC035A	Full	0.17	3.9	0.11	0.3 ± 0.2	0.2 -0.2	0.3 -0.0	-0.5 ± 0.2	-0.6 -0.1	-0.7 -0.2	-20 ± 15	-65 -45	-67 -46
DTC067B	Full	0.17	3.8	0.17	0.3 ± 0.1	0.2 -0.1	0.3 -0.1	-0.3 ± 0.1	-0.4 -0.0	-0.4 -0.1	-38 ± 9	-54 -15	-55 -16
							p-Xylene						
ETC196	Mini	0.52	5.0	0.08	0.4 ± 0.3	1.3 +1.0	0.4 +0.1	1.7 ± 0.7	3.4 +1.7	0.9 -0.8	39 ± 27	91 +53	16 -23
							1,2,3-Trimethylbenzene						
ETC267	Mini	0.48	4.3	0.04	3.6 ± 0.7	2.7 -0.8	3.2 -0.3	9.6 ± 1.4	5.9 -3.7	5.8 -3.8	272 ± 57	168 -104	155 -117
ETC269	Mini	0.46	4.3	0.04	4.1 ± 0.6	2.8 -1.3	3.3 -0.7	9.9 ± 1.1	6.2 -3.7	6.1 -3.8	284 ± 48	183 -101	167 -117
							1,2,4-Trimethylbenzene						
ETC348	Mini	0.49	4.5	0.04	1.8 ± 0.6	2.5 +0.6	1.2 -0.6	5.1 ± 1.2	5.7 +0.7	2.4 -2.7	72 ± 53	152 +80	49 -23
ETC249	Mini	0.48	4.4	0.04	1.6 ± 0.6	2.7 +1.0	1.3 -0.3	4.9 ± 1.1	6.1 +1.2	2.5 -2.4	115 ± 47	166 +51	53 -62
							1,3,5-Trimethylbenzene						
ETC344	Mini	0.49	4.9	0.05	4.5 ± 0.5	8.0 +3.4	8.3 +3.8	12.1 ± 1.1	19.0 +6.9	18.2 +6.1	314 ± 43	416 +102	385 +71

[a] Surrogates: "Mini" = n-hexane, ethene, m-xylene; "Full" = n-butane, n-octane, ethene, trans-2-butene, toluene, m-xylene and formaldehyde; "4-HC" = n-butane, propene, trans-2-butene, and m-xylene.

[b] Model calculations using the SAPRC-93 and the reoptimized aromatics mechanisms. Second number is difference between calculation and experiment.

The data in Table 15 indicate that the modifications to the mechanism did not significantly improve the model performance in the simulations of these blacklight chamber incremental reactivity experiments. The revised mechanism has a somewhat greater tendency to underpredict reactivities of toluene in the mini-surrogate runs than does the SAPRC-93 mechanism, and tends to underpredict the reactivity of 1,2,4-trimethylbenzene and (to a lesser extent) m-xylene in the mini-surrogate and the higher NO_x full surrogate runs. However, the two mechanisms have no significant differences in the simulations of the toluene runs using the full surrogate at low NO_x levels. The revised mechanism gives somewhat higher reactivity predictions for ethylbenzene than the previous version, though predictions of both are not outside the relatively large uncertainty of the data. The reactivity predictions are not significantly affected for o-xylene and 1,2,3- and 1,2,5-trimethylbenzenes. *p*-Xylene is the only compound where the reactivity predictions are improved by the reoptimization of the mechanism.

An improvement in model performance for toluene, m-xylene, or 1,3,5-trimethylbenzene is not expected because the previous mechanism was optimized in part to fit blacklight experiments with these compounds. The slight deterioration in reactivity predictions in the blacklight experiments is a result of giving the CTC experiments equal weight in the optimizations for the new mechanism, making the result somewhat less than optimal for blacklight conditions. The fact that the reoptimized mechanism does not perform as well as SAPRC-93 in the simulations of the 1,2,4-trimethylbenzene runs is somewhat surprising, in view of the opposite result observed in the simulations of the 1,2,4-trimethylbenzene - NO_x experiments. Presumably this situation will improve when more detailed information concerning aromatic photooxidation products is available for incorporation into the mechanisms.

CONCLUSIONS

This phase of our program has been useful in filling, at least in part, several important gaps in the existing environmental chamber data base for chemical mechanism evaluation and VOC reactivity assessment. The absolute light intensity measurements in indoor chamber experiments were verified using alternative actinometry methods. Information was obtained concerning the effects of humidity on results of environmental chamber experiments and the reproducibility of environmental chamber data. The large data base of incremental reactivity experiments from blacklight-irradiated chambers was extended to chambers using a light source whose spectrum more closely resembles sunlight. In addition, data from an extensive series of aromatic isomer - NO_x environmental chamber experiments, carried out using differing light sources, has provided the ability to systematically evaluate and optimize mechanisms for individual aromatic isomers which are applicable to varying lighting conditions. The conclusions and recommendations resulting from these new data are summarized below.

Evaluation of Light Intensity Measurements for Indoor Chambers. Accurate light source measurement is critical in mechanism evaluation, so one component of this program consisted of evaluating alternative methods for determining absolute light intensity in our indoor chamber experiments. Two alternative methods for measuring light intensity were evaluated: one based on the photostationary relationship between NO, NO_2, and O_3, and the other based on measuring the rate of photolysis of Cl_2. These were compared with the quartz tube method which has been the primary indoor chamber light intensity monitoring method in our previous studies. The steady-state method (at least as applied in our laboratories) proved to be unsatisfactory for routine monitoring of light intensity, since it was prone to giving variable results and occasionally gave anomalously low readings which could not always be explained by long sample lines. However, if the apparently anomalously low data are rejected, then its results are quite consistent with the quartz tube method in the blacklight chamber, and with the Cl_2 actinometry method in both chambers. The Cl_2 actinometry method appears to be the more useful alternative actinometry method. It gave more reproducible results which were also consistent with the other methods. The agreement between the Cl_2 actinometry results and the NO_2 actinometry using the quartz tube method in the blacklight chamber tends to validate both approaches, since they are based on quite different principles.

The quartz tube method was found to be unsatisfactory for obtaining absolute light intensities in the xenon arc chamber, and presumably other chambers which use nonhomogeneous light sources. This is because the light intensity entering the tube is not the same as the spherically integrated intensity in the

chamber. In the case of our xenon arc chamber, where in most actinometry experiments the tube was located outside the chamber in front of the lights, the quartz tube method gave NO_2 photolysis rates which were consistently ~30% higher than indicated by the results of the Cl_2 photolysis or the non-anomalous steady-state experiments. Since the latter two methods measure photolysis rates inside the chamber, they are not prone to biases introduced by inhomogeneity of the light source. Because of this, and because of the greater reproducibility and reliability of the Cl_2 actinometry method compared to the steady-state method, we conclude that the Cl_2 actinometry is the best approach for measuring absolute light intensity in the xenon arc chamber. This will therefore become the primary actinometry method for future programs using this chamber. The quartz tube, if always located in the same place, can provide information about how relative light intensity varies with time. However, the spectral intensity data from the LiCor spectraradiometer, which is available for almost all experiments in our xenon arc chamber, provides much more extensive and precise information in this regard. Consequently, the quartz tube actinometry data appear to be of limited utility to light characterization in our xenon arc chamber.

On the other hand, the quartz tube method still provides probably the best indication of both absolute and relative trends in light intensity in our blacklight chambers. The Cl_2 actinometry method appears to have similar precision, but the data for it are, thus far, quite limited. Both the quartz tube and Cl_2 actinometry method will be used in conjunction with future runs in the blacklight chamber. At present, there are insufficient data where both methods are applied to assess whether there may be biases involved in the application of the Cl_2 actinometry method, as might result if Cl_2 photodecomposed with less than unit quantum yields, or if there are inaccuracies in the absorption cross section data used to relate Cl_2 photolysis rates to NO_2 photolysis rates. Once a larger data base is obtained where both methods are employed, we can examine whether there might be non-negligible biases involved, and thus whether corrections may need to be applied when applying Cl_2 actinometry data to estimating NO_2 photolysis rates in the xenon arc chamber. However, the data obtained thus far indicate that the bias is unlikely to be large.

Humidity Effects. The existing chamber data base for mechanism evaluation has been carried out in chambers using differing humidities, but until this program systematic studies of effects of humidity on results of environmental chamber experiments and experimental reproducibility have been limited. At the time this program was designed we were unable to explain variabilities that were observed in the ability of the model to simulate results of replicate propene - NO_x which were periodically carried out in our laboratories, so one element of this study had been to determine whether humidity, or previous exposure of the chamber walls, might affect this. Therefore, a large number of replicate propene - NO_x and (to provide information concerning such effects on a different chemical system) toluene - NO_x

experiments were carried out at varying humidities. However, it was subsequently determined that the apparent unexplainable irreproducibility was due to the model using incorrect initial propene concentrations due to sporadic analytical problems. If runs where measured initial reactants disagree with amounts injected are rejected, then good reproducibility is obtained for all runs carried out with similar initial reactant concentrations and humidities. Therefore, we conclude that humidity is not a significant factor affecting reproducibility of chamber experiments for mechanism evaluation.

However, there are humidity effects which apparently are not appropriately represented by the current gas-phase mechanism or the current chamber effects model. In particular, increasing the humidity to near 100% causes reduction in peak O_3 concentration in both the propene - NO_x and toluene - NO_x systems, which is not accounted for by the model. It is not due to N_2O_5 wall hydrolysis because the model predicts that N_2O_5 hydrolysis is unimportant in the toluene system, presumably because N_2O_5 levels are suppressed by the rapid reaction of NO_3 radicals with the cresols formed in that system. Although this O_3 suppression occurs to a small extent in the ~50% RH runs, it is more than twice as great at ~100% RH, indicating that it is not a simple process which is first order in $[H_2O]$. It is almost certainly some sort of heterogeneous effect which becomes important as the system approaches saturation. An additional indication of problems with the chamber characterization model for experiments approaching water saturation comes from the inconsistency between the results of the ~100% RH n-butane - NO_x and propene or toluene - NO_x experiments, where the former indicated a much larger chamber radical source than was indicated by modeling the latter. Because of this, it is concluded that experiments with humidities near 100% should not be used for mechanism evaluation until we have a much better understanding of the surface processes which may be operating as the system approaches saturation.

Fortunately, most of the existing chamber data base for mechanism evaluation consist of experiments carried out under dry to ~50% RH conditions. Earlier SAPRC chamber experiments were carried out at ~50% RH air, while most of the more recent runs were carried out using dry air to minimize surface effects. Although the University of North Carolina (UNC) uses ambient air, steps are taken now to dry the air to minimize condensation on the walls in the morning (Jeffries et al. 1985a-c), and the humidity would tend to decrease during the run due to heating. However, earlier UNC runs should be examined for possible high humidity conditions when being used for mechanism evaluation. It is uncertain at which humidity level between ~50% and ~100% RH the problems indicated by our data may become significant. It may be that these problems may be near-saturation effects which become important primarily as the humidity approaches ~100%. However, experiments evaluating humidity effects in the ~60-90% range would be necessary to evaluate this.

It was also observed that the apparent formaldehyde yields in both the toluene and the propene systems declined as the humidity was increased. This is not a saturation effect since, unlike the O_3 suppression discussed above, the change in going from dry to ~50% RH was about the same as the change in going from ~50% to near 100% RH. It could possibly be due to a humidity effect in the gas-phase reaction of HO_2 with formaldehyde, though losses on the sample lines is a more likely explanation. However, one would think that sample line losses would increase more than linearly as the system approaches saturation, which was not observed. We will be obtaining additional data needed to resolve this issue in ongoing programs.

Other than the formaldehyde yields, the differences between results of experiments with dry air and those at ~50% RH are minor, and almost within the normal run-to-run variability of chamber experiments. The small difference should not significantly affect results of most mechanism evaluations. Therefore, we conclude that there are no significant humidity effects which complicate use of chamber data obtained from dry to ~50% RH conditions. This indicates that humidity should not be a significant complication in modeling chamber experiments with actual auto exhaust (where humidity is also a component) provided that the humidity in such experiments are not allowed to approach saturation.

Xenon Arc Reactivity Experiments. Much of the work in the first two phases consisted of incremental reactivity experiments carried out using blacklight light sources, and this phase of the program provided the first data concerning incremental reactivities using the more realistic xenon arc light source. Although the data obtained were not as comprehensive as the blacklight chamber data base, the compounds studied consisted of representatives of the major classes of compounds present in vehicle emissions and ambient air. Therefore, if any unexpected light source effect was important in affecting incremental reactivities of these major classes of compounds, they should be seen in at least some of these experiments.

The major conclusion arising from these experiments is that there are no unexplained light source effects on incremental reactivities of these compounds. The model which gave good simulations of the incremental reactivities of the non-aromatic compounds in the blacklight chamber experiments gave equally good (and in some cases slightly better) simulations of the incremental reactivities observed in these xenon arc chamber experiments. In the case of the aromatics, good simulations of the results of the xenon arc reactivity experiments were obtained once the mechanisms were reoptimized to be consistent with the single aromatic - NO_x experiments carried out in this chamber. Thus, the same mechanism gives similar (and, after reoptimization of the aromatics mechanisms generally satisfactory) predictions of incremental reactivities with both light sources. Thus, the differences between blacklights and solar

lighting can be accounted for in model simulations of incremental reactivity. This supports the applicability of the large blacklight chamber reactivity data base for mechanism evaluation for ambient air reactivity predictions.

Aromatic Isomer Mechanism Evaluation Data. Despite progress in recent years in our understanding of aromatic chemistry, it is still necessary to use parameritized mechanisms, optimized to fit chamber data, to model the atmospheric reactions of these compounds. Prior to this phase of the program there were inadequate chamber data to evaluate mechanisms to account for reactivity differences among aromatic isomers, and to account for the effect of changing light source on aromatic reactivity. This study provided the data needed to significantly improve the parameterization and performance of aromatics mechanisms. The data base obtained confirmed that the existing detailed SAPRC mechanism (SAPRC-93) did not correctly predict reactivity differences among aromatic isomers, and tended to underpredict aromatic reactivities when irradiated with the xenon arc light source. Therefore, a reparameterization of the aromatic mechanism was indicated.

The performance of the aromatic mechanism in simulating these data can be improved dramatically by a relatively simple reparameterization, without adding any new species or reactions to the mechanism. This involved allowing the yield of the methyl glyoxal ("MGLY") model species to be adjusted along with that for the uncharacterized product species "AFG2". Allowing the MGLY yields to increase at the expense of decreasing the AFG2 yield resulted in the model being able to adequately represent the reactivity with the xenon arc light source, while still satisfactorily simulating the blacklight chamber experiments. Since previously the α-dicarbonly model species used in the mechanism (of which MGLY is the most reactive) were based on measured glyoxal or methylglyoxal yields, this means that there are apparently other uncharacterized photoreactive aromatic fragmentation products with action spectra more closely representing that for methylglyoxal than that of acrolein (which is used for AFG2).

It was also found that, as expected, separate optimizations of MGLY and AFG2 yields for each aromatic isomer, rather than assuming that ethylbenzene reacts like toluene, that all dialkylbenzens react like m-xylene, and that all trialkylbenzenes react like the 1,3,5 isomer, resulted in significantly improved model performance for these compounds. Ethylbenzene appears to have much lower yields of photoreactive ring fragmentation products than does toluene, and likewise p-xylene and 1,2,4-trimethylbenzene also have lower yields of these products than do their other isomers. On the other hand, the overall reactive fragmentation product yields for o- and m-xylene are quite similar, as are 1,2,3- and 1,3,5-trimethylbenzene. This suggests that there may be a "para" substituent effect which somehow causes reduced total yields of photoreactive fragmentation products, since this is the one feature that distinguishes

p-xylene and 1,2,4-trimethylbenzene from their other isomers. Although this may be merely a coincidence, until we have a better understanding of the details of the aromatic ring fragmentation process and the reactivity characteristics of the products formed, this provides the best basis for estimating mechanistic parameters for the higher aromatic isomer for which evaluation data are not available for mechanism optimization.

A discussion of how these changes to the aromatic mechanisms affect atmospheric reactivity assessments is beyond the scope of this report, since we are still in the process of updating the overall mechanism. However, preliminary calculations indicate that the MIRs, relative to the base ROG mixture, increase by ~50% for toluene and m-xylene, decrease by ~50% for ethylbenzene, p-xylene, and 1,2,4-trimethylbenzene, and change by less than 10% for o-xylene and 1,2,3- and 1,3,5-trimethylbenzene. Relative MIRs for most of the non-aromatic VOCs (excluding those whose mechanisms were changed because of new data) decrease by ~6-10%, presumably because of the net increase for the aromatics in the base ROG. Reactivity Adjustment Factors of M85, CNG, LPG and E85 exhausts (CARB, 1993; Croes, private communication, 1991-1992) change by less than 10%.

Although the new parameterized mechanism performs significantly better in simulating the new, more comprehensive aromatic mechanism evaluation data base, it is not satisfactory in every respect, and is clearly an oversimplification to what is actually happening. A few experiments were carried out with benzene, and no mechanism could satisfactorily simulate both the blacklight and xenon arc chamber data for this compound. Although benzene is not a particularly important compound to predicting ozone formation, poor model performance for the simplest aromatic suggests fundamental problems with the aromatic mechanism. The reoptimized mechanism also systematically overpredicts the initial rate of O_3 formation at the beginning of the blacklight experiments for toluene, while underpredicting the ozone formation rate in the middle periods of both chambers, has similar discrepancies for many of the other isomers, and tends to underpredict the maximum ozone yields for most xylenes and trialkylbenzenes. Various other adjustments and optimizations, such as assuming that some aromatic products react with O_3, have been tried without significantly improving overall model performance.

Clearly, a better understanding of the details of the aromatic photooxidation process, and the reactivitity characteristics of the major reactive products formed, will result in improved aromatic mechanisms. This will require an identification *and quantification* of the major aromatic ring opening products which account for their reactivity, and, equally important, information on their rates and mechanisms. Such studies are being carried out at a number of laboratories, though it will probably be a number of years before sufficient information is available to have a significant impact on predictive

reactivity modeling. Until such information is available, we will have no choice but to use parameterized mechanisms. We are in the process of a complete update of the SAPRC mechanisms, which will include a re-assessment of how aromatics mechanisms are parameterized. The data obtained in this work will play a crucial role in the development, evaluation, and optimization of any new aromatics mechanisms which may result from this ongoing mechanism development effort.

REFERENCES

Atkinson, R. (1989): "Kinetics and Mechanisms of the Gas-Phase Reactions of the Hydroxyl Radical with Organic Compounds," J. Phys. Chem. Ref. Data, Monograph No 1.

Atkinson, R. (1990): "Gas-Phase Tropospheric Chemistry of Organic Compounds: A Review," Atmos. Environ., 24A, 1-24.

Atkinson, R. (1994): "Gas-Phase Tropospheric Chemistry of Organic Compounds," J. Phys. Chem. Ref. Data, Monograph No. 2.

Atkinson, R., D. L. Baulch, R. A. Cox, R. F. Hampson, Jr., J. A. Kerr, M. J. Rossi, and J. Troe (1996): "Evaluated Kinetic, Photochemical and Heterogeneous Data for Atmospheric Chemistry: Supplement V., IUPAC Subcommittee on Gas Kinetic Data Evaluation for Atmospheric Chemistry," J. Phys. Chem. Ref. Data, in press.

CARB (1993): "Proposed Regulations for Low-Emission Vehicles and Clean Fuels — Staff Report and Technical Support Document," California Air Resources Board, Sacramento, CA, August 13, 1990. See also Appendix VIII of "California Exhaust Emission Standards and Test Procedures for 1988 and Subsequent Model Passenger Cars, Light Duty Trucks and Medium Duty Vehicles," as last amended September 22, 1993. Incorporated by reference in Section 1960.1 (k) of Title 13, California Code of Regulations.

Carter, W. P. L. (1990): "A Detailed Mechanism for the Gas-Phase Atmospheric Reactions of Organic Compounds," Atm. Environ., 24A, 481-518.

Carter, W. P. L. (1994): "Development of Ozone Reactivity Scales for Volatile Organic Compounds," J. Air & Waste Manage. Assoc., 44, 881-899.

Carter, W. P. L. (1995a): "Computer Modeling of Environmental Chamber Measurements of Maximum Incremental Reactivities of Volatile Organic Compounds," Atmos. Environ., 29, 2513-2517.

Carter, W. P. L. (1995b): "Experimental Evaluation of Ozone Forming Potentials of Motor Vehicle Emissions," Research Proposal Submitted to the California Air Resources Board, July.

Carter, W. P. L., R. Atkinson, A. M. Winer, and J. N. Pitts, Jr. (1982): "Experimental Investigation of Chamber-Dependent Radical Sources," Int. J. Chem. Kinet., 14, 1071.

Carter, W. P. L. and R. Atkinson (1987): "An Experimental Study of Incremental Hydrocarbon Reactivity," Environ. Sci. Technol., 21, 670-679

Carter, W. P. L. and R. Atkinson (1989): "A Computer Modeling Study of Incremental Hydrocarbon Reactivity", Environ. Sci. Technol., 23, 864.

Carter, W. P. L., and F. W. Lurmann (1990): "Evaluation of the RADM Gas-Phase Chemical Mechanism," Final Report, EPA-600/3-90-001.

Carter, W. P. L. and F. W. Lurmann (1991): "Evaluation of a Detailed Gas-Phase Atmospheric Reaction Mechanism using Environmental Chamber Data," Atm. Environ. 25A, 2771-2806.

Carter, W. P. L., J. A. Pierce, I. L. Malkina, and D. Luo (1992): "Investigation of the Ozone Formation Potential of Selected Volatile Silicone Compounds," Final Report to Dow Corning Corporation, Midland, MI, November.

Carter, W. P. L., J. A. Pierce, I. L. Malkina, D. Luo and W. D. Long (1993a): "Environmental Chamber Studies of Maximum Incremental Reactivities of Volatile Organic Compounds," Report to Coordinating Research Council, Project No. ME-9, California Air Resources Board Contract No. A032-0692; South Coast Air Quality Management District Contract No. C91323, United States Environmental Protection Agency Cooperative Agreement No. CR-814396-01-0, University Corporation for Atmospheric Research Contract No. 59166, and Dow Corning Corporation. April 1.

Carter, W. P. L, D. Luo, I. L. Malkina, and J. A. Pierce (1993b): "An Experimental and Modeling Study of the Photochemical Ozone Reactivity of Acetone," Final Report to Chemical Manufacturers Association Contract No. KET-ACE-CRC-2.0. December 10.

Carter, W. P. L., D. Luo, I. L. Malkina, and C. Venkataraman (1994): "Screening Experiments to Evaluate the Aerosol Forming Potential of Selected Volatile Silicone Compounds," Final Report to Dow Corning Corporation, Midland, MI, May

Carter, W. P. L., D. Luo, I. L. Malkina, and J. A. Pierce (1995a): "Environmental Chamber Studies of Atmospheric Reactivities of Volatile Organic Compounds. Effects of Varying ROG Surrogate and NO_x," Final Report to Coordinating Research Council, Inc., Project ME-9, California Air Resources Board, Contract A032-0692, and South Coast Air Quality Management District, Contract C91323. March 24.

Carter, W. P. L., D. Luo, I. L. Malkina, and D. Fitz (1995b): "The University of California, Riverside Environmental Chamber Data Base for Evaluating Oxidant Mechanism. Indoor Chamber Experiments through 1993," Report submitted to the U. S. Environmental Protection Agency, EPA/AREAL, Research Triangle Park, NC, March 20.

Carter, W. P. L., D. Luo, I. L. Malkina, and J. A. Pierce (1995c): "Environmental Chamber Studies of Atmospheric Reactivities of Volatile Organic Compounds. Effects of Varying Chamber and Light Source," Final report to National Renewable Energy Laboratory, Contract XZ-2-12075, Coordinating Research Council, Inc., Project M-9, California Air Resources Board, Contract A032-0692, and South Coast Air Quality Management District, Contract C91323, March 26.

Carter, W. P. L., J. A. Pierce, D. Luo, and I. L. Malkina (1995d): "Environmental Chamber Studies of Maximum Incremental Reactivities of Volatile Organic Compounds," Atmos. Environ. 29, 2499-2511.

Gery, M. W., G. Z. Whitten, and J. P. Killus (1988): "Development and Testing of the CBM-IV For Urban and Regional Modeling," EPA-600/ 3-88-012, January.

Jeffries, H. E., R. M. Kamens, K. G. Sexton, and A. A. Gerhardt (1982): "Outdoor Smog Chamber Experiments to Test Photochemical Models", EPA-600/3-82-016a, April.

Jeffries, H. E., Sexton, K. G., Kamens, R. M. and Holleman, M. S. (1985a): "Outdoor Smog Chamber Experiments to Test Photochemical Models: Phase II," Final Report, EPA-600/3-85-029.

Jeffries, H. E., Sexton, K. G., Morris, T. P., Jackson, H., Goodman, R. G., Kamens, R. M. and Holleman, M. S. (1985b): "Outdoor Smog Chamber Experiments Using Automobile Exhaust," Final Report, EPA-600/3-85-032.

Jeffries, H. E., K. G. Sexton, and M. S. Holleman (1985c): "Outdoor Smog Chamber experiments: Reactivity of Methanol Exhaust," Final Report, EPA-600/3-85-009a, September.

Jeffries, H. E., K. G. Sexton, J. R. Arnold, Y. Bai, J. L. Li, and R. Crouse (1990): "A Chamber and Modeling Study to Assess the Photochemistry of Formaldehyde," Report on EPA Cooperative Agreement CR-813964, Atmospheric Research and Exposure Assessment Laboratory, EPA, Research Triangle Park, NC.

Jeffries, H. E., M. W. Gery and W. P. L. Carter (1992): "Protocol for Evaluating Oxidant Mechanisms for Urban and Regional Models," Report for U. S. Environmental Protection Agency Cooperative Agreement No. 815779, Atmospheric Research and Exposure Assessment Laboratory, Research Triangle Park, NC.

Johnson, G. M. (1983): "Factors Affecting Oxidant Formation in Sydney Air," in "The Urban Atmosphere -- Sydney, a Case Study." Eds. J. N. Carras and G. M. Johnson (CSIRO, Melbourne), pp. 393-408.

NRC (1991): "Rethinking the Ozone Problem in Urban and Regional Air Pollution," National Research Council Committee on Tropospheric Ozone Formation and Measurement. National Academy Press, Washington, DC.

Pitts, J. N., Jr., R. Atkinson, W. P. L. Carter, A. M. Winer, and E. C. Tuazon (1983): "Chemical Consequences of Air Quality Standard and of Control Implementation Programs," Final Report to the California ARB Contract No. A1-030-32, April.

Pitts, J. N., Jr., E. Sanhueza, R. Atkinson, W. P. L. Carter, A. M. Winer, G. W. Harris, and C. N. Plum (1984): "An Investigation of the Dark Formation of Nitrous Acid in Environmental Chambers," Int. J. Chem. Kinet., 16, 919-939.

Stockwell, W. R., P. Middleton, J. S. Chang, and X. Tang (1990): "The Second Generation Regional Acid Deposition Model Chemical Mechanism for Regional Air Quality Modeling," J. Geophys. Res. 95, 16343- 16376.

Tuazon, E. C., R. Atkinson, C. N. Plum, A. M. Winer, and J. N. Pitts, Jr. (1983): "The Reaction of Gas-Phase N_2O_5 with Water Vapor," Geophys. Res. Lett. 10, 953-956.

Zafonte, L., P. L. Rieger, and J. R. Holmes (1977): "Nitrogen Dioxide Photolysis in the Los Angeles Atmosphere," Environ. Sci. Technol. 11, 483-487.

APPENDIX A
LISTING OF THE CHEMICAL MECHANISM

The chemical mechanism used in the simulations discussed in this report is given in Tables A-1 through A-3. Table A-1 lists the species used in the mechanism, Table A-2 gives the reactions and rate constants, and Table A-3 gives the parameters used to calculate the rates of the photolysis reactions. Footnotes to Table A-2 indicate the format used for the reaction listing.

Table A-1. List of species in the chemical mechanism used in the model simulations for this study.

Name	Description
Constant Species.	
O2	Oxygen
M	Air
H2O	Water
Active Inorganic Species.	
O3	Ozone
NO	Nitric Oxide
NO2	Nitrogen Dioxide
NO3	Nitrate Radical
N2O5	Nitrogen Pentoxide
HONO	Nitrous Acid
HNO3	Nitric Acid
HNO4	Peroxynitric Acid
HO2H	Hydrogen Peroxide
Active Radical Species and Operators.	
HO2.	Hydroperoxide Radicals
RO2.	Operator to Calculate Total Organic Peroxy Radicals
RCO3.	Operator to Calculate Total Acetyl Peroxy Radicals
Active Reactive Organic Product Species.	
CO	Carbon Monoxide
HCHO	Formaldehyde
CCHO	Acetaldehyde
RCHO	Lumped C3+ Aldehydes
ACET	Acetone
MEK	Lumped Ketones
PHEN	Phenol

Table A-1, (continued)

Name	Description
CRES	Cresols
BALD	Aromatic aldehydes (e.g., benzaldehyde)
GLY	Glyoxal
MGLY	Methyl Glyoxal
AFG1	Reactive Aromatic Fragmentation Products from benzene and naphthalene
AFG2	Other Reactive Aromatic Fragmentation Products
AFG3	Aromatic Fragmentation Products used in adjusted m-xylene mechanism
RNO3	Organic Nitrates
NPHE	Nitrophenols
PAN	Peroxy Acetyl Nitrate
PPN	Peroxy Propionyl Nitrate
GPAN	PAN Analogue formed from Glyoxal
PBZN	PAN Analogues formed from Aromatic Aldehydes
-OOH	Operator Representing Hydroperoxy Groups
Non-Reacting Species	
CO2	Carbon Dioxide
-C	"Lost Carbon"
-N	"Lost Nitrogen"
H2	Hydrogen
Steady State Species and Operators.	
HO.	Hydroxyl Radicals
O	Ground State Oxygen Atoms
O*1D2	Excited Oxygen Atoms
RO2-R.	Peroxy Radical Operator representing NO to NO_2 conversion with HO_2 formation.
RO2-N.	Peroxy Radical Operator representing NO consumption with organic nitrate formation.
RO2-NP.	Peroxy Radical Operator representing NO consumption with nitrophenol formation
R2O2.	Peroxy Radical Operator representing NO to NO_2 conversion.
CCO-O2.	Peroxy Acetyl Radicals
C2CO-O2.	Peroxy Propionyl Radicals
HCOCO-O2.	Peroxyacyl Radical formed from Glyoxal
BZ-CO-O2.	Peroxyacyl Radical formed from Aromatic Aldehydes
HOCOO.	Intermediate formed in Formaldehyde + HO_2 reaction
BZ-O.	Phenoxy Radicals
BZ(NO2)-O.	Nitratophenoxy Radicals
HOCOO.	Radical Intermediate formed in the HO_2 + Formaldehyde system.
(HCHO2)	Excited Criegee biradicals formed from $=CH_2$ groups
(CCHO2)	Excited Criegee biradicals formed from $=CHCH_3$ groups
(RCHO2)	Excited Criegee biradicals formed from =CHR groups, where R not CH_3
(C(C)CO2)	Excited Criegee biradicals formed from $=C(CH_3)_2$ groups
(C(R)CO2)	Excited Criegee biradicals formed from $=C(CH_3)R$ or CR_2 groups
(BZCHO2)	Excited Criegee biradicals formed from styrenes

Table A-1, (continued)

Name	Description
Hydrocarbon species represented explicitly	
N-C4	n-Butane
N-C6	n-Hexane
N-C8	n-Octane
ETHE	Ethene
PROPENE	Propene
T-2-BUTE	trans-2-Butene
BENZENE	Benzene
TOLUENE	Toluene
C2-BENZ	Ethylbenzene
O-XYLENE	o-Xylene
M-XYLENE	m-Xylene
P-XYLENE	p-Xylene
123-TMB	1,2,3-Trimethylbenzene
124-TMB	1,2,4-Trimethylbenzene
135-TMB	1,3,5-Trimethylbenzene

Table A-2. List of reactions in the chemical mechanism used in the model simulations for this study.

Rxn. Label	Kinetic Parameters [a] k(300)	A	Ea	B	Reactions [b]
Inorganic Reactions					
1	(Phot. Set = NO2)				NO2 + HV = NO + O
2	6.00E-34	6.00E-34	0.00	-2.30	O + O2 + M = O3 + M
3A	9.69E-12	6.50E-12	-0.24	0.00	O + NO2 = NO + O2
3B	1.55E-12	(Falloff Kinetics)			O + NO2 = NO3 + M
	k0 =	9.00E-32	0.00	-2.00	
	kINF =	2.20E-11	0.00	0.00	
		F= 0.60	n= 1.00		
4	1.88E-14	2.00E-12	2.78	0.00	O3 + NO = NO2 + O2
5	3.36E-17	1.40E-13	4.97	0.00	O3 + NO2 = O2 + NO3
6	2.80E-11	1.70E-11	-0.30	0.00	NO + NO3 = 2 NO2
7	1.92E-38	3.30E-39	-1.05	0.00	NO + NO + O2 = 2 NO2
8	1.26E-12	(Falloff Kinetics)			NO2 + NO3 = N2O5
	k0 =	2.20E-30	0.00	-4.30	
	kINF =	1.50E-12	0.00	-0.50	
		F= 0.60	n= 1.00		
9	5.53E+10	9.09E+26	22.26	0.00	N2O5 + #RCON8 = NO2 + NO3
10	1.00E-21	(No T Dependence)			N2O5 + H2O = 2 HNO3
11	4.17E-16	2.50E-14	2.44	0.00	NO2 + NO3 = NO + NO2 + O2
12A	(Phot. Set = NO3NO)				NO3 + HV = NO + O2
12B	(Phot. Set = NO3NO2)				NO3 + HV = NO2 + O
13A	(Phot. Set = O3O3P)				O3 + HV = O + O2
13B	(Phot. Set = O3O1D)				O3 + HV = O*1D2 + O2
14	2.20E-10	(No T Dependence)			O*1D2 + H2O = 2 HO.
15	2.92E-11	1.92E-11	-0.25	0.00	O*1D2 + M = O + M
16	4.81E-12	(Falloff Kinetics)			HO. + NO = HONO
	k0 =	7.00E-31	0.00	-2.60	
	kINF =	1.50E-11	0.00	-0.50	
		F= 0.60	n= 1.00		
17	(Phot. Set = HONO)				HONO + HV = HO. + NO
18	1.13E-11	(Falloff Kinetics)			HO. + NO2 = HNO3
	k0 =	2.60E-30	0.00	-3.20	
	kINF =	2.40E-11	0.00	-1.30	
		F= 0.60	n= 1.00		
19	1.03E-13	6.45E-15	-1.65	0.00	HO. + HNO3 = H2O + NO3
21	2.40E-13	(No T Dependence)			HO. + CO = HO2. + CO2
22	6.95E-14	1.60E-12	1.87	0.00	HO. + O3 = HO2. + O2
23	8.28E-12	3.70E-12	-0.48	0.00	HO2. + NO = HO. + NO2
24	1.37E-12	(Falloff Kinetics)			HO2. + NO2 = HNO4
	k0 =	1.80E-31	0.00	-3.20	
	kINF =	4.70E-12	0.00	-1.40	
		F= 0.60	n= 1.00		
25	7.92E+10	4.76E+26	21.66	0.00	HNO4 + #RCON24 = HO2. + NO2
27	4.61E-12	1.30E-12	-0.75	0.00	HNO4 + HO. = H2O + NO2 + O2
28	2.08E-15	1.10E-14	0.99	0.00	HO2. + O3 = HO. + 2 O2
29A	1.73E-12	2.20E-13	-1.23	0.00	HO2. + HO2. = HO2H + O2
29B	5.00E-32	1.90E-33	-1.95	0.00	HO2. + HO2. + M = HO2H + O2
29C	3.72E-30	3.10E-34	-5.60	0.00	HO2. + HO2. + H2O = HO2H + O2 + H2O
29D	2.65E-30	6.60E-35	-6.32	0.00	HO2. + HO2. + H2O = HO2H + O2 + H2O
30A	1.73E-12	2.20E-13	-1.23	0.00	NO3 + HO2. = HNO3 + O2
30B	5.00E-32	1.90E-33	-1.95	0.00	NO3 + HO2. + M = HNO3 + O2
30C	3.72E-30	3.10E-34	-5.60	0.00	NO3 + HO2. + H2O = HNO3 + O2 + H2O
30D	2.65E-30	6.60E-35	-6.32	0.00	NO3 + HO2. + H2O = HNO3 + O2 + H2O
31	(Phot. Set = H2O2)				HO2H + HV = 2 HO.
32	1.70E-12	3.30E-12	0.40	0.00	HO2H + HO. = HO2. + H2O
33	9.90E-11	4.60E-11	-0.46	0.00	HO. + HO2. = H2O + O2
Peroxy Radical Operators					
B1	7.68E-12	4.20E-12	-0.36	0.00	RO2. + NO = NO
B2	2.25E-11	(Falloff Kinetics)			RCO3. + NO = NO
	k0 =	5.65E-28	0.00	-7.10	
	kINF =	2.64E-11	0.00	-0.90	
		F= 0.27	n= 1.00		
B4	1.04E-11	(Falloff Kinetics)			RCO3. + NO2 = NO2
	k0 =	2.57E-28	0.00	-7.10	
	kINF =	1.20E-11	0.00	-0.90	
		F= 0.30	n= 1.00		
B5	4.90E-12	3.40E-13	-1.59	0.00	RO2. + HO2. = HO2. + RO2-HO2-PROD
B6	4.90E-12	3.40E-13	-1.59	0.00	RCO3. + HO2. = HO2. + RO2-HO2-PROD
B8	1.00E-15	(No T Dependence)			RO2. + RO2. = RO2-RO2-PROD
B9	1.09E-11	1.86E-12	-1.05	0.00	RO2. + RCO3. = RO2-RO2-PROD

Table A-2 (continued)

Rxn. Label	Kinetic Parameters [a] k(300)	A	Ea	B	Reactions [b]
B10	1.64E-11	2.80E-12	-1.05	0.00	RCO3. + RCO3. = RO2-RO2-PROD
B11	(Same k as for RO2.)				RO2-R. + NO = NO2 + HO2.
B12	(Same k as for RO2.)				RO2-R. + HO2. = -OOH
B13	(Same k as for RO2.)				RO2-R. + RO2. = RO2. + 0.5 HO2.
B14	(Same k as for RO2.)				RO2-R. + RCO3. = RCO3. + 0.5 HO2.
B19	(Same k as for RO2.)				RO2-N. + NO = RNO3
B20	(Same k as for RO2.)				RO2-N. + HO2. = -OOH + MEK + 1.5 -C
B21	(Same k as for RO2.)				RO2-N. + RO2. = RO2. + 0.5 HO2. + MEK + 1.5 -C
B22	(Same k as for RO2.)				RO2-N. + RCO3. = RCO3. + 0.5 HO2. + MEK + 1.5 -C
B15	(Same k as for RO2.)				R2O2. + NO = NO2
B16	(Same k as for RO2.)				R2O2. + HO2. =
B17	(Same k as for RO2.)				R2O2. + RO2. = RO2.
B18	(Same k as for RO2.)				R2O2. + RCO3. = RCO3.
B23	(Same k as for RO2.)				RO2-XN. + NO = -N
B24	(Same k as for RO2.)				RO2-XN. + HO2. = -OOH
B25	(Same k as for RO2.)				RO2-XN. + RO2. = RO2. + 0.5 HO2.
B26	(Same k as for RO2.)				RO2-XN. + RCO3. = RCO3. + HO2.
G2	(Same k as for RO2.)				RO2-NP. + NO = NPHE
G3	(Same k as for RO2.)				RO2-NP. + HO2. = -OOH + 6 -C
G4	(Same k as for RO2.)				RO2-NP. + RO2. = RO2. + 0.5 HO2. + 6 -C
G5	(Same k as for RO2.)				RO2-NP. + RCO3. = RCO3. + HO2. + 6 -C
Excited Criegee Biradicals					
RZ1	(fast)				(HCHO2) = 0.7 HCOOH + 0.12 "HO. + HO2. + CO" + 0.18 "H2 + CO2"
RZ2	(fast)				(CCHO2) = 0.25 CCOOH + 0.15 "CH4 + CO2" + 0.6 HO. + 0.3 "CCO-O2. + RCO3." + 0.3 "RO2-R. + HCHO + CO + RO2."
RZ3	(fast)				(RCHO2) = 0.25 CCOOH + 0.15 CO2 + 0.6 HO. + 0.3 "C2CO-O2. + RCO3." + 0.3 "RO2-R. + CCHO + CO + RO2." + 0.55 -C
RZ4	(fast)				(C(C)CO2) = HO. + R2O2. + HCHO + CCO-O2. + RCO3. + RO2.
RZ5	(fast)				(C(R)CO2) = HO. + CCO-O2. + CCHO + R2O2. + RCO3. + RO2.
RZ6	(fast)				(CYCCO2) = 0.3 "HO. + C2CO-O2. + R2O2. + RCO3. + RO2." + 0.3 RCHO + 4.2 -C
RZ8	(fast)				(BZCHO2) = 0.5 "BZ-O. + R2O2. + CO + HO."
ISZ1	(fast)				(C:CC(C)O2) = HO. + R2O2. + HCHO + C2CO-O2. + RO2. + RCO3.
ISZ2	(fast)				(C:C(C)CHO2) = 0.75 RCHO + 0.25 ISOPROD + 0.5 -C
MAZ1	(fast)				(C2(O2)CHO) = HO. + R2O2. + HCHO + HCOCO-O2. + RO2. + RCO3.
M1Z1	(fast)				(HOCCHO2) = 0.6 HO. + 0.3 "CCO-O2. + RCO3." + 0.3 "RO2-R. + HCHO + CO + RO2." + 0.8 -C
M2Z1	(fast)				(HCOCHO2) = 0.12 "HO2. + 2 CO + HO." + 0.74 -C + 0.51 "CO2 + HCHO"
M2Z2	(fast)				(C2(O2)COH) = HO. + MGLY + HO2. + R2O2. + RO2.
Organic Product Species					
B7	(Phot. Set = CO2H)				-OOH + HV = HO2. + HO.
B7A	1.81E-12	1.18E-12	-0.25	0.00	HO. + -OOH = HO.
B7B	3.71E-12	1.79E-12	-0.44	0.00	HO. + -OOH = RO2-R. + RO2.
C1	(Phot. Set = HCHONEWR)				HCHO + HV = 2 HO2. + CO
C2	(Phot. Set = HCHONEWM)				HCHO + HV = H2 + CO
C3	9.76E-12	1.13E-12	-1.29	2.00	HCHO + HO. = HO2. + CO + H2O
C4	7.79E-14	9.70E-15	-1.24	0.00	HCHO + HO2. = HOCOO.
C4A	1.77E+02	2.40E+12	13.91	0.00	HOCOO. = HO2. + HCHO
C4B	(Same k as for RO2.)				HOCOO. + NO = -C + NO2 + HO2.
C9	6.38E-16	2.80E-12	5.00	0.00	HCHO + NO3 = HNO3 + HO2. + CO
C10	1.57E-11	5.55E-12	-0.62	0.00	CCHO + HO. = CCO-O2. + H2O + RCO3.
C11A	(Phot. Set = CCHOR)				CCHO + HV = CO + HO2. + HCHO + RO2-R. + RO2.
C12	2.84E-15	1.40E-12	3.70	0.00	CCHO + NO3 = HNO3 + CCO-O2. + RCO3.
C25	1.97E-11	8.50E-12	-0.50	0.00	RCHO + HO. = C2CO-O2. + RCO3.
C26	(Phot. Set = RCHO)				RCHO + HV = CCHO + RO2-R. + RO2. + CO + HO2.
C27	2.84E-15	1.40E-12	3.70	0.00	NO3 + RCHO = HNO3 + C2CO-O2. + RCO3.
C38	2.23E-13	4.81E-13	0.46	2.00	ACET + HO. = R2O2. + HCHO + CCO-O2. + RCO3. + RO2.

Table A-2 (continued)

Rxn. Label	Kinetic Parameters [a] k(300)	A	Ea	B	Reactions [b]
C39	(Phot. Set = ACET-93C)				ACET + HV = CCO-O2. + HCHO + RO2-R. + RCO3. + RO2.
C44	1.16E-12	2.92E-13	-0.82	2.00	MEK + HO. = H2O + 0.5 "CCHO + HCHO + CCO-O2. + C2CO-O2." + RCO3. + 1.5 "R2O2. + RO2."
C57	(Phot. Set = KETONE)				MEK + HV + #0.1 = CCO-O2. + CCHO + RO2-R. + RCO3. + RO2.
C95	2.07E-12	2.19E-11	1.41	0.00	RNO3 + HO. = NO2 + 0.155 MEK + 1.05 RCHO + 0.48 CCHO + 0.16 HCHO + 0.11 -C + 1.39 "R2O2. + RO2."
C58A	(Phot. Set = GLYOXAL1)				GLY + HV = 0.8 HO2. + 0.45 HCHO + 1.55 CO
C58B	(Phot. Set = GLYOXAL2)				GLY + HV + #0.029 = 0.13 HCHO + 1.87 CO
C59	1.14E-11 (No T Dependence)				GLY + HO. = 0.6 HO2. + 1.2 CO + 0.4 "HCOCO-O2. + RCO3."
C60	(Same k as for CCHO)				GLY + NO3 = HNO3 + 0.6 HO2. + 1.2 CO + 0.4 "HCOCO-O2. + RCO3."
C68A	(Phot. Set = MEGLYOX1)				MGLY + HV = HO2. + CO + CCO-O2. + RCO3.
C68B	(Phot. Set = MEGLYOX2)				MGLY + HV + 0.107 = HO2. + CO + CCO-O2. + RCO3.
C69	1.72E-11 (No T Dependence)				MGLY + HO. = CO + CCO-O2. + RCO3.
C70	(Same k as for CCHO)				MGLY + NO3 = HNO3 + CO + CCO-O2. + RCO3.
G7	1.14E-11 (No T Dependence)				HO. + AFG1 = HCOCO-O2. + RCO3.
G8	(Phot. Set = ACROLEIN)				AFG1 + HV + #0.029 = HO2. + HCOCO-O2. + RCO3.
U2OH	1.72E-11 (No T Dependence)				HO. + AFG2 = C2CO-O2. + RCO3.
U2HV	(Phot. Set = ACROLEIN)				AFG2 + HV = HO2. + CO + CCO-O2. + RCO3.
G46	2.63E-11 (No T Dependence)				HO. + PHEN = 0.15 RO2-NP. + 0.85 RO2-R. + 0.2 GLY + 4.7 -C + RO2.
G51	3.60E-12 (No T Dependence)				NO3 + PHEN = HNO3 + BZ-O.
G52	4.20E-11 (No T Dependence)				HO. + CRES = 0.15 RO2-NP. + 0.85 RO2-R. + 0.2 MGLY + 5.5 -C + RO2.
G57	2.10E-11 (No T Dependence)				NO3 + CRES = HNO3 + BZ-O. + -C
G30	1.29E-11 (No T Dependence)				BALD + HO. = BZ-CO-O2. + RCO3.
G31	(Phot. Set = BZCHO)				BALD + HV + #0.05 = 7 -C
G32	2.61E-15	1.40E-12	3.75	0.00	BALD + NO3 = HNO3 + BZ-CO-O2.
G58	3.60E-12 (No T Dependence)				NPHE + NO3 = HNO3 + BZ(NO2)-O.
G59	(Same k as for BZ-O.)				BZ(NO2)-O. + NO2 = 2 -N + 6 -C
G60	(Same k as for RO2.)				BZ(NO2)-O. + HO2. = NPHE
G61	(Same k as for BZ-O.)				BZ(NO2)-O. = NPHE
C13	(Same k as for RCO3.)				CCO-O2. + NO = CO2 + NO2 + HCHO + RO2-R. + RO2.
C14	(Same k as for RCO3.)				CCO-O2. + NO2 = PAN
C15	(Same k as for RCO3.)				CCO-O2. + HO2. = -OOH + CO2 + HCHO
C16	(Same k as for RCO3.)				CCO-O2. + RO2. = RO2. + 0.5 HO2. + CO2 + HCHO
C17	(Same k as for RCO3.)				CCO-O2. + RCO3. = RCO3. + HO2. + CO2 + HCHO
C18	6.50E-04 (Falloff Kinetics)				PAN = CCO-O2. + NO2 + RCO3.
	k0 =	4.90E-03	23.97	0.00	
	kINF =	4.00E+16	27.08	0.00	
		F= 0.30	n= 1.00		
C28	(Same k as for RCO3.)				C2CO-O2. + NO = CCHO + RO2-R. + CO2 + NO2 + RO2.
C29	8.40E-12 (No T Dependence)				C2CO-O2. + NO2 = PPN
C30	(Same k as for RCO3.)				C2CO-O2. + HO2. = -OOH + CCHO + CO2
C31	(Same k as for RCO3.)				C2CO-O2. + RO2. = RO2. + 0.5 HO2. + CCHO + CO2
C32	(Same k as for RCO3.)				C2CO-O2. + RCO3. = RCO3. + HO2. + CCHO + CO2
C33	6.78E-04	1.60E+17	27.97	0.00	PPN = C2CO-O2. + NO2 + RCO3.
C62	(Same k as for RCO3.)				HCOCO-O2. + NO = NO2 + CO2 + CO + HO2.
C63	(Same k as for RCO3.)				HCOCO-O2. + NO2 = GPAN
C65	(Same k as for RCO3.)				HCOCO-O2. + HO2. = -OOH + CO2 + CO
C66	(Same k as for RCO3.)				HCOCO-O2. + RO2. = RO2. + 0.5 HO2. + CO2 + CO
C67	(Same k as for RCO3.)				HCOCO-O2. + RCO3. = RCO3. + HO2. + CO2 + CO
C64	(Same k as for PAN)				GPAN = HCOCO-O2. + NO2 + RCO3.
G33	(Same k as for RCO3.)				BZ-CO-O2. + NO = BZ-O. + CO2 + NO2 + R2O2. + RO2.
G43	3.53E-11	1.30E-11	-0.60	0.00	BZ-O. + NO2 = NPHE
G44	(Same k as for RO2.)				BZ-O. + HO2. = PHEN
G45	1.00E-03 (No T Dependence)				BZ-O. = PHEN
G34	8.40E-12 (No T Dependence)				BZ-CO-O2. + NO2 = PBZN
G36	(Same k as for RCO3.)				BZ-CO-O2. + HO2. = -OOH + CO2 + PHEN
G37	(Same k as for RCO3.)				BZ-CO-O2. + RO2. = RO2. + 0.5 HO2. + CO2 + PHEN

Table A-2 (continued)

Rxn. Label	Kinetic Parameters [a] k(300)	A	Ea	B	Reactions [b]
G38	(Same k as for RCO3.)				BZ-CO-O2. + RCO3. = RCO3. + HO2. + CO2 + PHEN
G35	2.17E-04	1.60E+15	25.90	0.00	PBZN = BZ-CO-O2. + NO2 + RCO3.
Hydrocarbon Species Represented Explicitly [c]					
	2.56E-12	1.36E-12	-0.38	2.00	N-C4 + HO. = 0.076 RO2-N. + 0.924 RO2-R. + 0.397 R2O2. + 0.001 HCHO + 0.571 CCHO + 0.14 RCHO + 0.533 MEK + -0.076 -C + 1.397 RO2.
	5.63E-12	1.35E-11	0.52	0.00	N-C6 + HO. = 0.185 RO2-N. + 0.815 RO2-R. + 0.738 R2O2. + 0.02 CCHO + 0.105 RCHO + 1.134 MEK + 0.186 -C + 1.738 RO2.
	8.76E-12	3.15E-11	0.76	0.00	N-C8 + HO. = 0.333 RO2-N. + 0.667 RO2-R. + 0.706 R2O2. + 0.002 RCHO + 1.333 MEK + 0.998 -C + 1.706 RO2.
	8.43E-12	1.96E-12	-0.87	0.00	ETHENE + HO. = RO2-R. + RO2. + 1.56 HCHO + 0.22 CCHO
	1.68E-18	9.14E-15	5.13	0.00	ETHENE + O3 = HCHO + (HCHO2)
	2.18E-16	4.39E-13	4.53	2.00	ETHENE + NO3 = R2O2. + RO2. + 2 HCHO + NO2
	7.42E-13	1.04E-11	1.57	0.00	ETHENE + O = RO2-R. + HO2. + RO2. + HCHO + CO
	2.60E-11	4.85E-12	-1.00	0.00	PROPENE + HO. = RO2-R. + RO2. + HCHO + CCHO
	1.05E-17	5.51E-15	3.73	0.00	PROPENE + O3 = 0.6 HCHO + 0.4 CCHO + 0.4 (HCHO2) + 0.6 (CCHO2)
	9.74E-15	4.59E-13	2.30	0.00	PROPENE + NO3 = R2O2. + RO2. + HCHO + CCHO + NO2
	4.01E-12	1.18E-11	0.64	0.00	PROPENE + O = 0.4 HO2. + 0.5 RCHO + 0.5 MEK + -0.5 -C
	6.30E-11	1.01E-11	-1.09	0.00	T-2-BUTE + HO. = RO2-R. + RO2. + 2 CCHO
	1.95E-16	6.64E-15	2.10	0.00	T-2-BUTE + O3 = CCHO + (CCHO2)
	3.92E-13	1.10E-13	-0.76	2.00	T-2-BUTE + NO3 = R2O2. + RO2. + 2 CCHO + NO2
	2.34E-11	2.26E-11	-0.02	0.00	T-2-BUTE + O = 0.4 HO2. + 0.5 RCHO + 0.5 MEK + 0.5 -C
	1.28E-12	2.50E-12	0.40	0.00	BENZENE + HO. = 0.236 PHEN + 0.207 GLY + 1.75 AFG1 + 0.764 RO2-R. + 0.236 HO2. + 0.67 -C + 0.764 RO2.
	5.91E-12	1.81E-12	-0.70	0.00	TOLUENE + HO. = 0.085 BALD + 0.26 CRES + 0.118 GLY + 0.847 MGLY + 0.276 AFG2 + 0.74 RO2-R. + 0.26 HO2. + 0.981 -C + 0.74 RO2.
	7.10E-12	(No T Dependence)			C2-BENZ + HO. = 0.085 BALD + 0.26 CRES + 0.118 GLY + 0.19 MGLY + 0.19 AFG2 + 0.74 RO2-R. + 0.26 HO2. + 4.209 -C + 0.74 RO2.
	1.37E-11	(No T Dependence)			O-XYLENE + HO. = 0.04 BALD + 0.18 CRES + 0.108 GLY + 0.61 MGLY + 0.6 AFG2 + 0.82 RO2-R. + 0.18 HO2. + 2.614 -C + 0.82 RO2.
	2.36E-11	(No T Dependence)			M-XYLENE + HO. = 0.04 BALD + 0.18 CRES + 0.108 GLY + 1.554 MGLY + 0.505 AFG2 + 0.82 RO2-R. + 0.18 HO2. + 0.068 -C + 0.82 RO2.
	1.43E-11	(No T Dependence)			P-XYLENE + HO. = 0.04 BALD + 0.18 CRES + 0.108 GLY + 0.03 MGLY + 0.19 AFG2 + 0.82 RO2-R. + 0.18 HO2. + 5.584 -C + 0.82 RO2.
	3.27E-11	(No T Dependence)			123-TMB + HO. = 0.03 BALD + 0.18 CRES + MGLY + 0.69 AFG2 + 0.82 RO2-R. + 0.18 HO2. + 2.46 -C + 0.82 RO2.
	3.25E-11	(No T Dependence)			124-TMB + HO. = 0.03 BALD + 0.18 CRES + 0.31 MGLY + 0.3 AFG2 + 0.82 RO2-R. + 0.18 HO2. + 5.7 -C + 0.82 RO2.
	5.75E-11	(No T Dependence)			135-TMB + HO. = 0.03 BALD + 0.18 CRES + 0.93 MGLY + 0.66 AFG2 + 0.82 RO2-R. + 0.18 HO2. + 2.76 -C + 0.82 RO2.
Reoptimized Aromatic Reactions [d]					
	1.28E-12	2.50E-12	0.40	0.00	BENZENE + HO. = 0.236 PHEN + 0.207 GLY + 1.44 AFG1 + 0.764 RO2-R. + 0.236 HO2. + 1.29 -C + 0.764 RO2.
	5.91E-12	1.81E-12	-0.70	0.00	TOLUENE + HO. = 0.085 BALD + 0.26 CRES + 0.118 GLY + 0.964 MGLY + 0.259 AFG2 + 0.74 RO2-R. + 0.26 HO2. + 0.681 -C + 0.74 RO2.

Table A-2 (continued)

Rxn. Label	Kinetic Parameters [a] k(300)	A	Ea	B	Reactions [b]
	7.10E-12	(No T Dependence)			C2-BENZ + HO. = 0.085 BALD + 0.26 CRES + 0.118 GLY + 0.199 MGLY + 0.181 AFG2 + 0.74 RO2-R. + 0.26 HO2. + 4.207 -C + 0.74 RO2.
	1.37E-11	(No T Dependence)			O-XYLENE + HO. = 0.04 BALD + 0.18 CRES + 0.108 GLY + 0.805 MGLY + 0.582 AFG2 + 0.82 RO2-R. + 0.18 HO2. + 2.083 -C + 0.82 RO2.
	2.36E-11	(No T Dependence)			M-XYLENE + HO. = 0.04 BALD + 0.18 CRES + 0.108 GLY + 1.599 MGLY + 0.461 AFG2 + 0.82 RO2-R. + 0.18 HO2. + 0.063 -C + 0.82 RO2.
	1.43E-11	(No T Dependence)			P-XYLENE + HO. = 0.04 BALD + 0.18 CRES + 0.108 GLY + 0.168 MGLY + 0.15 AFG2 + 0.82 RO2-R. + 0.18 HO2. + 5.289 -C + 0.82 RO2.
	3.27E-11	(No T Dependence)			123-TMB + HO. = 0.03 BALD + 0.18 CRES + 1.12 MGLY + 0.658 AFG2 + 0.82 RO2-R. + 0.18 HO2. + 2.195 -C + 0.82 RO2.
	3.25E-11	(No T Dependence)			124-TMB + HO. = 0.03 BALD + 0.18 CRES + 0.405 MGLY + 0.256 AFG2 + 0.82 RO2-R. + 0.18 HO2. + 5.546 -C + 0.82 RO2.
	5.75E-11	(No T Dependence)			135-TMB + HO. = 0.03 BALD + 0.18 CRES + 1.164 MGLY + 0.61 AFG2 + 0.82 RO2-R. + 0.18 HO2. + 2.207 -C + 0.82 RO2.
Reactions used to Represent Chamber-Dependent Processes [e]					
O3W	(varied)	(No T Dependence)			O3 =
N25I	(varied)	(No T Dependence)			N2O5 = 2 NOX-WALL
N25S	(varied)	(No T Dependence)			N2O5 + H2O = 2 NOX-WALL
NO2W	(varied)	(No T Dependence)			NO2 = (yHONO) HONO + (1-yHONO) NOX-WALL
XSHC	(varied)	(No T Dependence)			HO. = HO2.
RSI	(Phot. Set = NO2)				HV + #RS/K1 = HO.
ONO2	(Phot. Set = NO2)				HV + #E-NO2/K1 = NO2 + #-1 NOX-WALL

[a] Except as noted, expression for rate constant is $k = A\ e^{Ea/RT}\ (T/300)^{B}$. Rate constants and A factor are in ppm, min units. Units of Ea is kcal $mole^{-1}$. "Phot Set" means this is a photolysis reaction, with the absorption coefficients and quantum yields given in Table A-3. In addition, if "#(number)" or "#(parameter)" is given as a reactant, then the value of that number or parameter is multiplied by the result in the "rate constant expression" columns to obtain the rate constant used. Furthermore, "#RCONnn" as a reactant means that the rate constant for the reaction is obtained by multiplying the rate constant given by that for reaction "nn". Thus, the rate constant given is actually an equilibrium constant.
[b] Format of reaction listing same as used in documentation of the detailed mechanism (Carter 1990).
[c] Aromatic reactions are standard for the SAPRC-93 mechanism.
[d] All other reactions in the reoptimized aromatics mechanisms are the same as those listed elsewhere on this table.
[e] See Table 1 for the values of the parameters used for the specific chambers modeled in this study.

Table A-3. Absorption cross sections and quantum yields for photolysis reactions.

WL (nm)	Abs (cm^2)	QY	WL (nm)	Abs (cm^2)	QY	WL (nm)	Abs (cm^2)	QY	WL (nm)	Abs (cm^2)	QY	WL (nm)	Abs (cm^2)	QY
Photolysis File = NO2														
250.0	2.83E-20	1.000	255.0	1.45E-20	1.000	260.0	1.90E-20	1.000	265.0	2.05E-20	1.000	270.0	3.13E-20	1.000
275.0	4.02E-20	1.000	280.0	5.54E-20	1.000	285.0	6.99E-20	1.000	290.0	8.18E-20	0.999	295.0	9.67E-20	0.998
300.0	1.17E-19	0.997	305.0	1.66E-19	0.996	310.0	1.76E-19	0.995	315.0	2.25E-19	0.994	320.0	2.54E-19	0.993
325.0	2.79E-19	0.992	330.0	2.99E-19	0.991	335.0	3.45E-19	0.990	340.0	3.88E-19	0.989	345.0	4.07E-19	0.988
350.0	4.10E-19	0.987	355.0	5.13E-19	0.986	360.0	4.51E-19	0.984	365.0	5.78E-19	0.983	370.0	5.42E-19	0.981
375.0	5.35E-19	0.979	380.0	5.99E-19	0.975	381.0	5.98E-19	0.974	382.0	5.97E-19	0.973	383.0	5.96E-19	0.972
384.0	5.95E-19	0.971	385.0	5.94E-19	0.969	386.0	5.95E-19	0.967	387.0	5.96E-19	0.966	388.0	5.98E-19	0.964
389.0	5.99E-19	0.962	390.0	6.00E-19	0.960	391.0	5.98E-19	0.959	392.0	5.96E-19	0.957	393.0	5.93E-19	0.953
394.0	5.91E-19	0.950	395.0	5.89E-19	0.942	396.0	6.06E-19	0.922	397.0	6.24E-19	0.870	398.0	6.41E-19	0.820
399.0	6.59E-19	0.760	400.0	6.76E-19	0.695	401.0	6.67E-19	0.635	402.0	6.58E-19	0.560	403.0	6.50E-19	0.485
404.0	6.41E-19	0.425	405.0	6.32E-19	0.350	406.0	6.21E-19	0.290	407.0	6.10E-19	0.225	408.0	5.99E-19	0.185
409.0	5.88E-19	0.153	410.0	5.77E-19	0.130	411.0	5.88E-19	0.110	412.0	5.98E-19	0.094	413.0	6.09E-19	0.083
414.0	6.19E-19	0.070	415.0	6.30E-19	0.059	416.0	6.29E-19	0.048	417.0	6.27E-19	0.039	418.0	6.26E-19	0.030
419.0	6.24E-19	0.023	420.0	6.23E-19	0.018	421.0	6.18E-19	0.012	422.0	6.14E-19	0.008	423.0	6.09E-19	0.004
424.0	6.05E-19	0.000	425.0	6.00E-19	0.000									
Photolysis File = NO3NO														
585.0	2.77E-18	0.000	590.0	5.14E-18	0.250	595.0	4.08E-18	0.400	600.0	2.83E-18	0.250	605.0	3.45E-18	0.200
610.0	1.48E-18	0.200	615.0	1.96E-18	0.100	620.0	3.58E-18	0.100	625.0	9.25E-18	0.050	630.0	5.66E-18	0.050
635.0	1.45E-18	0.030	640.0	1.11E-18	0.000									
Photolysis File = NO3NO2														
400.0	0.00E+00	1.000	405.0	3.00E-20	1.000	410.0	4.00E-20	1.000	415.0	5.00E-20	1.000	420.0	8.00E-20	1.000
425.0	1.00E-19	1.000	430.0	1.30E-19	1.000	435.0	1.80E-19	1.000	440.0	1.90E-19	1.000	445.0	2.20E-19	1.000
450.0	2.80E-19	1.000	455.0	3.30E-19	1.000	460.0	3.70E-19	1.000	465.0	4.30E-19	1.000	470.0	5.10E-19	1.000
475.0	6.00E-19	1.000	480.0	6.40E-19	1.000	485.0	6.90E-19	1.000	490.0	8.80E-19	1.000	495.0	9.50E-19	1.000
500.0	1.01E-18	1.000	505.0	1.10E-18	1.000	510.0	1.32E-18	1.000	515.0	1.40E-18	1.000	520.0	1.45E-18	1.000
525.0	1.48E-18	1.000	530.0	1.94E-18	1.000	535.0	2.04E-18	1.000	540.0	1.81E-18	1.000	545.0	1.81E-18	1.000
550.0	2.36E-18	1.000	555.0	2.68E-18	1.000	560.0	3.07E-18	1.000	565.0	2.53E-18	1.000	570.0	2.54E-18	1.000
575.0	2.74E-18	1.000	580.0	3.05E-18	1.000	585.0	2.77E-18	1.000	590.0	5.14E-18	0.750	595.0	4.08E-18	0.600
600.0	2.83E-18	0.550	605.0	3.45E-18	0.400	610.0	1.45E-18	0.300	615.0	1.96E-18	0.250	620.0	3.58E-18	0.200
625.0	9.25E-18	0.150	630.0	5.66E-18	0.050	635.0	1.45E-18	0.000						
Photolysis File = O3O3P														
280.0	3.97E-18	0.100	281.0	3.60E-18	0.100	282.0	3.24E-18	0.100	283.0	3.01E-18	0.100	284.0	2.73E-18	0.100
285.0	2.44E-18	0.100	286.0	2.21E-18	0.100	287.0	2.01E-18	0.100	288.0	1.76E-18	0.100	289.0	1.58E-18	0.100
290.0	1.41E-18	0.100	291.0	1.26E-18	0.100	292.0	1.10E-18	0.100	293.0	9.89E-19	0.100	294.0	8.59E-19	0.100
295.0	7.70E-19	0.100	296.0	6.67E-19	0.100	297.0	5.84E-19	0.100	298.0	5.07E-19	0.100	299.0	4.52E-19	0.100
300.0	3.92E-19	0.100	301.0	3.42E-19	0.100	302.0	3.06E-19	0.100	303.0	2.60E-19	0.100	304.0	2.37E-19	0.100
305.0	2.01E-19	0.112	306.0	1.79E-19	0.149	307.0	1.56E-19	0.197	308.0	1.38E-19	0.259	309.0	1.25E-19	0.339
310.0	1.02E-19	0.437	311.0	9.17E-20	0.546	312.0	7.88E-20	0.652	313.0	6.77E-20	0.743	314.0	6.35E-20	0.816
315.0	5.10E-20	0.872	316.0	4.61E-20	0.916	317.0	4.17E-20	0.949	318.0	3.72E-20	0.976	319.0	2.69E-20	0.997
320.0	3.23E-20	1.000	330.0	6.70E-21	1.000	340.0	1.70E-21	1.000	350.0	4.00E-22	1.000	355.0	0.00E+00	1.000
400.0	0.00E+00	1.000	450.0	1.60E-22	1.000	500.0	1.34E-21	1.000	550.0	3.32E-21	1.000	600.0	5.06E-21	1.000
650.0	2.45E-21	1.000	700.0	8.70E-22	1.000	750.0	3.20E-22	1.000	800.0	1.60E-22	1.000	900.0	0.00E+00	1.000
Photolysis File = O3O1D														
280.0	3.97E-18	0.900	281.0	3.60E-18	0.900	282.0	3.24E-18	0.900	283.0	3.01E-18	0.900	284.0	2.73E-18	0.900
285.0	2.44E-18	0.900	286.0	2.21E-18	0.900	287.0	2.01E-18	0.900	288.0	1.76E-18	0.900	289.0	1.58E-18	0.900
290.0	1.41E-18	0.900	291.0	1.26E-18	0.900	292.0	1.10E-18	0.900	293.0	9.89E-19	0.900	294.0	8.59E-19	0.900
295.0	7.70E-19	0.900	296.0	6.67E-19	0.900	297.0	5.84E-19	0.900	298.0	5.07E-19	0.900	299.0	4.52E-19	0.900
300.0	3.92E-19	0.900	301.0	3.42E-19	0.900	302.0	3.06E-19	0.900	303.0	2.60E-19	0.900	304.0	2.37E-19	0.900
305.0	2.01E-19	0.888	306.0	1.79E-19	0.851	307.0	1.56E-19	0.803	308.0	1.38E-19	0.741	309.0	1.25E-19	0.661
310.0	1.02E-19	0.563	311.0	9.17E-20	0.454	312.0	7.88E-20	0.348	313.0	6.77E-20	0.257	314.0	6.35E-20	0.184
315.0	5.10E-20	0.128	316.0	4.61E-20	0.084	317.0	4.17E-20	0.051	318.0	3.72E-20	0.024	319.0	2.69E-20	0.003
320.0	3.23E-20	0.000												
Photolysis File = HONO														
311.0	0.00E+00	1.000	312.0	2.00E-21	1.000	313.0	4.20E-21	1.000	314.0	4.60E-21	1.000	315.0	4.20E-21	1.000
316.0	3.00E-21	1.000	317.0	4.60E-21	1.000	318.0	3.60E-20	1.000	319.0	6.10E-20	1.000	320.0	2.10E-20	1.000
321.0	4.27E-20	1.000	322.0	4.01E-20	1.000	323.0	3.93E-20	1.000	324.0	4.01E-20	1.000	325.0	4.04E-20	1.000
326.0	3.13E-20	1.000	327.0	4.12E-20	1.000	328.0	7.55E-20	1.000	329.0	6.64E-20	1.000	330.0	7.29E-20	1.000
331.0	8.70E-20	1.000	332.0	1.38E-19	1.000	333.0	5.91E-20	1.000	334.0	5.91E-20	1.000	335.0	6.45E-20	1.000
336.0	5.91E-20	1.000	337.0	4.58E-20	1.000	338.0	1.91E-19	1.000	339.0	1.63E-19	1.000	340.0	1.05E-19	1.000
341.0	8.70E-20	1.000	342.0	3.35E-19	1.000	343.0	2.01E-19	1.000	344.0	1.02E-19	1.000	345.0	8.54E-20	1.000
346.0	8.32E-20	1.000	347.0	8.20E-20	1.000	348.0	7.49E-20	1.000	349.0	7.13E-20	1.000	350.0	6.83E-20	1.000
351.0	1.74E-19	1.000	352.0	1.14E-19	1.000	353.0	3.71E-19	1.000	354.0	4.96E-19	1.000	355.0	2.46E-19	1.000
356.0	1.19E-19	1.000	357.0	9.35E-20	1.000	358.0	7.78E-20	1.000	359.0	7.29E-20	1.000	360.0	6.83E-20	1.000
361.0	6.90E-20	1.000	362.0	7.32E-20	1.000	363.0	9.00E-20	1.000	364.0	1.21E-19	1.000	365.0	1.33E-19	1.000
366.0	2.13E-19	1.000	367.0	3.52E-19	1.000	368.0	4.50E-19	1.000	369.0	2.93E-19	1.000	370.0	1.19E-19	1.000
371.0	9.46E-20	1.000	372.0	8.85E-20	1.000	373.0	7.44E-20	1.000	374.0	4.77E-20	1.000	375.0	2.70E-20	1.000
376.0	1.90E-20	1.000	377.0	1.50E-20	1.000	378.0	1.90E-20	1.000	379.0	5.80E-20	1.000	380.0	7.78E-20	1.000
381.0	1.14E-19	1.000	382.0	1.40E-19	1.000	383.0	1.72E-19	1.000	384.0	1.99E-19	1.000	385.0	1.90E-19	1.000
386.0	1.19E-19	1.000	387.0	5.65E-20	1.000	388.0	3.20E-20	1.000	389.0	1.90E-20	1.000	390.0	1.20E-20	1.000
391.0	5.00E-21	1.000	392.0	0.00E+00	1.000									
Photolysis File = H2O2														
250.0	8.30E-20	1.000	255.0	6.70E-20	1.000	260.0	5.20E-20	1.000	265.0	4.20E-20	1.000	270.0	3.20E-20	1.000
275.0	2.50E-20	1.000	280.0	2.00E-20	1.000	285.0	1.50E-20	1.000	290.0	1.13E-20	1.000	295.0	8.70E-21	1.000
300.0	6.60E-21	1.000	305.0	4.90E-21	1.000	310.0	3.70E-21	1.000	315.0	2.80E-21	1.000	320.0	2.00E-21	1.000
325.0	1.50E-21	1.000	330.0	1.20E-21	1.000	335.0	9.00E-22	1.000	340.0	7.00E-22	1.000	345.0	5.00E-22	1.000
350.0	3.00E-22	1.000	355.0	0.00E+00	1.000									

Table A-3. (continued)

WL (nm)	Abs (cm^2)	QY	WL (nm)	Abs (cm^2)	QY	WL (nm)	Abs (cm^2)	QY	WL (nm)	Abs (cm^2)	QY	WL (nm)	Abs (cm^2)	QY
Photolysis File = CO2H														
210.0	3.75E-19	1.000	220.0	2.20E-19	1.000	230.0	1.38E-19	1.000	240.0	8.80E-20	1.000	250.0	5.80E-20	1.000
260.0	3.80E-20	1.000	270.0	2.50E-20	1.000	280.0	1.50E-20	1.000	290.0	9.00E-21	1.000	300.0	5.80E-21	1.000
310.0	3.40E-21	1.000	320.0	1.90E-21	1.000	330.0	1.10E-21	1.000	340.0	6.00E-22	1.000	350.0	4.00E-22	1.000
360.0	0.00E+00	1.000												
Photolysis File = HCHONEWR														
280.0	2.49E-20	0.590	280.5	1.42E-20	0.596	281.0	1.51E-20	0.602	281.5	1.32E-20	0.608	282.0	9.73E-21	0.614
282.5	6.76E-21	0.620	283.0	5.82E-21	0.626	283.5	9.10E-21	0.632	284.0	3.71E-20	0.638	284.5	4.81E-20	0.644
285.0	3.95E-20	0.650	285.5	2.87E-20	0.656	286.0	2.24E-20	0.662	286.5	1.74E-20	0.668	287.0	1.13E-20	0.674
287.5	1.10E-20	0.680	288.0	2.62E-20	0.686	288.5	4.00E-20	0.692	289.0	3.55E-20	0.698	289.5	2.12E-20	0.704
290.0	1.07E-20	0.710	290.5	1.35E-20	0.713	291.0	1.99E-20	0.717	291.5	1.56E-20	0.721	292.0	8.65E-21	0.724
292.5	5.90E-21	0.727	293.0	1.11E-20	0.731	293.5	6.26E-20	0.735	294.0	7.40E-20	0.738	294.5	5.36E-20	0.741
295.0	4.17E-20	0.745	295.5	3.51E-20	0.749	296.0	2.70E-20	0.752	296.5	1.75E-20	0.755	297.0	1.16E-20	0.759
297.5	1.51E-20	0.763	298.0	3.69E-20	0.766	298.5	4.40E-20	0.769	299.0	3.44E-20	0.773	299.5	2.02E-20	0.776
300.0	1.06E-20	0.780	300.4	7.01E-21	0.780	300.6	8.63E-21	0.779	300.8	1.47E-20	0.779	301.0	2.01E-20	0.779
301.2	2.17E-20	0.779	301.4	1.96E-20	0.779	301.6	1.54E-20	0.778	301.8	1.26E-20	0.778	302.0	1.03E-20	0.778
302.2	8.53E-21	0.778	302.4	7.13E-21	0.778	302.6	6.61E-21	0.777	302.8	1.44E-20	0.777	303.0	3.18E-20	0.777
303.2	3.81E-20	0.777	303.4	5.57E-20	0.777	303.6	6.91E-20	0.776	303.8	6.58E-20	0.776	304.0	6.96E-20	0.776
304.2	5.79E-20	0.776	304.4	5.24E-20	0.776	304.6	4.30E-20	0.775	304.8	3.28E-20	0.775	305.0	3.60E-20	0.775
305.2	5.12E-20	0.775	305.4	4.77E-20	0.775	305.6	4.43E-20	0.774	305.8	4.60E-20	0.774	306.0	4.01E-20	0.774
306.2	3.28E-20	0.774	306.4	2.66E-20	0.774	306.6	2.42E-20	0.773	306.8	1.95E-20	0.773	307.0	1.58E-20	0.773
307.2	1.37E-20	0.773	307.4	1.19E-20	0.773	307.6	1.01E-20	0.772	307.8	9.01E-21	0.772	308.0	8.84E-21	0.772
308.2	2.08E-20	0.772	308.4	2.39E-20	0.772	308.6	3.08E-20	0.771	308.8	3.39E-20	0.771	309.0	3.18E-20	0.771
309.2	3.06E-20	0.771	309.4	2.84E-20	0.771	309.6	2.46E-20	0.770	309.8	1.95E-20	0.770	310.0	1.57E-20	0.770
310.2	1.26E-20	0.767	310.4	9.26E-21	0.764	310.6	7.71E-21	0.761	310.8	6.05E-21	0.758	311.0	5.13E-21	0.755
311.2	4.82E-21	0.752	311.4	4.54E-21	0.749	311.6	6.81E-21	0.746	311.8	1.04E-20	0.743	312.0	1.43E-20	0.740
312.2	1.47E-20	0.737	312.4	1.35E-20	0.734	312.6	1.13E-20	0.731	312.8	9.86E-21	0.728	313.0	7.82E-21	0.725
313.2	6.48E-21	0.722	313.4	1.07E-20	0.719	313.6	2.39E-20	0.716	313.8	3.80E-20	0.713	314.0	5.76E-20	0.710
314.2	6.14E-20	0.707	314.4	7.45E-20	0.704	314.6	5.78E-20	0.701	314.8	5.59E-20	0.698	315.0	4.91E-20	0.695
315.2	4.37E-20	0.692	315.4	3.92E-20	0.689	315.6	2.89E-20	0.686	315.8	2.82E-20	0.683	316.0	2.10E-20	0.680
316.2	1.66E-20	0.677	316.4	2.05E-20	0.674	316.6	4.38E-20	0.671	316.8	5.86E-20	0.668	317.0	6.28E-20	0.665
317.2	5.07E-20	0.662	317.4	4.33E-20	0.659	317.6	4.17E-20	0.656	317.8	3.11E-20	0.653	318.0	2.64E-20	0.650
318.2	2.24E-20	0.647	318.4	1.70E-20	0.644	318.6	1.24E-20	0.641	318.8	1.11E-20	0.638	319.0	7.70E-21	0.635
319.2	6.36E-21	0.632	319.4	5.36E-21	0.629	319.6	4.79E-21	0.626	319.8	6.48E-21	0.623	320.0	1.48E-20	0.620
320.2	1.47E-20	0.614	320.4	1.36E-20	0.608	320.6	1.69E-20	0.601	320.8	1.32E-20	0.595	321.0	1.49E-20	0.589
321.2	1.17E-20	0.583	321.4	1.15E-20	0.577	321.6	9.64E-21	0.570	321.8	7.26E-21	0.564	322.0	5.94E-21	0.558
322.2	4.13E-21	0.552	322.4	3.36E-21	0.546	322.6	2.39E-21	0.539	322.8	2.01E-21	0.533	323.0	1.76E-21	0.527
323.2	2.82E-21	0.521	323.4	4.65E-21	0.515	323.6	7.00E-21	0.508	323.8	7.80E-21	0.502	324.0	7.87E-21	0.496
324.2	6.59E-21	0.490	324.4	5.60E-21	0.484	324.6	4.66E-21	0.477	324.8	4.21E-21	0.471	325.0	7.77E-21	0.465
325.2	2.15E-20	0.459	325.4	3.75E-20	0.453	325.6	4.10E-20	0.446	325.8	6.47E-20	0.440	326.0	7.59E-20	0.434
326.2	6.51E-20	0.428	326.4	5.53E-20	0.422	326.6	5.76E-20	0.415	326.8	4.43E-20	0.409	327.0	3.44E-20	0.403
327.2	3.22E-20	0.397	327.4	2.13E-20	0.391	327.6	1.91E-20	0.384	327.8	1.42E-20	0.378	328.0	9.15E-21	0.372
328.2	6.79E-21	0.366	328.4	4.99E-21	0.360	328.6	4.77E-21	0.353	328.8	1.75E-20	0.347	329.0	3.27E-20	0.341
329.2	3.99E-20	0.335	329.4	5.13E-20	0.329	329.6	4.00E-20	0.322	329.8	3.61E-20	0.316	330.0	3.38E-20	0.310
330.2	3.08E-20	0.304	330.4	2.16E-20	0.298	330.6	2.09E-20	0.291	330.8	1.41E-20	0.285	331.0	9.95E-21	0.279
331.2	7.76E-21	0.273	331.4	6.16E-21	0.267	331.6	4.06E-21	0.260	331.8	3.03E-21	0.254	332.0	2.41E-21	0.248
332.2	1.74E-21	0.242	332.4	1.33E-21	0.236	332.6	2.70E-21	0.229	332.8	1.65E-21	0.223	333.0	1.17E-21	0.217
333.2	9.84E-22	0.211	333.4	8.52E-22	0.205	333.6	6.32E-22	0.198	333.8	5.21E-22	0.192	334.0	1.46E-21	0.186
334.2	1.80E-21	0.180	334.4	1.43E-21	0.174	334.6	1.03E-21	0.167	334.8	7.19E-22	0.161	335.0	4.84E-22	0.155
335.2	2.73E-22	0.149	335.4	1.34E-22	0.143	335.6	-1.62E-22	0.136	335.8	1.25E-22	0.130	336.0	4.47E-22	0.124
336.2	1.23E-21	0.118	336.4	2.02E-21	0.112	336.6	3.00E-21	0.105	336.8	2.40E-21	0.099	337.0	3.07E-21	0.093
337.2	2.29E-21	0.087	337.4	2.46E-21	0.081	337.6	2.92E-21	0.074	337.8	8.10E-21	0.068	338.0	1.82E-20	0.062
338.2	3.10E-20	0.056	338.4	3.24E-20	0.050	338.6	4.79E-20	0.043	338.8	5.25E-20	0.037	339.0	5.85E-20	0.031
339.2	4.33E-20	0.025	339.4	4.20E-20	0.019	339.6	3.99E-20	0.012	339.8	3.11E-20	0.006	340.0	2.72E-20	0.000
Photolysis File = HCHONEWM														
280.0	2.49E-20	0.350	280.5	1.42E-20	0.346	281.0	1.51E-20	0.341	281.5	1.32E-20	0.336	282.0	9.73E-21	0.332
282.5	6.76E-21	0.327	283.0	5.82E-21	0.323	283.5	9.10E-21	0.319	284.0	3.71E-20	0.314	284.5	4.81E-20	0.309
285.0	3.95E-20	0.305	285.5	2.87E-20	0.301	286.0	2.24E-20	0.296	286.5	1.74E-20	0.291	287.0	1.13E-20	0.287
287.5	1.10E-20	0.282	288.0	2.62E-20	0.278	288.5	4.00E-20	0.273	289.0	3.55E-20	0.269	289.5	2.12E-20	0.264
290.0	1.07E-20	0.260	290.5	1.35E-20	0.258	291.0	1.99E-20	0.256	291.5	1.56E-20	0.254	292.0	8.65E-21	0.252
292.5	5.90E-21	0.250	293.0	1.11E-20	0.248	293.5	6.26E-20	0.246	294.0	7.40E-20	0.244	294.5	5.36E-20	0.242
295.0	4.17E-20	0.240	295.5	3.51E-20	0.238	296.0	2.70E-20	0.236	296.5	1.75E-20	0.234	297.0	1.16E-20	0.232
297.5	1.51E-20	0.230	298.0	3.69E-20	0.228	298.5	4.40E-20	0.226	299.0	3.44E-20	0.224	299.5	2.02E-20	0.222
300.0	1.06E-20	0.220	300.4	7.01E-21	0.220	300.6	8.63E-21	0.221	300.8	1.47E-20	0.221	301.0	2.01E-20	0.221
301.2	2.17E-20	0.221	301.4	1.96E-20	0.221	301.6	1.54E-20	0.222	301.8	1.26E-20	0.222	302.0	1.03E-20	0.222
302.2	8.53E-21	0.222	302.4	7.13E-21	0.222	302.6	6.61E-21	0.223	302.8	1.44E-20	0.223	303.0	3.18E-20	0.223
303.2	3.81E-20	0.223	303.4	5.57E-20	0.223	303.6	6.91E-20	0.224	303.8	6.58E-20	0.224	304.0	6.96E-20	0.224
304.2	5.79E-20	0.224	304.4	5.24E-20	0.224	304.6	4.30E-20	0.225	304.8	3.28E-20	0.225	305.0	3.60E-20	0.225
305.2	5.12E-20	0.225	305.4	4.77E-20	0.225	305.6	4.43E-20	0.226	305.8	4.60E-20	0.226	306.0	4.01E-20	0.226
306.2	3.28E-20	0.226	306.4	2.66E-20	0.226	306.6	2.42E-20	0.227	306.8	1.95E-20	0.227	307.0	1.58E-20	0.227
307.2	1.37E-20	0.227	307.4	1.19E-20	0.227	307.6	1.01E-20	0.228	307.8	9.01E-21	0.228	308.0	8.84E-21	0.228
308.2	2.08E-20	0.228	308.4	2.39E-20	0.228	308.6	3.08E-20	0.229	308.8	3.39E-20	0.229	309.0	3.18E-20	0.229
309.2	3.06E-20	0.229	309.4	2.84E-20	0.229	309.6	2.46E-20	0.230	309.8	1.95E-20	0.230	310.0	1.57E-20	0.230
310.2	1.26E-20	0.233	310.4	9.26E-21	0.236	310.6	7.71E-21	0.239	310.8	6.05E-21	0.242	311.0	5.13E-21	0.245
311.2	4.82E-21	0.248	311.4	4.54E-21	0.251	311.6	6.81E-21	0.254	311.8	1.04E-20	0.257	312.0	1.43E-20	0.260
312.2	1.47E-20	0.263	312.4	1.35E-20	0.266	312.6	1.13E-20	0.269	312.8	9.86E-21	0.272	313.0	7.82E-21	0.275
313.2	6.48E-21	0.278	313.4	1.07E-20	0.281	313.6	2.39E-20	0.284	313.8	3.80E-20	0.287	314.0	5.76E-20	0.290
314.2	6.14E-20	0.293	314.4	7.45E-20	0.296	314.6	5.78E-20	0.299	314.8	5.59E-20	0.302	315.0	4.91E-20	0.305
315.2	4.37E-20	0.308	315.4	3.92E-20	0.311	315.6	2.89E-20	0.314	315.8	2.82E-20	0.317	316.0	2.10E-20	0.320
316.2	1.66E-20	0.323	316.4	2.05E-20	0.326	316.6	4.38E-20	0.329	316.8	5.86E-20	0.332	317.0	6.28E-20	0.335
317.2	5.07E-20	0.338	317.4	4.33E-20	0.341	317.6	4.17E-20	0.344	317.8	3.11E-20	0.347	318.0	2.64E-20	0.350
318.2	2.24E-20	0.353	318.4	1.70E-20	0.356	318.6	1.24E-20	0.359	318.8	1.11E-20	0.362	319.0	7.70E-21	0.365

Table A-3. (continued)

WL (nm)	Abs (cm^2)	QY	WL (nm)	Abs (cm^2)	QY	WL (nm)	Abs (cm^2)	QY	WL (nm)	Abs (cm^2)	QY	WL (nm)	Abs (cm^2)	QY
319.2	6.36E-21	0.368	319.4	5.36E-21	0.371	319.6	4.79E-21	0.374	319.8	6.48E-21	0.377	320.0	1.48E-20	0.380
320.2	1.47E-20	0.386	320.4	1.36E-20	0.392	320.6	1.69E-20	0.399	320.8	1.32E-20	0.405	321.0	1.49E-20	0.411
321.2	1.17E-20	0.417	321.4	1.15E-20	0.423	321.6	9.64E-21	0.430	321.8	7.26E-21	0.436	322.0	5.94E-21	0.442
322.2	4.13E-21	0.448	322.4	3.36E-21	0.454	322.6	2.39E-21	0.461	322.8	2.01E-21	0.467	323.0	1.76E-21	0.473
323.2	2.82E-21	0.479	323.4	4.65E-21	0.485	323.6	7.00E-21	0.492	323.8	7.80E-21	0.498	324.0	7.87E-21	0.504
324.2	6.59E-21	0.510	324.4	5.60E-21	0.516	324.6	4.66E-21	0.523	324.8	4.21E-21	0.529	325.0	7.77E-21	0.535
325.2	2.15E-20	0.541	325.4	3.75E-20	0.547	325.6	4.10E-20	0.554	325.8	6.47E-20	0.560	326.0	7.59E-20	0.566
326.2	6.51E-20	0.572	326.4	5.53E-20	0.578	326.6	5.76E-20	0.585	326.8	4.43E-20	0.591	327.0	3.44E-20	0.597
327.2	3.22E-20	0.603	327.4	2.13E-20	0.609	327.6	1.91E-20	0.616	327.8	1.42E-20	0.622	328.0	9.15E-21	0.628
328.2	6.79E-21	0.634	328.4	4.99E-21	0.640	328.6	4.77E-21	0.647	328.8	1.75E-20	0.653	329.0	3.27E-20	0.659
329.2	3.99E-20	0.665	329.4	5.13E-20	0.671	329.6	4.00E-20	0.678	329.8	3.61E-20	0.684	330.0	3.38E-20	0.690
330.2	3.08E-20	0.694	330.4	2.16E-20	0.699	330.6	2.09E-20	0.703	330.8	1.41E-20	0.708	331.0	9.95E-21	0.712
331.2	7.76E-21	0.717	331.4	6.16E-21	0.721	331.6	4.06E-21	0.726	331.8	3.03E-21	0.730	332.0	2.41E-21	0.735
332.2	1.74E-21	0.739	332.4	1.33E-21	0.744	332.6	2.70E-21	0.748	332.8	1.65E-21	0.753	333.0	1.17E-21	0.757
333.2	9.84E-22	0.762	333.4	8.52E-22	0.766	333.6	6.32E-22	0.771	333.8	5.21E-22	0.775	334.0	1.46E-21	0.780
334.2	1.80E-21	0.784	334.4	1.43E-21	0.789	334.6	1.03E-21	0.793	334.8	7.19E-22	0.798	335.0	4.84E-22	0.802
335.2	2.73E-22	0.798	335.4	1.34E-22	0.794	335.6	0.00E+00	0.790	335.8	1.25E-22	0.786	336.0	4.47E-22	0.782
336.2	1.23E-21	0.778	336.4	2.02E-21	0.773	336.6	3.00E-21	0.769	336.8	2.40E-21	0.764	337.0	3.07E-21	0.759
337.2	2.29E-21	0.754	337.4	2.46E-21	0.749	337.6	2.92E-21	0.745	337.8	8.10E-21	0.740	338.0	1.82E-20	0.734
338.2	3.10E-20	0.729	338.4	3.24E-20	0.724	338.6	4.79E-20	0.719	338.8	5.25E-20	0.714	339.0	5.85E-20	0.709
339.2	4.33E-20	0.703	339.4	4.20E-20	0.698	339.6	3.99E-20	0.693	339.8	3.11E-20	0.687	340.0	2.72E-20	0.682
340.2	1.99E-20	0.676	340.4	1.76E-20	0.671	340.6	1.39E-20	0.666	340.8	1.01E-20	0.660	341.0	6.57E-21	0.655
341.2	4.83E-21	0.649	341.4	3.47E-21	0.643	341.6	2.23E-21	0.638	341.8	1.55E-21	0.632	342.0	3.70E-21	0.627
342.2	4.64E-21	0.621	342.4	1.08E-20	0.616	342.6	1.14E-20	0.610	342.8	1.79E-20	0.604	343.0	2.33E-20	0.599
343.2	1.72E-20	0.593	343.4	1.55E-20	0.588	343.6	1.46E-20	0.582	343.8	1.38E-20	0.576	344.0	1.00E-20	0.571
344.2	8.26E-21	0.565	344.4	6.32E-21	0.559	344.6	4.28E-21	0.554	344.8	3.22E-21	0.548	345.0	2.54E-21	0.542
345.2	1.60E-21	0.537	345.4	1.15E-21	0.531	345.6	8.90E-22	0.525	345.8	6.50E-22	0.520	346.0	5.09E-22	0.514
346.2	5.15E-22	0.508	346.4	3.45E-22	0.503	346.6	3.18E-22	0.497	346.8	3.56E-22	0.491	347.0	3.24E-22	0.485
347.2	3.34E-22	0.480	347.4	2.88E-22	0.474	347.6	2.84E-22	0.468	347.8	9.37E-22	0.463	348.0	9.70E-22	0.457
348.2	7.60E-22	0.451	348.4	6.24E-22	0.446	348.6	4.99E-22	0.440	348.8	4.08E-22	0.434	349.0	3.39E-22	0.428
349.2	1.64E-22	0.423	349.4	1.49E-22	0.417	349.6	8.30E-23	0.411	349.8	2.52E-23	0.406	350.0	2.57E-23	0.400
350.2	0.00E+00	0.394	350.4	5.16E-23	0.389	350.6	0.00E+00	0.383	350.8	2.16E-23	0.377	351.0	7.07E-23	0.371
351.2	3.45E-23	0.366	351.4	1.97E-22	0.360	351.6	4.80E-22	0.354	351.8	3.13E-21	0.349	352.0	6.41E-21	0.343
352.2	8.38E-21	0.337	352.4	1.55E-20	0.331	352.6	1.86E-20	0.326	352.8	1.94E-20	0.320	353.0	2.78E-20	0.314
353.2	1.96E-20	0.309	353.4	1.67E-20	0.303	353.6	1.75E-20	0.297	353.8	1.63E-20	0.291	354.0	1.36E-20	0.286
354.2	1.07E-20	0.280	354.4	9.82E-21	0.274	354.6	8.66E-21	0.269	354.8	6.44E-21	0.263	355.0	4.84E-21	0.257
355.2	3.49E-21	0.251	355.4	2.41E-21	0.246	355.6	1.74E-21	0.240	355.8	1.11E-21	0.234	356.0	7.37E-22	0.229
356.2	4.17E-22	0.223	356.4	1.95E-22	0.217	356.6	1.50E-22	0.211	356.8	8.14E-23	0.206	357.0	0.00E+00	0.200
Photolysis File = CCHOR														
260.0	2.00E-20	0.310	270.0	3.40E-20	0.390	280.0	4.50E-20	0.580	290.0	4.90E-20	0.530	295.0	4.50E-20	0.480
300.0	4.30E-20	0.430	305.0	3.40E-20	0.370	315.0	2.10E-20	0.170	320.0	1.80E-20	0.100	325.0	1.10E-20	0.040
330.0	6.90E-21	0.000												
Photolysis File = RCHO														
280.0	5.26E-20	0.960	290.0	5.77E-20	0.910	300.0	5.05E-20	0.860	310.0	3.68E-20	0.600	320.0	1.66E-20	0.360
330.0	6.49E-21	0.200	340.0	1.44E-21	0.080	345.0	0.00E+00	0.020						
Photolysis File = ACET-93C														
250.0	2.37E-20	0.760	260.0	3.66E-20	0.800	270.0	4.63E-20	0.640	280.0	5.05E-20	0.550	290.0	4.21E-20	0.300
300.0	2.78E-20	0.150	310.0	1.44E-20	0.050	320.0	4.80E-21	0.026	330.0	8.00E-22	0.017	340.0	1.00E-22	0.000
350.0	3.00E-23	0.000	360.0	0.00E+00	0.000									
Photolysis File = KETONE														
210.0	1.10E-21	1.000	220.0	1.20E-21	1.000	230.0	4.60E-21	1.000	240.0	1.30E-20	1.000	250.0	2.68E-20	1.000
260.0	4.21E-20	1.000	270.0	5.54E-20	1.000	280.0	5.92E-20	1.000	290.0	5.16E-20	1.000	300.0	3.44E-20	1.000
310.0	1.53E-20	1.000	320.0	4.60E-21	1.000	330.0	1.10E-21	1.000	340.0	0.00E+00	1.000			
Photolysis File = GLYOXAL1														
230.0	2.87E-21	1.000	235.0	2.87E-21	1.000	240.0	4.30E-21	1.000	245.0	5.73E-21	1.000	250.0	8.60E-21	1.000
255.0	1.15E-20	1.000	260.0	1.43E-20	1.000	265.0	1.86E-20	1.000	270.0	2.29E-20	1.000	275.0	2.58E-20	1.000
280.0	2.87E-20	1.000	285.0	3.30E-20	1.000	290.0	3.15E-20	1.000	295.0	3.30E-20	1.000	300.0	3.58E-20	1.000
305.0	2.72E-20	1.000	310.0	2.72E-20	1.000	312.5	2.87E-20	1.000	315.0	2.29E-20	1.000	320.0	1.43E-20	1.000
325.0	1.15E-20	1.000	327.5	1.43E-20	1.000	330.0	1.15E-20	1.000	335.0	2.87E-21	1.000	340.0	0.00E+00	1.000
Photolysis File = GLYOXAL2														
355.0	0.00E+00	1.000	360.0	2.29E-21	1.000	365.0	2.87E-21	1.000	370.0	8.03E-21	1.000	375.0	1.00E-20	1.000
380.0	1.72E-20	1.000	382.0	1.58E-20	1.000	384.0	1.49E-20	1.000	386.0	1.49E-20	1.000	388.0	2.87E-20	1.000
390.0	3.15E-20	1.000	391.0	3.24E-20	1.000	392.0	3.04E-20	1.000	393.0	2.23E-20	1.000	394.0	2.63E-20	1.000
395.0	3.04E-20	1.000	396.0	2.63E-20	1.000	397.0	2.43E-20	1.000	398.0	3.24E-20	1.000	399.0	3.04E-20	1.000
400.0	2.84E-20	1.000	401.0	3.24E-20	1.000	402.0	4.46E-20	1.000	403.0	5.27E-20	1.000	404.0	4.26E-20	1.000
405.0	3.04E-20	1.000	406.0	3.04E-20	1.000	407.0	2.84E-20	1.000	408.0	2.43E-20	1.000	409.0	2.84E-20	1.000
410.0	6.08E-20	1.000	411.0	5.07E-20	1.000	411.5	6.08E-20	1.000	412.0	4.86E-20	1.000	413.0	8.31E-20	1.000
413.5	6.48E-20	1.000	414.0	7.50E-20	1.000	414.5	8.11E-20	1.000	415.0	8.11E-20	1.000	415.5	6.89E-20	1.000
416.0	4.26E-20	1.000	417.0	4.86E-20	1.000	418.0	5.88E-20	1.000	419.0	6.69E-20	1.000	420.0	3.85E-20	1.000
421.0	5.67E-20	1.000	421.5	4.46E-20	1.000	422.0	5.27E-20	1.000	422.5	1.05E-19	1.000	423.0	8.51E-20	1.000
424.0	6.08E-20	1.000	425.0	7.29E-20	1.000	426.0	1.18E-19	1.000	426.5	1.30E-19	1.000	427.0	1.07E-19	1.000
428.0	1.66E-19	1.000	429.0	4.05E-20	1.000	430.0	5.07E-20	1.000	431.0	4.86E-20	1.000	432.0	4.05E-20	1.000
433.0	3.65E-20	1.000	434.0	4.05E-20	1.000	434.5	6.08E-20	1.000	435.0	5.07E-20	1.000	436.0	8.11E-20	1.000
436.5	1.13E-19	1.000	437.0	5.27E-20	1.000	438.0	1.01E-19	1.000	438.5	1.38E-19	1.000	439.0	7.70E-20	1.000
440.0	2.47E-19	1.000	441.0	8.11E-20	1.000	442.0	6.08E-20	1.000	443.0	7.50E-20	1.000	444.0	9.32E-20	1.000
445.0	1.13E-19	1.000	446.0	5.27E-20	1.000	447.0	2.43E-20	1.000	448.0	2.84E-20	1.000	449.0	3.85E-20	1.000
450.0	6.08E-20	1.000	451.0	1.09E-19	1.000	451.5	9.32E-20	1.000	452.0	1.22E-19	1.000	453.0	2.39E-19	1.000
454.0	1.70E-19	1.000	455.0	3.40E-19	1.000	455.5	4.05E-19	1.000	456.0	1.01E-19	1.000	457.0	1.62E-20	1.000

Table A-3. (continued)

WL (nm)	Abs (cm^2)	QY	WL (nm)	Abs (cm^2)	QY	WL (nm)	Abs (cm^2)	QY	WL (nm)	Abs (cm^2)	QY	WL (nm)	Abs (cm^2)	QY
458.0	1.22E-20	1.000	458.5	1.42E-20	1.000	459.0	4.05E-21	1.000	460.0	4.05E-21	1.000	460.5	6.08E-21	1.000
461.0	2.03E-21	1.000	462.0	0.00E+00	1.000									
Photolysis File = MEGLYOX1														
220.0	2.10E-21	1.000	225.0	2.10E-21	1.000	230.0	4.21E-21	1.000	235.0	7.57E-21	1.000	240.0	9.25E-21	1.000
245.0	8.41E-21	1.000	250.0	9.25E-21	1.000	255.0	9.25E-21	1.000	260.0	9.67E-21	1.000	265.0	1.05E-20	1.000
270.0	1.26E-20	1.000	275.0	1.43E-20	1.000	280.0	1.51E-20	1.000	285.0	1.43E-20	1.000	290.0	1.47E-20	1.000
295.0	1.18E-20	1.000	300.0	1.14E-20	1.000	305.0	9.25E-21	1.000	310.0	6.31E-21	1.000	315.0	5.47E-21	1.000
320.0	3.36E-21	1.000	325.0	1.68E-21	1.000	330.0	8.41E-22	1.000	335.0	0.00E+00	1.000			
Photolysis File = MEGLYOX2														
350.0	0.00E+00	1.000	354.0	4.21E-22	1.000	358.0	1.26E-21	1.000	360.0	2.10E-21	1.000	362.0	2.10E-21	1.000
364.0	2.94E-21	1.000	366.0	3.36E-21	1.000	368.0	4.21E-21	1.000	370.0	5.47E-21	1.000	372.0	5.89E-21	1.000
374.0	7.57E-21	1.000	376.0	7.99E-21	1.000	378.0	8.83E-21	1.000	380.0	1.01E-20	1.000	382.0	1.09E-20	1.000
384.0	1.35E-20	1.000	386.0	1.51E-20	1.000	388.0	1.72E-20	1.000	390.0	2.06E-20	1.000	392.0	2.10E-20	1.000
394.0	2.31E-20	1.000	396.0	2.48E-20	1.000	398.0	2.61E-20	1.000	400.0	2.78E-20	1.000	402.0	2.99E-20	1.000
404.0	3.20E-20	1.000	406.0	3.79E-20	1.000	408.0	3.95E-20	1.000	410.0	4.33E-20	1.000	412.0	4.71E-20	1.000
414.0	4.79E-20	1.000	416.0	4.88E-20	1.000	418.0	5.05E-20	1.000	420.0	5.21E-20	1.000	422.0	5.30E-20	1.000
424.0	5.17E-20	1.000	426.0	5.30E-20	1.000	428.0	5.21E-20	1.000	430.0	5.55E-20	1.000	432.0	5.13E-20	1.000
434.0	5.68E-20	1.000	436.0	6.22E-20	1.000	438.0	6.06E-20	1.000	440.0	5.47E-20	1.000	441.0	6.14E-20	1.000
442.0	5.47E-20	1.000	443.0	5.55E-20	1.000	443.5	6.81E-20	1.000	444.0	5.97E-20	1.000	445.0	5.13E-20	1.000
446.0	4.88E-20	1.000	447.0	5.72E-20	1.000	448.0	5.47E-20	1.000	449.0	6.56E-20	1.000	450.0	5.05E-20	1.000
451.0	3.03E-20	1.000	452.0	4.29E-20	1.000	453.0	2.78E-20	1.000	454.0	2.27E-20	1.000	456.0	1.77E-20	1.000
458.0	8.41E-21	1.000	460.0	4.21E-21	1.000	464.0	1.68E-21	1.000	468.0	0.00E+00	1.000			
Photolysis File = BZCHO														
299.0	1.78E-19	1.000	304.0	7.40E-20	1.000	306.0	6.91E-20	1.000	309.0	6.41E-20	1.000	313.0	6.91E-20	1.000
314.0	6.91E-20	1.000	318.0	6.41E-20	1.000	325.0	8.39E-20	1.000	332.0	7.65E-20	1.000	338.0	8.88E-20	1.000
342.0	8.88E-20	1.000	346.0	7.89E-20	1.000	349.0	7.89E-20	1.000	354.0	9.13E-20	1.000	355.0	8.14E-20	1.000
364.0	5.67E-20	1.000	368.0	6.66E-20	1.000	369.0	8.39E-20	1.000	370.0	8.39E-20	1.000	372.0	3.45E-20	1.000
374.0	3.21E-20	1.000	376.0	2.47E-20	1.000	377.0	2.47E-20	1.000	380.0	3.58E-20	1.000	382.0	9.90E-21	1.000
386.0	0.00E+00	1.000												
Photolysis File = ACROLEIN														
250.0	1.80E-21	1.000	252.0	2.05E-21	1.000	253.0	2.20E-21	1.000	254.0	2.32E-21	1.000	255.0	2.45E-21	1.000
256.0	2.56E-21	1.000	257.0	2.65E-21	1.000	258.0	2.74E-21	1.000	259.0	2.83E-21	1.000	260.0	2.98E-21	1.000
261.0	3.24E-21	1.000	262.0	3.47E-21	1.000	263.0	3.58E-21	1.000	264.0	3.93E-21	1.000	265.0	4.67E-21	1.000
266.0	5.10E-21	1.000	267.0	5.38E-21	1.000	268.0	5.73E-21	1.000	269.0	6.13E-21	1.000	270.0	6.64E-21	1.000
271.0	7.20E-21	1.000	272.0	7.77E-21	1.000	273.0	8.37E-21	1.000	274.0	8.94E-21	1.000	275.0	9.55E-21	1.000
276.0	1.04E-20	1.000	277.0	1.12E-20	1.000	278.0	1.19E-20	1.000	279.0	1.27E-20	1.000	280.0	1.27E-20	1.000
281.0	1.26E-20	1.000	282.0	1.26E-20	1.000	283.0	1.28E-20	1.000	284.0	1.33E-20	1.000	285.0	1.38E-20	1.000
286.0	1.44E-20	1.000	287.0	1.50E-20	1.000	288.0	1.57E-20	1.000	289.0	1.63E-20	1.000	290.0	1.71E-20	1.000
291.0	1.78E-20	1.000	292.0	1.86E-20	1.000	293.0	1.95E-20	1.000	294.0	2.05E-20	1.000	295.0	2.15E-20	1.000
296.0	2.26E-20	1.000	297.0	2.37E-20	1.000	298.0	2.48E-20	1.000	299.0	2.60E-20	1.000	300.0	2.73E-20	1.000
301.0	2.85E-20	1.000	302.0	2.99E-20	1.000	303.0	3.13E-20	1.000	304.0	3.27E-20	1.000	305.0	3.39E-20	1.000
306.0	3.51E-20	1.000	307.0	3.63E-20	1.000	308.0	3.77E-20	1.000	309.0	3.91E-20	1.000	310.0	4.07E-20	1.000
311.0	4.25E-20	1.000	312.0	4.39E-20	1.000	313.0	4.44E-20	1.000	314.0	4.50E-20	1.000	315.0	4.59E-20	1.000
316.0	4.75E-20	1.000	317.0	4.90E-20	1.000	318.0	5.05E-20	1.000	319.0	5.19E-20	1.000	320.0	5.31E-20	1.000
321.0	5.43E-20	1.000	322.0	5.52E-20	1.000	323.0	5.60E-20	1.000	324.0	5.67E-20	1.000	325.0	5.67E-20	1.000
326.0	5.62E-20	1.000	327.0	5.63E-20	1.000	328.0	5.71E-20	1.000	329.0	5.76E-20	1.000	330.0	5.80E-20	1.000
331.0	5.95E-20	1.000	332.0	6.23E-20	1.000	333.0	6.39E-20	1.000	334.0	6.38E-20	1.000	335.0	6.24E-20	1.000
336.0	6.01E-20	1.000	337.0	5.79E-20	1.000	338.0	5.63E-20	1.000	339.0	5.56E-20	1.000	340.0	5.52E-20	1.000
341.0	5.54E-20	1.000	342.0	5.53E-20	1.000	343.0	5.47E-20	1.000	344.0	5.41E-20	1.000	345.0	5.40E-20	1.000
346.0	5.48E-20	1.000	347.0	5.90E-20	1.000	348.0	6.08E-20	1.000	349.0	6.00E-20	1.000	350.0	5.53E-20	1.000
351.0	5.03E-20	1.000	352.0	4.50E-20	1.000	353.0	4.03E-20	1.000	354.0	3.75E-20	1.000	355.0	3.55E-20	1.000
356.0	3.45E-20	1.000	357.0	3.46E-20	1.000	358.0	3.49E-20	1.000	359.0	3.41E-20	1.000	360.0	3.23E-20	1.000
361.0	2.95E-20	1.000	362.0	2.81E-20	1.000	363.0	2.91E-20	1.000	364.0	3.25E-20	1.000	365.0	3.54E-20	1.000
366.0	3.30E-20	1.000	367.0	2.78E-20	1.000	368.0	2.15E-20	1.000	369.0	1.59E-20	1.000	370.0	1.19E-20	1.000
371.0	8.99E-21	1.000	372.0	7.22E-21	1.000	373.0	5.86E-21	1.000	374.0	4.69E-21	1.000	375.0	3.72E-21	1.000
376.0	3.57E-21	1.000	377.0	3.55E-21	1.000	378.0	2.83E-21	1.000	379.0	1.69E-21	1.000	380.0	8.29E-24	1.000
381.0	0.00E+00	1.000												

APPENDIX B
PLOTS OF RESULTS OF AROMATIC - NO_x EXPERIMENTS

Figures B-1 through B-28 give time series plots of selected results of the aromatic - NO_x experiments carried out or modeled for this program. Results of model simulations, using both the SAPRC-93 mechanism and the reoptimized aromatics mechanisms, are also shown. Experimental and calculated $\Delta([O_3]-[NO])$ data are shown on Figures B-1 through B-12, where B-1 through B-9 show the experiments for this program, and Figures B-9 through B-12 show pervious experiments which were used to evaluate the reoptimized aromatics mechanisms. Experimental and calculated for the reactant aromatic are shown on Figures B-13 through B-20, and those formaldehyde are shown on Figures B-21 through B-28.

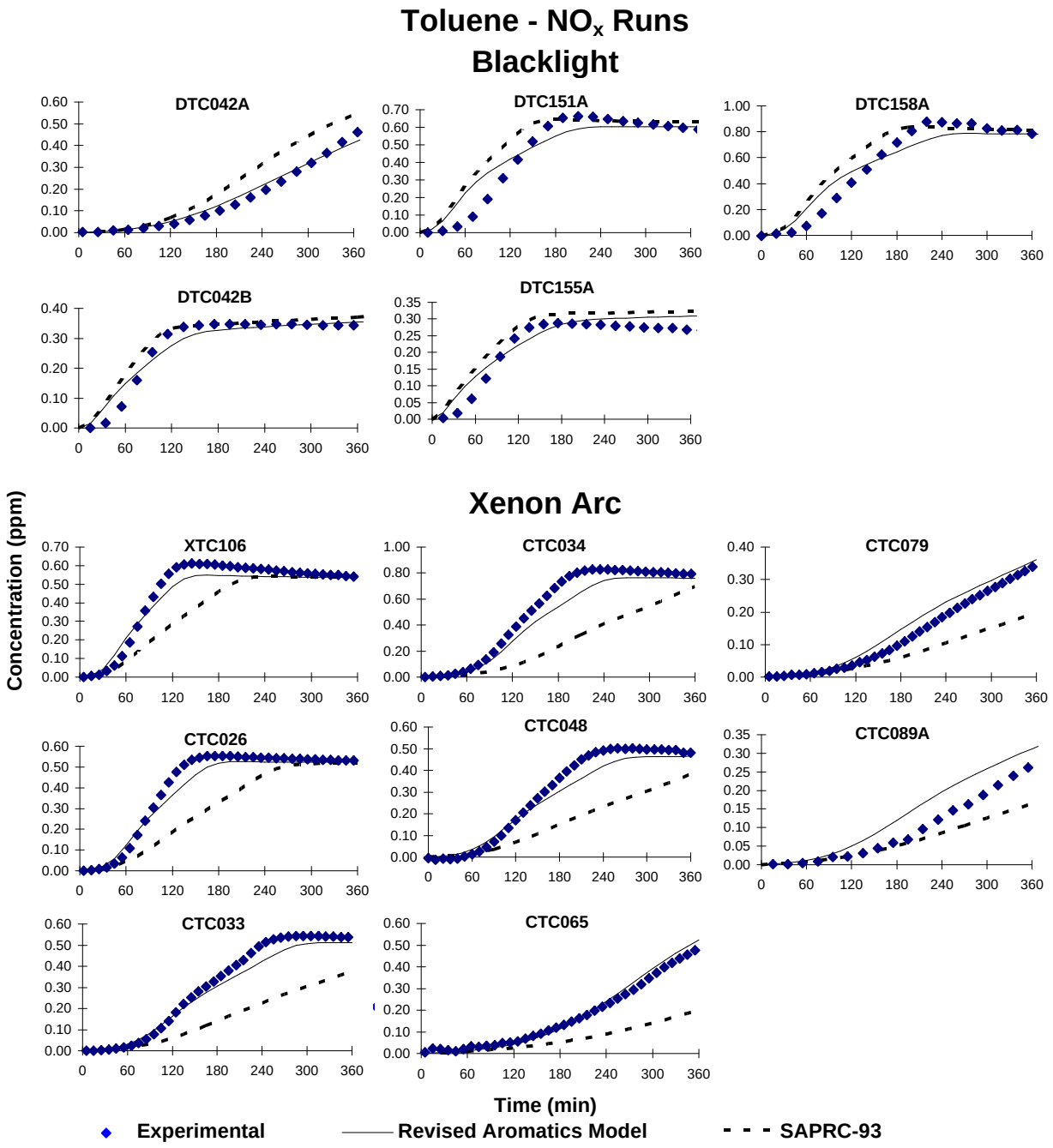

Figure B-1. Experimental and calculated concentration - time plots for $\Delta([O_3]-[NO])$ for the toluene - NO_x experiments carried out for this program and used for mechanism evaluation.

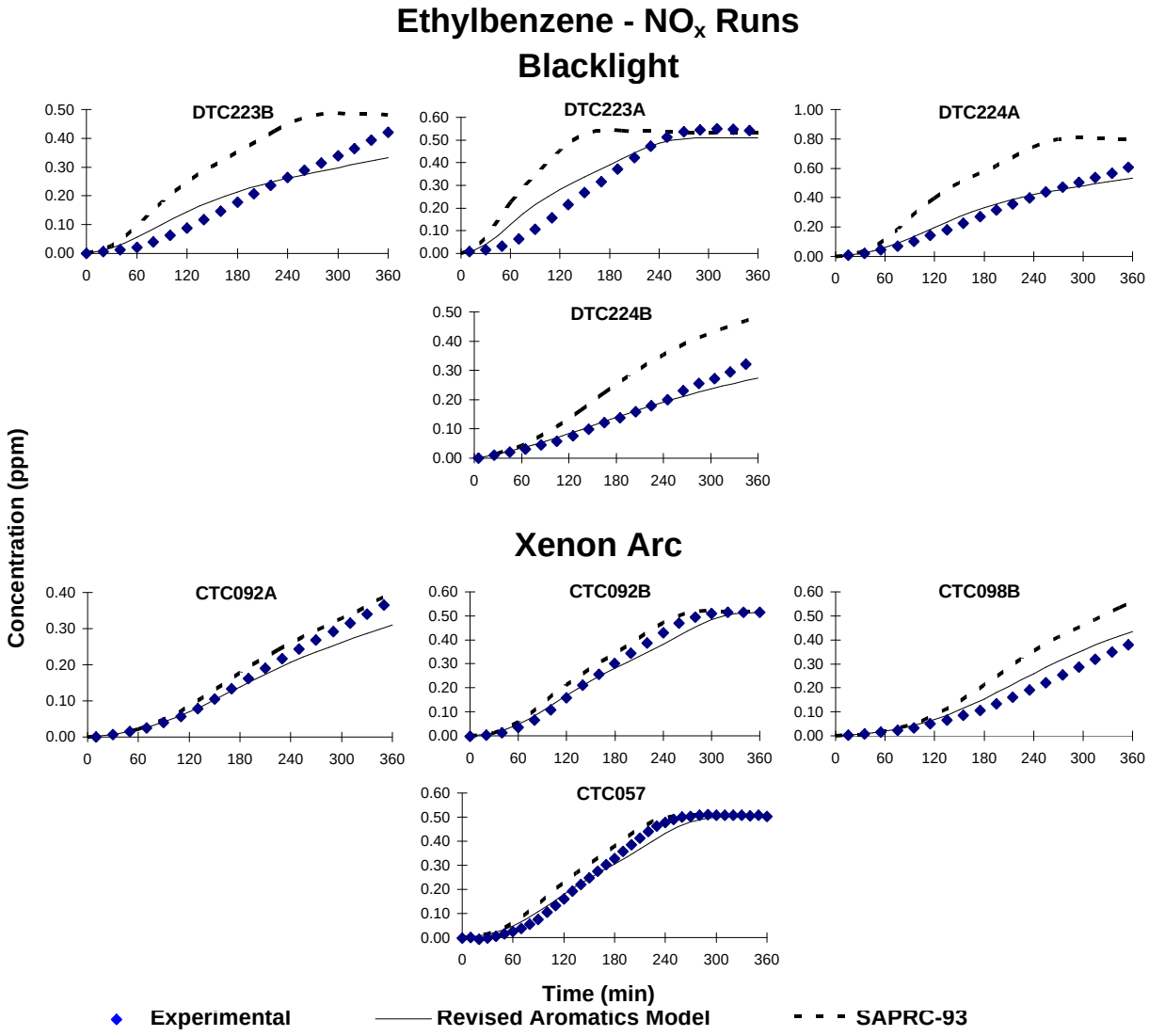

Figure B-2. Experimental and calculated concentration - time plots for $\Delta([O_3]-[NO])$ for the ethylbenzene - NO_x experiments carried out for this program.

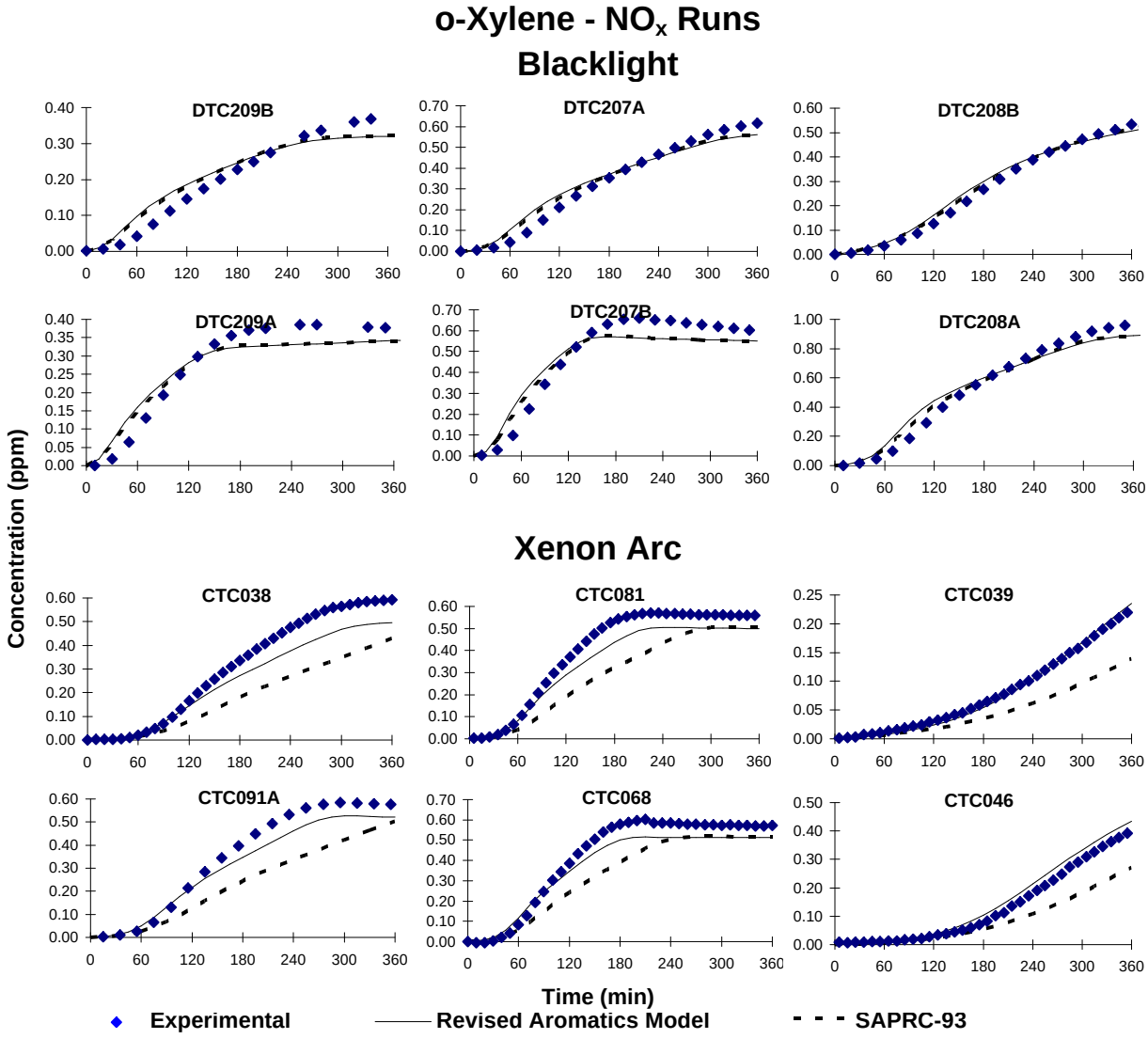

Figure B-3. Experimental and calculated concentration - time plots for $\Delta([O_3]-[NO])$ for the o-xylene - NO_x experiments carried out for this program.

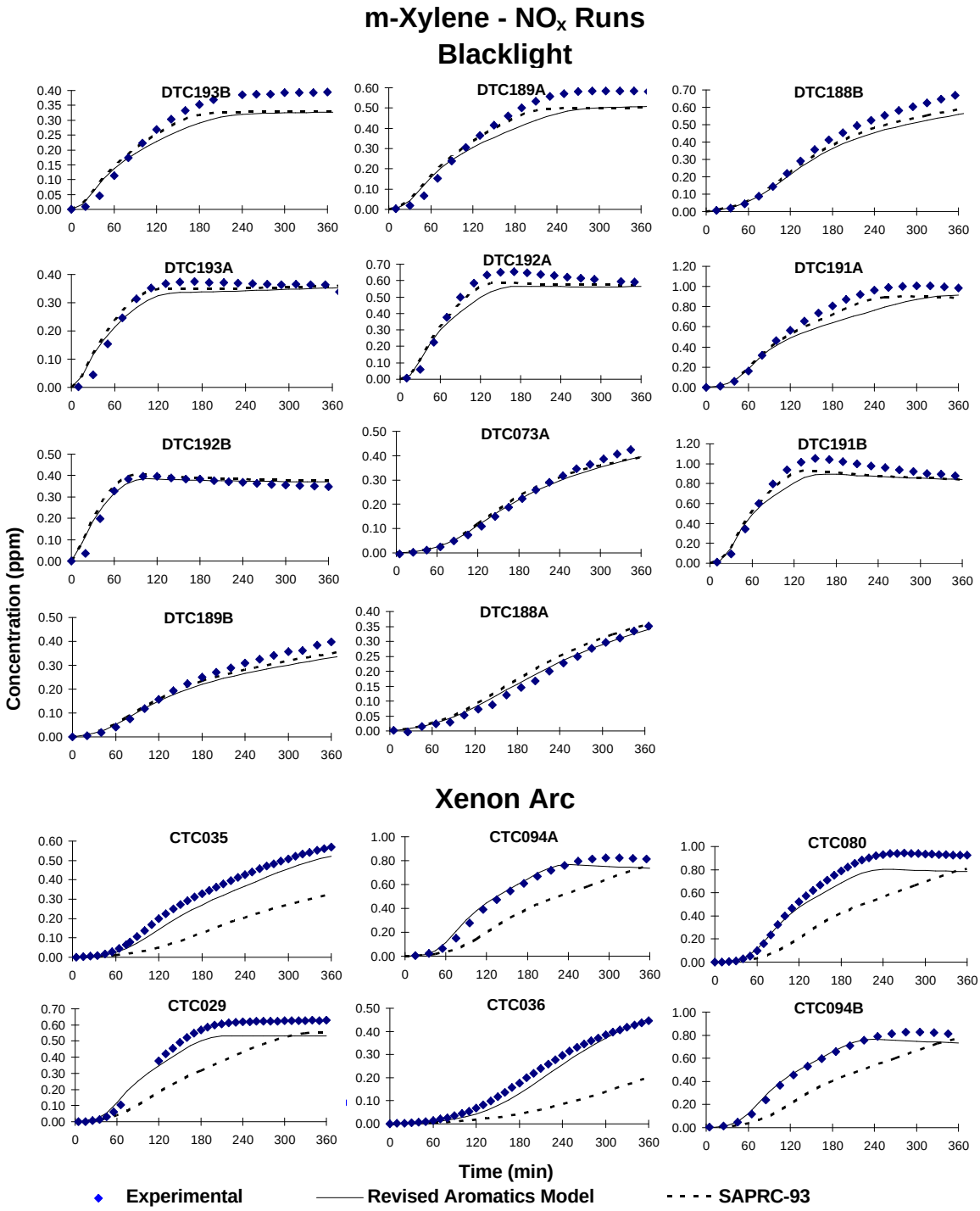

Figure B-4. Experimental and calculated concentration - time plots for $\Delta([O_3]-[NO])$ for the m-xylene - NO_x experiments carried out for this program.

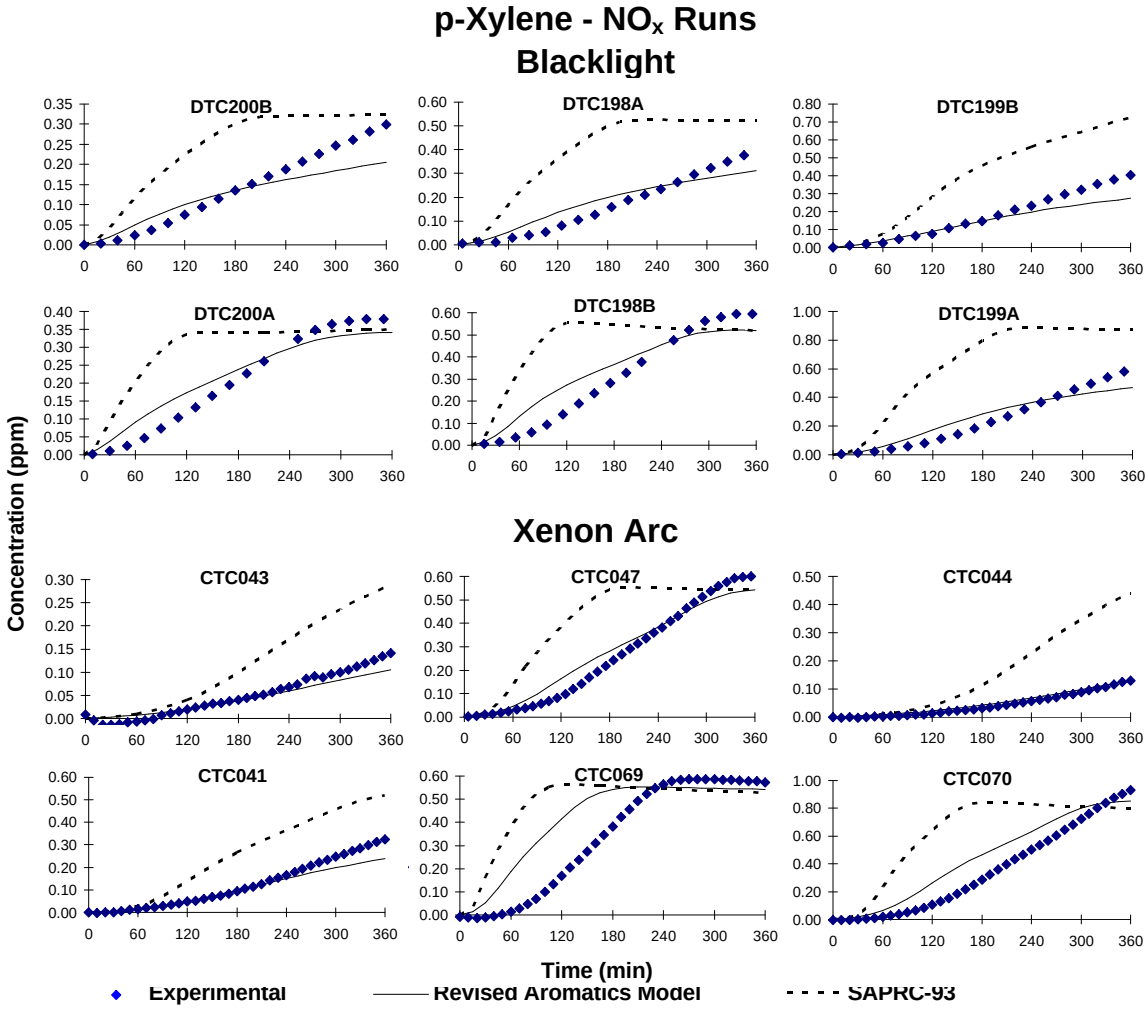

Figure B-5. Experimental and calculated concentration - time plots for $\Delta([O_3]-[NO])$ for the p-xylene - NO_x experiments carried out for this program.

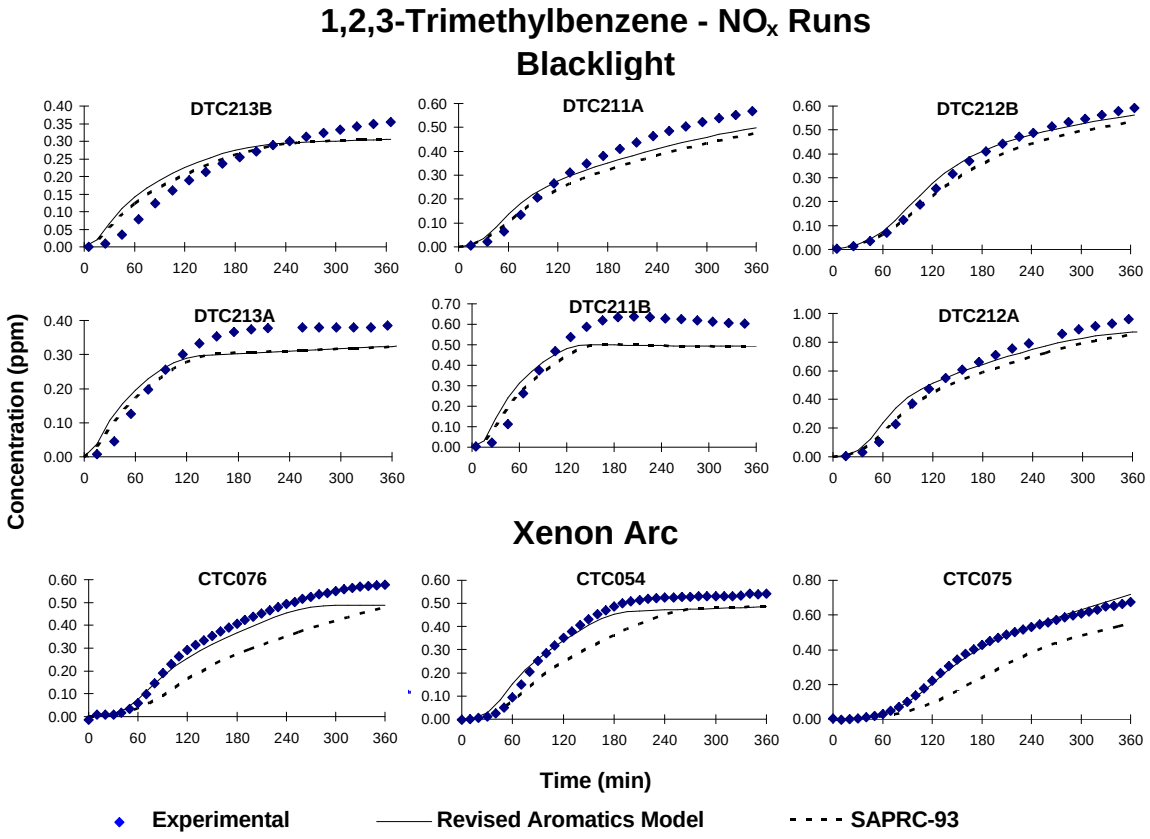

Figure B-6. Experimental and calculated concentration - time plots for $\Delta([O_3]-[NO])$ for the 1,2,3-trimethylbenzene - NO_x experiments carried out for this program.

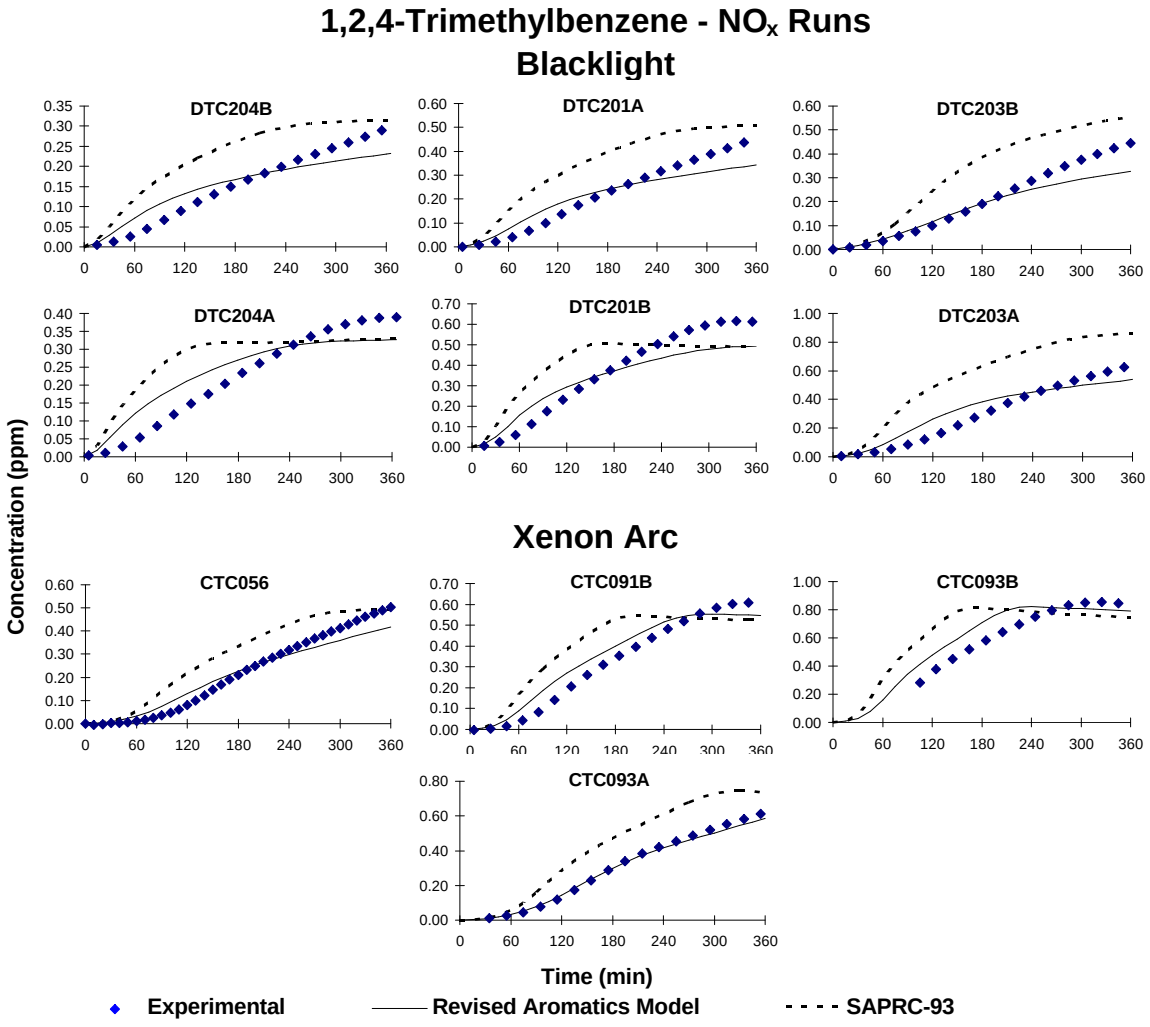

Figure B-7. Experimental and calculated concentration - time plots for $\Delta([O_3]-[NO])$ for the 1,2,4-trimethylbenzene - NO_x experiments carried out for this program.

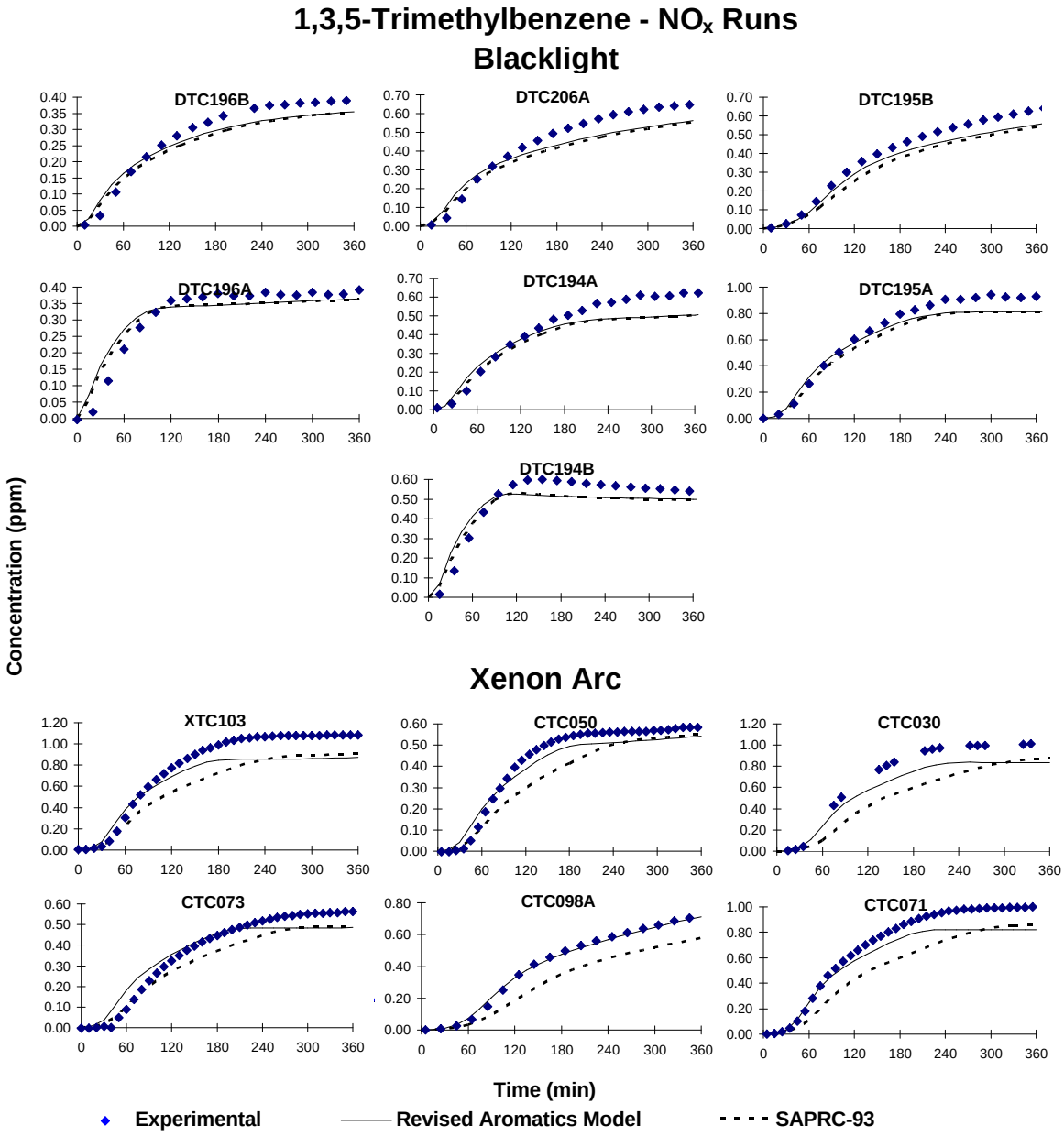

Figure B-8. Experimental and calculated concentration - time plots for $\Delta([O_3]-[NO])$ for the 1,3,5-trimethylbenzene - NO_x experiments carried out for this program.

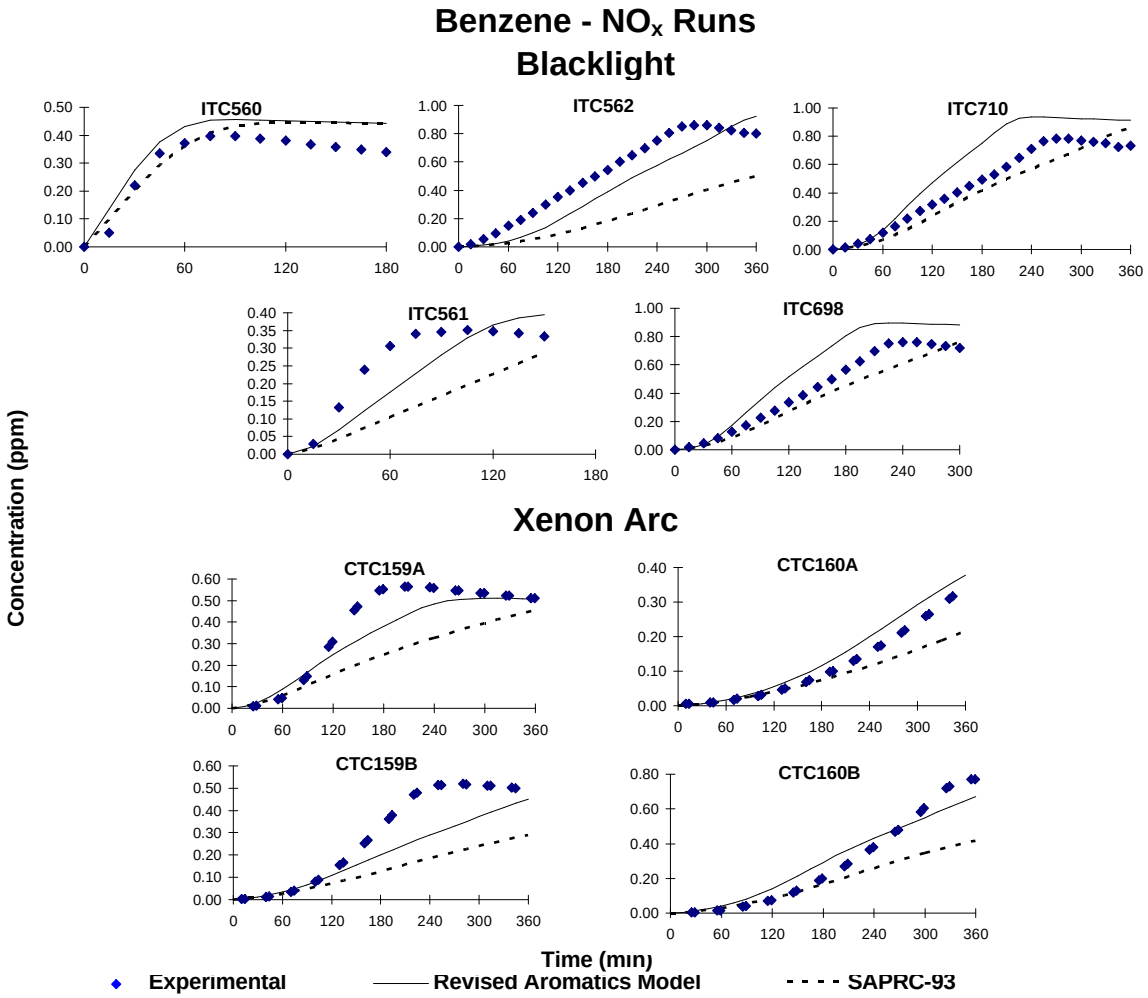

Figure B-9. Experimental and calculated concentration - time plots for D([O3]-[NO]) for the benzene - NOx experiments used for mechanism evaluation. The CTC experiments were carried out for this program, and the ITC runs were carried out previously and used in the development of the SAPRC-93 mechanism.

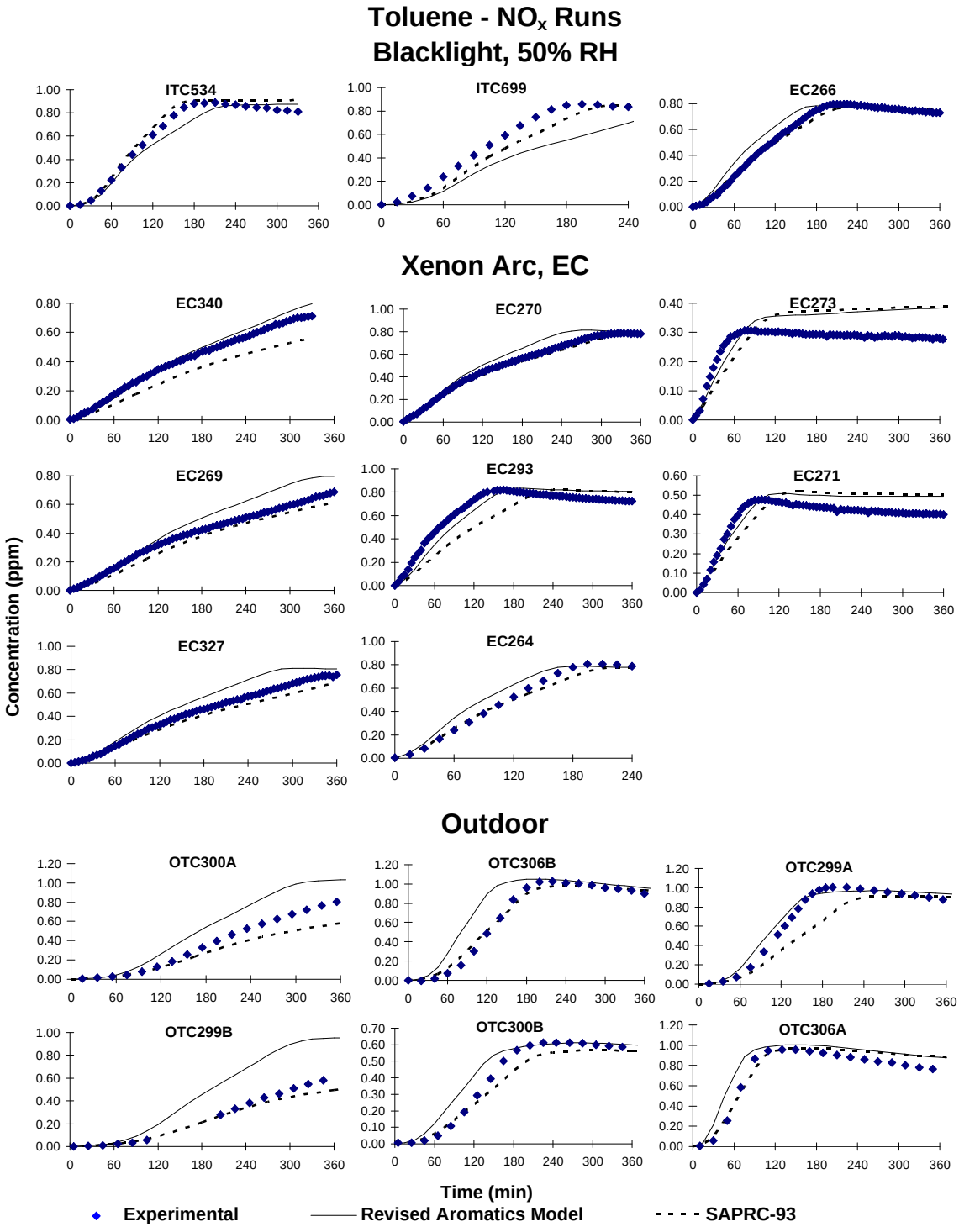

Figure B-10. Experimental and calculated concentration - time plots for D([O3]-[NO]) for the toluene - NOx experiments carried out previously for mechanism evaluation.

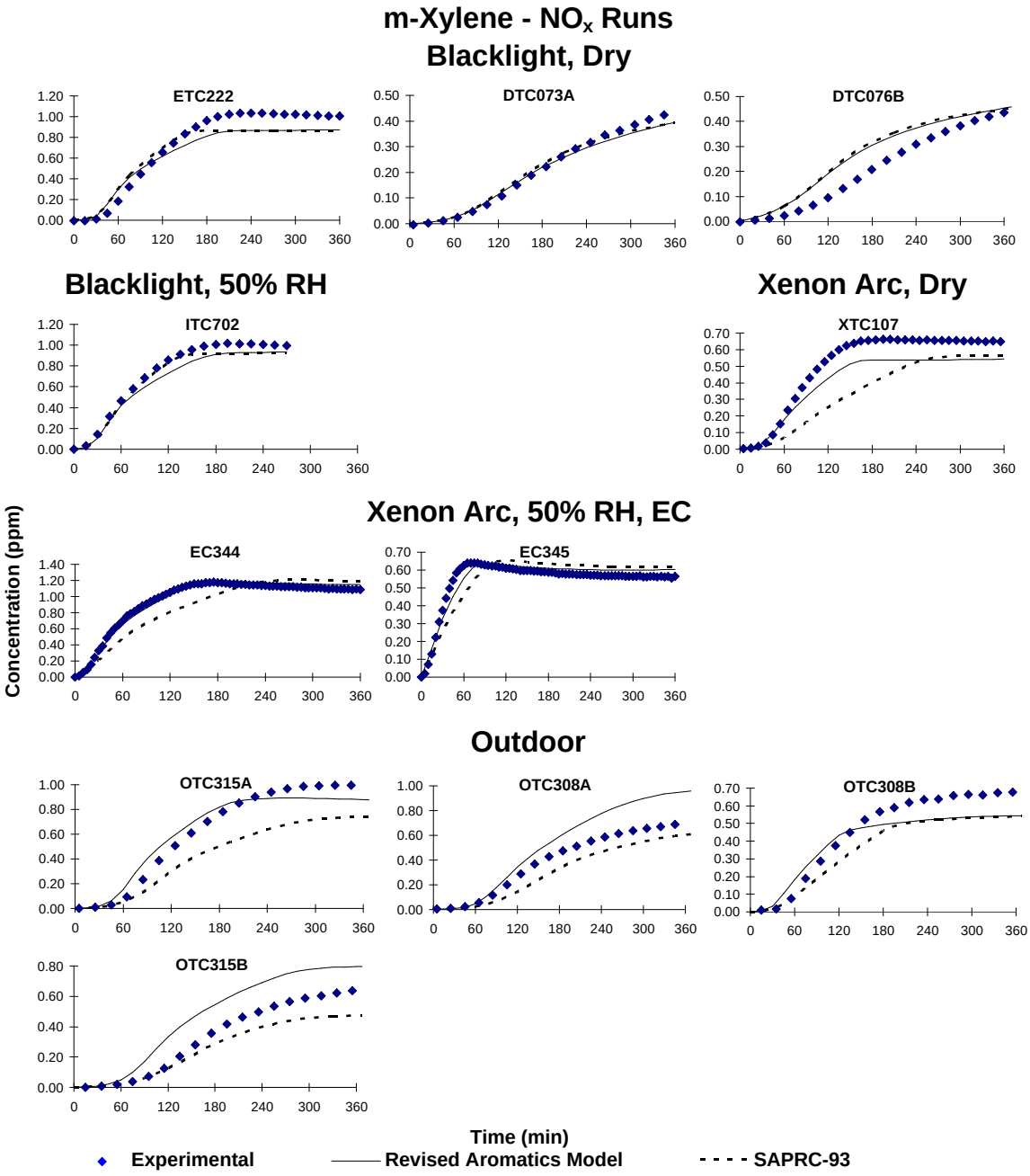

Figure B-11. Experimental and calculated concentration - time plots for D([O3]-[NO]) for the m-xylene - NOx experiments carried out previously for mechanism evaluation.

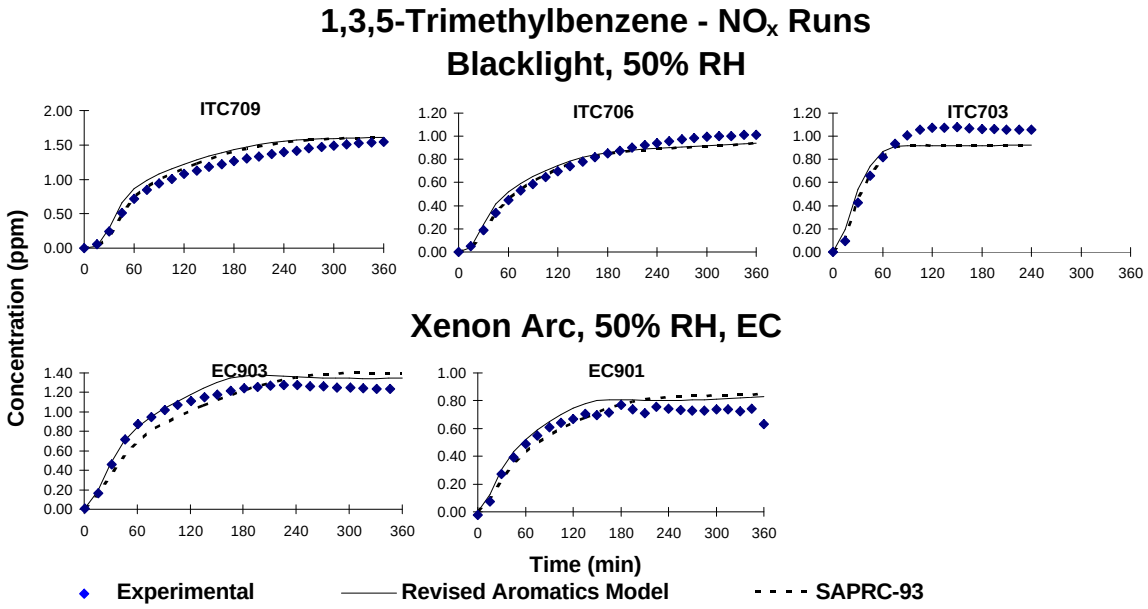

Figure B-12. Experimental and calculated concentration - time plots for D([O3]-[NO]) for the 1,3,5-trimethylbenzene - NOx experiments carried out previously for mechanism evaluation.

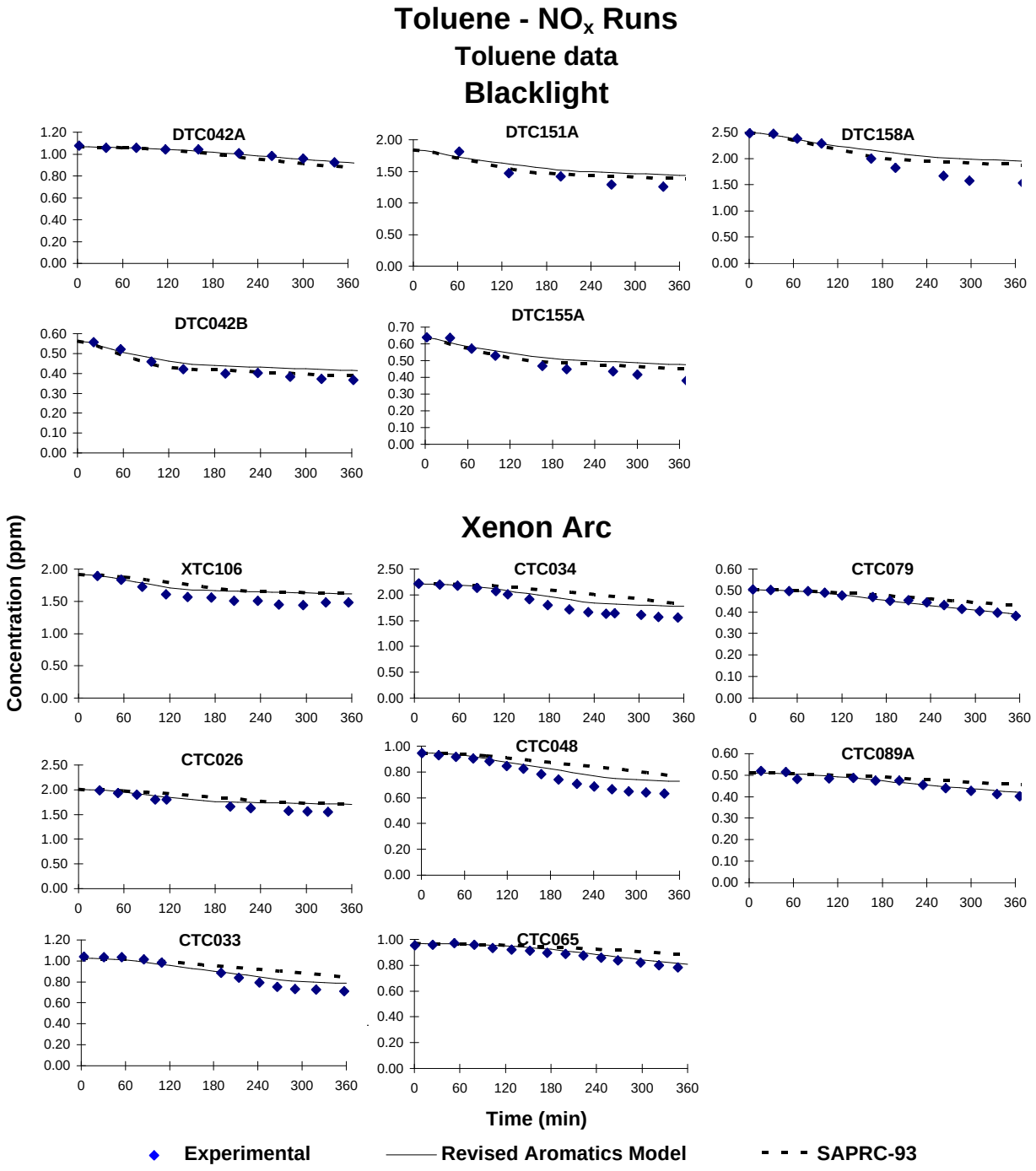

Figure B-13. Experimental and calculated concentration - time plots for toluene for the toluene - NO_x experiments carried out for this program and used for mechanism evaluation.

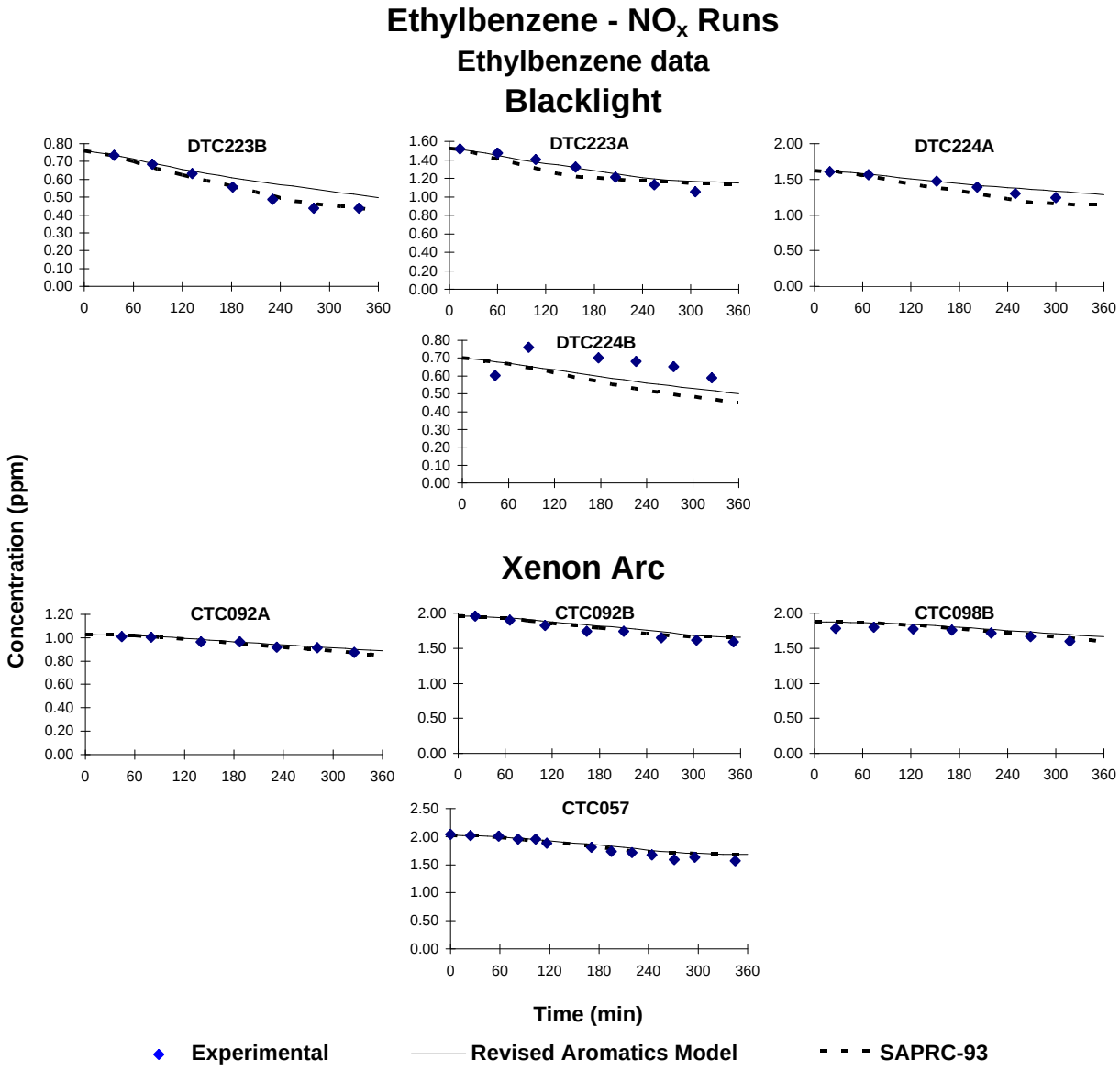

Figure B-14. Experimental and calculated concentration - time plots for ethylbenzene for the ethylbenzene - NO_x experiments carried out for this program.

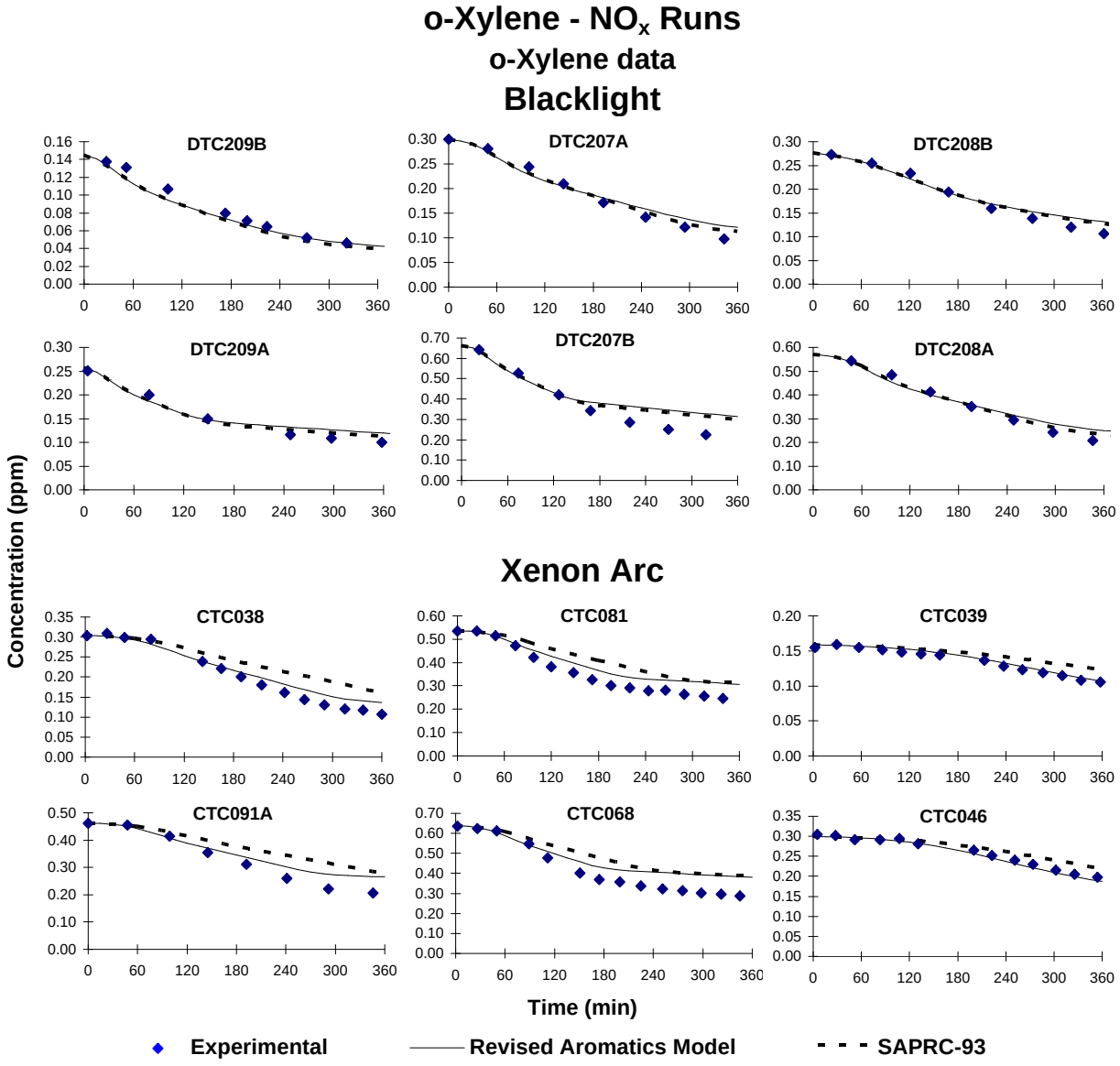

Figure B-15. Experimental and calculated concentration - time plots for o-xylene for the o-xylene - NO_x experiments carried out for this program.

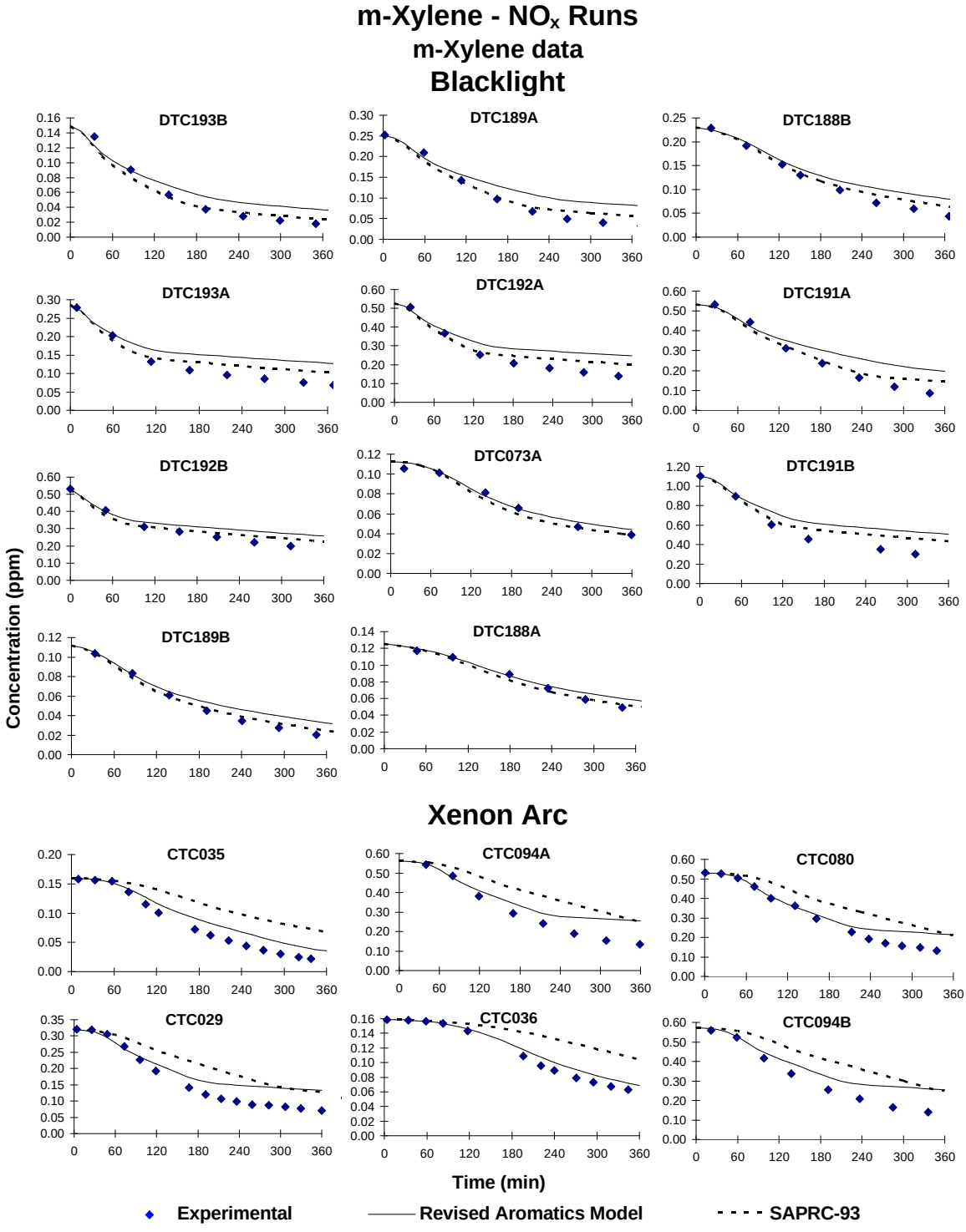

Figure B-16. Experimental and calculated concentration - time plots for m-xylene for the m-xylene - NO_x experiments carried out for this program.

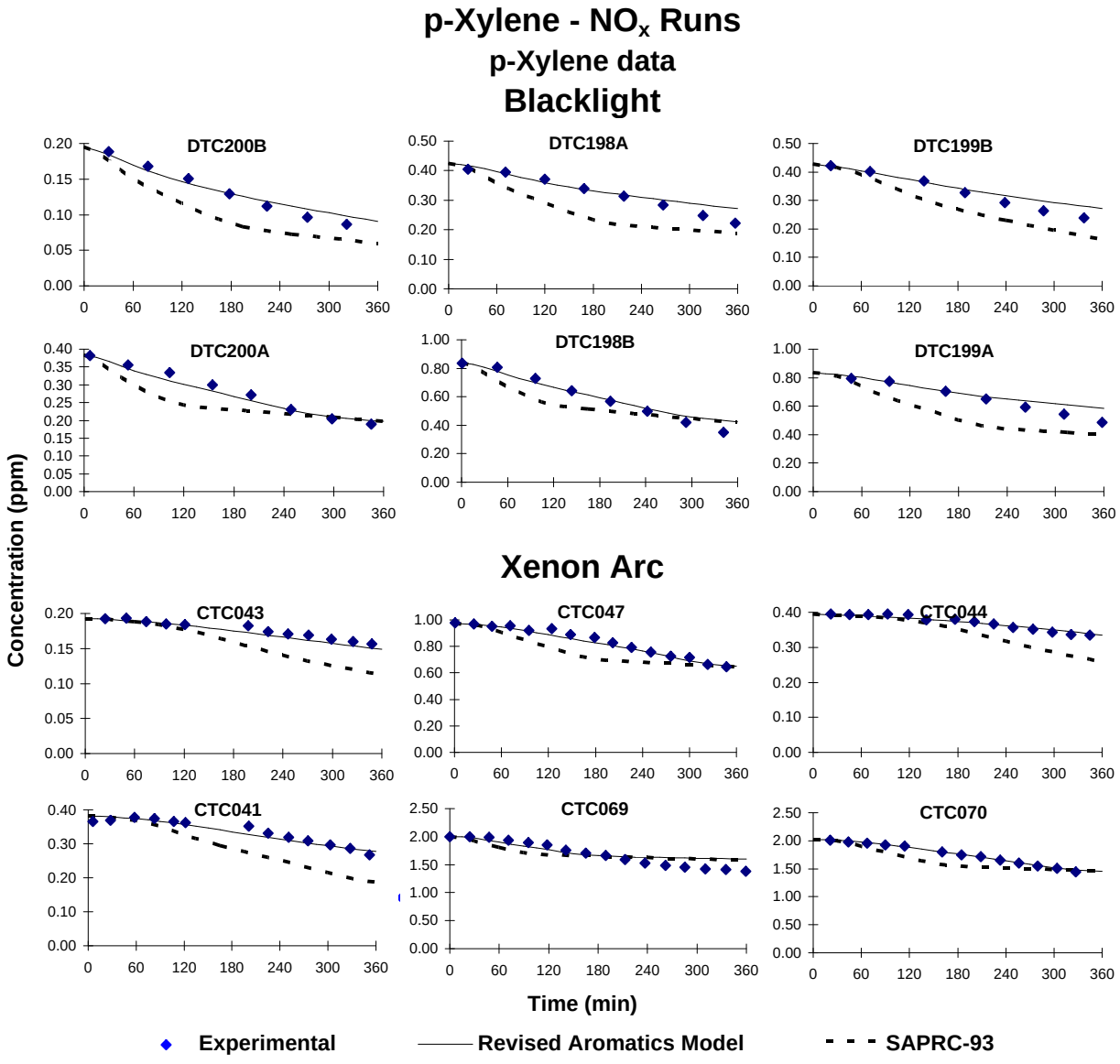

Figure B-17. Experimental and calculated concentration - time plots for p-xylene for the p-xylene - NO_x experiments carried out for this program.

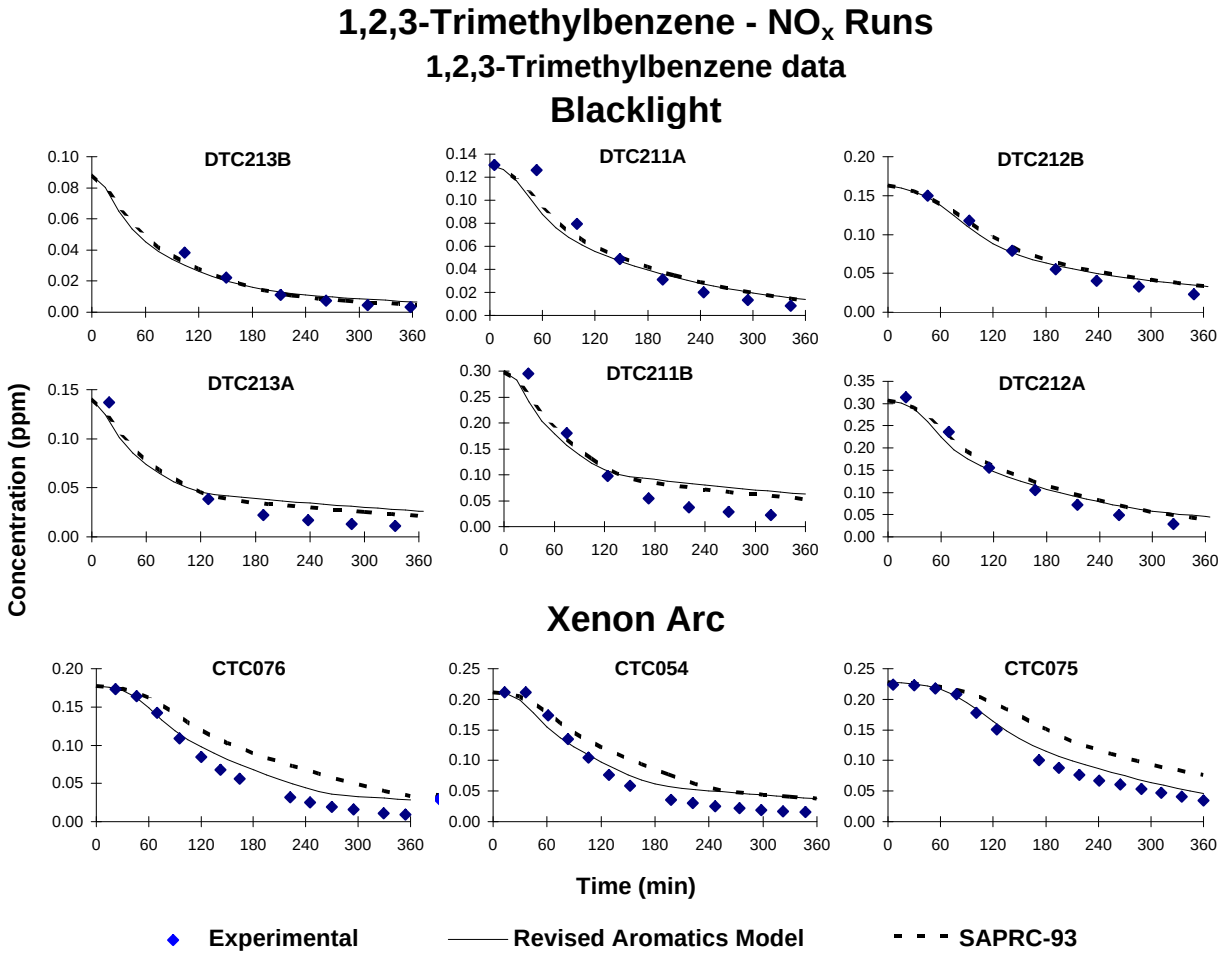

Figure B-18. Experimental and calculated concentration - time plots for 1,2,3-trimethylbenzene for the 1,2,3-trimethylbenzene - NO_x experiments carried out for this program.

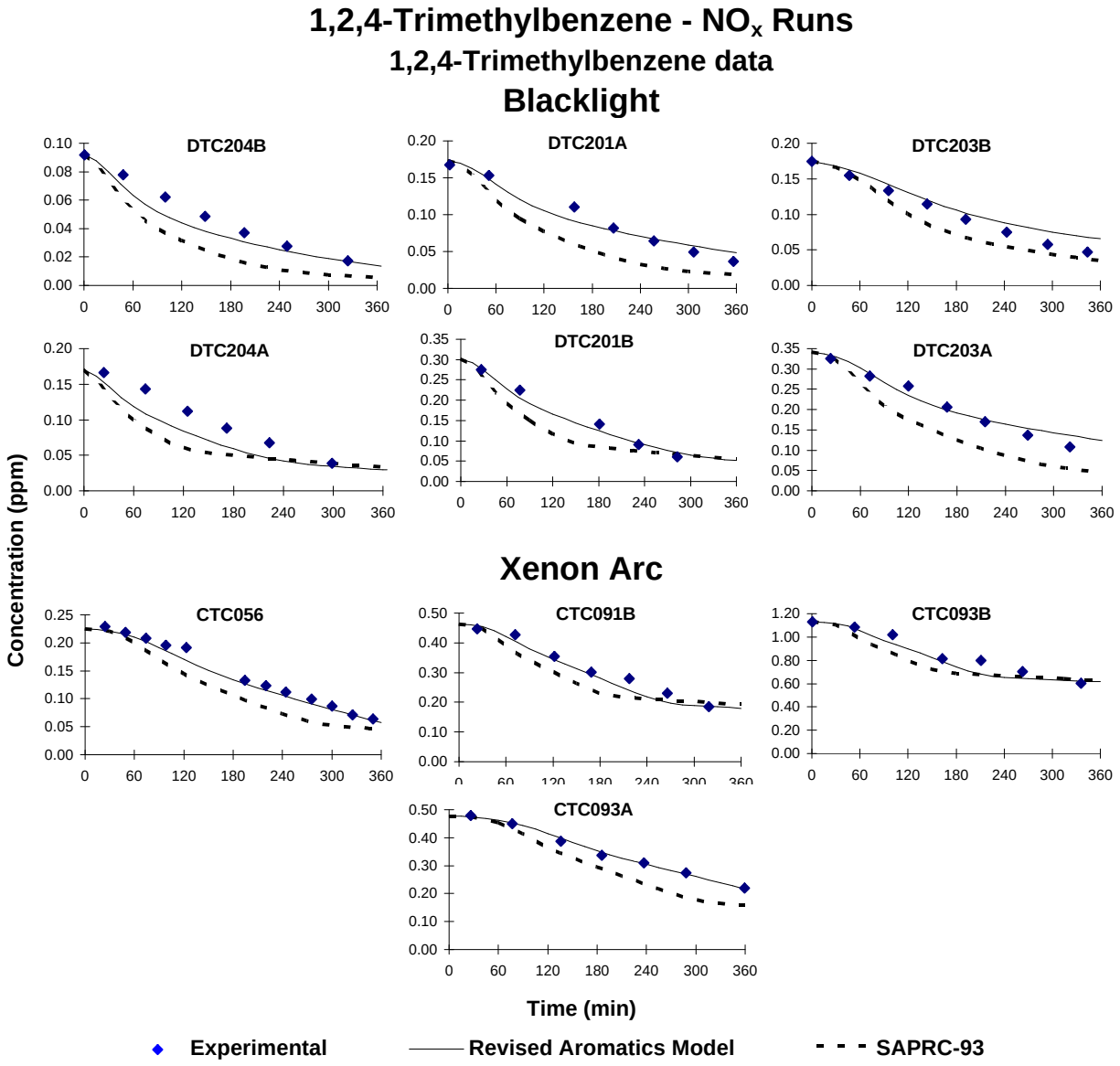

Figure B-19. Experimental and calculated concentration - time plots for 1,2,4-trimethylbenzene for the 1,2,4-trimethylbenzene - NO_x experiments carried out for this program.

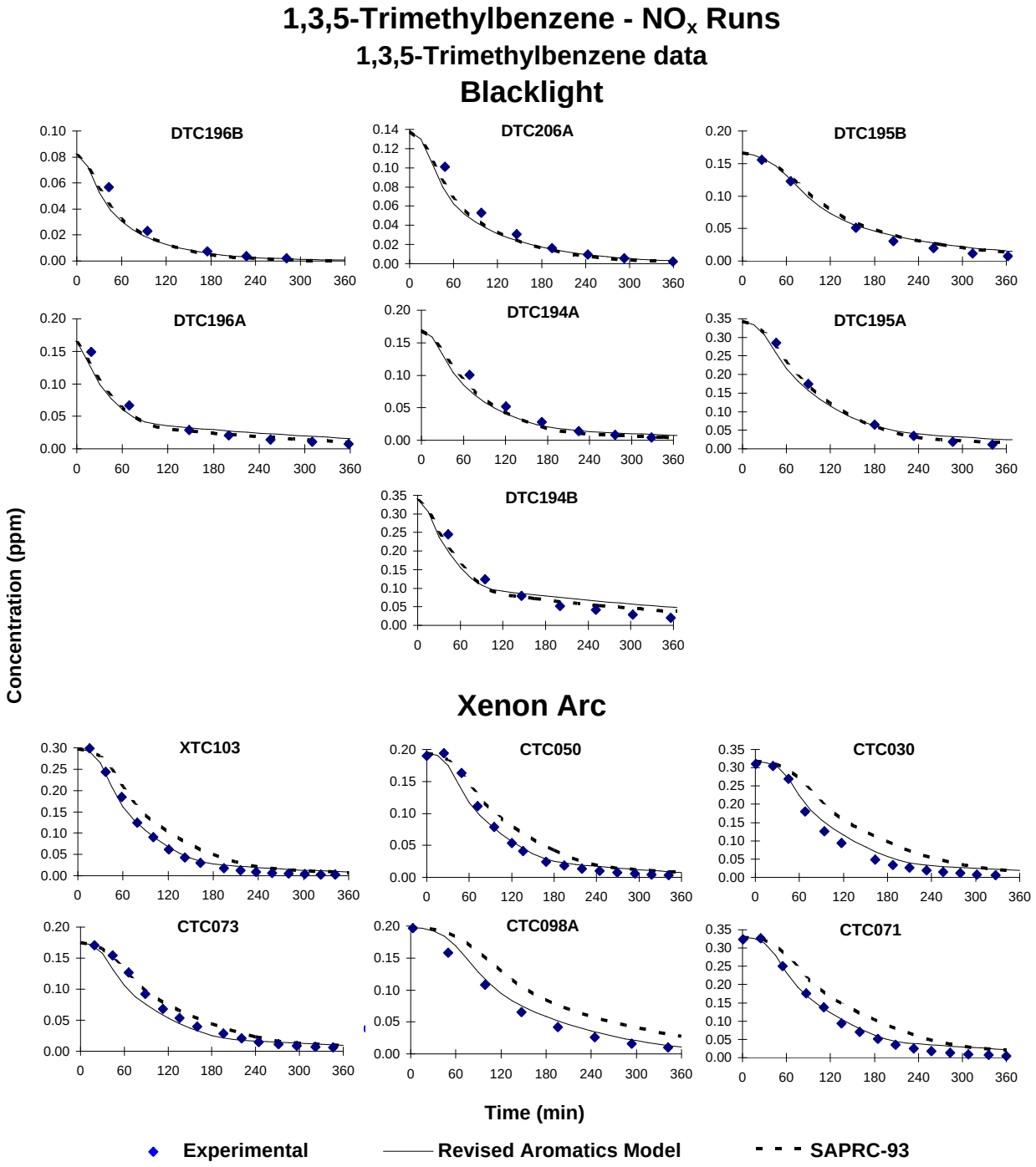

Figure B-20. Experimental and calculated concentration - time plots for 1,3,5-trimethylbenzene for the 1,3,5-trimethylbenzene - NO_x experiments carried out for this program.

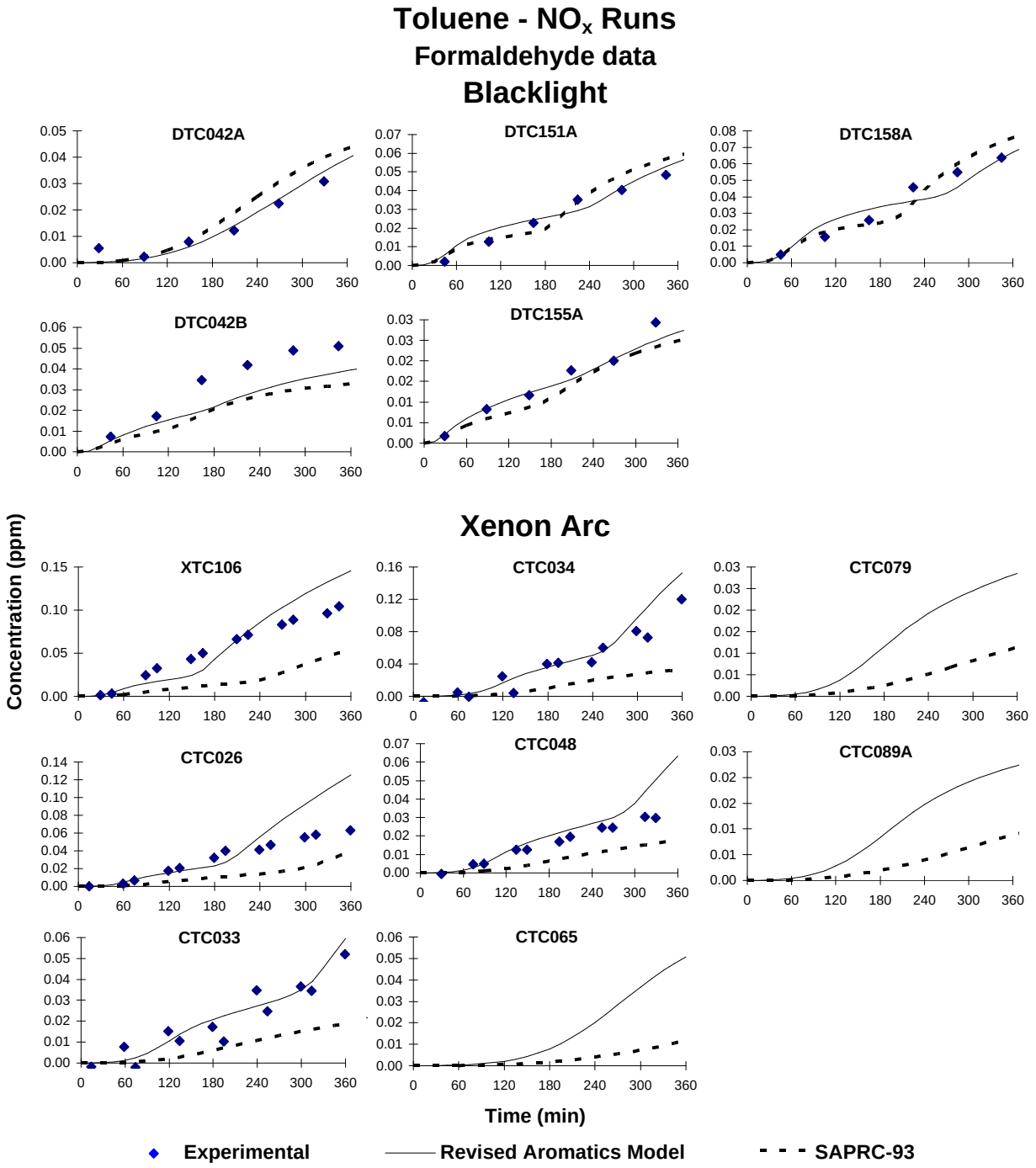

Figure B-21. Experimental and calculated concentration - time plots for formaldehyde for the toluene - NO_x experiments carried out for this program and used for mechanism evaluation.

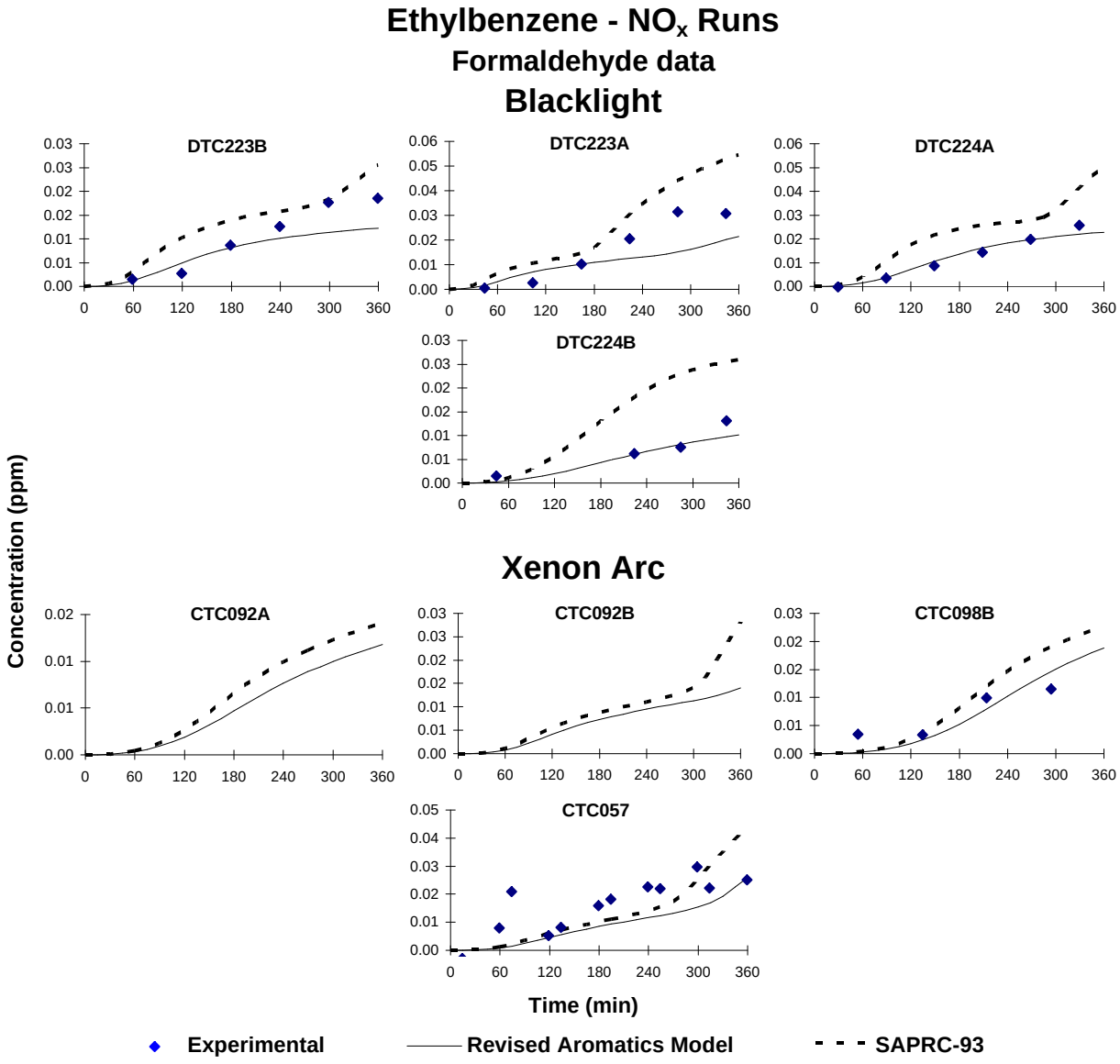

Figure B-22. Experimental and calculated concentration - time plots for formaldehyde for the ethylbenzene - NO_x experiments carried out for this program.

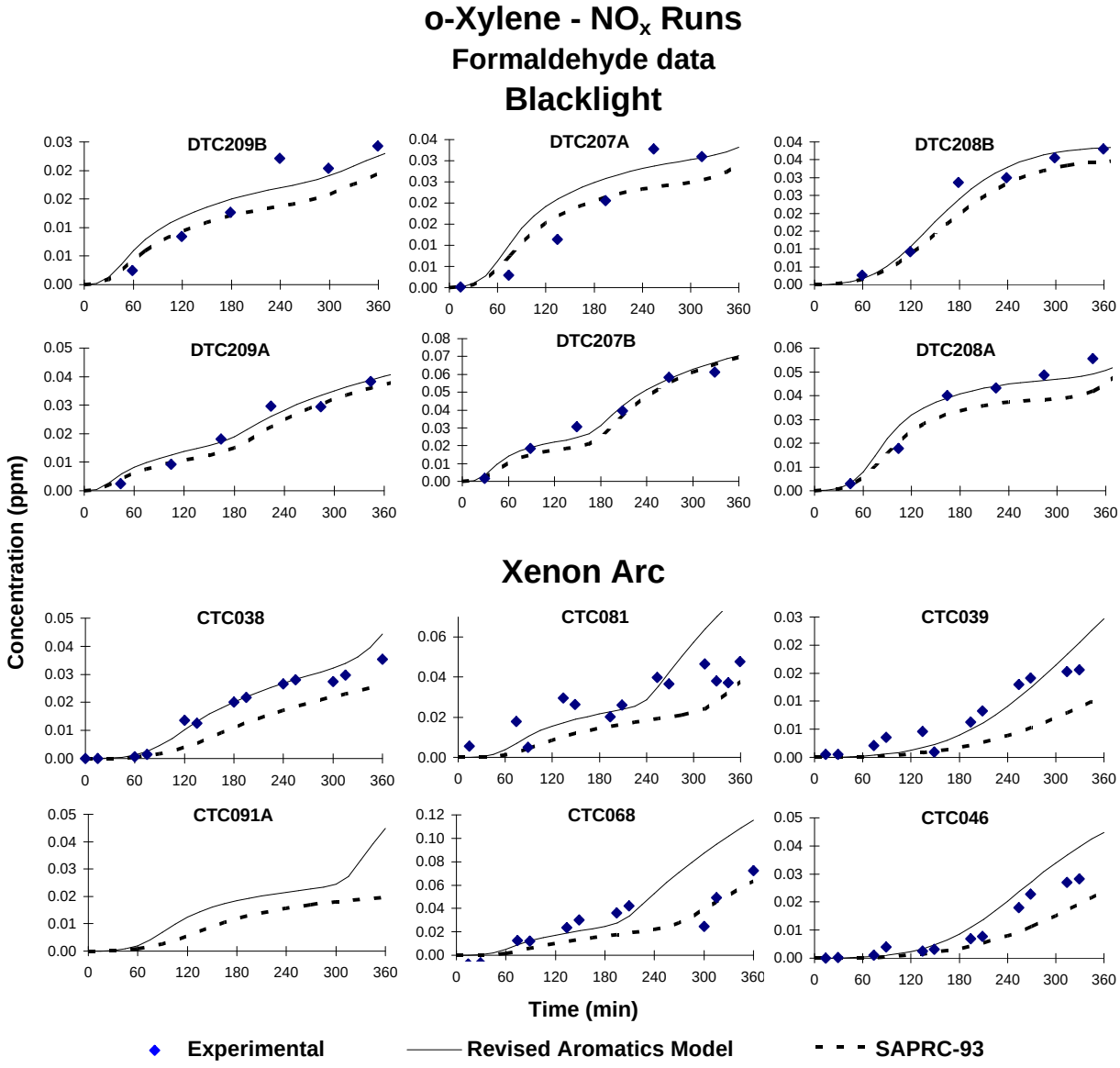

Figure B-23. Experimental and calculated concentration - time plots for formaldehyde for the o-xylene - NO_x experiments carried out for this program.

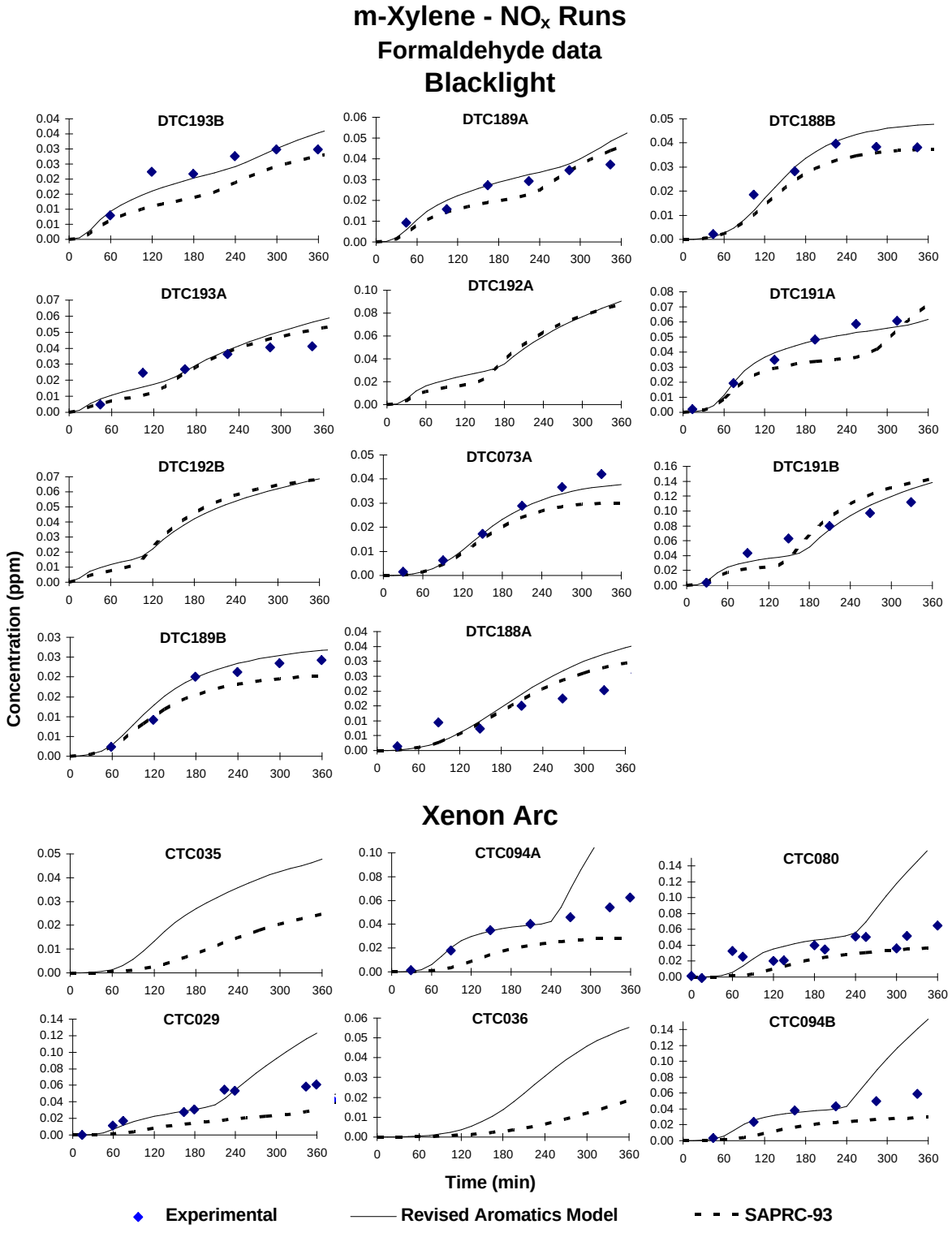

Figure B-24. Experimental and calculated concentration - time plots for formaldehyde for the m-xylene - NO_x experiments carried out for this program.

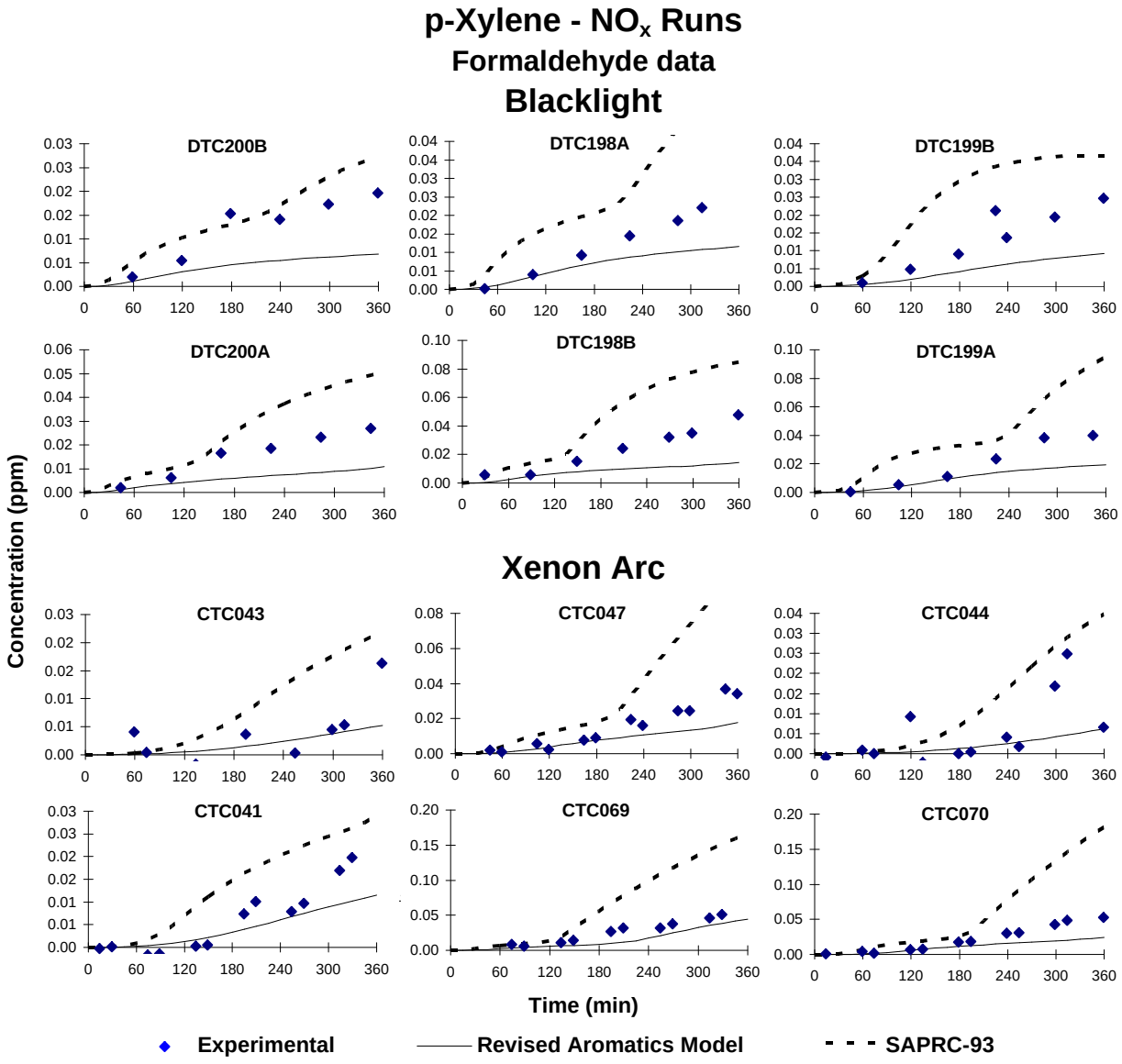

Figure B-25. Experimental and calculated concentration - time plots for formaldehyde for the p-xylene - NOx experiments carried out for this program.

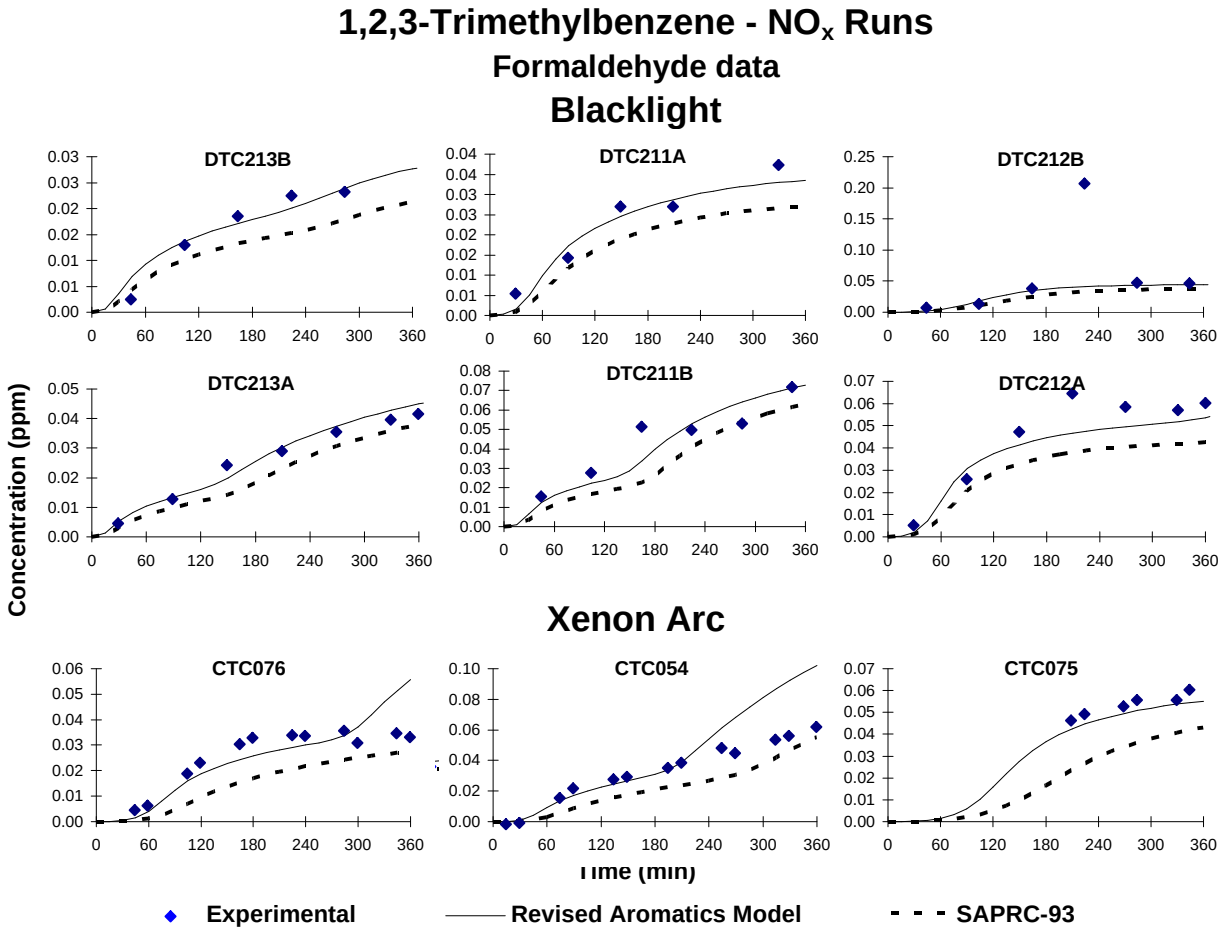

Figure B-26. Experimental and calculated concentration - time plots for formaldehyde for the 1,2,3-trimethylbenzene NOx experiments carried out for this program.

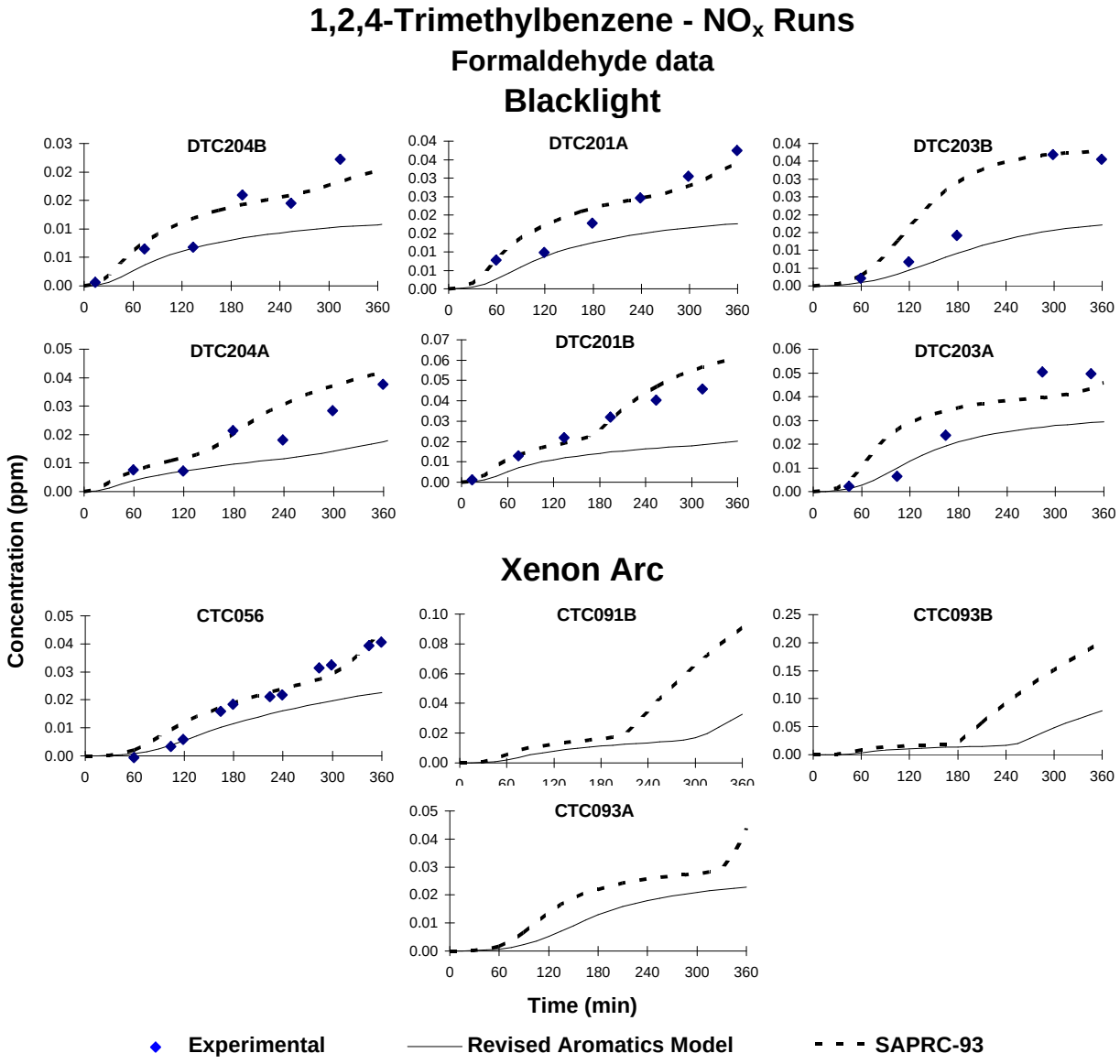

Figure B-27. Experimental and calculated concentration - time plots for formaldehyde for the 1,2,4-trimethylbenzene - NO_x experiments carried out for this program.

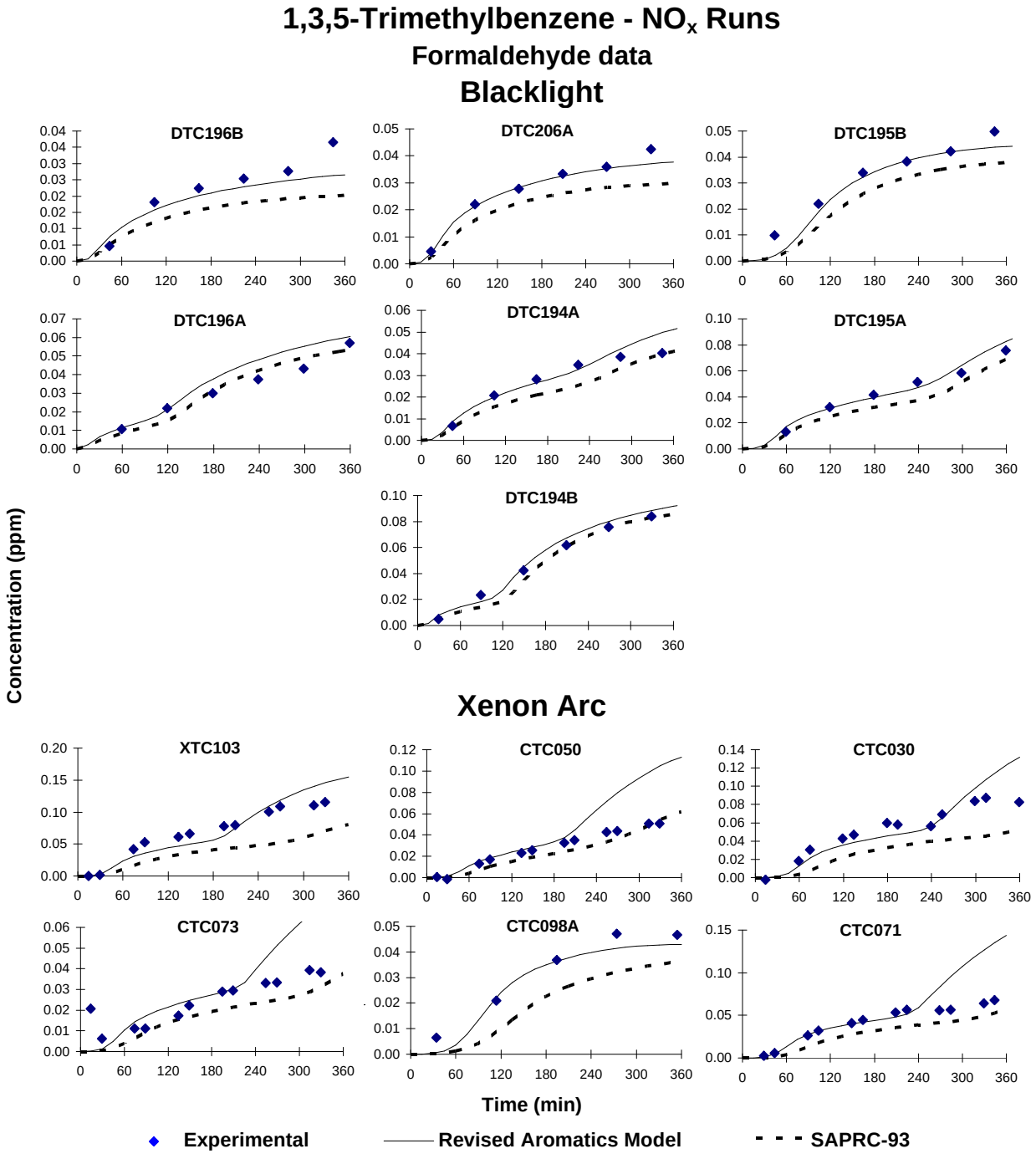

Figure B-28. Experimental and calculated concentration - time plots for formaldehyde for the 1,3,5-trimethylbenzene - NO_x experiments carried out for this program.